Universitat Autònoma de Barcelona

When oncology meets immunology: improving GL261 glioblastoma treatment through cancer-related immunity and MRSI-based non-invasive follow-up of response

SHUANG WU

Universitat Autònoma de Barcelona

Department of Biochemistry and Molecular Biology

DOCTORAL THESIS

When oncology meets immunology: improving GL261 glioblastoma treatment through cancer-related immunity and MRSI-based non-invasive follow-up of response

SHUANG WU

September 2020

Universitat Autònoma de Barcelona

Thesis presented by **SHUANG WU** to obtain the degree of doctor in Biochemistry, Molecular Biology and Biomedicine

Supervised by:

PhD Ana Paula Candiota and **PhD Carles Arús Caraltó**

Signatures of the supervisors

PhD Ana Paula Candiota

PhD Carles Arús Caraltó

Signature of the Ph.D. thesis author

Shuang Wu

Biochemistry and Molecular Biology Department

Biosciences Faculty, Campus UAB

Cerdanyola del Vallès, Spain.

September 2020

ACKNOWLEDGEMENTS

The completion of the thesis is attributed to many people's support and encouragement.

First and foremost, I want to extend my heartfelt gratitude to my supervisors, Dr. Ana Paula Candiota and Dr. Carles Arús, whose patient guidance, valuable suggestions and constant encouragement make me successfully complete this thesis. Their conscientious academic spirit, open-minded personality and positive attitude toward life inspire me both in academic study and daily life. They give me much help and advice during the whole period of my Ph.D study, which has made my accomplishments possible.

Also, I would like to express my sincere gratitude to all the member of our group - *Grup d'Aplicacions Biomèdiques de la Ressonància Magnètica Nuclear* (GABRMN). Thanks to Pilar Calero, we have been working together for almost 3 years, you are my best working partner often gives me creative suggestions, and I have always infected by your cheerful spirit. Thanks to Lucia, Elena, Nuria and Laura, since I came here, you taught me a lot of experimental skills, which are indispensable for the completion of this thesis. Thanks to other members in GABRMN group, Marga, Yeni, LuisMi and Daniel, thank you for helping me in your specific field and for your kindness.

My thanks also go to the SeRMN members, Silvia and Miquel, thank you for your help and support during the Biospec experiment. Even on weekends, you are always there.

In addition, I want to say to the colleagues in our department: “I am very happy to meet you, you make me feel less lonely abroad, y me has hecho sentir la buena cultura de un país extranjero, gracias por tu ayuda.” To: Lu, Jiarui, Pablo, Guillem, Sergi, Helena, Mohhammed, Valentin, Francisca, Samuel, Jaime, Jordi, Gabriel, Alejandro, Jofre, Rafa, Raquel, Gisela, Marta, Nuria, Salvador, Santiago, Elena, Magda, Juan Carlos, Maria.

Thanks to China Scholarship Council, who financed the expenses of my Ph.D. study here.

Last but not least, I would like to express my special thanks to my parents, whose care and support motivate me to move on and make me want to be a better person.

Table of Contents

Index of figures

Index of tables

MAJOR ABBREVIATIONS

3D	Three dimensional
Ala	Alanine
ALK	Anaplastic lymphoma kinase
APC	Antigen presenting cells
AS	Surface area
ASCII	American Standard Code for Information Interchange
BBB	Blood–brain barrier
BTDP	Below threshold detection period
BER	Base excision repair
CA	Contrast agent
CAR-T	Chimeric antigen receptor T-cell
Cho	Choline
CK2	Protein Kinase CK2
cNMF	Convex-Non-negative matrix factorization
CNS	Central nervous system
CPA	Cyclophosphamide
Cr	Creatine
CT	Computed tomography
CTLs	Cytotoxic T-lymphocytes
CTLA-4	Cytotoxic T-Lymphocyte Antigen 4
CX-4945	5-(3-Chlorophenylamino) benzo[c] [2,6] naphthyridine-8-carboxylic acid
DAMPs	Damage-associated molecular patterns
DCs	Dendritic cells
DIPG	Diffuse intrinsic pontine glioma
DMSO	Dimethyl sulfoxide
DNA	Deoxyribonucleic acid
DSB	Double-strand break
DTT	Dithiothreitol
EC50	Half maximal effective concentration
EDTA	Ethylenediaminetetraacetic acid

EE	Enriched environment
EML4	Echinoderm microtubule-associated protein-like 4
ERK	Extracellular signal-regulated kinases
E3D	Every 3 days dosing schedule
FACS	Fluorescence-activated cell sorting
FASTMAP	Fast Automatic Shimming Technique by Mapping Along Projections
FOV	Field of view
Foxp3	Forkhead box P3
GABRMN	Grup d'Aplicacions Biomèdiques de la Ressonància Magnètica Nuclear
GAMs	Glioma-associated microglia/macrophages
GB	Glioblastoma
Gln	Glutamine
Glu	Glutamate
Gly	Glycine
Gy	Gray
HGGs	High-grade gliomas
HIF	Hypoxia-inducible factor
IFN-γ	Interferon-γ
IgG	Immunoglobulin G
IHC	Immunohistochemistry
IL	Interleukin
IMS	Immune-Enhancing Metronomic Schedule
Ins	myo-Inositol
IP	Intraperitoneal Injection
IT	inter-slice thickness
ITIM	Immune receptor tyrosine-based inhibitory motif
ITSM	Immune receptor tyrosine-based switch motif
JAK	Janus kinases
Lac	Lactate
LGGs	Low-grade gliomas
Lkb1	Liver kinase B1

LN	lymph nodes
mAbs	Monoclonal antibodies
MEK	Mitogen-activated protein kinase kinase
MDSC	Myeloid-derived suppressor cell
MGMT	O6-methylguanine-DNA-methyltransferase
MHC	Major histocompatibility complex
MLs	Mobile Lipids
MMR	Mismatch repair
MR	Magnetic resonance
MRI	Magnetic resonance imaging
MRS	Magnetic Resonance Spectroscopy
MRSI	Magnetic resonance spectroscopic imaging
MTIC	Methyl-triazeno imidazole-carboxamide
MTX	Matrix size
MW	Molecular weight
NA	Number of averages
NAA	N-Acetyl Aspartate
NK	Natural killer cells
NMR	Nuclear Magnetic Resonance
N3-MedA	N3-methyl-adenine
N7-MedG	N7-methyl-guanine
OS	Overall survival
O6-MedG	O6-methyl-guanine
PBS	Phosphate buffered saline
PD	Progressive disease
PD-1	Programmed cell death protein 1
PD-L1	Programmed death-ligand 1
PFS	Progression-free survival
p.i.	post-implantation
PMSF	Phenylmethylsulfonylfluoride
PPi	Phosphatase inhibitor

ppm	Part per million
PR	Pattern recognition
PRe	Partial response
PRESS	Point-resolved spectroscopy
PTEN	Phosphatase and tensin homolog
PUFAs	Polyunsaturated fatty acids
PVDF	Polyvinylidene fluoride
RARE	Rapid acquisition with relaxation enhancement
RECIST	Response Evaluation Criteria in Solid Tumours
RF	Radiofrequency
RNA	Ribonucleic acid
ROI	Region of interest
ROS	Reactive oxygen species
RPMI	Roswell Park Memorial Institute
RT	Radiotherapy
SDi	Stable disease
SDS-PAGE	Sodium dodecyl sulphate polyacrylamide gel electrophoresis
SHP-2	Src homology 2-containing tyrosine phosphatase
ST	Slice thickness
STAT	Signal transducer and activator of transcription
SPION	Superparamagnetic iron oxide nanoparticle
SV	Single voxel
SW	Sweep Width
T1	Longitudinal relaxation time
T2	Transverse relaxation time
TAMs	Tumour-associated macrophages
TAT	Total acquisition time
TBS	Tris Buffered Saline
TCGA	The Cancer Genome Atlas
TCR	T cell receptor
TE	Echo time

TEeff	Effective echo time
TILs	Tumour-infiltrating lymphocytes
TIM	Tumour immune microenvironment
TIMCs	Tumour-infiltrating myeloid cells
TMZ	Temozolomide
TNF-α	Tumour necrosis factor-α
TP53	Tumor protein P53
Treg	Regulatory T cells
TTBS	TBS buffer containing 0.1% Tween-20
T2w	T2-weighted MRI
TR	Recycling time
TRI	Tumour Responding Index
TV	Tumour Volume
U.S. FDA	United States Food and Drug Administration
VAPOR	Variable Power and Optimized Relaxation Delay
VEGF	Vascular endothelial growth factor
VOI	Volume of interest
WB	Western blot
WHO	World health organization
wt	Wild type

1 INTRODUCTION

1.1 GLIOMA

1.1.1 Concept & Classification

Gliomas are the commonest malignant tumours of the central nervous system (CNS) in adults, which accounts for approximately 30% of all CNS tumour and 80% of all malignant brain tumours [1]. The average annual incidence of glioma is 5.26 per 100,000 people (Figure 1.1), or 17,000 new diagnoses per year, and the tendency is rising [2].

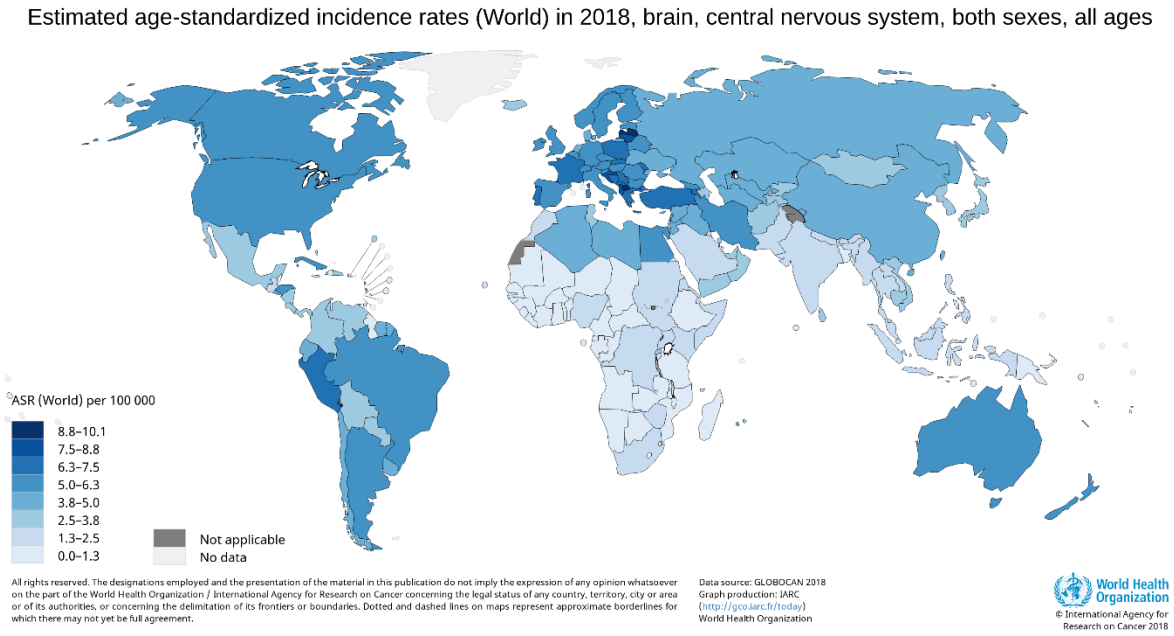

Figure 1.1 Worldwide incidence of malignant brain tumours in 2018 ASR (Age Standardized Rate).

Figure extracted from Global Cancer observatory https://gco.iarc.fr/

Based on the cell type they originate from or their histological appearance, gliomas are conventionally classified as astrocytoma, oligodendroglioma or ependymal tumours and attributed by the World Health Organization grades I- IV, where I and II are low-grade gliomas (LGGs) and III and IV are high-grade gliomas (HGGs) [3]. Astrocytoma is a tumour that develops from astrocytic glial cells, most possibly stem cells [4], [5] accounting for more than 60% of all gliomas, among which the most common and fatal form is glioblastoma (GB, grade IV astrocytoma) [6]. Gliomas are typically characterized by rapid growth, high infiltration and difficulty in surgical resection. Besides, most patients with gliomas are diagnosed at stage IV [2]. Clinically, the 5-year survival rate of patients with GB is less than 9 %, and the median survival time of them is only 1 year after diagnosis despite the availability of multimodal therapies [7].

1.1.2 Glioblastoma (GB) therapy

1.1.2.1 Surgery

Currently, surgery is the most traditional and effective method for the clinical treatment of GB, being the first step of the current clinical guidelines. The maximal safe resection of tumour lesion can effectively prolong the survival of patients with GB and significantly improve the quality of patient's life [8]. However, GBs exhibit infiltrating growth and have no distinct boundary with the normal brain tissue, thus it is hard to completely resect the tumour through surgery, often resulting in tumour recurrence after surgical resection (Figure 1.2). After recurrence, reoperation may improve the outcome of some patients. With the rapid development of glioma diagnosis and treatment technology, advanced specialized knowledge was progressively incorporated in surgery to remove tumour. For instance, intraoperative ultrasound localization, intraoperative neurophysiological monitoring, neuronavigation techniques, intraoperative magnetic resonance imaging and fluorescence-guided surgery, which assist in judging the location and boundary of tumour from different angles, removing the tumour as much as possible without damage the surrounding normal brain tissue needed for neurological function [9].

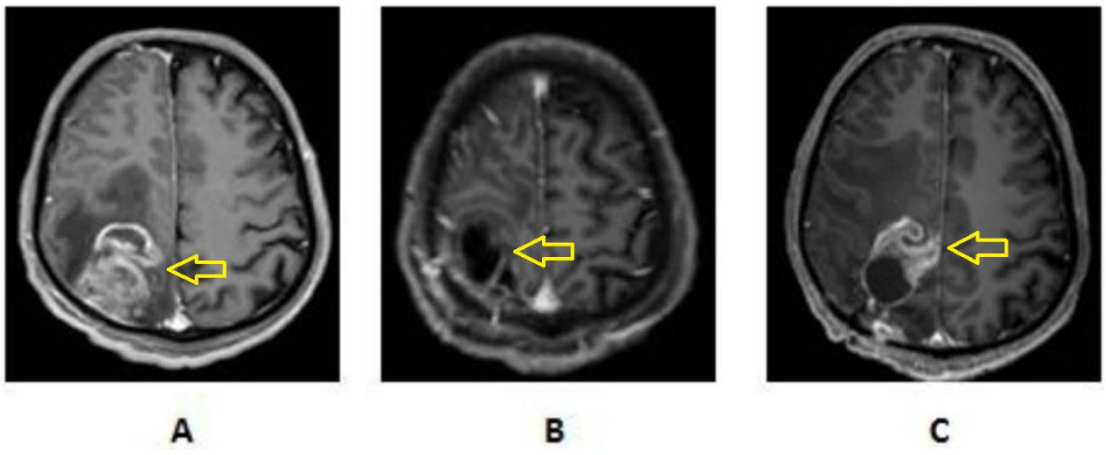

Figure 1.2 Magnetic resonance imaging (T1w post CE MRI) of local recurrent glioma. *A) Contrast enhanced axial magnetic resonance imaging scan at the time of diagnosis, showing an abnormal region with contrast enhanced hyperintensity, the tumour site is indicated by yellow arrow. B) post-operative scan showing gross total resection, black region at the centre of the previously tumour occupied volume (yellow arrow). C) Recurrent tumour adjacent to the resection cavity*

(hyperintensity region, yellow arrow) extending from the resection cavity). Figure modified from B. van der Sanden et al [10].

1.1.2.2 Radiotherapy

GB presents unique challenges to therapy. Due to its aggressive biological behaviour and diffuse infiltrative growth, it is extremely difficult to ensure complete removal even after precise resection. Thus, adjuvant postoperative radiotherapy has had an important role in the treatment of GB. In general, radiotherapy is usually performed within 1-2 weeks after the surgery, with doses of 60 Gy (30 fractions of 1.8 – 2.0 Gy) providing enlarged survival when compared to lower doses [11]. Radiation therapy affects tumour cells by directly or indirectly damaging cellular deoxyribonucleic acid (DNA) that leads to mitotic catastrophe and apoptosis [12]. After the radiation causes water ionization, the reactive oxygen species (ROS) and hydroxyl free radicals are formed by oxidative stress, which results in the increase of DNA damage in targeted cells (Figure 1.3). However, the radiation-induced DNA damage occurs not only in tumour cells but also in normal tissue, which often causes severe complications during or after radiotherapy [13]. Additionally, RT has been shown to trigger the host immune system concomitantly with the improved survival of patients [14][15]. RT does not cure GB patients, therefore, other therapeutic strategies are needed.

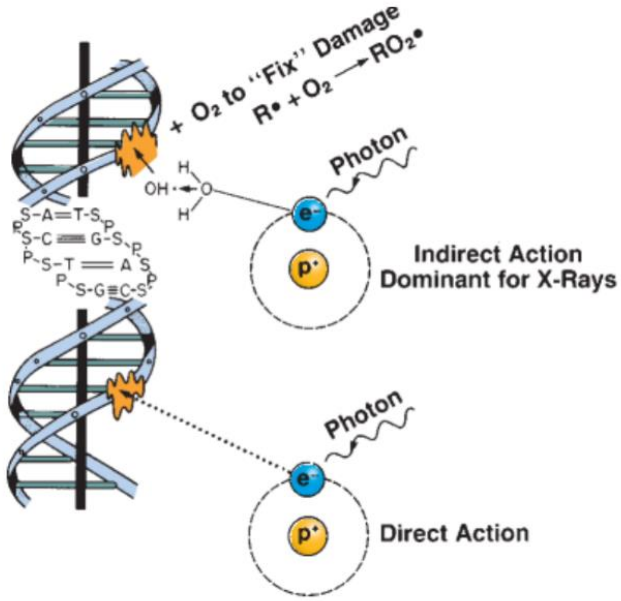

Figure 1.3 Direct and indirect actions of radiation on DNA. *Incident photons transfer part of their energy to free electrons; Direct Action: these electrons directly interact with DNA to induce DNA damage. Indirect Action: these electrons first interact with water to produce hydroxyl radicals that can then induce DNA damage. Figure modified from E. J. Hall et al* [12].

1.1.2.3 Chemotherapy - Temozolomide

Despite surgical resection and radiotherapy, the prognosis of GB patients remains dismal. Chemotherapy is an indispensable adjuvant therapeutic approach for the treatment of GB. While different chemotherapeutic drugs have different mechanisms of action, most of them have one thing in common: they trigger tumour cell cytotoxicity through apoptosis activation [16]. The most conventional chemotherapy drug for newly diagnosed GB is temozolomide (TMZ), which has been the standard chemotherapy for GB treatment for more than a decade [17].

TMZ has an obvious curative effect on various brain tumour types. It is an imidazotetrazine anti-tumour drug (194 MW), belonging to the second-generation alkylating chemotherapeutic agent [18]. As a new alkylating agent that can be administered orally, TMZ features high bioavailability and can penetrate through the blood-brain barrier to reach an effective concentration in brain and cerebral spinal fluid [19]. TMZ is stable at the acid pH of the stomach and is quickly absorbed through the gastro-intestinal tract. However, at neutral pH such as in the brain tissue, TMZ is first hydrolysed to the short-lived active compound Monomethyl Triazene 5-(3-methyltriazen-l-yl)-Imidazole-4-Carboxamide (MTIC), then rapidly breaks down to the methyl-diazonium ion (diazomethane), which is its reactive form. The diazomethane formed by the breakdown of MTIC primarily alkylates guanine residues in the DNA molecule, producing the formation of O6- and N7-methylguanines, and the O6-MedG is the most cytotoxic form (Figure 1.4). Eventually, blocking DNA synthesis triggered by TMZ induces cell cycle arrest at G2/M, which promotes apoptosis [20].

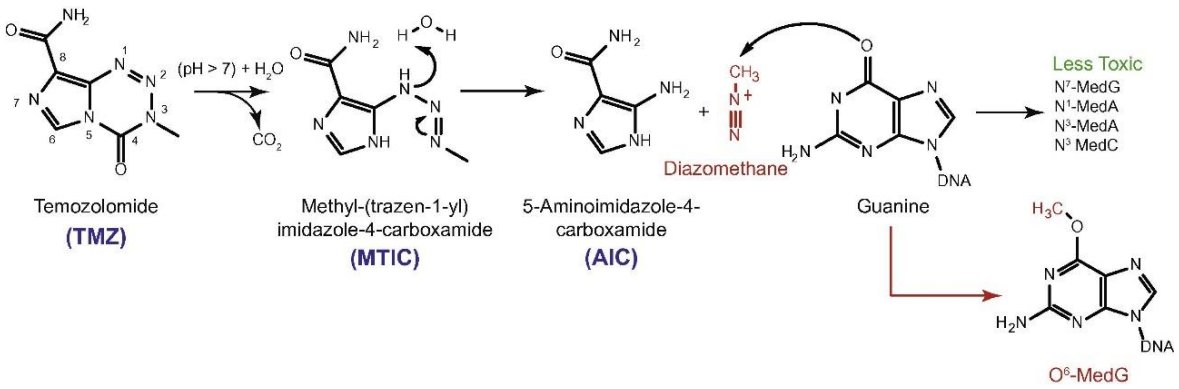

Figure 1.4 Mechanism of action of TMZ. *Schematic illustrating the release of diazomethane, which alkylates DNA and further promotes apoptosis. Figure modified from R. Rai et al* [20].

The combined usage of TMZ-mediated chemotherapy and radiotherapy to treat GB patients has improved the 2-year survival rate from 10.9% (adjuvant radiotherapy alone) to 27.2% [21], which has represented a significant improvement in GB therapy. Even so, the recurrence of GB remains inevitable and the clinical therapeutic outcome is still unsatisfying. The reason for the failure of adjuvant chemotherapy is often attributed to GB heterogeneity and mutations leading to resistance to TMZ [22].

1.1.2.4 Temozolomide resistance in GB

Chemotherapy with the alkylating agent TMZ is essentially a DNA-damaging treatment, although other factors may be also involved (see section 1.1.3). As previously stated, the active species diazomethane released from TMZ commonly methylate purine DNA bases (N7-MedG [60%-80%], N3-MedA [10%-20%] and O6-MedG [10%]) [23]. Under these circumstances, DNA repair mechanisms are activated in order to eliminate DNA damage, maintaining cell homeostasis and reducing apoptosis. The methylated DNA lesions induced by TMZ can be removed by base excision repair (BER) by DNA glycosylase, or dealkylated by a suicide DNA-repair enzyme, O6-methylguanine methyltransferase (MGMT). Temozolomide cytotoxicity is primarily mediated through the O6-MedG lesion, therefore the MGMT enzyme has been widely considered as a major mechanism of TMZ resistance [24].

MGMT is a small enzyme which removes the alkyl group from DNA restoring guanine to normal. If an O6-medG DNA adduct escapes the MGMT repair, it will form a base pair with thymine during DNA replication. The mismatched base pair of the persistent O6-medG with thymine may be recognized by the mismatch repair (MMR) pathway, resulting in futile repair

cycles leading to DNA double-strand break and apoptosis (Figure 1.5). Increased expression of MGMT in patients of GB is reported to produce poor prognosis compared to those having lower MGMT expression [25]. Both preclinical and clinical studies have reported MGMT as the responsible factor in decreasing TMZ-mediated death of GB cells [26][27]. MGMT-mediated demethylation is considered to be an important predictive feature for clinical response to TMZ therapy and associated survival in GB [24][28]

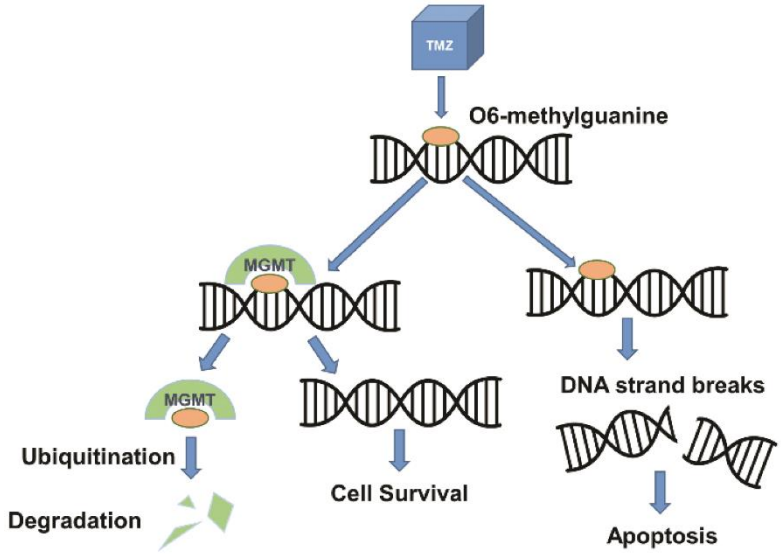

Figure 1.5 Mechanisms of TMZ and MGMT in DNA damage and repair. *TMZ methylates DNA at the O6 position of guanine, resulting in DNA damage and apoptosis of tumour cells. MGMT, a DNA repair protein, removes alkyl adducts from the O6 position of guanine, inhibiting the potentially therapeutic effect of TMZ. Figure modified from M. Esteller et al* [24].

In addition, MGMT expression in cells is regulated by hypermethylation of the CpG islands within the promoter and enhancer regions of the gene [29]. In tumours with a methylated MGMT promoter, MGMT deficiency is presumed, resulting in the enhanced effects of TMZ [30]. However, even patients with MGMT promoter methylated tumours eventually progress and succumb to GB [31]. The progression occurring in MGMT promoter methylated tumours suggests that other pathways must be activated to escape from TMZ treatment. Apart from MGMT pathway, the tumour suppressor p53 [32], MMR deficiencies [33][34], p-glycoprotein expression [34] and certain microRNAs [35] are all well described and studied mechanisms of resistance.

The most potent chemotherapeutic drug currently used in GB treatment is TMZ, but the development of resistance limits its effectiveness. Since the mechanism behind TMZ

resistance in GB is still debatable, further understanding about pathways in TMZ resistance is essential and important for GB therapy efficacy.

1.1.3 Immune system role in cancer fighting

The development and growth of tumours is known to be associated with decreased/impaired tumour immunosurveillance and anti-tumour immune response. Research over the last decades has shown that the immune system not only deals with neoplasm growth but can also eradicate damaged cells that are more vulnerable to being malignant [36], and it has been found that the immune system also plays a crucial role in responding to many malignancies [37]. The development of successful antitumor immune response depends on organized interactions between host immunocompetent cells and the production of tumour antigen-specific cytotoxic T lymphocytes (CTLs), which play an important role in the defence against cancer recognising specific antigens presented on the surface of transformed cells. Naive lymphocytes require the priming by dendritic cells (DCs) which are antigen-presenting cells (APCs) and also need the assistance of CD4 + T-cells (helper) to become effective killer cells.

As schematised in Figure 1.6, malignant cells may express pathogen-associated molecular patterns (PAMPs) that can be recognized by pattern recognition receptors (PRRs) on dendritic cells (DCs) precursors, triggering the local release of cytokines and chemokines. Then, DCs migrate to local lymph nodes (LN) and present processed tumour-derived peptides to naïve T and B lymphocytes, which are then activated in case of antigen (Ag) match to become plasma cells producing antibodies and CD4+ helper T lymphocytes or CD8+ T lymphocytes. CD8+ T lymphocytes leave LN to infiltrate tumour tissues and exert effector functions once activated to cytotoxic T lymphocytes (CTLs) by encounter with target cells.

In the end, it is worth mentioning that the process known as “immunogenic death” may also be relevant in the recruitment if immunological response against the tumour [38], [39]. In this respect, TMZ has been suggested as one of the chemotherapeutic agents which trigger immunogenic death after administration [40]. Besides, chemotherapy (cyclophosphamide) administration with every 6 days consecutive cycles triggered immune system activation and immune memory in a subcutaneous GB model [36] and we coined the expression “Immune-Enhancing Metronomic Schedule” (IMS) for this immune-friendly “every 6 days” administration protocol in our system.

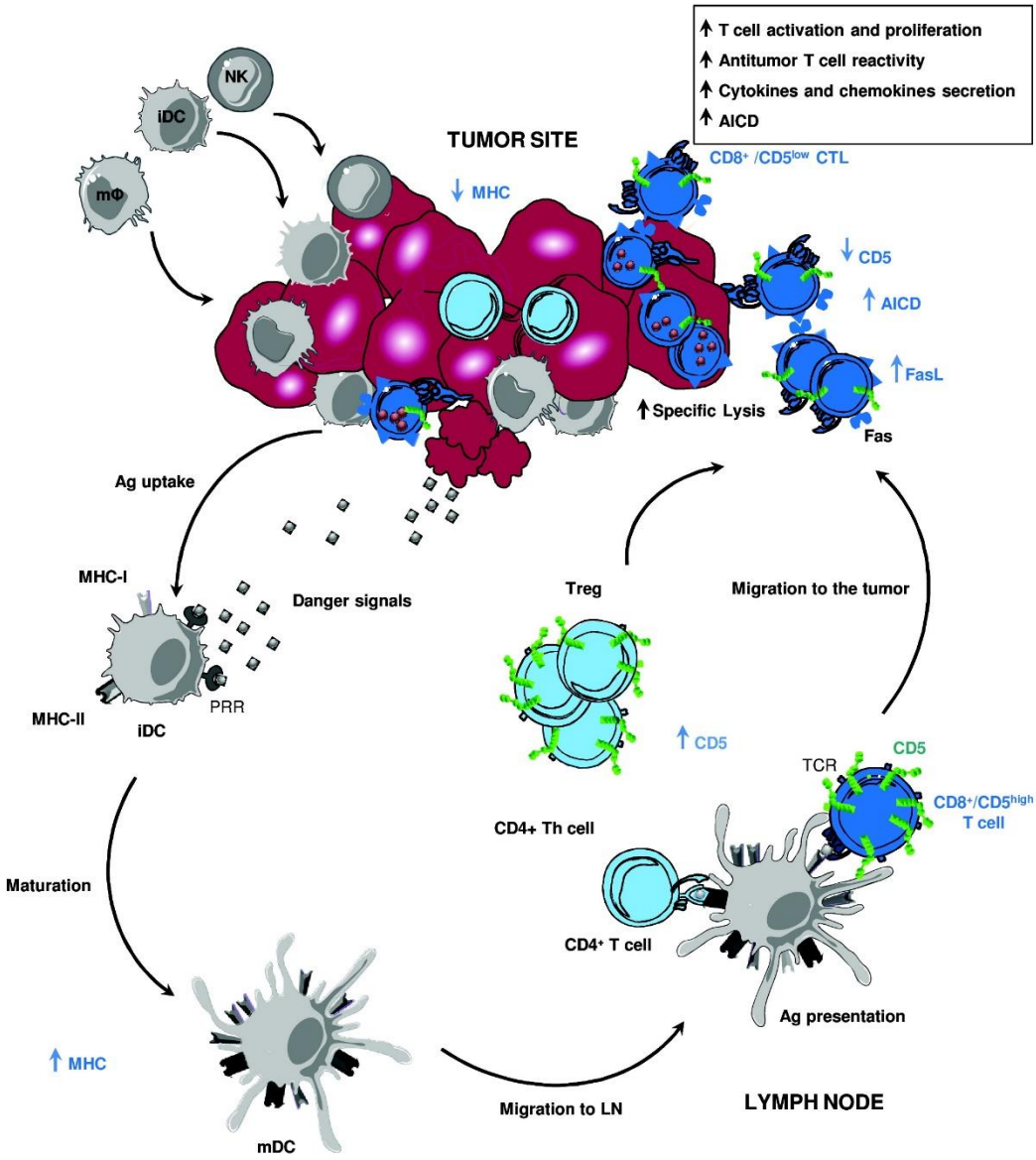

Figure 1.6 Scheme of the cycle for immune response against a tumour. *MHC: Major histocompatibility complex, Mφ: macrophages, NK: natural killer, NKT: natural killer T, TCR: T-cell receptor, and Treg: Lymphocyte T regulatory. Figure modified from Tabbekh M et al* [41].

1.1.4 Immunosuppression and immunotherapy in GB

With the rapid development of tumour immunotherapy, an increasing number of studies suggested that immune escape plays an important role in tumour progression. In other words, resistance to chemotherapy is not only related to intrinsic properties of tumour cells but also to other cellular or acellular parameters of the tumour microenvironment [42]. Tumours have evolved multiple ways to evade the immune system by creating a strong immunosuppressive microenvironment, which protects tumour cells from the immune attack by generating

immunosuppressive signals that target T-lymphocytes and dendritic cells. Ultimately, the final phase of escape from immune surveillance allows the tumour cells to thrive unchecked in such an immunosuppressive tumour microenvironment. Accordingly, by ameliorating the immunosuppressive tumour microenvironment and triggering an anti-tumour immune response, immunotherapy brings new strategies and hope to the treatment of GB.

In recent years, the field of tumour immunotherapy is growing remarkably, such as chimeric antigen receptor T-cell (CAR-T) therapy, cancer vaccinations or immune checkpoint blockade therapy [43][44]. Among them, immune checkpoint blockade has emerged as one of the most promising modalities in tumour immunotherapy. Cytotoxic T-Lymphocyte Antigen 4, CTLA-4, and Programmed cell death protein 1/Programmed death-ligand 1, PD-1/PD-L1, are the main checkpoints to be targeted [45][46]. Specifically, CTLA4 is involved in early phases by reducing T-cell response to self-antigens, while the axis PD-1/PD-L1 participates in the active stage of T-cell response in the tumour microenvironment (Figure 1.7).

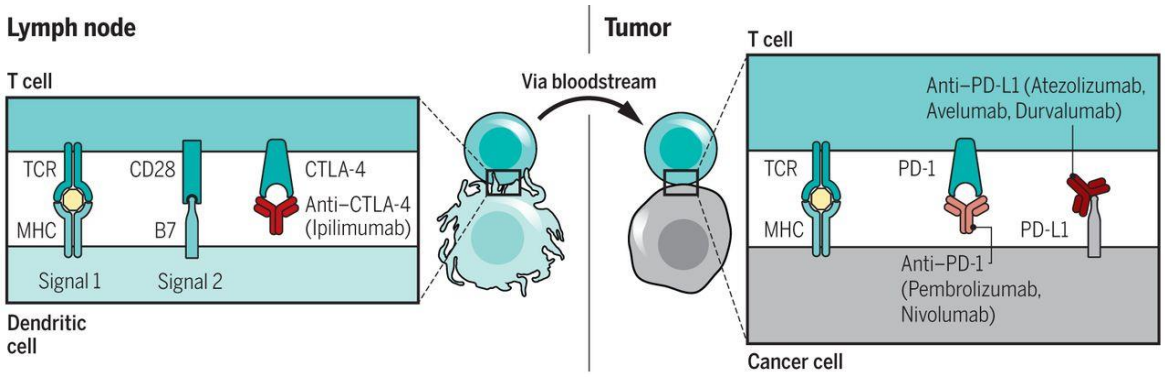

Figure 1.7 Blockade of CTLA-4 and of PD-1 and PD-L1 induce antitumour responses. *Left: The activation of T cells is mediated by the interaction of T cell receptor (TCR) and the CD28 receptor with class II major histocompatibility complex (MHC) and B7 co-stimulatory molecule located on the antigen presenting cells. The interaction of CTLA-4 with the B7 molecule delivers an inhibitory signal, which can be blocked with anti–CTLA-4 antibodies.*

Right: Once T cells are activated, they circulate throughout the body to find their cognate antigen presented by cancer cells. Upon recognition, the triggering of the TCR leads to the expression of the negative regulatory receptor PD-1, and the production of interferon-γ (IFN-γ) results in the reactive expression of PD-L1, turning off the antitumour T cell responses. This negative interaction can be blocked by anti–PD-1 or anti–PD-L1 antibodies. Figure modified from A. Ribas et al [47].

While anti-CTLA-4 antibody treatment leads to immune activation in central lymphoid organs, anti-PD-1 or anti-PD-L1 antibodies reactivate peripheral immunity within the tumour microenvironment (Figure 1.8).

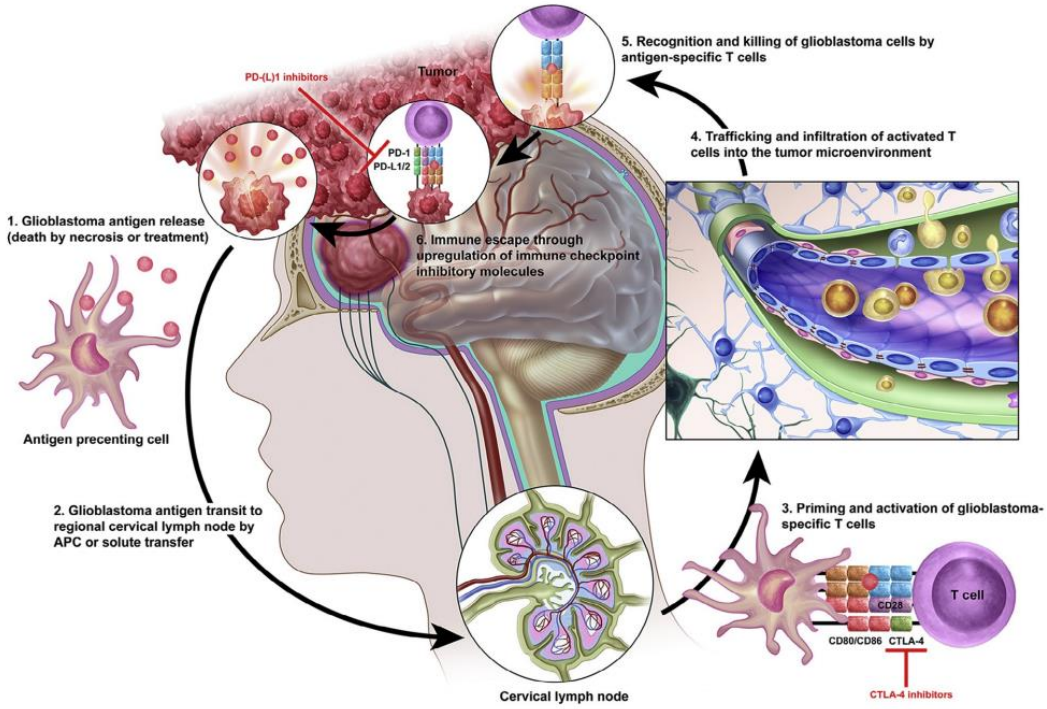

Figure 1.8 In the cancer immune cycle, targeting PD-1/PD-L1 axis plays a key role in fighting GB.

Figure modified from Johanns T M et al [48].

GB is known to grow in a highly immunosuppressive microenvironment that is favoured by tumour hypoxia and the presence of immunosuppressive cytokines [49], thus targeting PD-1/PD-L1 axis plays an important role in downregulating immunologic tumour escape mechanisms.

1.1.4.1 Expression and functions of PD-1 and its ligand PD-L1

Programmed death-1 (PD-1, also known as CD279) is a type I transmembrane receptor belonging to the immunoglobulin superfamily [50][51], transcriptionally expressed on $CD4^+$ and $CD8^+$ T cells, B cells, monocytes, macrophages, natural killer cells (NK cells) and dendritic cells (DCs) [52][53]. $CD8^+$ T cells differentiate into cytotoxic T lymphocytes (CTLs), which are primarily responsible for the removal of target cells, including tumour ones. PD-1 is an important inhibitory receptor that induces the exhaustion of $CD8^+$ T cells. Typically, exhausted CD8+ T cells lose their ability to proliferate and to produce cytokines, such as interleukin-2 (IL-2), tumour necrosis factor-α (TNF-α) and interferon-γ (IFN-γ). Finally upon exhaustion,

effector and memory functions of $CD8^+$ T cells are also substantially lost, $CD8^+$ T cells undergo apoptosis and are eliminated by phagocytic cells [54]. Moreover, regulatory T cells ($CD4^+$ and $Foxp3^+$ Treg) are immunosuppressive cells in the body, inhibiting $CD8^+$ T cell proliferation and cytotoxic activity of other major immune cells [55][56]. When the PD-1 expressed on $CD4^+$ T cells is bound by its ligand programmed death-ligand 1 (PD-L1, also known as B7-H1 or CD274), the naive $CD4^+$ T cells differentiate into Treg cells, which will inhibit the immune activation and effector response [57]. Finally, PD-1 is also expressed on activated NK cells [58], B cells [59], macrophages [60] and DCs [61] and these cells can be also affected through the PD-1 pathway modulation (Figure 1.9).

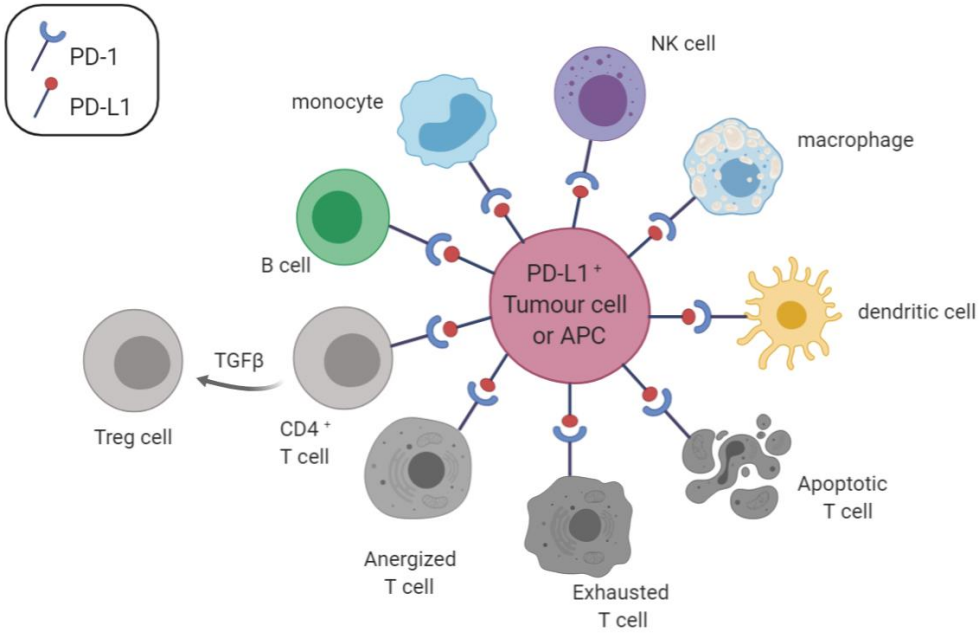

Figure 1.9 Multiple lymphoid and myeloid cell populations express PD-1 and are inhibited by PD-L1+ tumour cells or APCs. *Binding of PD-L1$^+$ cells to PD-1$^+$ activated T cells can result in T cell dysfunction by causing T cell anergy, T cell exhaustion, and T cell apoptosis, as well as by inducing the differentiation of Treg cells. PD-1 is also expressed by activated B cells, monocytes, NKT cells, macrophages, and DCs and suppresses these cells. Figure modified from Ostrand-Rosenberg S et al* [62].

PD-1 has two known ligands PD-L1 and PD-L2, which are expressed in tumour cells and antigen-presenting cells (APC), such as B lymphocytes, macrophages, etc. Both ligand types

engage the PD-1 receptor and induce PD-1 signalling and associated T-cell "exhaustion" [63][64]. PD-L1 is more extensively expressed than PD-L2 and can be found in a variety of tumour cells, such as glioma, ovarian cancer, melanoma and lung cancer [65]. A growing amount of evidence enlighten the intrinsic and extrinsic mechanisms of PD-L1 expression regulation in tumour cells [66]. Inflammatory cytokines, such as IFN-γ, can induce PD-L1 expression through the MEK/ERK or JAK/STAT pathways [67][68]. The EML4-ALK fusion gene and loss of Lkb1 and PTEN have been reported to be involved in the intrinsic regulation of PD-L1 expression in non-small-cell lung cancer [69]. In addition to tumour cells, research shows that PD-L1 expression is also detected in tumour-associated macrophages (TAMs). Namely, it is worth mentioning that gliomas can upregulate PD-L1 expression in circulating monocytes and tumour-infiltrative macrophages through modulation of autocrine/paracrine interleukin (IL)-10 signalling, resulting in an immunosuppressive phenotype [70].

1.1.4.2 PD-1/PD-L1 prognostic role in glioma.

PD-1, as a negative regulator, plays an important role in enforcing T cell exhaustion. Tumour-infiltrating lymphocytes (TILs) typically express PD-1 which impairs anti-tumour function when bound to its ligand in situ [71]. The presence of PD-1 on TILs has been described as a strong prognostic and predictive negative feature in different types of tumours [72][73][74]. In glioma, it has been revealed that PD-1 expression on $CD4^+$ and $CD8^+$ peripheral T cells was significantly increased in glioma patients compared with healthy controls [75]. In addition, PD-1 was found significantly elevated in TILs when compared with peripheral blood T cell in glioma patients [76]. In general, high expression of PD-1 either on TILs or peripheral blood T cell subsets is correlated with poor prognosis.

PD-L1 acts as a PD-1 ligand, and has been reported to be highly expressed in various types of cancers and associated with tumour prognosis [77][78][79][80]. Furthermore, numerous studies have found that PD-L1 overexpression could be considered a predictive biomarker for response to immune checkpoint inhibitors [81][82]. In recent years, the correlation between PD-L1 expression levels and prognosis of glioma patients has been extensively studied. Using mRNA expression level, high PD-L1 was found to be associated with significantly shorter overall survival (OS) of glioma patients [83][84]. Similar results were also reported in other studies based on immunohistochemistry (IHC) [85][86][87][88]. However, there is some controversy in this respect: other IHC analyses and a TCGA (The Cancer Genome Atlas)

database analysis involving 444 GB patients showed no significant relationship between PD-L1 expression and overall survival of glioma patients [89][90][91]. There is a lack of consistency between these studies though, which may be probably explained by relying on relatively small cohorts. Besides, several studies reported that PD-L1 in glioma microenvironment is contributed mainly by tumour-infiltrating myeloid cells (TIMCs, including macrophages and T-regulatory cells) rather than tumour cells themselves [92][93]. Some authors describe that lower PD-L1 level in glioma cells is not associated with either decreased immune inhibition or better prognosis of glioma, reinforcing the idea of elevated PD-L1 in glioma TIM [94]. Thus, PD-L1 expression on TIM in glioma microenvironment may also be an important factor affecting the prognostic value of PD-L1 and should not be neglected.

1.1.4.3 Mechanisms of immunotherapy via PD-1/PD-L1 pathway blockade.

The structure of PD-1 contains an extracellular domain, a transmembrane region and a cytoplasmic tail. The cytoplasmic tail of PD-1 possesses two signalling motifs, one is an immune receptor tyrosine-based inhibitory motif (ITIM) and the other is an immune receptor tyrosine-based switch motif (ITSM) [95]. Binding of PD-L1 to PD-1 on activated T cells, along with TCR signalling, leads to phosphorylation of the cytoplasmic domain tyrosine residues and recruitment of an Src homology 2-containing tyrosine phosphatase (SHP-2) to the ITSM. Consequently, SHP-2 dephosphorylates TCR-associated CD3 ζ, resulting in inhibition of TCR signalling, cytokine production and altered T cell metabolism (Figure 1.10) [96][97].

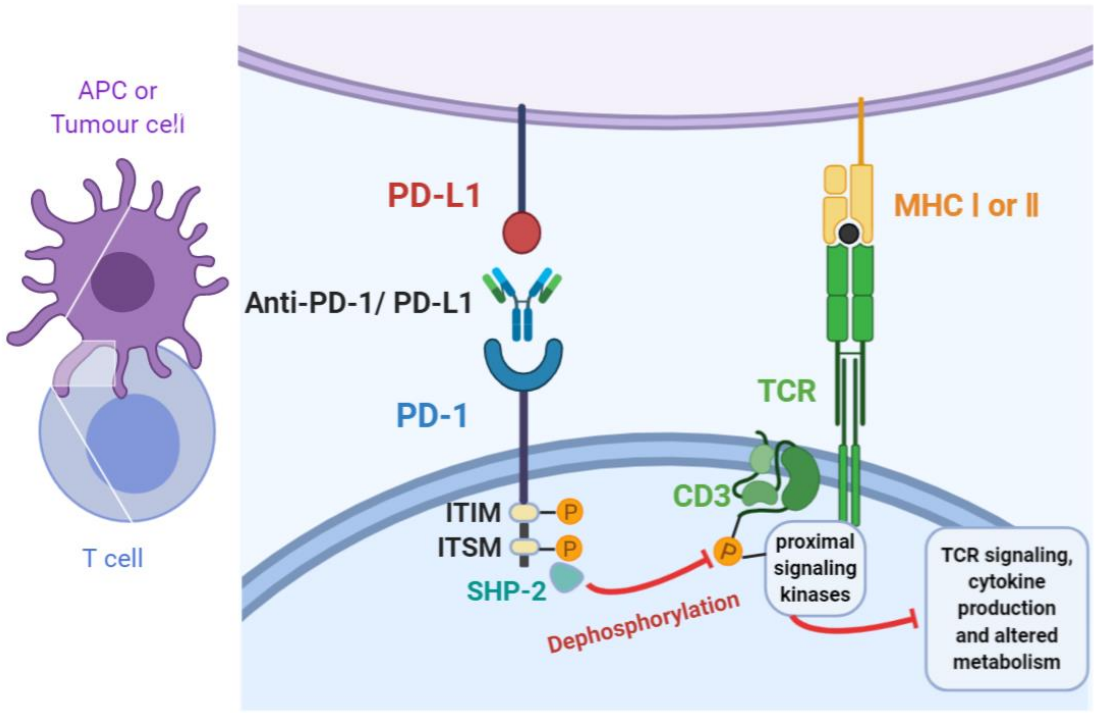

Figure 1.10 PD-1/PD-L1 pathway and therapeutic targeting. *PD-1 contains an extracellular domain, transmembrane region, and cytoplasmic tail with ITIM and ITSM. During T cell activation through TCR crosslinking with antigen presented by MHC, PD-L1 expressed on cancer cells downregulate T cell activity by binding to PD-1, unless blocked by anti-PD-1 or anti-PD-L1. Red curving lines indicate inhibitory signals. Figure modified from Long J et al* [98].

Thus, monoclonal antibodies (mAbs) blocking the PD-1/PD-L1 axis are recognized as an attractive strategy for cancer immunotherapy. There are evidences that blockade of PD-1 or PD-L1 leads to an increase in T-cell proliferation and interferon-gamma (IFNγ) production at the tumour site [99], which is accompanied by decrease of the highly immunosuppressive myeloid-derived suppressor cell (MDSC) populations [100]. In summary, anti-PD-1 and anti-PD-L1 antibodies to the PD-L1/PD-1 axis have been shown to be encouraging as immunotherapies for changing the dynamics of the tumour microenvironment in order to control tumour growth.

1.1.4.4 Clinical application of PD-1/PD-L1 antibody in glioma.

Currently, several antibodies for PD-1 (e.g. nivolumab, pembrolizumab and pidilizumab) are extensively being used in the clinic. They were approved by the U.S. FDA (United States Food and Drug Administration) for the treatment of melanoma, non-small cell lung cancer, renal cell cancer, Hodgkin's lymphoma, and bladder cancer [101][102][103][104]. Preclinical studies revealed that PD-1 antibodies exhibit strong potential for enhancing anti-tumour immune

response in an immune-competent mouse model of glioma [105], and a large group of anti-PD-1 immunotherapy protocols are under study for safety and efficacy in the treatment of gliomas. For example, in a clinical trial involving 24 patients with high grade gliomas, pembrolizumab (PD-1 antibody) treatment response and toxicity was evaluated [106]. The median progression free survival (PFS) was 1.4 months and median overall survival (OS) was 4 months, along with very few serious adverse events occurring during treatment. Besides, in a clinical trial (NCT01952769) using pidilizumab (PD-1 antibody) for diffuse intrinsic pontine glioma (DIPG) in children, 9 patients were treated with pidilizumab after radiotherapy [107]. Treated patients showed a median PFS of 9.3 months and a median OS of 15.3 months, PFS of 2 of them were of nearly 30 months, suggesting that pidilizumab is a safe and effective treatment option for DIPG. Based on these evidences, a number of clinical trials are still underway, such as clinical trials (NCT02617589), which is a randomized Phase III open-label study of nivolumab (PD-1 antibody) compared to TMZ, each given with RT, in newly diagnosed GB patients.

PD-L1 antibody treatment is another promising immunotherapy strategy to block the PD-1/PD-L1 pathway. Antibody-mediated blockade of PD-L1 induced durable tumour regression and prolonged stabilization of disease in patients with advanced cancers, including non–small-cell lung cancer, melanoma, and renal-cell cancer [108][109]. Durvalumab is one of the anti-PD-L1 blocking mAb, currently undergoing phase II clinical trial (NCT02336165) for the treatment of GB, to evaluate the treatment effectiveness and quality of patient's life.

1.1.4.5 PD-1/PD-L1 antibody combined with other therapeutic approaches in glioma treatment

Cancer involves multiple mechanisms to promote its own progression and metastasis. In this sense, combination therapy has the advantage of targeting different pathways in comparison with monotherapy, thus avoiding tumour escape. According to the different benefits, PD-1/PD-L1 antibody could be combined with other immune checkpoint inhibitors or different therapeutic strategies.

In a preclinical study with different immune checkpoint inhibitors in a GL261 GB murine model, Reardon, D. A. et al [105] found that combination of anti-PD-1 and anti-CTLA-4 was more effective and presented significantly higher survival rate compared with monotherapy. From the clinical side, a phase III clinical trial evaluating safety and tolerability of nivolumab (anti-

PD-1) plus ipilimumab (anti-CTLA-4) compared with nivolumab alone in GB patients is still in progress (NCT02017717).

The standard therapy for GB is composed of surgical resection, radio-chemotherapy and adjuvant chemotherapy with TMZ, but the standard treatment is not capable of curing patients or preventing tumour recurrence, since tumour cells present infiltrative growth pattern and chemoresistance (see section 1.1.2.). Immunotherapy could help the host immune system to recognize and eliminate tumour cells specifically, thus immune checkpoint inhibitors combined with standard therapy may enhance the overall treatment effect for GB. In preclinical studies, the combination of PD-1 antibody and localized radiation therapy showed prolonged survival in an orthotopic GB mouse model [110]. Also, combination therapy of PD-1 antibody and a chemotherapeutic drug (carmustine) greatly decreased tumour size and improved survival rate in GB animal models [111]. Furthermore, phase I and II trials were launched to assess safety, toxicity, and efficacy of pembrolizumab (PD-1 antibody) in combination with MRI-guided laser ablation in recurrent glioblastoma (NCT02311582).

Rapid development in the immunotherapy field has occurred in the recent decades. Accordingly, a variety of preclinical studies and clinical trials for GB immunotherapy are ongoing. Although PD-1 checkpoint blockade strategy has not been approved by the US FDA to treat patients with GB, the existing studies have shown its therapeutic benefit in preclinical models and a future approval is foreseen. Due to the poor outcome from traditional treatment, immunotherapy is expected to help eliminating tumour cells completely with its unique advantages, which brings new hope for curing patients with GB.

1.2 PRECLINICAL MODELS OF GB

For obvious ethical reasons, repeated collection of brain tumour tissue from human subjects along treatment is not feasible/advisable, thus preclinical models are a powerful surrogate for investigating and understanding the mechanisms underlying human GB. Indeed, research into GB relies heavily on preclinical models, particularly rodent models, as experimental systems.

Ideally, glioma models should present reproducible growth patterns, mimic the histopathology and appearance/evolution of human gliomas in vivo, be able to grow in immunocompetent models preferably in the same site of origin as human GB, do not present

intrinsic immunogenicity, and have consistent tumour evolution in vivo, as their human counterparts. However, the ideal GB preclinical model that meets all the above conditions does not exist. Thus, it is important to identify the advantages and disadvantage of different preclinical models in order to select the most suitable GB model based on the nature of the experiment to be conducted.

There are several types of preclinical models of brain tumours (Figure 1.11). Rodent models could be spontaneous, which are experimental mice that develop tumours under ordinarily natural conditions. Spontaneous models could emulate better the human tumour appearance at early stage, however it is very difficult to have control over the tumour initiation time [112], at least in our hands, incidence was much lower than expected and it was not feasible to generate cohorts of animals with similar tumours [113].

Apart from spontaneous strategies, tumour rodent models can also be induced, being this divided into syngeneic or xenografts. Syngeneic models are transplantation models obtained by injecting a recipient of a specific genetic background with cell lines previously established through isolation of tumour cells from a mouse of the same genetic background. On the other hand, a xenograft model is transplanted with human tumour cells, either under the skin or into the organ type in which the tumour originates in humans, but using immunocompromised mice, that do not reject human cells.

Moreover, if we take into account the transplantation location, rodent models can be orthotopic or ectopic. Orthotopic models involve implantation of tumour cell lines or patient-derived cell xenografts into animal tumour models into the organ or tissue which matches the original tumour histotype. This creates a more disease-relevant environment for the assessment of tumour growth, which can be analysed by imaging. Ectopic models are similar to orthotopic models of metastasis, however, cells or graft material is delivered to a location that differs from the origin of the original tumour, sub-cutaneous injections are the most common location for these models.

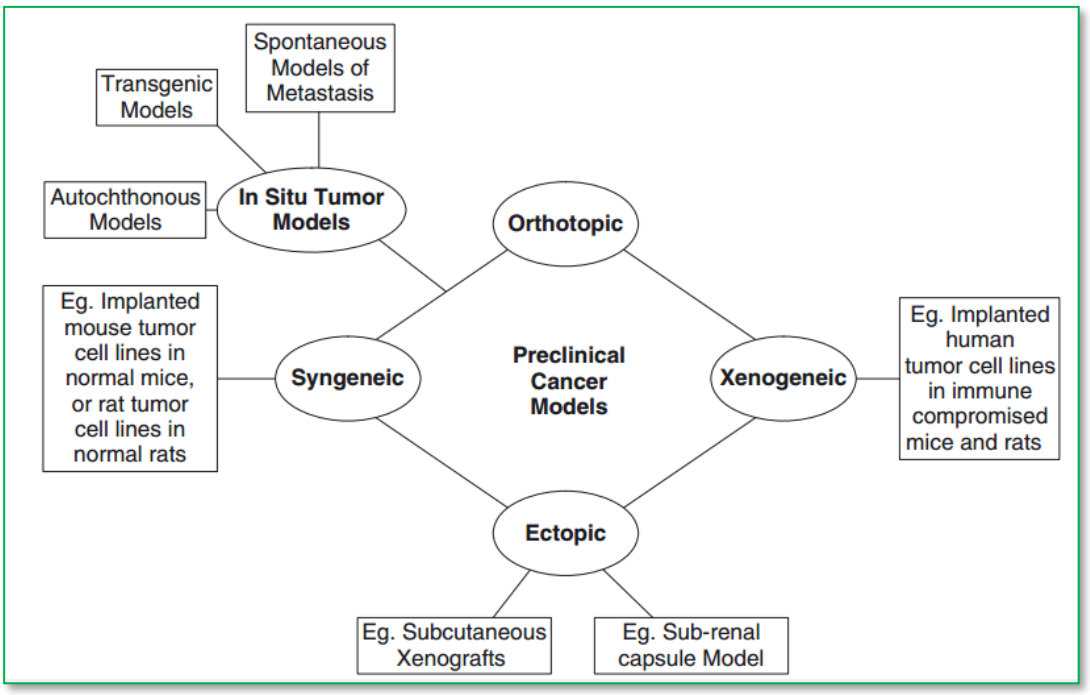

Figure 1.11 Preclinical cancer model scheme. The model studied in this thesis belongs to an implanted, orthotopic model from glioblastoma murine cells in C57BL/6J mice. *Figure modified from L. Ferrer Font* [114]

There is a large number of cell lines that simulate human GB and which can grow on rodent models. The most commonly used include human-derived cell lines U251 and U87, rat cell line C6 and murine cell lines GL261 and CT-2A. The characteristics of the tumours obtained with these lines are briefly summarised below.

U251 human GB xenograft model - The U251 malignant glioma cell line was originally established from a 75-year-old male patient with GB; to establish the preclinical model, cells are injected intracranially in the striatum of athymic Balb/c nude mice [115]. It is known to mimic the features of human GB and received a lot of attention over the last decades [115][116]. However, as a xenogeneic mouse model, U251 model is criticized for not reproducing the tumour host immune system interactions and for not accurately representing the cellular composition of the original tumours [117].

U87 human GB xenograft model - The U87 GB cell line was originally established from a female patient with GB, and it is often subcutaneously or intracranially implanted in the athymic Balb/c nude mice [118]. The U87 human xenograft model is the most abundantly

vascularized tumour among the GB rodent models, and its profuse angiogenesis allows it to test therapeutic approaches that target neovascularization. Unfortunately, the U87 model fails to reproduce the necrotic foci of the human GB tumours and its invasion pattern is less aggressive than the U251 tumour [119]. Furthermore, research shows that U87 incorporate host (non-human) glycolipids, possibly altering the biochemical and immunogenic properties of the model [120], which is a common drawback of the xenograft models. Besides, authors find that the DNA profile of the widely used glioma cell line U87MG is different from that of the original cells and that it is likely to presently be a human glioblastoma cell line of unknown origin [121].

C6 rat GB allogeneic model – the C6 cell line was obtained from methyl-nitrosourea-induced glioma in Wistar-Furth rats [122]. Although it was originally developed in Wistar rats, C6 can be implanted in Sprague–Dawley and Long–Evans rats as allogeneic model [123][124]. Both in vitro and in vivo, C6 cells present stable growth, express glioma specific markers and are consistent with the pathological characteristics of human GB [125]. However, it has been reported that C6 tumour loose its invasive characteristics and grow in an encapsulated way, no longer diffusely infiltrating the whole brain like human GB [126]. Besides, the immunogenicity of the C6 model is an important factor that needs to be considered, Parsa and col. [127] demonstrated strong antibody responses to C6, even when grown in Wistar rats.

GL261 mouse GB syngeneic model – The GL261 model is one of the best characterised orthotopic allograft mouse models of human malignant glioma, and it was initially generated by chemical mutagenesis in the early 1940's, in the C3H mice strain [128][129]. The GL261 murine model has a high tumour take rate, tumours grow aggressively in vivo, and to our knowledge there is no description of spontaneous regression of the tumours for the GL261 model, as has been reported for the C6 model [130]. Moreover, the GL261 model shares several molecular biological alterations, characteristic of human gliomas, such as TP53 gene mutation, which is known to be a common alteration in human glioma and is often accompanied by a bad prognosis [131]. Still, GL261 is a moderately immunogenic tumour model; the immunogenicity may be due to a basal MHCI expression on its cell surface [132] jointly to the usual practice after the 1970s of growing GL261 tumours in the C57BL/6 mice

strain[133], different from the early C3H one. Still, tumours grow in a consistent way and usually kill animals in three weeks after inoculation.

CT-2A mouse GB syngeneic model – The CT-2A cell line was established by Seyfried and col [134] in 1992 through chemical induction with 20-methylcholanthrene. Following serial transplantation of tumour fragments into C57BL/6 mice, this syngeneic model for highly malignant, poorly differentiated anaplastic astrocytoma resulted in 100% mortality within 3–8 weeks. In 2007, Martinez-Murillo and col [135] standardized techniques for establishing CT-2A tumours from cultured CT-2A cells, as opposed to solid tumours, and demonstrated a survival range of 15–20 days with intracranial injections of 8×10^4 tumour cells/4 µl. Histologically, CT-2A tumours manifest features of high-grade astrocytomas including pleomorphism and high cellular density, but can undergo malignant transformation with evidence of pseudopalisading necrosis [135]. Tumours are angiogenic, occasionally cystic, and infiltrative, with tumorigenesis rates reported up to 100% [135], [136]. Compared to established glioma cell lines, CT-2A cells are significantly more proliferative and invasive [137] but less invasive than other mouse brain tumours [138]. Overall, the CT-2A model is considered to accurately represent several GB characteristics including intra-tumoral heterogeneity, in vivo migratory patterns, radio-resistance, and chemo-resistance [135].

Overall, human lines usually will need an immunocompromised mouse to grow as tumours, which would prevent us to observe and study several aspects of the host immune system that that be relevant in therapy response. There are strategies to tolerize postnatal mice from to make it possible the growth of human glioma cells [139] that may be of interest in future work if robust and reproducible to generate large enough mice cohorts for evaluation.

On the other hand, with the rodent lines, although “inducing” the tumour prevents us to monitore the typical evolution of a spontaneous human tumour, they allow us to work with immunocompetent models, such as the GL261 model, which can mimic more closely the growth and immune response of human GB when compared with xenograft and allogeneic models. Due to its immune competent feature and the availability of many mice raised antibodies and immune markers available, several advances in preclinical GB immunotherapy have been achieved by using the GL261 model[140].

After comparing the strengths and weaknesses of different preclinical models, GL261 is one of the optimal models for studying GB therapies, particularly immune system-based therapies, thus it was chosen for conducting experiments in this thesis. Besides, using the GL261 model allowed us to compare ourselves with previous therapeutic studies by others [105], [141], [142].

1.3 MAGNETIC RESONANCE

Magnetic resonance (MR) techniques are non-invasive measurements utilizing the phenomenon of nuclear magnetic resonance (NMR) for detecting tissue structure and function in the body of living humans or animal models of the human pathology. This technique has evolved from promising beginnings in the 1970s to become nowadays a cornerstone technology in clinical diagnostics and basic research. The most used nucleus in clinics is proton, ^{1}H, due to its abundance and suitable characteristics. In particular, in the diagnosis and follow-up of GB, MR techniques are the most common clinical tools among the many non-invasive imaging modalities (such as computed tomography and positron-emission tomography) due to its harmless, non-ionizing radiation features. Magnetic resonance imaging (MRI) is the most spread MR technique allowing us to acquire high-quality images of brain tissue. It provides anatomical information about any brain lesion and its surrounding parenchyma, as well as biophysical measurements related to function, such as perfusion or diffusion.

However, phenomena such as pseudoprogression and pseudoresponse which could take place during GB follow-up can lead to misinterpretation of MRI features [143]. Thus, a single MRI exploration may not provide confident information about therapy response in GB patients and an additional exploration may be needed, causing a delay of several weeks in proper prognosis. Magnetic resonance spectroscopy (MRS) is an application of MR that permits the non-invasive quantification of different metabolites in living tissue, informing about its biochemical environment and complementing the anatomical information obtained by conventional MRI. With the development of improved techniques for spatial localization and water suppression, research in the MR field has promoted the production of more advanced technology -- magnetic resonance spectroscopic imaging (MRSI). Unlike MRS which reveals metabolic information only from a single region of interest (single voxel), MRSI can superimpose multi-voxel metabolic information on the corresponding MRI to study the spatial

distribution of some metabolites along brain anatomy. This section will emphasize the key aspects related to MR techniques which could be essential for the proper understanding of the results obtained in this thesis, while a detailed description of the physics behind the NMR phenomenon goes beyond this thesis scope and can be found in various sources such as [144].

1.3.1 Magnetic Resonance Imaging (MRI)

MRI was commonly used in diagnostic imaging for general clinical evaluation, with a particular relevance in brain disease detection and diagnosis. In brief, MR Images are obtained by positioning the patient within a large magnet, which generates a powerful external magnetic field. This leads the magnetic moment of the nuclei of many atoms in the body, including hydrogen proton, to align them with the magnetic field. Subsequent application of suitable radio frequency (RF), excite these nuclei, which may further return to equilibrium releasing energy (a process known as relaxation). The transient perturbation from equilibrium of the system is detected and used to provide anatomical imaging. Protons in different chemical environments (e.g. water, fat, metabolites, gray matter, skull, ventricles) will behave in different ways and will give rise to signals with different features (absorption frequency, relative intensity). Proton density (mostly water in classical MRI), longitudinal relaxation (T1) and transverse relaxation (T2) of protons are important factors determining signal intensity, and image contrast depends on the difference of signal intensity between two adjacent tissues or areas. The adjustment of different acquisition parameters such as repetition time (TR) or echo time (TE) can “weigh” images and reinforce differences in T1, T2 or proton density (Figure 1.12) which informs about the characteristic of protons present in tissues. The intrinsic MRI contrast can be also enhanced by administration of exogenous contrast agents (CA) which improve the specificity and sensitivity of MRI. Currently, the most commonly used CA for diagnosis and monitoring diseases are gadolinium-based "positive" CA and superparamagnetic iron oxide nanoparticle (SPION)-based "negative" CA[145]. Most of clinical CA have been shown to not adequately permeate through the BBB, but they can reach brain lesions (ex. GB) if this barrier is disrupted (figure 1.2). Thus, in vivo administration of CA may provide information about the integrity of BBB, as a valuable diagnostic strategy. T2 weighted images are most commonly used when searching for inflammatory changes and tumours, while T1 weighted images are more common for inspection of contrast enhancement in brain tumours.

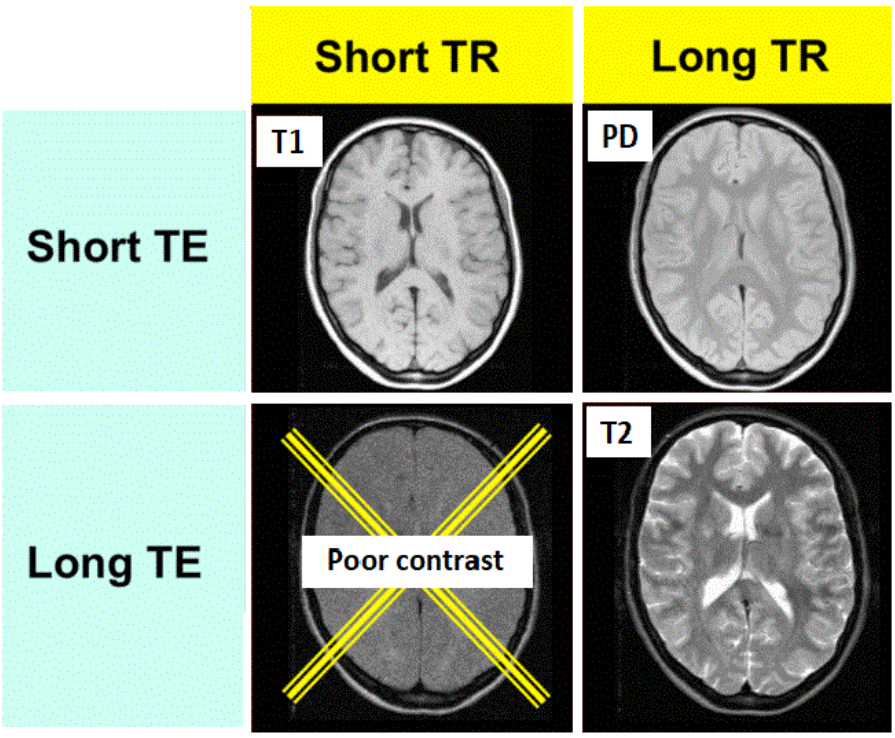

Figure 1.12 Tissue contrast dependence on TR, TE.

Axialimage from human brain. A short TR and short TE will result in a T1 weighted image (T1 label in the upper left box), fluids are dark, water-rich tissues are mid-grey and water-poor (high myeline/fat-tissues) are bright.

A long TR and long TE will result in a T2 weighted image, fluids have the highest intensity (bright), and water- and fat-based tissues are mid-grey.

A long TR and short TE will result in a PD weighted image, the signal of water is in the mid gray scale and myelin/fat appears bright. Figure extracted from http://mriquestions.com/

1.3.2 Magnetic Resonance Spectroscopy (MRS)

MRS is a technique that allows to measure the content of metabolites in a sample or tissue non-invasively. It has been widely used for the study and characterisation of brain tumours since it can detect metabolite patterns which are characteristic of different type and states of a tumour [146]. Compared with other nuclei such as ^{13}C-MRS and ^{31}P-MRS, ^{1}H-MRS based on recording signals from the hydrogen nucleus (proton), has become the most widely adopted quantitative method for non-invasive detection of metabolites in vivo. ^{1}H-MRS can detect a wide variety of pharmacologically important low molecular weight metabolites in the millimolar range. Still, before observing metabolites, it is important to suppress the large signal arising from the water protons, which is three to five orders of magnitude larger than the signal of the detectable metabolites in brain/tumour. MRS data are presented as spectra

(Figure 1.13) rather than images. The x-axis refers to the frequency shift which locates the metabolite in chemical shift (parts per million (ppm)), and the area below each peak reflecting the relative concentration of nuclei detected for a given chemical species. The chemical shift is characteristic of each metabolite and it is related with its chemical environment. Still, in order to be seen protons may have enough mobility, otherwise their extremely short relaxation times will prevent their observation. Appearance of signals can vary with application of different acquisition parameters such as TE. A basic explanation of these variations and its meaning can be found in [147].

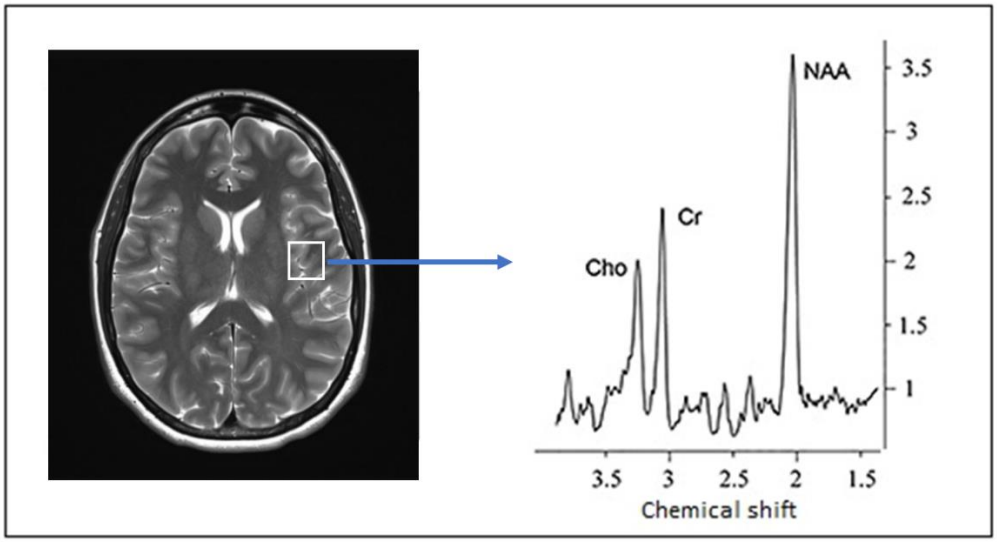

Figure 1.13 Example of a T2w MRI and a single voxel spectrum of human brain. *Left, axial T2w MRI of normal human brain acquired at 3 T. Right, long echo time (TE= 136 ms) single voxel (white square) spectrum acquired from the left precentral gyrus, X-axis correspond to the metabolites shift frequency (ppm adimensional units) and Y-axis to amplitude. Major labelled resonances from several functional groups of major metabolites are indicated: Cho, choline (3.21 ppm); Cr, total creatine (3.03 ppm); NAA, N-acetyl aspartate (2.01 ppm). Figure adapted from* [148]. *See* [149]*for resonance chemical shifts of major tissue metabolites detectable from tissue MRS.*

Even when the metabolites cannot be separated spectrally, differences in spectral patterns can be used to distinguish between different tissue types, tumour classes, or the same tumour under different conditions (e.g. before or after therapy) (see section 1.3.4).

Metabolites: localization and importance

With current ^{1}H-MRS systems used in clinics and research, the presence of certain metabolites in brain tissue can be detected in vivo as resolved resonances when the minimum concentrations range between 0.5 and 1.0 mM. Some of these metabolites have high clinical importance, such as:

N-Acetyl Aspartate (NAA) – its main signal appears at 2.01 ppm. NAA is a neuronal marker that is present in neurons and axons, indicating their density and viability. Its production takes place in the brain tissue mitochondria. Due to these factors, the NAA peak in ^{1}H-MRS will be decreased whenever neuron loss occurs, such as in GB.

Creatine (Cr) – its main signal can be seen at 3.03 ppm, although a 3.93 ppm signal is also present. Cr is a marker of the brain cells' energy, being considered as mostly constant and used as reference value to evaluate relative changes of other metabolites. Occasionally, a decrease in the Cr peak takes place, particularly in metastases or other brain tumours.

Choline (Cho) – usually detected as a strong signal at 3.21 ppm, although its different components overlap at clinical magnetic fields (glycerophosphocoline, phosphocoline and free choline, known as choline-containing compounds). Choline-containing compounds are intermediary molecules of the cell membrane phospholipid metabolism and can be associated to the turnover of those membranes. Thus, increased Cho, when originated by phosphocholine, suggests greater synthesis of the cell membrane and proliferation of cells. So, its concentration is usually increased in cases of fast proliferation in a brain tumour.

Lactate (Lac) – signals are observed at 1.33 and 4.10 ppm. In normal human brain tissue Lac is usually below detection. Its presence usually suggests a pathological condition with increased anaerobic metabolism of glucose. In cysts, hypoxic / ischaemic tissues, and some brain tumours, lactate can be detected. The main signal at 1.33 ppm can also be contributed by MR visible mobile lipids.

Mobile Lipids (MLs) – major signals observed at 0.9 and 1.3 ppm. Normally, MLs are not observed by ^{1}H-MRS in brain tissue. However, in pathological circumstances involving necrosis, for example in malignant brain tumours and inflammatory / infectious processes, increased ML peaks are observed, although its overlap with lactate signal at 1.33 ppm may complicate interpretation in *in vivo* spectra unless different echo time acquisitions are inspected.

Myoinositol – this metabolite has several signals in MRS brain spectra but the main signal is observed at 3.55-3.56 ppm, overlapping with glycine at clinical magnetic fields. Myoinositol is a glial function marker and an essential osmotic agent regulator for cell volume. It typically reduces its content in hepatic encephalopathy and increases in Alzheimer's disease.

Other metabolites that can be investigated with ^{1}H-MRS include the following: glutamine plus glutamate (Glx 2.10-2.40 and 3.8 ppm) and glycine (partially overlapping with myoinositol at 3.55 ppm), alanine (Ala, 1.5 ppm). For a detailed description of the brain MRS pattern, please refer to the review by Evanthia Kousi and col [150]. In the frame of tumour therapy response in preclinical GB, one of the main focus of this PhD thesis, a metabolite appears at 2.8 ppm – Polyunsaturated Fatty Acids (PUFAs) shows a small but consistent difference between treated and non-treated tumour [151], in line with findings described by other authors while assessing response to treatment in preclinical models [152]. Changes in this metabolite, in addition to main changes observed between control and treated, responding GL261 GB tumours, can be appreciated in Figure 1.14 [151].

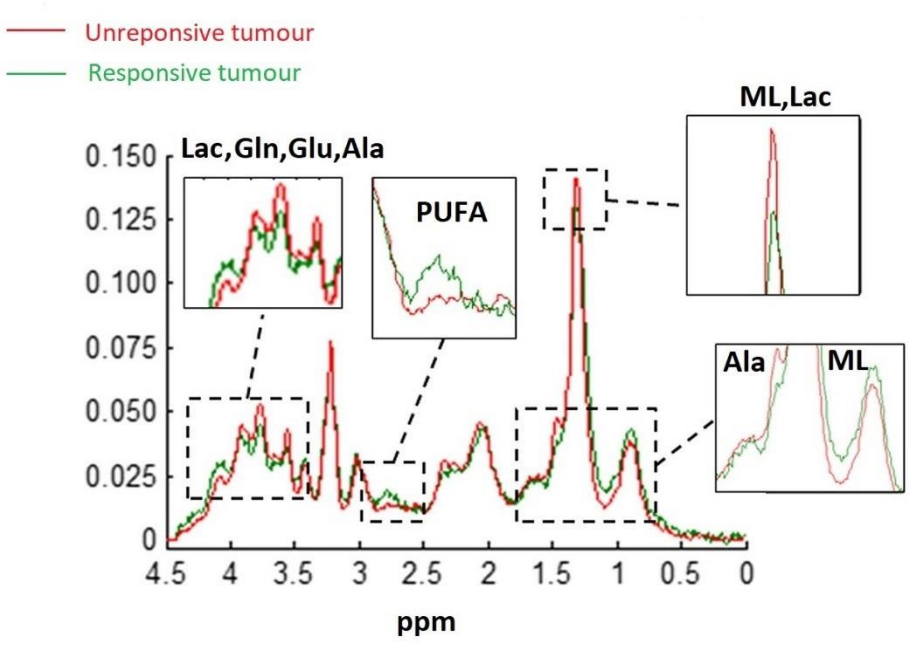

Figure 1.14 Main differences of spectral patterns of "sources" (see section 1.3.5) between responsive and unresponsive GL261 tumour. *Tumour responding to TMZ showed higher total ML (0.9 ppm), PUFA (2.8 PPM), and Lac (4.1 ppm), combined with lower Gln/Glu/ Ala (ca. 3.8 ppm) and fatty acid MLs/Lac (1.3 ppm). Figure adapted from* [151].

1.3.3 Magnetic Resonance Spectroscopic Imaging (MRSI)

MRSI is an extension of the MRS technique, which is widely used in both clinical and preclinical research for non-invasive investigation of normal or pathological tissue metabolism. MRSI combines metabolomics and anatomical information, superimposing a grid of MR spectra to different anatomical locations to obtain a spatial distribution of metabolites. Besides, metabolic changes can precede structural changes observed in MR images. Then, MRSI provides a feasible way of gathering more complete information than with MRI alone (Figure 1.15). MRSI was accredited and approved by the United States FDA as a clinical research tool in 1995 [153] and it is constantly gaining relevance in human GB therapy/relapse follow-up [154].

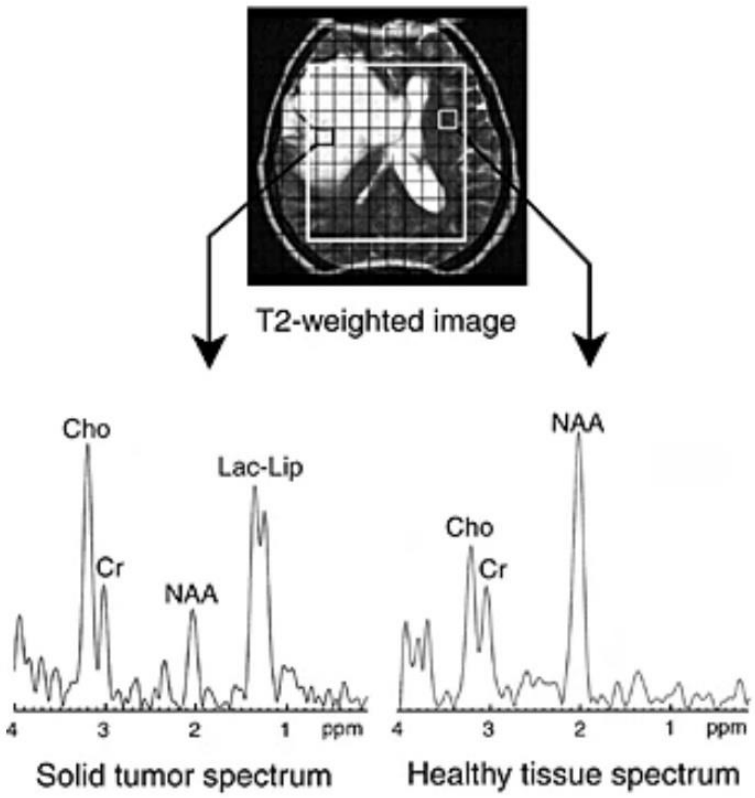

Figure 1.15 MRSI information from a human glioblastoma. *Upper part: T2-weighted MRI image of a glioblastoma with a necrotic region. The grid superimposed on the MRI image shows the voxels of MRSI. Signal was obtained only in the volume of interest (white square) selected for MRSI analysis. Lower part: ^{1}H MR spectra from different voxels located within the solid tumour and within the healthy tissue showing label of main metabolites. Figure adapted from* [155].

After suitable processing, MRSI information can be convert into an “image-like” output. In this respect, several studies generated single metabolite maps using MRSI data (e.g. Cho map, NAA map, Cre map) [155][156]. However, the rich information contained in the whole spectral pattern would be omitted and some specific distinctions such as tumours before and after treatment may be not straightforward to perform if only few metabolites are analysed, since in this case several metabolites can be changing simultaneously in minor percentages. In this case, the optimal way to gain information from these MRSI data is by using pattern recognition techniques, which take the whole spectral pattern changes into account and are currently recognized to be useful both in clinical and preclinical studies [151], [157], [158].

1.3.4 Pattern Recognition (PR) techniques

Pattern recognition (PR) is a concept that encompasses a wide variety of techniques that search for patterns in data groups in order to distinguish between different subgroups. Once these patterns have been identified, unknown individuals can be further assigned to a certain subgroup classification. The changes in MRSI data can determine specific biochemical information related to pathological or biological processes. In therapy response assessment, subtle changes in several metabolites can take place, which may be difficult to spot even for an expert observer. Combining MRSI techniques with robust PR algorithms makes it possible to identify the relationship between quantitative changes of different metabolites happening at the same time and to detect even minor variations in metabolic profiles. Based on the mathematical models used for classification, there are three major classification strategies used in PR: supervised, unsupervised and semi-supervised classification, summarized below.

The supervised PR methods use a defined *training* group of cases in order to develop a mathematical model. In case of brain tumours, spectra can be assigned to a certain class according to the post-surgical resection histopathological analysis criteria. After the classifier has been trained, it can be applied to a totally independent *test set* to check for robustness. On the contrary, in the unsupervised classification, the classes are unknown a priori and need to be discovered from the data based on their similarities. Non-negative matrix factorization (NMF) [156] is a popular unsupervised technique, which can provide an advantage as each class is represented by a complete “paradigmatic spectroscopic pattern”, also known as “source”. Biochemically, the source extraction technique for classifying the MRSI data assumes that a mixture of the heterogeneous tissue pattern is present in each voxel and that

the contribution of individual sources to the final pattern can be calculated. Finally, semi-supervised methods [151], [156] are based on a successful combination of supervised and unsupervised PR methods, using both labelled and unlabelled data for training and benefits from the prior knowledge regarding class membership to guide the source extraction. In this PhD thesis, the semi-supervised classifiers previously developed in our group were applied to new data with no new source extraction or retraining.

1.3.5 Nosological imaging: segmentation and classification using MRI and MRSI

Being one of our goals to increase the translational potential of our preclinical approaches, we should be able to transform the complex information coming from MRSI and PR analysis into visual representations that can be more friendly for straightforward interpretation by radiologists. One way to achieve this objective is through nosological imaging generation. More than a “spectroscopic imaging”, the nosological imaging is a colour-coded representation of some condition (diagnostic, pathologic…). In our case, the nosological imaging will reflect whether a tissue is responding or not to a given therapeutic strategy, by means of PR analysis of previous cases and development of a classification method.

The nosological imaging in our case is generated estimating the contribution of each source (“paradigmadic spectra”) to the individual voxels in the MRSI grid. Accordingly, once the main contribution is established, we assign each acquired voxel to one of the predetermined classes, namely normal brain tissue, treated/responding or untreated/unresponsive tumour. The quantitatively most relevant paradigmatic spectrum of the voxel is selected as the "winning source" and the voxel is correspondingly coloured, finally represented as nosological maps for each matrix. These nosological images can provide a visual description of MRSI results and be used as an imaging biomarker to determine therapeutic responses. For example normal brain parenchyma may be coloured blue, actively proliferating tumour red, and therapy responding tumour green, depending on the spectral pattern (source) that mostly contributes to the spectrum of a given voxel (figure 1.16).

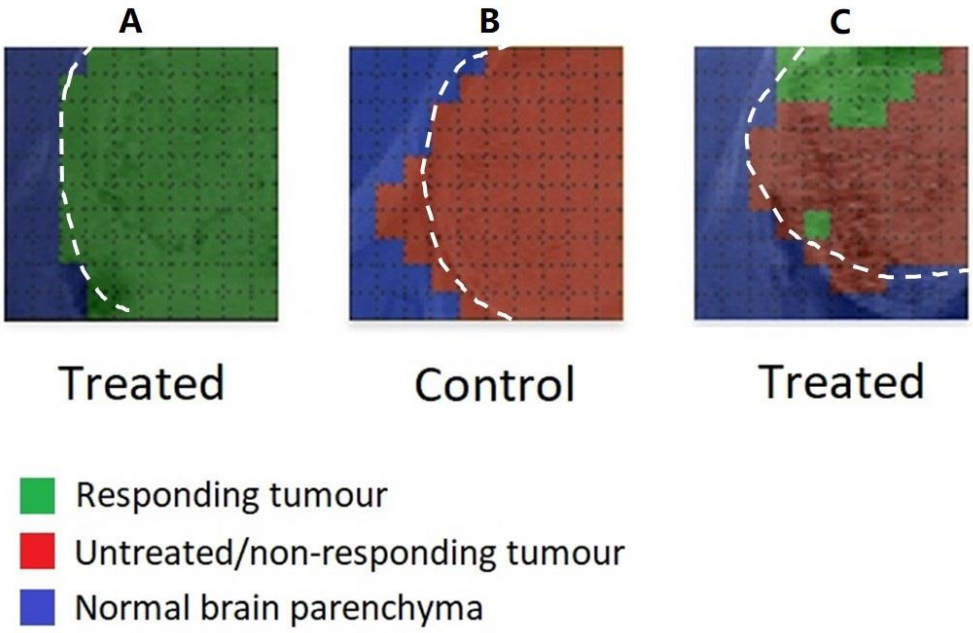

Figure 1.16 Examples of nosological images obtained with the semi-supervised PR method in control and TMZ-treated GL261 GB tumour-bearing mice. *Figure adapted from* [151] *A) homogeneous treated case C586 mostly identified as responding, B) control case C583, mostly identified as non-responding/control, and C) treated case C418 with partial response.*

Within the GABRMN group, this semi-supervised PR method has been used to test the therapy response, primarily with TMZ treated GL261 GB [151] [158], then it also proved effective for the evaluation of CPA therapy [159], which suggested the promising potential of this classification therapy response biomarker strategy. These PR methods and nosological images were therefore used for the follow-up of GL261 tumour-bearing treated mice analysed with MRSI during this thesis.

2 GENERAL OBJECTIVES

The main objectives of this PhD thesis were:

1. To investigate the potential of anti-PD1 immunotherapy, alone or in TMZ combination, for preclinical GL261 GB treatment, with emphasis in IMS protocols.
2. To apply MRSI-based semi-supervised pattern recognition techniques for non-invasive therapy response follow-up in GL261 tumour-bearing mice treated with IMS-TMZ or anti-PD-1, either alone or in combination.
3. To check whether the oscillatory behaviour of the MRSI-based surrogate biomarker of therapy response studied with standard IMS-TMZ protocols would be also observed with immunotherapy.
4. To investigate the role of MGMT or PD-L1 for TMZ chemoresistance in GL261 GB.

3 GENERAL MATERIALS AND METHODS

3.1 GL261 MURINE GLIOMA CELLS

The mouse glioma cell line GL261 was obtained from the Tumour Bank Repository at the National Cancer Institute (Frederick/MD, USA). This cells batch have been tested for absence of pathogens and for being bona fide GL261 cells, without spurious contamination from other cell lines. These cells used in our group for a long time in several studies [151] – [157] because of its reproducibility and reliability when implanted into C57BL/6j mice to generate glioblastomas.

3.1.1 Cell culture

GL261 cells were grown in 75cm^2 cell-culture flasks with RPMI-1640 culture medium (Sigma-Aldrich, Madrid, Spain) supplemented with 10% fetal bovine serum (FBS) (Gibco, Invitrogen, UK), 0.285 g/L glutamine, 1% penicillin-streptomycin and 2.0 g/L of sodium bicarbonate (all from Sigma-Aldrich, Madrid, Spain). Cells were incubated at 37℃ in a 5% CO_2 and 95% humidity (incubator HERAcell, 150i, Thermo Scientific). When cells covered 75%-85% of the flask surface reaching confluence, cells were sub-cultured. The previous culture medium in the flask was removed by aspiration with a vacuum pump and the attached cells were washed with 10 ml of sterile phosphate buffered saline (PBS), then removing PBS by aspiration. This step was performed to ensure completely remove the medium since any remaining FBS would inactivate trypsin. Next, 2 ml of trypsin-ethylenediaminetetraacetic acid (EDTA) (0.5 g/L and 0.2 g/L, respectively) (Sigma-Aldrich, Madrid, Spain) was added to detach cells from the flask. After a 3 min incubation, cells were resuspended in 8 ml of RPMI medium and centrifuged, the cell pellet was collected and resuspended in 10 ml fresh medium for cell counting (see 3.1.2). Finally, the appropriate number of cells were seeded in a new culture flask containing 25 ml RPMI medium. The culture medium was changed on the day 3 and 5 during the new process of growth. Cells were discarded after 25 passages in order to avoid possible undesired mutations and ensure consistent tumour development and behaviour; in this case, a new aliquot was thawed and process restarted.

LN18 cells were provided directly from Victor Yuste's group and were cultured by them as described in [165].

3.1.2 Cell count

The cells were counted using the TC10^{TM} automatic cell counter (Biorad, Hercules, California) using Trypan Blue dye (Sigma-Aldrich, Madrid, Spain). Trypan blue is a stain used to distinguish living cells from dead cells, since dead cells do not have the required energy-dependent mechanisms in order to extrude Trypan blue, which remains inside the cells, being also detected by the counter. Aliquots of 10 µl of the cell suspension obtained in the sub-culturing step (see 3.1.1) were added to 10 µl of Trypan Blue dye. Then, 10 µl of the resulting mixture was added into the cell counting slide (Biorad, Hercules, California), two replicates for each sample. Finally, the counting slide was insert into the cell counter and the average number of cells/ml was quantitated.

3.2 GL261 MURINE GLIOMA MODEL

3.2.1 C57BL/6J mice

All animals used in this work were 14-18 weeks old C57BL/6 female mice (20-24 g), which were obtained from Charles River Laboratories (Charles River Laboratories International, l'Abresle, France) and housed in the animal facility (Servei d'Estabulari, https://estabulari.uab.cat/) of the *Universitat Autònoma de Barcelona*.

All animal studies were conducted according to the protocol approved by the local ethics committee (*Comissió d'Ètica en l'Experimentació Animal i Humana*, https://www.uab.cat/etica-recerca/) according to regional and state legislations (protocol CEEAH-3665). The laboratory animal supervision protocol mentioned in **Annex I** was performed by the veterinary staff of the animal facility to evaluate the physical condition of mice and notify the researcher whether euthanasia was recommended and halting of the experimental protocol should be considered for humanitary reasons.

In this thesis, each studied mouse was given a unique alphanumerical identifier. Identifiers of the type CXXXX belong to mice bearing GL261 tumours while WTXXXX belong to wild type (wt) mice without tumours. Besides, unique ear notch combinations were made with an ear punch device for differentiating animals in the same cage. As shown in Figure 3.1, single or combination of ear notches (1, 2 or 3) were made in one or both ears.

Figure 3.1 Scheme for unique identification in mice by ear punching.

3.2.2 Generation of tumours by stereotactic injection of cells

For GL261 murine GB generation, analgesia (Metacam, Boehringer Ingelheim) at 1 mg/kg was injected subcutaneously to each animal 15 minutes before anaesthesia, and also 24 and 48 hours after tumour implantation. Mice were anesthetized with a mixture of ketamine (Parke-Davis SL, Madrid) at 80 mg/kg and xylazine (Carlier, Barcelona, Spain) at 10 mg/kg, administered intraperitoneally. Once anesthetized, the mouse was immobilized on the stereotaxic holder (Kopf Instruments, Tujunga / CA, USA) in a prone position. Next, the head area was shaved, and the incision site was sterilised with iodophor disinfectant solution, a 1 cm incision was made exposing the skull and a 1 mm hole was drilled 0.1 mm posterior to the Bregma and 2.32 mm to the right of the midline using a microdrill (Fine Science Tools, Heidelberg, Germany). A 26G Hamilton syringe (Reno/NV, USA), positioned on a digital push-pull microinjector (Harvard Apparatus, Holliston/MA, USA) was them used for injection of 4 µl of RPMI cell culture medium containing 100,000 GL261 cells (obtained and counted as in section 3.1) at a depth of 3.35 mm from the surface of the skull at a rate of 2 µl/min.

Once the injection was completed, the Hamilton syringe was left untouched for 2 minutes more before its removal to prevent the cells liquid leaking out of the skull. Finally, the Hamilton syringe was gently and slowly taken out and the scission site were closed with suture silk 6.0 (Braun, Barcelona, Spain).

When the implantation was finished, mice were left in a warm environment to recover from anaesthesia. Authors in [166] reported that when C57BL/6 immunocompetent mice were exposed to an “enriched environment” (EE) for 3 weeks before tumour implantation could

significantly reduce glioma growth and improve mice survival by increasing immunological parameters in the brain of mice. Thus, different from previous work, all mice in this thesis were allowed to endure 3 weeks of guarantee housing in “enriched environment (EE)”-like caging before tumour generation, and were maintained there from beginning to end (Figure 3.2).

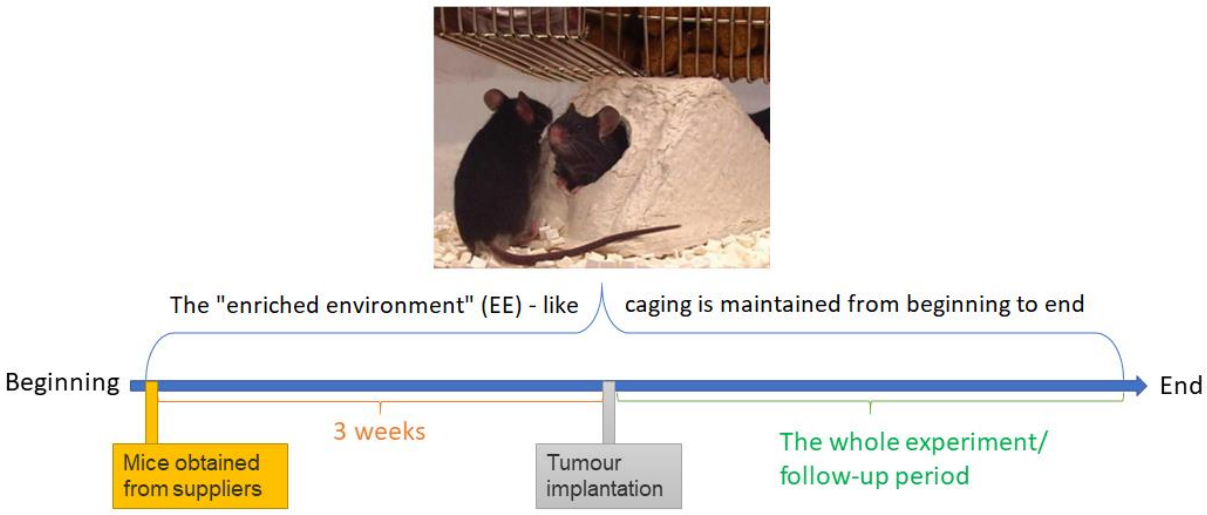

Figure 3.2 Scheme for “enriched environment”-like caging strategy.

Mice were allowed to endure 3 weeks of guarantee housing in “enriched environment (EE)”-like caging before tumour generation, and EE were also maintained during the whole experiment and follow-up period. The ‘Shepherd Shack’ is cage insert composed of autoclavable paper, mice can shred it and use the paper for nest building.

3.3 TISSUE PRESERVATION PROCEDURES

When animals died or were euthanized by cervical dislocation to prevent suffering (refer to **Annex 1** for the animal euthanasia criteria), the brain/tumour was excised and either frozen in liquid nitrogen or formalin fixed, depending on the purpose. In case of freezing, tumours were dissected from normal brain parenchyma, collected, and frozen in a liquid nitrogen container for further MGMT and PD-L1 expression analysis. In case of fixation, tissue was preserved in 4% formalin for further autopsy or histopathological analysis. Tissues were resected after visual inspection of the whole brain and tumour, avoiding as much as possible the crossed contamination of tumour with non-tumoral tissue.

3.4 IN VIVO MRI/MRSI

All MR studies in this thesis were carried out at the joint NMR facility of the *Universitat Autònoma de Barcelona* and CIBER-BBN (https://www.ciber-bbn.es, Cerdanyola del Vallès, Spain) Unit 25 of the ICTS NANOBIOSIS (https://www.nanbiosis.es) with a 7T horizontal magnet (BioSpec 70/30, Bruker BioSpin, Ettlingen, Germany) equipped with actively shielded gradients (B-GA12 gradient coil inserted into a B-GA20 gradient system) and a quadrature receive surface coil, actively decoupled from a volume resonator with 72 mm inner diameter.

Mice were anesthetized by inhalation of 0.5 -2.0% isoflurane in O_2 and placed on the scanner bed prior to the MR study, keeping the respiratory frequency at 60 – 80 breaths/min. Mice body temperature was controlled using a recirculating water system incorporated to the scanner bed and kept at ~ 37 ℃. Animal breathing was monitored constantly with a breathing sensor (SA Instruments, Inc., New York, USA).

3.4.1 High resolution MRI for tumour volume measurement

GL261 tumour-bearing mice were screened using the Rapid Acquisition with Relaxation Enhancement (RARE) sequence to acquire HR axial T2w images (TR / TEeff = 4200/36 ms) to detect brain tumour presence and track its evolution process. The acquisition parameters were as follows: turbo factor: 8, field of view (FOV): 19.2 x 19.2 mm, matrix size (MTX): 256 x 256 (75 x 75 µm/pixel), number of slices: 10, slice thickness (ST): 0.5 mm, inter slice thickness (IT): 0.6 mm, number of averages (NA): 4, total acquisition time (TAT): 6 min and 43 s. The acquired MRI data were processed on a Linux computer using software ParaVision 5.1 (Bruker BioSpin GmbH, Ettlingen, Germany).

To calculate the tumour volume from MRI acquisitions, an automated system for generating ROIs in the ParaVision software was used to measure the tumour area in each slice (Figure 3.3)

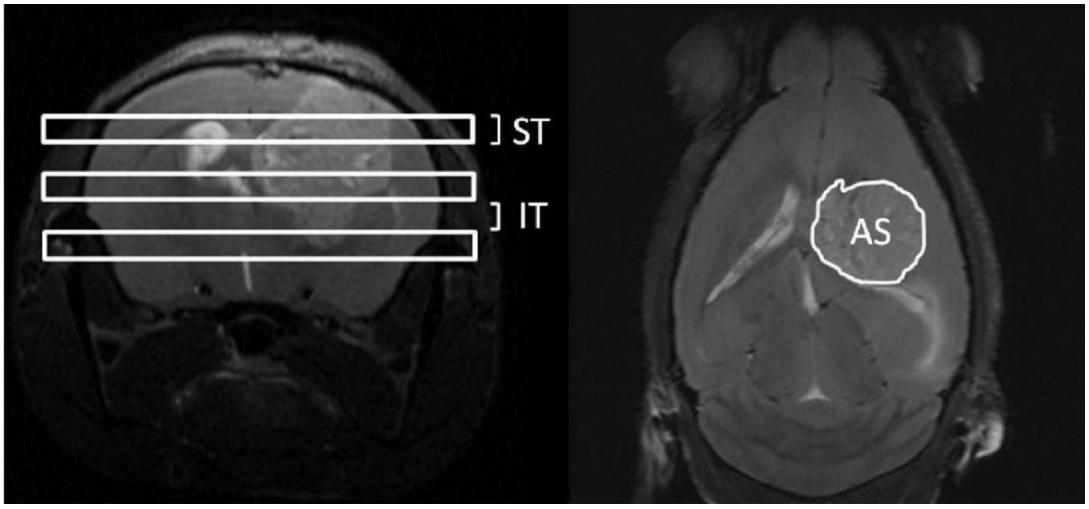

Figure 3.3 MRI measurement for tumour volume assessment. *HR axial T_2w images (right) were acquired for this purpose. The surface area (AS) of the tumour (white line contour at right) was measured in each slice of the axial T_2w images. The slice thickness (ST) and the inter-slice thickness (IT) (represented by horizontal slices over a coronal image on the left) were taken into account for final volume calculation. Figure adapted from* [114].

As shown above, the tumour volume of the studied mice was calculated from HR axial T2w images using the following equation:

$$TV\ (mm^3) = [(AS_1 \times ST) + [(AS_2 + (\ldots) + AS_{10}) \times (ST + IT)]] \times 0.075^2 \quad \text{(Equation 1)}$$

Where TV is the tumour volume, AS is the number of pixels contained in the region of interest delimited by the tumour boundaries in each slice of the MRI sequence, ST is the slice thickness (0.5 mm), IT the inter-slice thickness (0.1 mm) and 0.0752 the individual pixel surface area in mm^2.

3.4.2 MRSI data acquisition, processing and post-processing

The MRSI acquisitions were performed using a multi-slice, 3D-like acquisition protocol developed in our group [158] to obtain metabolic information across the entire volume of the tumour. Consecutive 14 ms echo time (TE) MRSI with point-resolved spectroscopy (PRESS) grids were acquired individually in the tumour, using HR T2w images as a reference. First upper (dorsal) grid (Grid 1) had a matrix size of 10 × 10. Then, Grid 2 was acquired 1 mm below Grid 1 with a matrix size of 12 × 12. Grid 3 was acquired 1 mm below Grid 2, also with a matrix size of 12 × 12. Finally, if the volume of the tumour was not fully covered by 3 grids, a final Grid 4 was acquired 1 mm below Grid 3 with a matrix size of 10 × 10. For each MRSI grid shimming was performed individually to ensure the quality of the acquired data. Spatial MRSI

grids were located such that the volume of interest (VOI) covered most of the tumour mass as well as normal / peritumoural brain parenchyma.

Acquisition parameters were: FOV, 17.6 mm × 17.6 mm; VOI in Grids 1 and 4 was 5.5 mm × 5.5 mm × 1.0 mm. VOI in Grids 2 and 3 was 6.6 mm × 6.6 mm × 1.0 mm. ST, 1 mm; TR, 2500 ms; Sweep Width (SW), 4006.41 Hz; NA, 512; TAT, 21 min 30 s. Water suppression was performed with Variable Power and Optimized Relaxation Delay (VAPOR), using a 300 Hz bandwidth. Linear and second order shims were automatically adjusted with Fast Automatic Shimming Technique by Mapping Along Projections (FASTMAP) in a 5.8 mm × 5.8 mm × 5.8 mm volume which contained the VOI region. Six saturation slices (ST, 10 mm; sech-shaped pulses: 1.0 ms/20250 Hz) were positioned around the VOI to minimize outer volume contamination in the signals obtained.

MRSI data were essentially post-processed as explained in [162]. Briefly, data were initially pre-processed at the MR workstation with ParaVision 5.1, and then post-processed with 3D Interactive Chemical Shift Imaging (3DiCSI) software package version 1.9.17 (Courtesy of Truman Brown, Ph.D., Columbia University, New York, NY, USA) for line broadening adjustment (Lorentzian filter, 4 Hz), zero-order phase correction and exporting the data in ASCII format. Dynamic MRSI processing module (DMPM[1]) running over MatLab 2013a (MathWorks Inc., Natick, MA, USA) was used to align all spectra within each MRSI matrix (using the choline peak as a reference, 3.21 ppm). The area between 0 – 4.5 ppm of each spectrum in the MRSI matrix was standardized individually to unit length and the normalized matrix were exported in ASCII format to perform the PR analysis. In those spectra, no baseline correction was performed.

The ASCII file resulting from the previous process was then further analysed with pattern recognition approaches. Namely, non-negative matrix factorization (NMF) semi-supervised methodology was applied for the extraction of meaningful source signals from the MRSI investigated tumours. The source extraction technique for classifying MRSI data, from a biochemical point of view, assumes that in each voxel there is a mixture of heterogeneous tissues and their metabolites from which the contribution of each source can be obtained. A previously described semi-supervised method [151] based on Convex-NMF for final source

[1] http://gabrmn.uab.es/dmpm

extraction was used to classify pixels into the normal brain parenchyma, actively proliferating tumours (i.e. non responding) and tumours responding to treatment, being further used to compute nosological maps that reflect the spatial response to treatment. The final image was colour-coded according to the source most contributing to each pixel/voxel. Green colour was shown when the GB response to the treatment source contributes the most, blue for normal brain parenchyma, red for aggressively proliferate GB and black to undetermined tissue.

Tumour Responding Index (TRI) calculations

In order to measure the extent of response to treatment using the obtained nosological images, a numerical parameter named TRI was calculated (Equation 2) [158].

$$TRI = (\text{Tumour responding pixels}) / (\text{Total tumour pixels}) \times 100 \qquad \text{(Equation 2)}$$

TRI is stated as the percentage of green (responding) tumour pixels of all grids over the total tumour pixels of all recorded grids. Then, tentative ranges of TRI categories were established to classify the different response to treatment levels observed in the studied animals, taking into account both TRI percentage and volumetric data from MRI measurements according to RECIST criteria [167] which was further adapted for preclinical assessment (Figure 3.4 and text below).

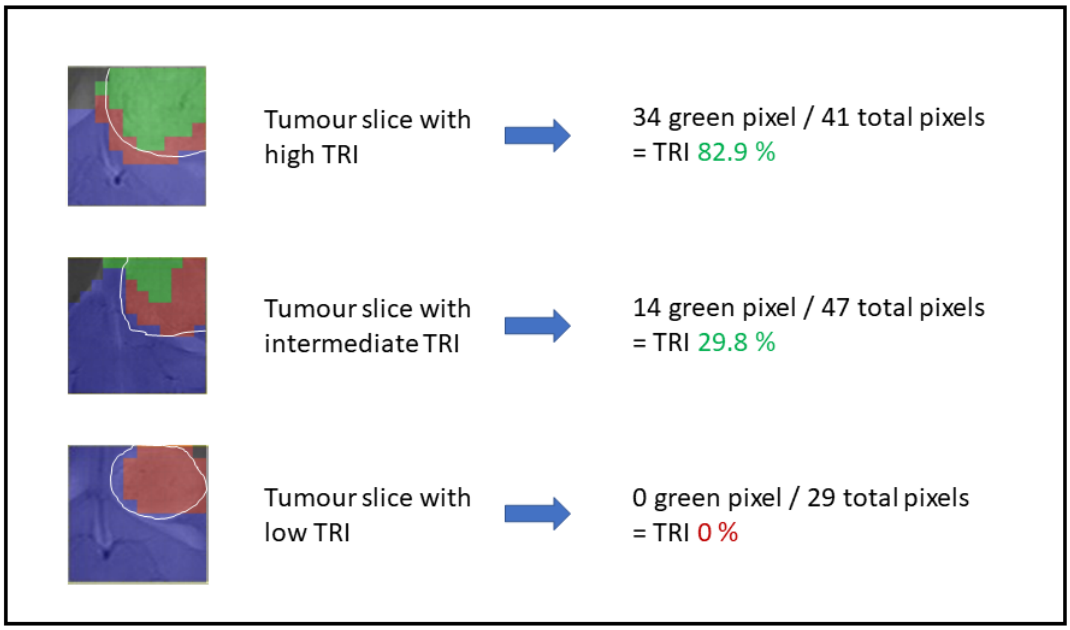

Figure 3.4 Demonstrating examples of tumour slice with high, intermediate and low TRI.

TRI was studied longitudinally along mice treatment to check whether TRI 'cycles' were present, as described in [158]. In this thesis, one TRI cycle means days from therapy administration to next TRI peak maxima, and a TRI peak was defined provided a change between maximum and minimum TRI values was above 10% (Figure 3.5). Values below this threshold were attributed to possible experimental variability and were not used to define "cycles".

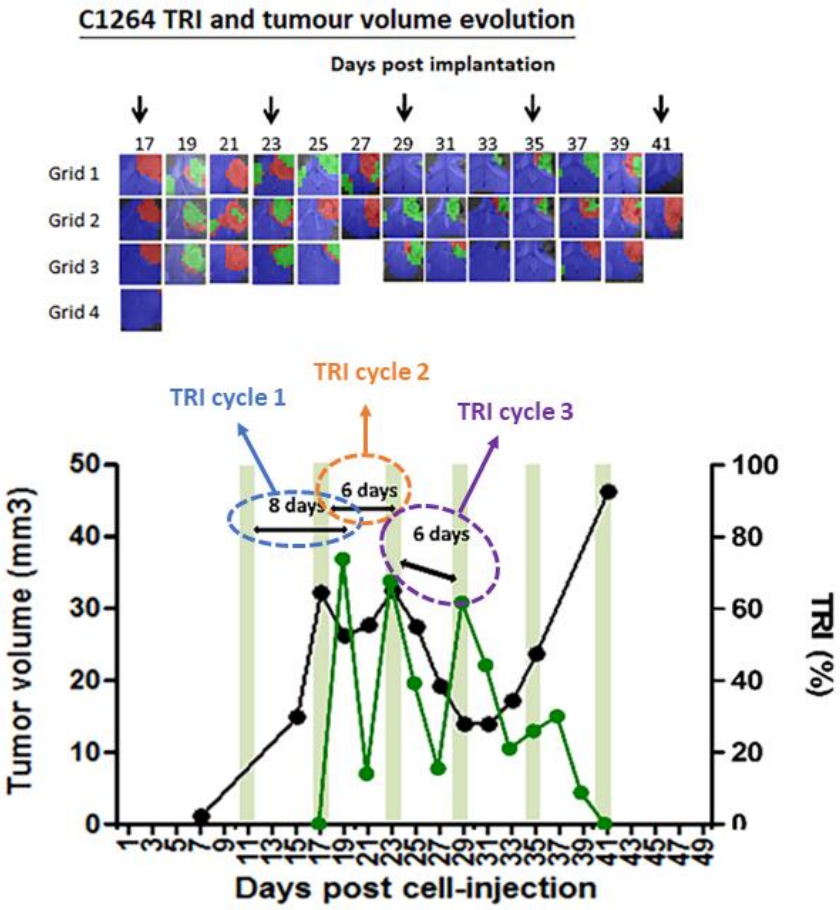

Figure 3.5 Demonstrating examples of TRI cycles. *Nosological images and graphical representation of the tumour volume evolution for the tumour region in the case C1264. Tumour volume in mm^3 (black line, left axis) and the percentage of green, responding pixels (TRI) obtained taking into account total tumour pixels counting (green line, right axis). In the upper part of every image, chosen time points show the evolution of the nosological images in four rows of colour-coded grids superimposed to the T2w-MRI for each slice. Vertical arrows indicate days of therapy administration. In the bottom graphs, green shaded columns indicate TMZ administration days. TRI cycle duration (therapy administration to next peak maxima) is highlighted in every image. TRI peaks appear after TMZ administration time points*

(day 11, day 17, and day 23 p.i.) with a period of 8 days (TRI cycle 1, indicated in blue), 6 days (TRI cycle 2, indicated in orange) and 6 days (TRI cycle 3, indicated in purple), respectively.

An adapted set of RECIST criteria was used to classify cases into Progressive disease (PD), Partial response (PRe) or Stable disease (SDi), namely:

Classification using adapted RECIST criteria: Progressive disease (PD): 20% increase with respect to the smallest tumour volume so far. Partial response (PRe): tumour decrease by 30%, taking into account the biggest volume so far. Stable disease (SDi): less than 20% increase and no more than 30% decrease in tumour volume.

3.5 STATISTICAL ANALYSES

Variance homogeneity was assessed with the Levene's test. Sample distribution was assessed with the Kolmogorov-Smirnov test. A two-tailed Student's t-test for independent measurements was used for comparisons, for samples of equal or different variances (depending on the Levene's test result). The global evolution of tumour growth curves or body weight measurements was evaluated with the UNIANOVA test. Comparisons of survival rates were performed with the Log-Rank test. The significance level for all tests was $p<0.05$.

4 RESULTS

4.1 ANTI-PD-1 OR TMZ METRONOMIC TREATMENT: A RAT RACE BETWEEN TUMOURS AND THE IMMUNE SYSTEM

4.1.1 Context and specific objectives

The immune system plays an important role in controlling and eradicating cancer. Both chemotherapy dose and schedule are critically important determinants to ensure proper action of the immune system during cancer treatment. It was described that chemotherapy (cyclophosphamide) administration with every 6 days consecutive cycles triggered immune system activation and immune memory in a subcutaneous GB model [38] and we coined the expression “Immune-Enhancing Metronomic Schedule” (IMS) for this immune-friendly “every 6 days” administration protocol in our system. Our group has tested the IMS-chemotherapeutic treatment in GL261 tumour bearing mice with TMZ (140, 200 and 240 mg/kg), which provided significantly better results when compared with standard “three cycles, 5-2-2” TMZ treatment at 60mg/kg [159]. However, hazardous effects such lymphomas were found later on in brain-tumour cured mice treated with high cumulative doses of IMS-TMZ therapy, in this sense, the decrease in TMZ dosage (returning to 60 mg/kg in this thesis and also preliminarily in [168]) would be advisable in order to reduce the side effects due to TMZ cumulative dosage upon IMS administration.

In the rat race between tumour and the immune system, in addition to indirectly enhancing the participation of the host immune system through IMS administration strategy, immunotherapy can strengthen the anti-tumour function of the immune system directly. Immune checkpoint inhibitors such as anti-PD-1 antibodies, which are increasingly being used as anticancer drugs [101]–[104], could restore the function of exhausted CD8+ cytotoxic T effector cells. Despite anti-PD-1 immunotherapeutic approaches are currently undergoing clinical study for safety and efficacy in GB, preclinical studies revealed that anti-PD-1 monotherapy exhibits considerable potential of enhancing anti-tumour immune response in the GL261 immune-competent mouse model [105], [110], [142]. However, the overall survival (OS) of mice under anti-PD-1 monotherapy was quite variable among these studies probably due to their different dosing scheme and therapy starting days. In this sense, we found relevant to assess the impact of initial tumour volume and dosing schedule on the anti-PD-1 monotherapy efficacy.

In addition, immune checkpoint inhibitors combined with the gold standard therapy could represent another way to enhance treatment effect for GB. In preclinical studies, the combination of anti-PD-1 antibody and localized radiation therapy have shown prolonged survival in GL261 immune-competent mouse model [110]. Also, combination therapy of anti-PD-1 antibody and chemotherapeutic drug (carmustine) greatly shrank the tumour size and improved survival rate in GL261 immune-competent mouse model [111]. Therefore, we should expect an improved therapeutic potency when administered IMS-TMZ is combined with anti-PD-1 antibody in GL261 immune-competent mice.

Tumour volume in this chapter was arbitrarily defined into three categories, namely, "normal tumour volume", "large tumour volume" and "small tumour volume". The "normal tumour volume" was defined based on average of the group evaluated GL261 tumour volumes in preceeding years, for example 5.4 ± 2.6 mm^3 described in [169]. Therefore, the "large tumour volume" group is considered for tumours above this volume range while the "small tumour volume" group refers to tumours are under this volume range.

In summary, the specific goals for this section were:

- To consistently evaluate the therapeutic effect of IMS-TMZ (60 mg/kg) in GL261 GB tumour growing in C57BL/6 immunocompetent mice (orthotopic tumour).
- To assess the efficacy of anti-PD-1 monotherapy alone and the effect of initial tumour volume at therapy start and dosing schedule in the outcome of GL261 GB-bearing mice.
- To evaluate the added value of anti-PD-1+TMZ combined therapy when administered in IMS to GL261 GB.
- To evaluate whether long-term anti-tumour immune memory would be induced by TMZ and/or anti-PD-1 treatment in GL261 GB tumour-bearing mice.

4.1.2 Specific materials and methods

Therapeutic agent preparations

For in vivo experiments in this section, TMZ (Sigma-Aldrich, Madrid, Spain) was dissolved in 10% dimethyl sulfoxide (DMSO) in sterile saline solution (0.9% NaCl). Anti-PD-1 (Bio X cell, Lebanon, USA) and isotype IgG (Bio X cell, Lebanon, USA) were diluted to the appropriate concentration in sterile saline solution (0.9% NaCl).

4.1.2.1 IMS-TMZ monotherapy: evaluation of the therapeutic effect against GL261 GB

A total of 19 C57BL/6 female wt mice weighting 23.2 ± 2.2 g were used in this study. The usual 1×10^5 GL261 cells were stereotactically implanted intracranially in C57BL/6 mice to induce the tumour, as explained in general materials and method section 3.2.2. Mice were weighted twice a week and tumour volumes were followed using T2-weighted MRI acquisition at day 8 and day 11 after implantation, then tumour volume was calculated. Mice with most homogeneous weights and tumour sizes were chosen to make experimental groups after randomization, and therapy started. IMS-TMZ 60 mg/kg was administered to n=13 tumour-bearing mice using an oral gavage, every 6 days, from day 11 post implantation (p.i.), while control mice (n = 6) received 10% DMSO vehicle. During the therapeutic period, mice were followed according to the supervision parameters for animal health status (Annex I) and weighted. MRI studies were performed twice a week to monitor tumour volume evolution and their real-time response to therapy. Therapeutic scheme and MRI (volumetric T2w) follow-up schedule are shown in Figure 4.1. After treatment, animals meeting endpoint criteria were euthanized by cervical dislocation according to animal welfare protocol advice for ethical reasons, the brain was removed and tumour resected.

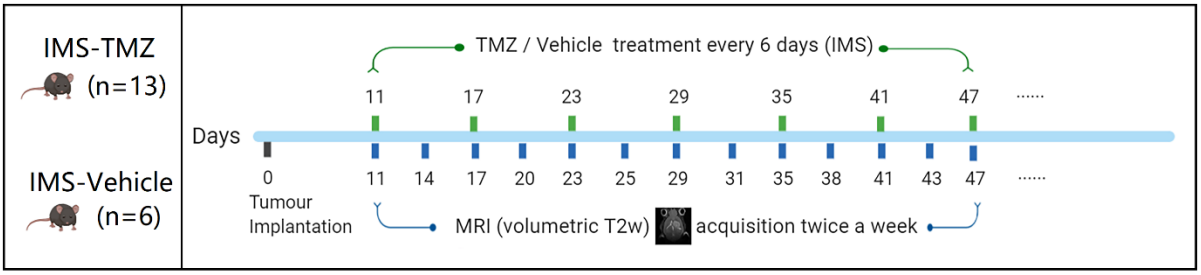

Figure 4.1 Immune-Enhancing Metronomic Schedule (IMS) used for GL261 GB therapy in mice. *TMZ (60 mg/kg) or Vehicle (10% DMSO) is administered every six days, volumetric T2w MRI were acquired twice a week.*

4.1.2.2 Assessing the added value of anti-PD-1 therapy in combination with TMZ against GL261 GB tumours, when administered in IMS

This experiment was designed to check whether the combined IMS anti-PD-1/TMZ therapy would be superior in fighting GL261 GB tumours in comparison with the corresponding monotherapies. The usual 1×10^5 GL261 cells were stereotactically implanted intracranially in C57BL/6 mice to induce the tumour, as explained in general materials and method section

3.2.2. Mice were weighted twice a week and tumour volumes were followed using T2-weighted MRI acquisition at day 8 and day 11 after implantation, then tumour volume was calculated. The dispersion of tumour volumes in this implantation round led us to split this cohort into two series: 1) *Normal* tumour volume (5.4 ± 1.8 mm^3 , n=6) at therapy starting day and also a 2) *Larger* tumour volume (10.8 ± 0.7 mm^3 n=4) at therapy starting day.

- **Normal tumour volume (5.4 ± 1.8 mm^3) at therapy starting day**

Mice with most homogeneous weights and tumour sizes were chosen for experimental groups after randomization (n = 6 in therapy combination group, n = 4 per group in other conditions), and therapy was launched. See group design, dosage, mice number, body weight and tumour size in Table 4.1.

		Body weight & Tumour volume (Day 11 p.i.)						
Anti-PD-1 100 µg /day (IMS) + TMZ 60 mg/kg (IMS)	**Mice**	**C1386**	**C1398**	**C1402**	**C1403**	**C1431**	**C1433**	**AV±SD**
	Weight (g)	21.5	22.1	21.3	22.2	22.3	20	**21.6 ± 0.9**
	Volume (mm^3)	5.1	3.6	8.6	5.9	4.8	4.3	**5.4 ± 1.8**
TMZ 60 mg/kg (IMS)	**Mice**	**C1382**	**C1383**	**C1394**	**C1395**			**AV±SD**
	Weight (g)	22.8	22.3	18.3	19.2			**20.7 ± 2.2**
	Volume (mm^3)	4.7	4.4	7.6	5.6			**5.6 ± 1.4**
Anti-PD-1 100 µg /day (IMS)	**Mice**	**C1321**	**C1326**	**C1330**	**C1335**			**AV±SD**
	Weight (g)	19.5	22.7	20.6	21.3			**21.0 ± 1.3**
	Volume (mm^3)	5.6	3.1	8.2	5.9			**5.7 ± 2.1**
Control isotype IgG 100 µg /day (IMS)	**Mice**	**C1324**	**C1325**	**C1329**	**C1332**			**AV±SD**
	Weight (g)	21.1	20.1	21.0	21.9			**21.0 ± 0.7**
	Volume (mm^3)	5.3	6.7	4.6	7.2			**5.9 ± 1.2**

Table 4.1 Average ± standard deviation (AV± SD) for body weight (g) and tumour volume (mm^3) for mice before starting therapy, at day 11 p.i. *No significant differences (p>0.05) were found among the four groups (n = 6 in combination group, n = 4 per group in others) neither for mice body weight, nor for tumour volumes before starting therapy.*

The dosage of TMZ remained the same (60 mg/kg) as described in section 4.2.1.1, and an optimum, low anti-PD1 therapy dosage (100 µg /day) was chosen from literature (see **Annex II**). Mice in anti-PD-1/TMZ combined therapy group were given TMZ (60 mg/kg) by intragastric administration in the morning and anti-PD1 (100 µg /day) via intra-peritoneal injection in the late afternoon. Both therapies were administrated in IMS (every 6 days) from day 11 post-implantation until tumour escape from therapy or transient tumour mass disappearance from MRI. Mice in monotherapy groups were treated with the corresponding individual drug dosing schedules. During the therapeutic period, mice were followed according to the supervision parameters for animal health status and weighted. MRI studies were performed twice a week to monitor tumour volume evolution and their response to therapy.

- **Larger tumour volume (10.8 ± 0.7 mm3) at therapy starting day**

Another group of mice (n =6) were treated with anti-PD-1/TMZ combined therapy but bearing larger tumour sizes at therapy start point. For comparison purposes, four mice with similar tumour volumes and treated with IMS-TMZ during the same time period or described in previous work [169] were integrated in this part. The effect of control isotype IgG was assumed to be similar in both tumour volume groups and was not repeated. See group design, dosage, mice number, body weight and tumour size in Table 4.2.

Body weight & Tumour volume (Day 11 p.i.)

anti-PD-1 100 µg /day (IMS) + TMZ 60 mg/kg (IMS)	**Mice**	**C1366**	**C1368**	**C1397**	**C1399**	**C1401**	**C1405**	**AV ± SD**
	Weight (g)	21.6	21.4	22	20.8	23	24.9	**22.3 ± 1.3**
	Volume (mm^3)	11.3	12.0	10.4	10.5	10.0	10.3	**10.8 ± 0.7**
TMZ 60 mg/kg (IMS)	**Mice**	**C1270**	**C1356**	**C1380**	**C1408**			**AV ± SD**
	Weight (g)	22.2	26	22.1	21.8			**23.0 ± 1.7**
	Volume (mm^3)	10.9	9.5	10.1	11.88			**10.6 ± 0.9**

Table 4.2 Average ± standard deviation (AV± SD) for body weight (g) and tumour volume (mm^3) for mice before starting therapy, at day 11 p.i. *No significant differences (p>0.05) were found between the two groups (n = 6 in combination group, n = 4 for TMZ monotherapy) neither for mice body weight, nor for tumour volumes before starting therapy.*

As described before, mice in anti-PD-1/TMZ combined therapy group were given TMZ (60 mg/kg) in the morning and anti-PD1 (100 µg /day) in the late afternoon, both of these therapies were administered in IMS from day 11 post-implantation until tumour escape from therapy or transient tumour mass disappearance from MRI?. Mice in IMS-TMZ group received equivalent doses of drug according to the same dosing schedule. During the therapeutic period, mice were followed according to the supervision parameters for animal health status and weighted. MRI studies were performed twice a week to monitor tumour volume evolution and their real-time response to therapy.

4.1.2.3 Anti-PD-1 monotherapy in optimized dosage: evaluation of tumour volume at therapy starting point and administration schedule

Since there was no consensus (or even lack of information) regarding the initial tumour volume or dosing schedule in the literature with anti-PD-1 treatment, we designed two series of experiments to assess these variables. The first series of experiments was designed to explore the impact of initial tumour size on treatment effect. Mice were divided into two groups according to the tumour size registered at day 11 post-implantation. As shown in Figure 4.2A, significant differences ($p<0.005$) were found between cases assigned to the *large* initial tumour group (n=4, 9.6 ±2.2 mm^3) and the *small* initial tumour group (n=4, 2.1 ± 1.1 mm^3). Since the first low anti-PD-1 dosage attempted did not prove effective to increase mice survival (see section 4.1.3.2, figure 4.10), a new therapeutic schedule and dose was adapted from [105]. Thus, anti-PD-1 was administered from day 11 p.i. (500 µg/dose) followed by repeated injections (250 µg/dose) every 3 days. Experimental schedule and tumour T2w MRI image of representative cases on the therapy starting day are shown in Figure 4.2B.

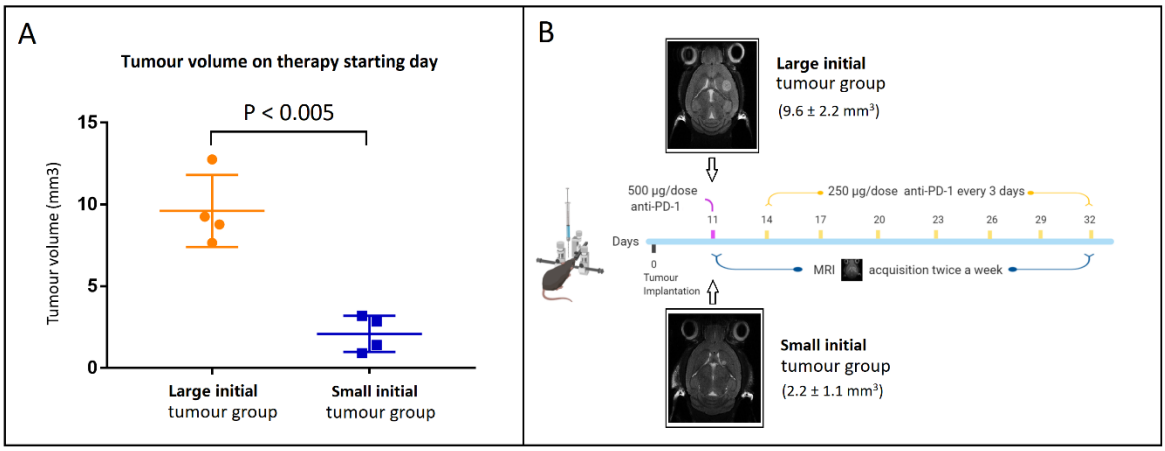

Figure 4.2 Mice bearing different size tumours at same post-implantation days and treated with same anti-PD-1 dosing schedule. *(A) Distribution of tumour volume on therapy starting day, large initial tumour volume group (orange dots, 9.6 ±2.2 mm^3, n = 4), small initial tumour volume group (blue dots, 2.1 ± 1.1 mm^3, n = 4). Significant differences (p<0.005) were found between two groups with Student's t-test. (B) Experimental treatment schedule and representative T2w tumour images of cases on the therapy starting day.*

The second series of experiments aimed to investigate the effect of changes in the dosing schedule while using similar tumour volumes. Mice bearing similar size tumours were divided randomly into two groups on day 6 post-implantation, being 0.39 ± 0.19 mm^3 in every 3 days dosing schedule (E3D) group and 0.37 ± 0.06 mm^3 in the standard IMS group. Figure 4.3A presents the tumour size distribution of each group, and no significant differences were found in groups (p > 0.05). In E3D group, anti-PD-1 was administered from day 6 p.i. (500 µg/dose) followed by repeated injections (250 µg/dose) every 3 day. In IMS group, anti-PD-1 was administered from day 6 p.i. (500 µg/dose) followed by repeated injections (250 µg/dose) with IMS (every 6 days). Experimental schedule for each group is shown in Figure 4.3B.

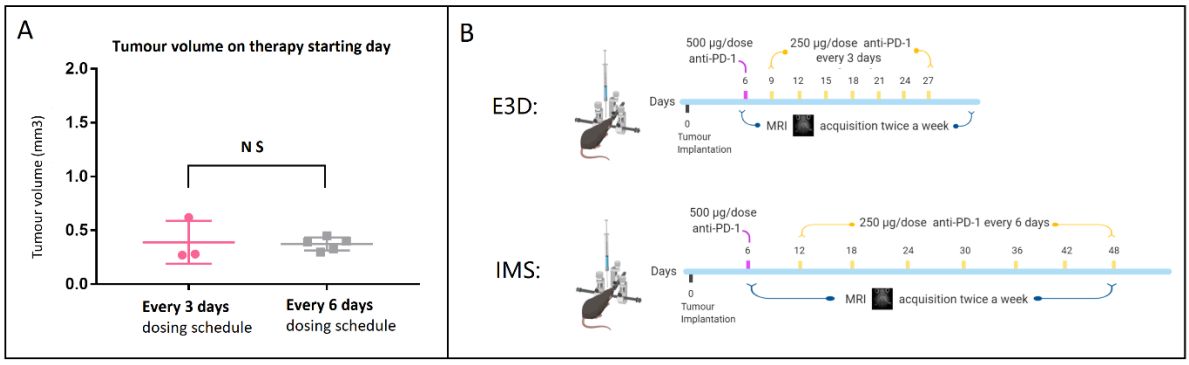

Figure 4.3 Mice bearing similar size tumours at same post-implantation days and treated with different anti-PD-1 dosing schedule. *(A) Distribution of tumour volume on therapy starting day, every 3 days dosing schedule group (pink dots, 0.4 ± 0.2 mm^3, n = 3), every 6 days group (grey dots, 0.4 ± 0.1 mm3, n = 5). No significant differences (p > 0.05) were found between two groups with Student's t-test. (B) Experimental schedule for administration of anti-PD-1 (500/250 µg) every 3 day (E3D) and IMS.*

4.1.2.4 Evaluation of the long-term anti-tumour immune memory induced by TMZ and/or anti-PD-1 treatment in mice harbouring GL261 tumour.

When GL261 tumours were reduced after treatment until abnormal mass detection by MRI was no longer possible, or its volume remained stable (usually below 2 mm^3) during at least 2 weeks, therapy administration was halted. Then, MR images were acquired twice a week. Whenever the volume of the residual/abnormal mass was stable or decreased for one month, mice were transiently declared "cured" as in [38].

We were interested in a preliminary evaluation of whether the anti-tumour immunity were induced in these cured C57BL/6 mice. For that, a re-challenge experiment was performed. Mice cured by TMZ and/or anti-PD-1 treatment (n = 23) were inoculated with GL261 cells again, symmetric but contralateral to the initial injection site. For re-implantation, three C57BL/6 female wt mice were also implanted as controls, to check for consistency and growth rate in contralateral side. All mice were followed-up (weight + welfare parameters) twice a week and volumetric T2w MRI was acquired once a week. In case of abnormal tumour growth, treatment was resumed at the same therapeutic schedule and dose.

4.1.3 Results

4.1.3.1 IMS-TMZ treatment strongly increased survival in orthotopic GL261 GB-bearing mice.

In this part of the study 19 mice were used. Among them, 13 mice were treated with TMZ using an IMS protocol and 6 were administered with vehicle, also in an IMS administration. All mice were followed-up according to the supervision parameters for animal health status and weighted (Figure 4.4). Results from this mice cohort were recently described in NMR in Biomedicine (https://pubmed.ncbi.nlm.nih.gov/31926117/).

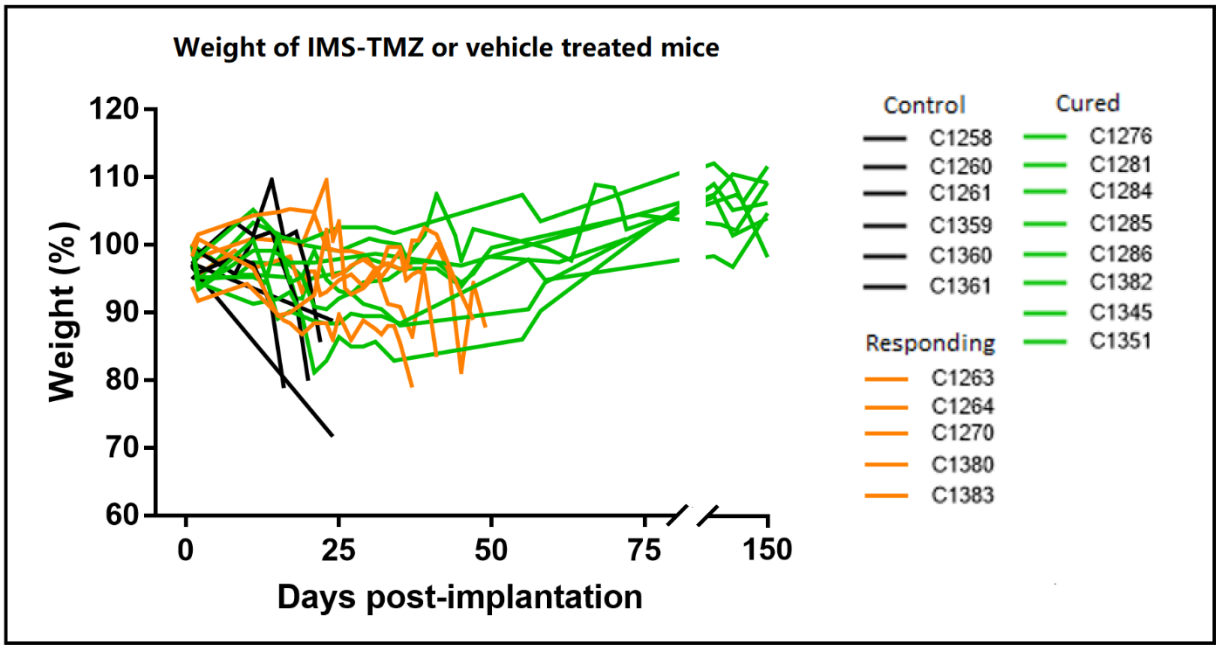

Figure 4.4 Body weight evolution of GL261 tumour-bearing mice during TMZ or vehicle treatment with IMS protocol. *Weight is expressed in %, assuming 100% for the weight at day 0; dashed horizontal blue line indicates the 20% weight reduction point, below which animals must be euthanized due to welfare parameters.*

The tumour volume at therapy starting (day 11 p.i.) in this section was 5.4 ± 2.6 mm^3, close to tumour volumes in previous work from our group with similar TMZ schedule (6.0 ± 1.2 mm^3) [168], indicating that the evolution is consistent along time in different cohorts. Tumour volume evolution of vehicle and TMZ-treated mice is shown in Figure 4.5. Five tumours in the IMS-TMZ monotherapy group showed transient growth arrest/shrinkage and eventually relapsed. The remaining 8 tumours were reduced to a small but stable abnormal mass (Figure 4.6). Finally, these eight mice were declared "cured" with the stablished criteria and re-challenge experiment was carried out (see section 4.1.3.2). Cured mice had a trend towards smaller volumes at therapy start (average 4.3 ± 1 .4 mm^3 vs 6.9 ± 3.4 mm^3 in non-cured mice from this work), although this difference was not statistically significant ($p = 0.099$). Finally, tumour volume evolution was significantly different ($p < 0.001$) when comparing control group with IMS-TMZ group.

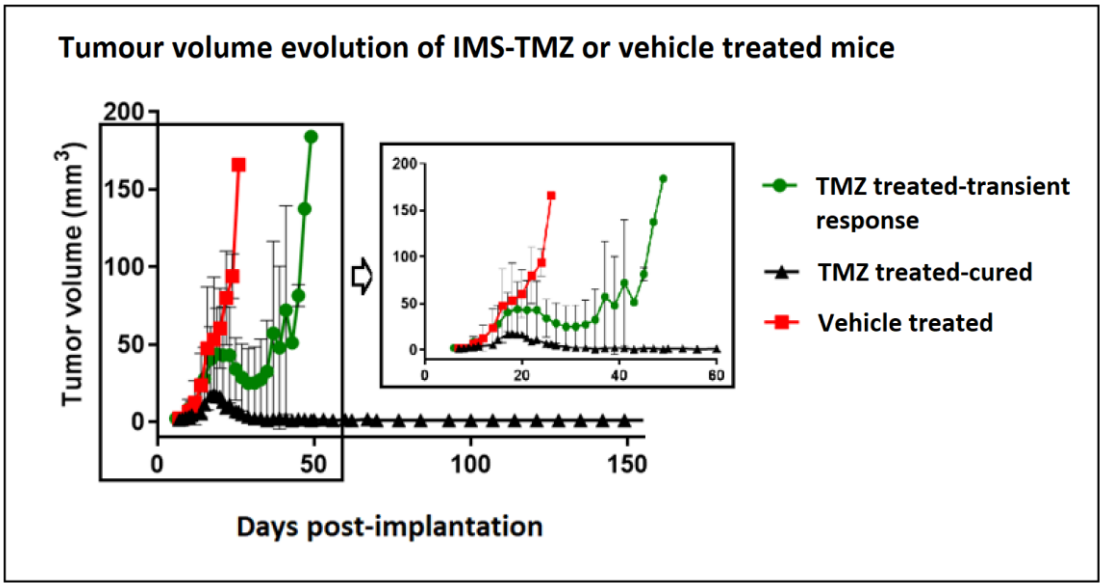

Figure 4.5 Tumour volume evolution for control (vehicle treated) and TMZ-treated GL261 GB-bearing mice with the IMS protocol. *Mice in control group (n=6, C1258, C1260, C1261, C1359, C1360 and C1361). For TMZ-treated mice two groups are shown: transient response mice (n=5, cases C1263, C1264, C1270, C1380 and C1383) and cured mice, in which tumour disappeared due to TMZ treatment (n=8, C1276, C1281, C1284, C1285, C1286, C1345, C1351 and C1382). Mean ± SD values are shown.*

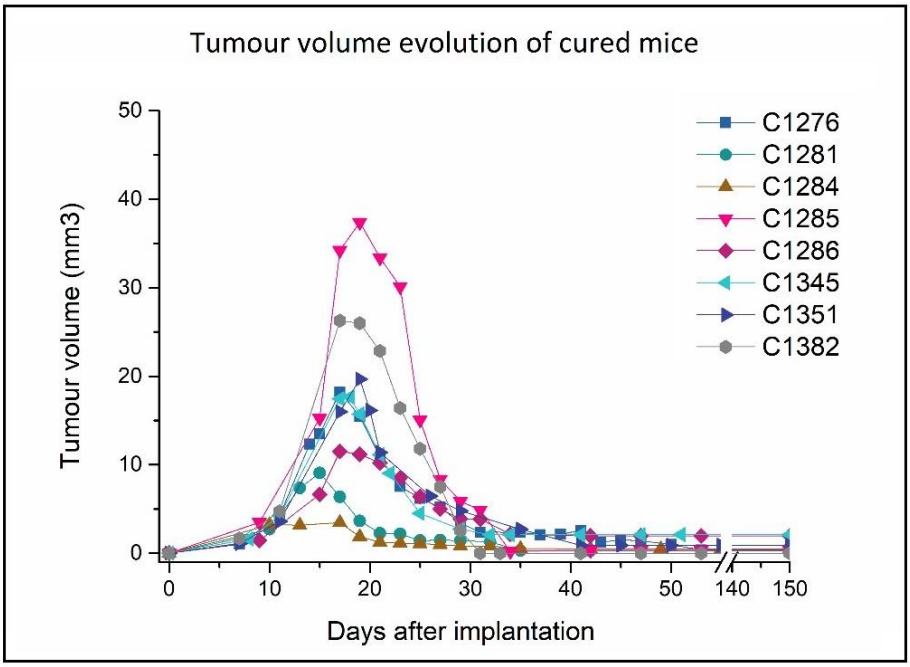

Figure 4.6 Tumour volume evolution of mice cured from the TMZ treated group. *(n=8, C1276, C1281, C1284, C1285, C1286, C1345, C1351 and C1382).*

TMZ treatment with the IMS administration has a positive impact in the survival of GL261 tumour-bearing mice (Figure 4.7), which is in agreement with results described previously by our group [159]. Thus, the average survival rate for control mice was 22.5 ± 3.0 days whereas

the IMS-TMZ-treated animals survived significantly more, 298 ± 285 days ($p<0.05$ according to Log Rank Test), being 61.5% of TMZ treated mice alive at day 150 p.i. and some individuals still alive at 845 days p.i. Considering previous survival of 33.9 ± 11.7 days with the standard 5-2-2 protocol [160][151], IMS administration greatly improved mice outcome. Our findings from IMS-TMZ therapy are also better than those published by other authors. For instance, in the same preclinical GB model, when TMZ was administered for 5 consecutive days, the median survival time of the treated mice was 30 days [170]. In another study, GL261 tumour-bearing mice were treated with TMZ in 2 different ways, one was TMZ 50 mg/kg for 5 consecutive days and another was TMZ 25 mg/kg in a 10-day metronomic way, but the longest survival time of those TMZ treated mice was no more than 50 days [171].

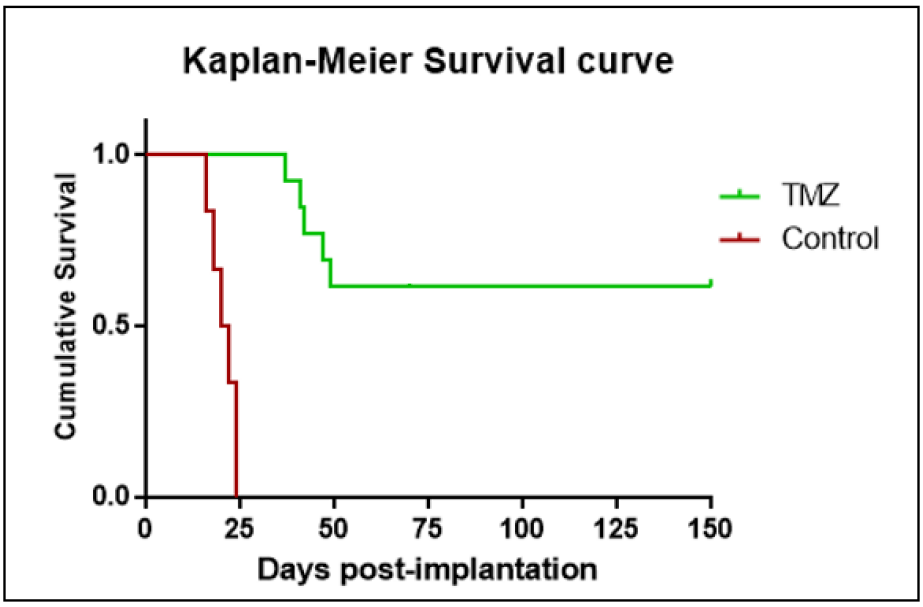

Figure 4.7 Kaplan Meier survival curve comparing GL261 GB-bearing mice treated with vehicle and TMZ in an IMS protocol. *Mice in vehicle-treated group (n=6) and in TMZ-treated group (n=13).*

Although it was an outstanding result, even displaying cure of a fraction of the investigated animals, we still lost some individuals due to tumour relapsing. Thus, we wondered whether the combination with immunotherapy such as the anti-PD-1 agent would help to 'rescue' this percentage of non-responding mice.

4.1.3.2 Combining anti-PD-1 with TMZ in an IMS administration improves monotherapy outcome.

- **Normal tumour volume (5.4 ± 1.8 mm^3) at therapy starting day**

Four treatment groups with IMS (every 6 days) were conducted as follows: isotype IgG control (n =4), anti-PD-1 (n = 4), TMZ (n = 4) and a combination of anti-PD-1 and TMZ (n = 6). Mice body weight and tumour volume were inspected twice a week (Figure 4.8 and 4.9).

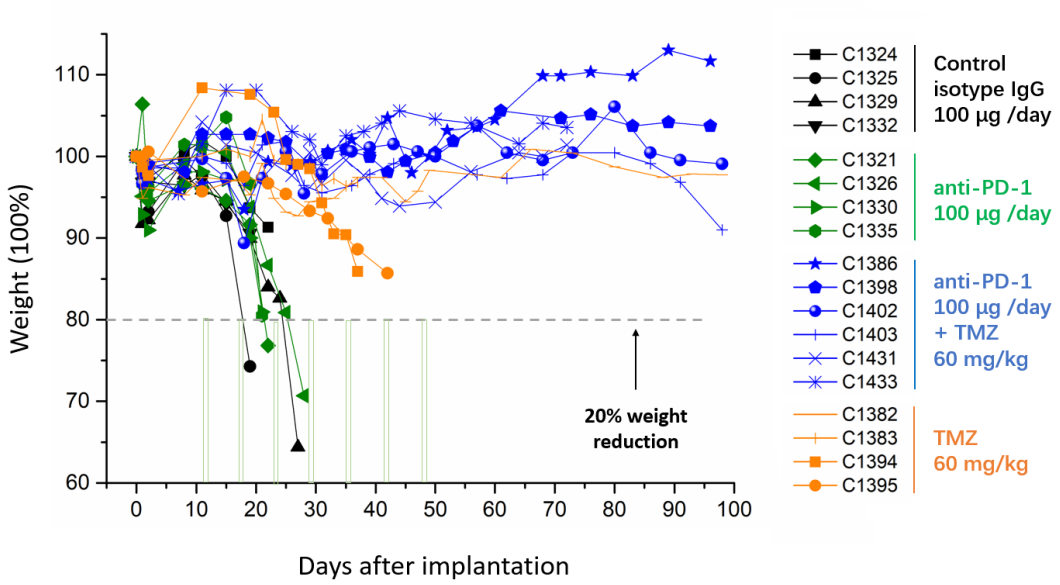

Figure 4.8 Body weight of mice in monotherapy and combination therapy groups. *Mice treated with control isotype murine IgG 100 µg/day (n=4, black lines), anti-PD-1 100 µg/day (n=4, green lines), anti-PD-1 100 µg/day combined with TMZ 60 mg/kg (n= 6, blue lines) and TMZ 60 mg/kg alone (n=4, orange lines), the green columns indicate therapy administration time points. Weight is expressed in %, assuming 100% for the weight at day 0; dashed horizontal grey line indicates the 20% weight reduction point, below which animals must be euthanized due to welfare parameters.*

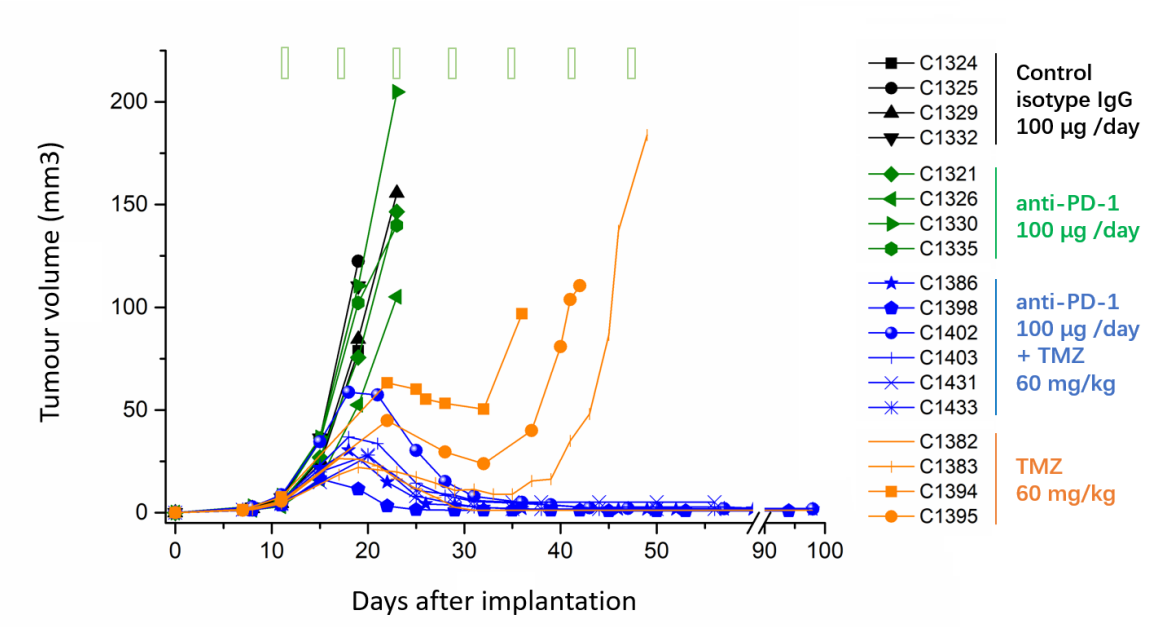

Figure 4.9 Tumour volume evolution of mice in monotherapy and combination therapy groups. *Mice treated with control isotype murine IgG 100 µg/day (n=4, black lines), anti-PD-1 100 µg/day (n=4, green lines), anti-PD-1 100 µg/day combined with TMZ 60 mg/kg (n= 6, blue lines) and TMZ 60 mg/kg alone (n=4, orange lines), the green columns at top indicate therapy administration time points.*

Tumours in anti-PD-1 monotherapy group and isotype murine IgG control presented similar results with no apparent response to therapy. Tumours in the TMZ monotherapy group showed transient shrinkage followed by relapse, except by one case (C1382) in the TMZ group which was cured after 6 doses of TMZ treatment. Notably, all mice in anti-PD-1/TMZ combined therapy group were declared cured, i.e. all these tumours reduced to a stable tissue scar for one month and mice were re-challenged (see section 4.1.3.3). Tumour volume evolution was significantly different ($p < 0.001$) when comparing control group with TMZ monotherapy group and combined anti-PD-1/TMZ group. Moreover, Kaplan-Meier curves were elaborated (Figure 4.10) to compare animal survival rate among four groups.

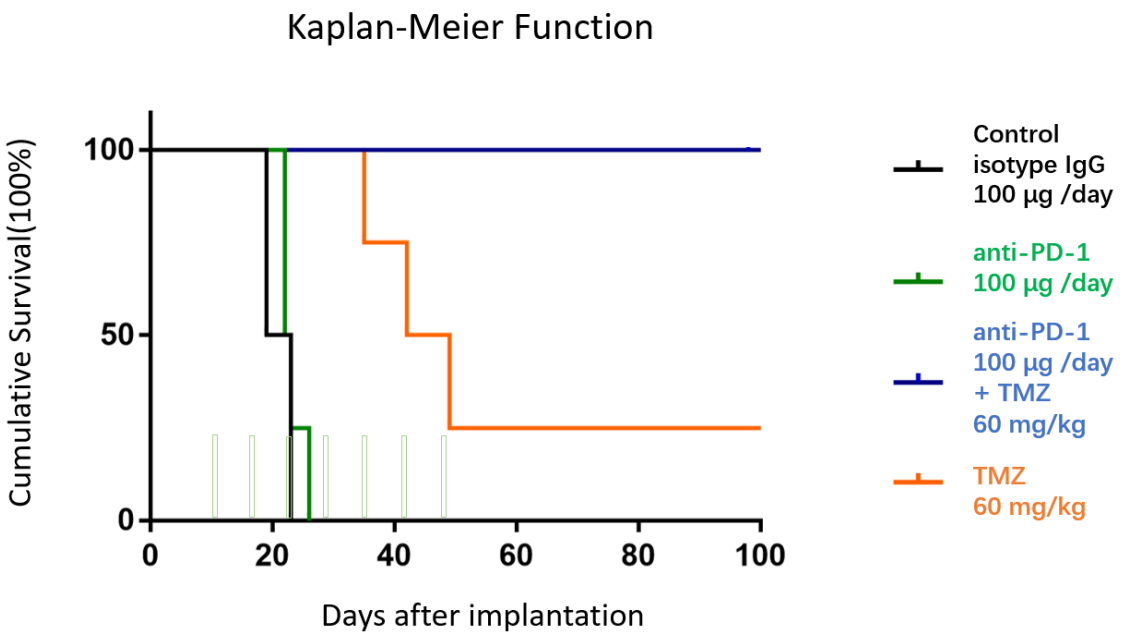

Figure 4.10 Survival Kaplan-Meier curves of mice in different therapy groups. *Mice treated with control isotype murine IgG 100 µg/day (n=4, black lines), anti-PD-1 100 µg/day (n=4, green lines), anti-PD-1 100 µg/day combined with TMZ 60 mg/kg (n= 5, blue lines) and TMZ 60 mg/kg alone (n=4, orange lines), the green columns indicate therapy administration time points*[2].

For the anti-PD-1 treatment (100µg/day), a survival rate of 23 ± 2.9 days was found, which was not significant different neither from isotype IgG control group (21.8 ± 3.3 days) nor from untreated (control) mice previously studied in our group, 19.7 ± 2.7 days. During the long-term survival observation period (100 days p.i.), the IMS-TMZ treatment led to a survival rate of 56.5 ± 29.6 days, somewhat lower than survival described in section 4.1.3.1 but still significantly different and improved when compared with anti-PD-1 monotherapy or control mice ($p < 0.001$). The best results were obtained with the combined anti-PD-1 and TMZ treatment, with an average survival rate of 100 ± 0 days, which is significantly different ($p = 0.02$) from IMS-TMZ alone. Importantly, at the time of comparing the different treated groups, significant differences were found regarding mice weight changes, tumour volume evolution and survival average, being the best overall outcome always obtained with the anti-PD-1/TMZ combined treatment in IMS, which proved clearly better than either monotherapy alone.

[2] *Note: mouse C1403 (combination therapy group) died on day 98 p.i. during the re-challenge experiment (not recovering from anesthesia). MRI scanning did not show relapsing tumour; accordingly, GB did not cause its death, and this individual was excluded from the survival curve since it died from unknown reasons.*

➢ **Larger tumour volume (10.8 ± 0.7 mm^3) at therapy starting day**

Two treatment groups in IMS (every 6 days) were conducted as follows: TMZ (n = 4) and a combination therapy of anti-PD-1 and TMZ (n = 6). Mice body weight and tumour volume were inspected twice a week (Figure 4.11 and 4.12).

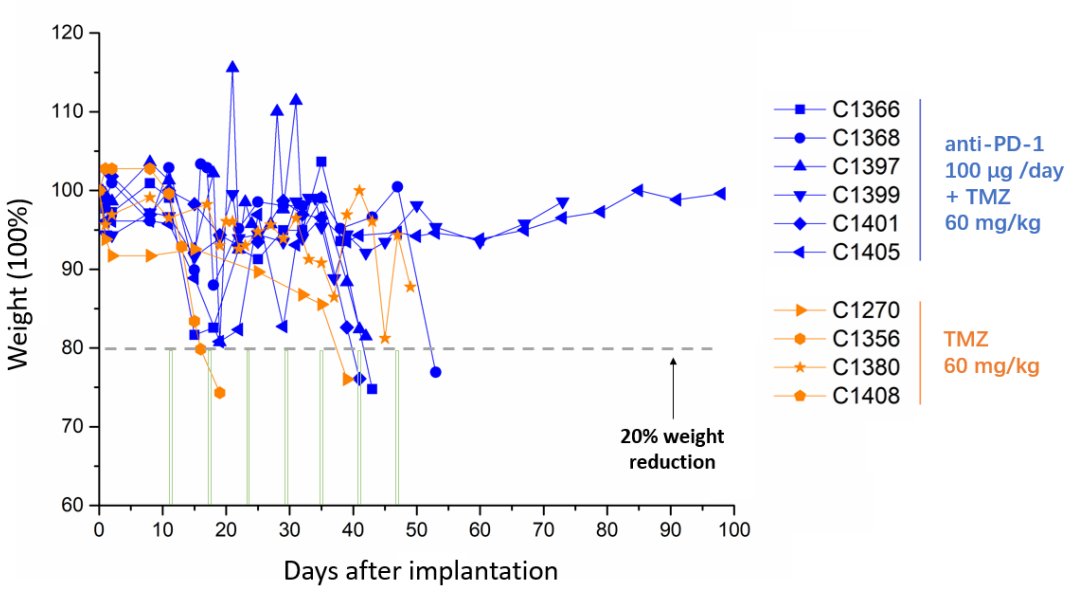

Figure 4.11 Body weight of mice (with larger tumour volume at day 11 p.i.) treated with different therapy. *Mice treated with anti-PD-1 100 µg/day combined with TMZ 60 mg/kg (n= 6, blue lines) and TMZ 60 mg/kg alone (n=4, orange lines), the green columns (note: green columns barely seen in this plot, perhaps use a darker green) indicate therapy administration time points. Weight is expressed in %, assuming 100% for the weight at day 0; dashed horizontal grey line indicates the 20% weight reduction point, below which animals must be euthanized due to welfare parameters.*

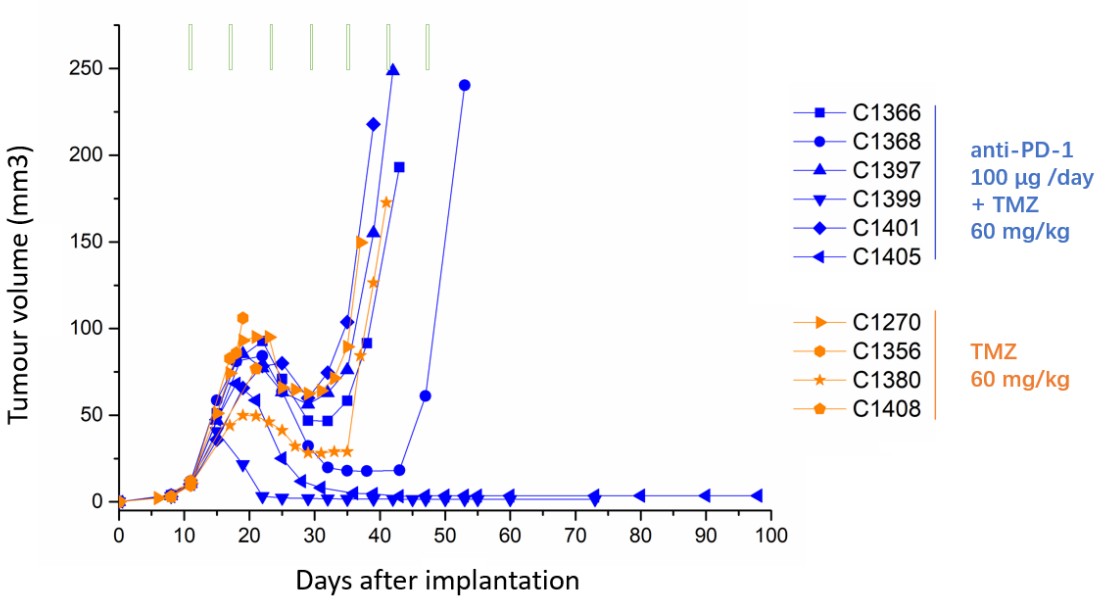

Figure 4.12 Tumour volume evolution of mice (with larger tumour volume at day 11 p.i.) treated with different therapy. *Mice treated with anti-PD-1 100 µg/day combined with TMZ 60 mg/kg (n= 6, blue lines) and TMZ 60 mg/kg alone (n=4, orange lines), the green columns indicate therapy administration time points.*

In these cohort with larger tumour volumes, two mice (C1270 and C1380) in TMZ monotherapy groups showed transient shrinkage but eventually relapsed, while the other two cases (C1356 and C1408) escaped TMZ therapy right from the start, then died on day 19 p.i. and 21 p.i respectively. However, all mice (n=6) in anti-PD-1/TMZ combined therapy group responded to therapy. Among them, 4 mice (C1366, C1368, C1397 and C1401) showed transient response followed by relapse, but it is worth mentioning the other two mice (C1399 and C1405) tumours were reduced to a small but stable abnormal mass. Finally, these two mice were declared "cured" with the stablished criteria and a re-challenge experiment was carried out (see section 4.1.3.2).

Furthermore, Kaplan-Meier curves were elaborated (Figure 4.13) to compare survival rate between the two groups.

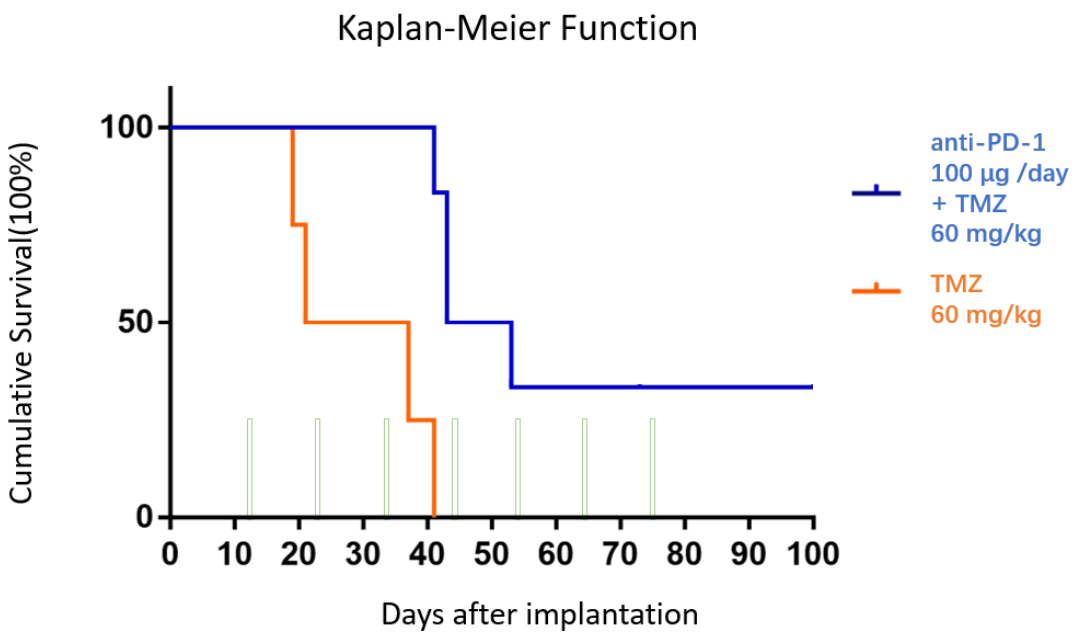

Figure 4.13 Survival Kaplan-Meier curves of mice (with large tumour volumes at day 11 p.i.) in different therapy group. *Mice treated with anti-PD-1 100 µg/day combined with TMZ 60 mg/kg (n= 5, blue lines) and TMZ 60 mg/kg alone (n=4, orange lines), the green columns indicate therapy administration time points*[3].

The average survival of TMZ monotherapy for this group was 29.5 ± 11.1 (n=4) days, significantly different from anti-PD-1 / TMZ combination therapy group (104 ± 131.3 days, n=6, one of them - C1405 is still alive at August 18, 2020) ($p < 0.001$ with Log-Rank test). Also, the survival for TMZ monotherapy in this "larger tumour volume" group was significantly different from a) "normal tumour volume" group (56.5 ± 29.6 days), b) TMZ-treated mice in section 4.3.1 (298 ± 285 days). These differences have probably an origin on tumour size at therapy starting point. Thus, significant difference in mice survival rate was found between "larger tumour volume" and "normal tumour volume" combination therapy groups.

It is important to emphasize that we had never been able to cure mice bearing large tumours (higher than 10 mm^3 on therapy starting day) in our group with standard TMZ therapy, meaning that combination of anti-PD-1 plus TMZ using an IMS schedule showed unprecedented therapeutic results in our preclinical glioblastoma model.

[3] *Note: mouse C1399 (combination therapy group) died on day 73 p.i. during the re-challenge experiment (not recovering from anesthesia). MRI scanning did not show relapsing tumour; accordingly, GB did not cause its death, and this individual was excluded from the survival curve since it died from unknown reasons.*

However, the subdivision of the investigated cohort in larger and smaller volume values brought to light that the tumour volume at the therapy starting point could be a determinant in the outcome; in addition, it could also explain different outcomes reported in literature. The poor survival results obtained with the anti-PD-1 alone were disappointing, and we wondered whether the dosage used was not suitable for our aggressive GB model, even for small volumes at therapy starting point. In this sense, we moved to a higher dosage described in literature [105] and further investigated the anti-PD-1 monotherapy performance.

4.1.3.3 Initial tumour volume and administration schedule are critical to the efficacy of anti-PD-1 monotherapy

Initial tumour volume

Under the higher dosage (500/250 µg) chosen for anti-PD-1 monotherapy at E3D schedule, mice survival rate was significantly different ($p<0.001$) according to tumour starting volumes. Survival was remarkably higher in the *small* initial tumour volume group (170 ± 90 days, 75% of mice cured) than in the *large* initial tumour group (17.8 ± 1.5 days, 0% cured) at the same dosing schedule, Figure 4.14A. The tumour growth curves (Figure 4.14 B and C) drawn from calculated tumour size demonstrated the regression of the tumour observed in most cases from the *small* initial tumour volume group.

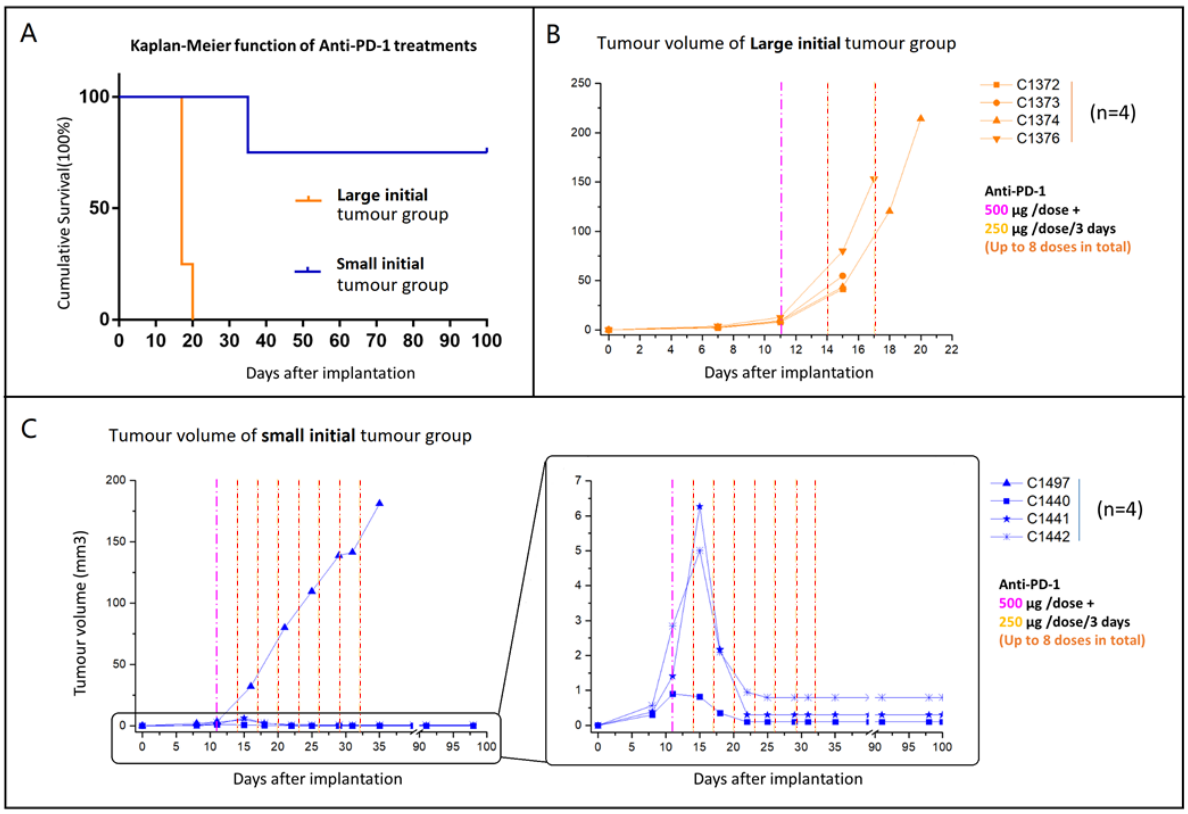

Figure 4.14 Mice bearing different size tumours and treated with same anti-PD-1 dosing schedule. *(A) Survival Kaplan-Meier curves for mice bearing large tumours (n=4, orange line) and small tumours (n=4, blue line) treated with anti-PD-1 every 3 days. (B) Tumour volume evolution of mice bearing large tumours treated with anti-PD-1 every 3 days (n=4, orange lines). (C) Tumour volume evolution of mice bearing small tumours treated with anti-PD-1 every 3 days (n=4, blue lines). The purple and red dashed line (500 µg/dose and 250 µg/dose separately) indicate therapy administration time points.*

Administration schedule: every 3 days vs 6 days

Regarding the series of mice bearing similar size tumour at therapy starting day treated with anti-PD-1 (500/250 µg) but different dosing schedule (i.e. E3D vs IMS), no significant differences were found between E3D group (91.3 ± 53.1 days) and IMS group (85.8 ± 49.6 days) ($p > 0.05$ Figure 4.15 B). The tumour volume evolution plot for each group is shown under their respective anti-PD-1 dosing scheme (Figure 4.15 C and D). The curative rate in E3D group was 66.6% and that in IMS group was 60.0 %.

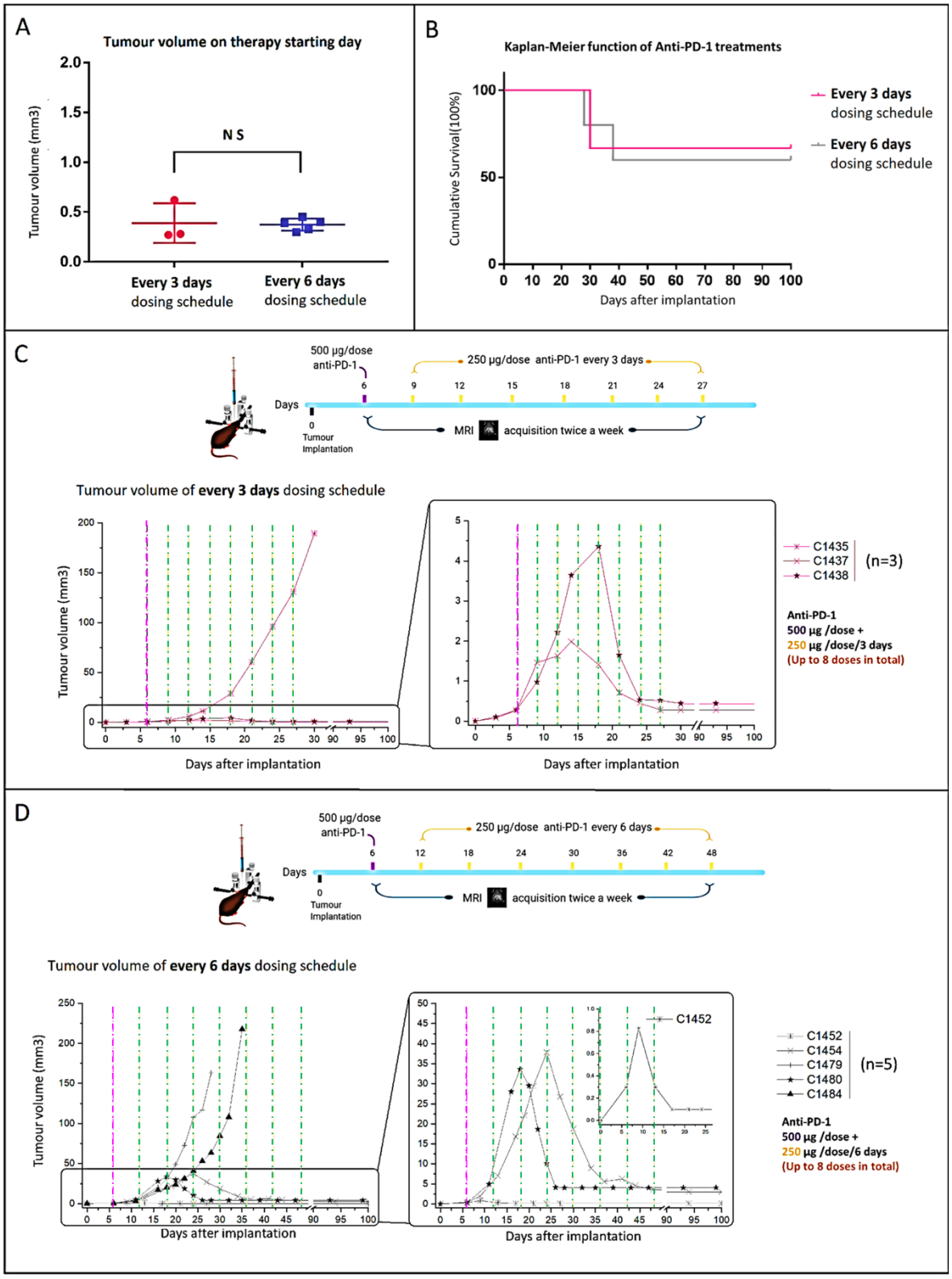

Figure 4.15 Mice bearing similar size tumours at therapy starting day and treated with different anti-PD-1 dosing schedule. *(A) Tumour volume at therapy starting day (B) Survival Kaplan-Meier curves for mice treated with anti-PD-1 every 3 days dosing schedule (n=3, pink line) and IMS (n = 5, grey line).(C) Tumour volume evolution of mice treated with anti-PD-1 every 3 days dosing schedule*

(n=3, pink lines). (D) Tumour volume evolution of mice treated with anti-PD-1 in IMS (n=5, grey lines). The purple and green dashed line (500 µg/dose and 250 µg/dose separately) indicate therapy administration time points.

Results show that, regarding the two parameters investigated, the tumour volume at therapy starting point is definitely a determinant for therapy outcome. On the other hand, and using the chosen dosage of 500/250 µg/dose, no significant differences are observed when treating mice every 3 days or every 6 days, with a survival rate and percentage of cure being similar in both cases. In this sense, there would be no improvement with the increase of anti-PD-1 frequency of administration and a 6-day schedule would be more suitable, since it produces the same results, consumes less therapeutic agent and produces less stress to animals.

4.1.3.4 IMS-TMZ and anti-PD-1 monotherapy shown to be more effective in establishing anti-tumour immune memory than combined therapy.

From the aforementioned work in this section, twenty-three mice had tumour which disappeared after TMZ and/or anti-PD-1 treatment (n = 8 in the IMS-TMZ group, n =7 in the IMS-TMZ/PD-1 combination group, and n = 8 in the anti-PD-1 monotherapy group, see Table 4.3 for individual codes).

TREATMENT	IMS-TMZ	IMS-ANTI-PD-1/TMZ	ANTI-PD-1 MONOTHERAPY
MICE CODE	C1276	C1386	C1440
	C1281	C1398	C1441
	C1284	C1402	C1442
	C1285	C1431	C1437
	C1286	C1433	C1438
	C1382	C1446	C1454
	C1345	C1405	C1480
	C1351		C1484
NUMBER OF ANIMALS	8	7	8

Table 4.3 Table illustrating cured animal distribution in different groups investigated in this section.

Although curing GL261 GB-bearing animals was already a big step along the work performed in this thesis, there was a great interest to assess whether treatments could lead to an immune memory that would prevent further development of the same type of tumours. To

investigate whether IMS-TMZ therapy, IMS-anti-PD-1/TMZ combined therapy or anti-PD-1 monotherapy could produce such immune memory, we performed tumour re-challenge studies with reimplantation of GL261 cells in the opposite side. Magnetic resonance imaging acquisitions (volumetric T2w) were acquired twice a week to check for tumour development and 3 wt C57BL/6 mice were implanted in parallel as controls. Figure 4.16 shows the tumour volume evolution after the re-challenge experiment.

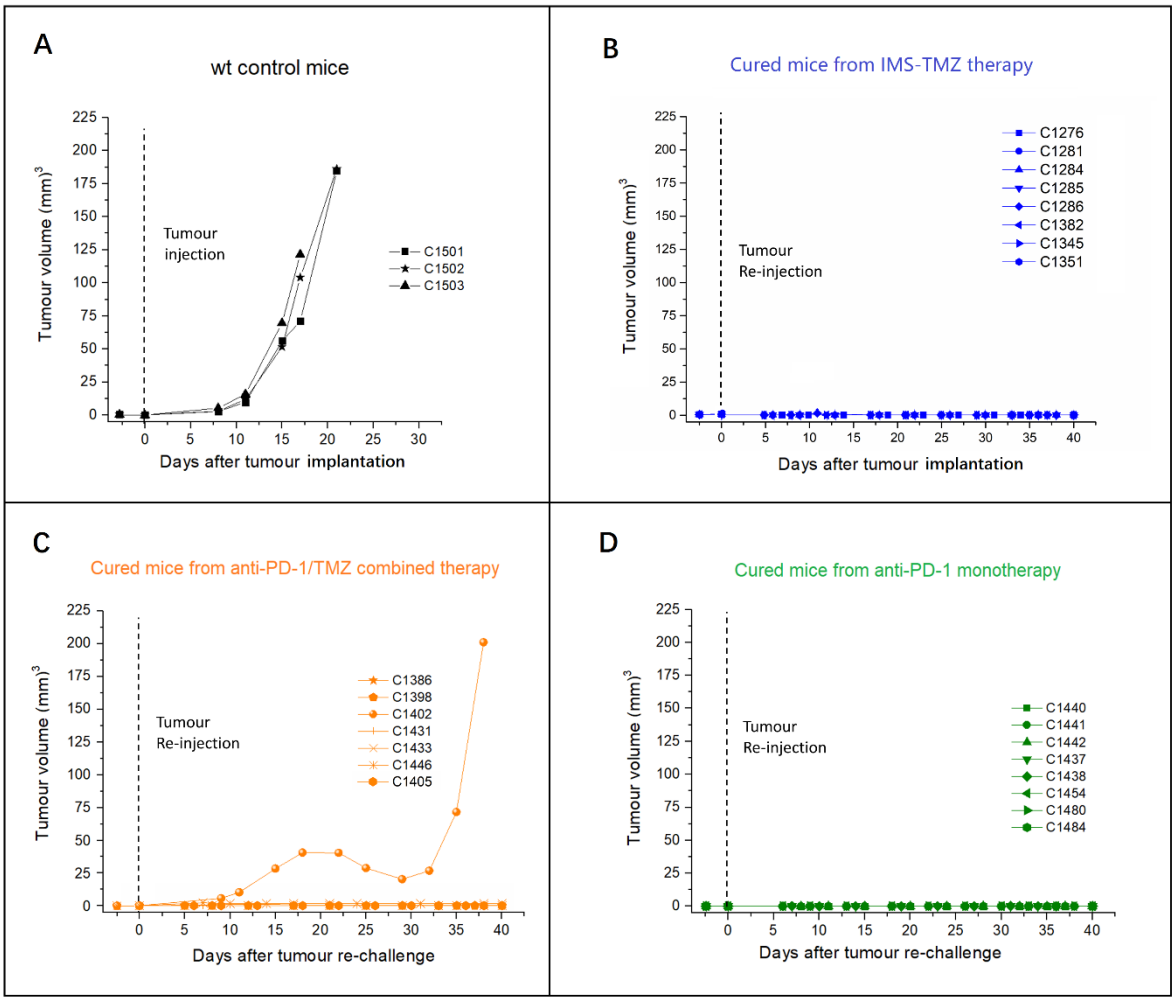

Figure 4.16 Tumour volume evolution after the re-challenge experiment with GL261 cells in cured mice. *(A) All wt control mice developed rapidly growing GL261 tumours, as expected. (B) In IMS-TMZ therapy group, one cured mouse (C1286) had transient tumour growth 10 days after reimplantation, which disappeared after only one TMZ dose. The rest of the mice remained tumour-free after rechallenge. (C) In IMS-anti-PD-1/TMZ combined therapy group, one cured mouse (C1402) exhibited progressively tumour regrowth and eventually died of the re-implanted tumour, meanwhile two cured mice (C1431 and C1433) had transient tumour growth 7 days after implantation, which were*

eliminated after 2 doses of IMS-anti-PD-1/TMZ therapy. (D) Mice cured from anti–PD-1 monotherapy rejected the tumour right away, showing no tumour growth at any time point.

Control mice

Mice in wt control group had a 0% tumour rejection rate and died by day 21 post-implantation, no significant difference was found when comparing to control mice in our group, 19.7 ± 2.7 days. Besides, control tumours grew normally and no significant differences were found with standard GL261 tumour doubling time of 2.4 ± 0.3 days [172].

IMS-TMZ cured mice

Regarding IMS-TMZ cured mice, only one of the re-implanted tumours (case C1286) grew after 10 days while the rest remained tumour-free until present time (range 150-464 days post-implantation). With respect to case C1286, TMZ was administered as usual in an IMS protocol and tumour disappeared after only one TMZ dose. After being cured again, this mouse has been followed-up (weight + welfare parameters) twice a week and MRI acquisitions were acquired once a week, for the rest of its lifetime (until 175 days post-implantation) and no tumour mass has been detected in its brain. Thus, 1/8 of IMS-TMZ mice had sub-optimal immune memory, and the tumour rejection rate of IMS-TMZ cured mice was 87.5% (7/8).

IMS-Anti-PD-1/TMZ cured mice

Regarding cured mice from IMS-Anti-PD-1/TMZ combined therapy group, three (C1402, C1431 and C1433) out of seven tumours (43%) re-implanted in the cured mice grew after 6 days. Anti-PD-1/ TMZ combined therapy was administered as usual in IMS immediately after regrowth detection. As shown in *Figure 4.16 C*, after therapy administration, C1402 showed transient response with tumour shrinkage but eventually died on day 38 post re-challenge, while C1431 and C1433 get cured again after 2 doses of anti-PD-1/TMZ therapy. Therefore, 3/7 of combined treatment showed “suboptimal memory”, and the tumour rejection rate of IMS-anti-PD-1/TMZ cured mice was 57% (4/7).

anti-PD-1 monotherapy cured mice

Cured mice that had received anti-PD-1 monotherapy exhibit the best tumour rejection rate (8/8, 100%), all of them have the optimal immune memory raised, with no tumour growth in any of the mice after the re-challenge experiment.

	Primary tumour implantation wt control mice	Tumour re-challenge IMS-TMZ cured mice	Tumour re-challenge IMS-anti-PD-1/TMZ cured mice	Tumour re-challenge anti-PD-1 monotherapy cured mice
Mice with growing tumour	3	1	3	0
Mice with upfront tumour rejection	0	7	4	8
Tumour rejection rate	0%	87.5%	57%	100%

Table 4.4 Comparison of GL261 tumour take rates between primary tumour implantation, and GL261 re-challenge in IMS-TMZ, IMS-anti-PD-1/TMZ and anti-PD-1 monotherapy cured mice.

As summarised in Table 4.4, the re-challenge survival experiments demonstrated that different therapies exhibited varying degrees (57%-100%) of long-term protective immune memory development against further development of GL261 GB.

4.1.4 Discussion

4.1.4.1 Harnessing the immune system to control the tumour progression

As a natural anti-tumour defence system, the immune system plays an important role in the response to anti-tumour therapy, and harnessing the immune system to control cancer has been highlighted in recent years [173][174].

Historically, conventional chemotherapy drugs were thought to work only through direct tumour cell killing. This concept comes from cytotoxic drugs interfering with DNA synthesis and replication (mentioned in section 1.2.2.3). However, further investigation proved that the anti-tumour actions of chemotherapeutic agents also rely on some indirect pathways for stimulating immune cells. Namely, some cytotoxic drugs have been shown to induce immunogenic cell death in tumour cells, resulting in the release of specific signals that trigger cell phagocytosis and encourage the maturation of dendritic cells [175][176], eventually

resulting in powerful anti-tumour response. Metronomic chemotherapy, which is described as continuous or periodic treatment with low doses of chemotherapeutic agents, is applied in patients who have been extensively pre-treated with cytotoxic drugs or who have poor performance status [177][178]. Intriguingly, in the past, metronomic chemotherapy used for palliation has resulted in favourable tumour responses and extended patient survival [179][180], opposed to the extended belief that, in chemotherapy, “more is better”. Similarly, in preclinical studies, research work with GL261 subcutaneous tumours in immunocompetent mice described an optimal immune-based regression achieved through a 6-day metronomic schedule of Cyclophosphamide (CPA) treatment. This 6-day repeating treatment schedule proved to trigger a strong, sustained CD8 + T-cell-dependent adaptive immune response and associated with long-term, tumour-specific anti-tumour immune memory [38][181][182]. Furthermore, the same authors also found that the optimal outcome of immune activation is mostly observed with the 6-day metronomic schedule, and such beneficial effects were not observed neither decreasing [183] nor increasing [181] the frequency of the chemotherapy administration. The underlying mechanism of this beneficial effect might be probably associated with the ca. 6-day cycle for immune cell recruitment in mouse brain [39]. In our group, we have coined a specific expression “Immune-enhancing Metronomic Schedule (IMS)” for this 6-day interval metronomic treatment schedule [169].

In previous work from our group, TMZ (60 mg/kg) administered in IMS improved the survival rate (38.7 ± 2.7 days) [168] in comparison with the standard “three cycles 5-2-2” administration schedule (33.8 ± 8.7 days) [160] in a reduced cohort of mice. Results obtained in this thesis with a larger cohort using the same dose and schedule (IMS-TMZ 60 mg/kg) achieved a significant better survival rate (298 ± 285 days) when compared to previous work [168]. The tumour volume at therapy starting day was not significantly different in both studies (5.4 ± 2.6 mm^3 vs 6.0 ± 1.2 mm^3), thus the difference observed is really surprising and should be attributed to other reasons. One possible explanation behind this significant improvement is the housing environment of mice, which may have an impact in the disease outcome. All mice studied in this thesis were allowed to endure 3 weeks of guaranteed housing in "Enriched Environment (EE)"-like caging before tumour generation and kept there from beginning to end, as opposed to our previous published work, in which EE was not contemplated. Literature evidence described that this EE-housing could modulate the NK cell

infiltration and anti-tumour activity in mice brain, thus consistently increasing the survival time of GB bearing mice[166]. In this sense, the improved outcome obtained with IMS-TMZ treatment in this thesis suggests that the IMS and EE-housing could play a cooperative role in improving the TMZ therapeutic effect of tumour-bearing mice.

Our results obtained from IMS-TMZ therapy is better than that reported by other authors. For example, in the same preclinical GB model, when TMZ was given with 5 consecutive days, the median survival time of treated mice was 30 days [170]. In another study, authors treated GL261 bearing mice with TMZ in both, standard way - 50 mg/kg for 5 consecutive days, and 25 mg/kg in a 10-day interval metronomic way, however, the maximum survival time of TMZ treated mice was no more than 50 days [171].

There are few studies with human GB and immune respectful cycles (see for example Brandes and col [184]). Fotemustine was used as a second line in patients that relapsed with the standard treatment, and a weekly schedule was established with promising results (6-8.5% PFS), although an interval time between TMZ and Fotemustine seems to be needed for better results.

Anti-tumour immune responses can be strongly stimulated by multimodal therapies targeting different aspects of cell killing. In our case, we aimed, on one hand, to induce immunogenic tumour cell damage while sparing replicating immune system cells (with IMS chemotherapy). On the other hand, we wanted to actively counteract the immune suppression microenvironment within the tumour (PD-1/PD-L1 pathway blockade). We have studied relapsing GL261 tumours treated with IMS-TMZ, and found that the upregulated PD-L1 content in tumour tissue could be a possible explanation for TMZ resistance (see details described in section 4.3). In this sense, we wondered whether the combination of IMZ-TMZ and PD-1 antibody in GL261 GB bearing mice, would produce more beneficial results in comparison with individual drug use. The results obtained in this thesis confirmed this possibility: the rate of cured animals with the combined therapy is as high as 100%, significantly higher than 0% (anti-PD-1) and 25%-60% (TMZ) of monotherapy. A synergistic effect is likely to result in enhanced survival of mice treated with combination therapy. One possible explanation is that PD-1 antibody blocked the PD-L1 binding to PD-1, strongly enhancing T cell proliferation and reducing the immunosuppressive effects in tumour microenvironment. Thus, the tumour cell sub-clones expressing high content of PD-L1 could

not supress anti-tumour immunity and failed to induce tumour escape. This is in line with work from other authors [141] which obtained 100% of cured mice with combination therapy, although with a different protocol of administration.

Another potential explanation is an intensification (synergism) of the anti-tumour effect taking place after a combined administration of TMZ and anti-PD-1 in IMS. The therapeutic effects of anti-PD-1 in GB have been reported to be associated with immune infiltration [185]. The most commonly used classifications for the patterns of immune cell infiltration include the "inflamed tumour" (tumour rich in tumour-infiltrating lymphocytes, “hot” tumour), the "immune-excluded" (presence of immune cells at the invasive margin but absence of immune cells at the centre of the tumour) and the "immune-desert " phenotype (absence of relevant immune cells at both the periphery and centre of the tumour, “cold” tumour)[186][187]. In our research, IMS-TMZ induced immunogenic cell death of tumour cells [188] which may trigger host immune system recruitment, and convert tumour microenvironment from an “immune desert (cold tumour)” to and “inflamed (“hot”) tumour”. This hypothesis is supported by previous results such as increased calreticulin (CRT) exposure after TMZ treatment in GL261 cells [188] and histopathological studies showing increase in microglia/macrophage in responding tumours after TMZ standard treatment [169]. Being this so, the tumour infiltrating lymphocytes action would be enhanced by the next turn of immune checkpoint inhibitor anti-PD-1 administration (see hypothetic schema in Figure 4.17) taking place 6 days later. Accordingly, during the second turn of combined therapy administration, the volume of all tumours in the combination therapy group decreased drastically, which could be used as an argument supporting the above mentioned hypothesis.

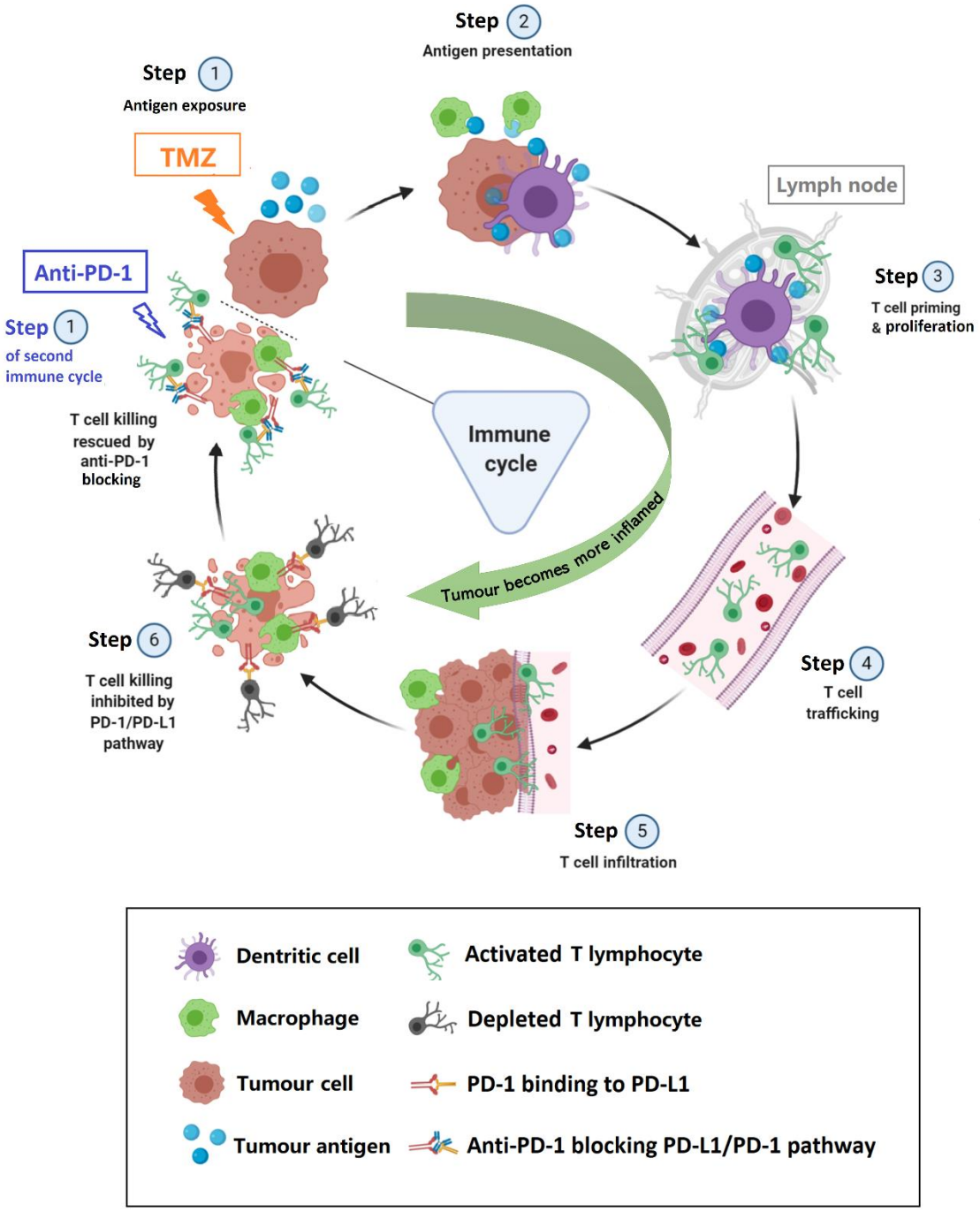

Figure 4.17 Hypothetic schema of the cycle for immune response against a preclinical GL261 GB tumour after two cycles of anti-PD-1/TMZ combined therapy. *The cancer-Immunity cycle is thought to last around 6 days in mouse brain and tumour microenvironment: when treated with combination therapy at day 1, tumour cells release and expose immunogenic signals which attract dendritic cells (DCs) and macrophages to the tumour site (Step 1 and 2). Initially, tumour cell killing/damaging mostly relies on the TMZ cytotoxic/cytostatic effect, the immune system is not*

especially active against these particular tumour cell clones. At days 3-5, primed DCs have migrated to the lymph nodes and prime naïve CD8+ effector T cells, which start to proliferate (Step3). At days 6 of the cycle, a new wave of effector T cells arrive to the tumour site and efficiently attack the tumour (Step 4-6). However, in this period, some tumour sub-clone cells and macrophages presenting an increased expression of PD-L1 may bind to PD-1 expressed by T cells to evade the immune system attack. At this critical juncture, anti-PD-1 administration from the next round of combination therapy (day 1 of next cycle) plays a key role to rescue and enhance the T lymphocytes killing ability.

4.1.4.2 *Relevance of tumour volume at therapy starting time and dosing schedule in anti-PD-1 monotherapy.*

When we treated GL261 GB bearing mice with anti-PD-1 monotherapy at the 100 µg dose, the therapeutic effect was not significantly different from that of the Isotype control group (23 ± 2.9 days vs 21.8 ± 3.3 days survival time), which was a disappointing result. Other authors had reported that anti-PD-1 at a higher dose and different schedule (500/250 µg) could significantly improve the long-term survival rate (50% mice survived over 100 days) [105]. Therefore, we moved to the higher dose (500/250 µg) of anti-PD-1 monotherapy with our GL261 GB bearing mice. From results described in section 4.1.3.2 it became evident that the tumour volume at therapy starting point was determinant in the outcome. Accordingly, we explored the impact of initial tumour size on therapy starting day with the new chosen dosage (500/250 µg from day 11 post-implantation) and found that the cure rate was significantly higher in the *small* initial tumour group when compared to the *large* initial tumour group (75 % vs 0 % long term survival). Some studies have pointed out that the tumour mass could probably hamper on its own immune system capability of the host [189] and in this context, our results are not surprising. Importantly, the main premise of cancer immunotherapy is to use/enhance the host immune system to attack the tumour cells. Thus, accurate initial tumour volume measurement at immunotherapy starting day is relevant to understand results and evaluate efficacy. However, most anti-PD-1 therapy studies in preclinical GB models focused on the starting time of administration rather than the initial tumour volume (Annex II), and even for the same preclinical model/cell line there could be variations in tumour development. Lacking this information may lead to a loss of accuracy and misinterpretation of the immunotherapy results in preclinical studies. Thus, determining the tumour volume before immunotherapy launch is very important in both preclinical development and clinical trials and would be strongly advised whenever possible. In our

hands, a suitable volume to start anti-PD-1 therapy with GL261 tumours is ca. 2.1 ± 1.1 mm^3, which finally lead to cure of 75% of animals, allowing ample time for evaluation of biomarker performance (section 4.2).

A second relevant question was related to timing in immunotherapy administration. We wondered whether the "every 3 days (E3D)" administration schedule described in [105] was more, less or equally efficient in comparison with "every 6 days (IMS)" for anti-PD-1 (500/250 µg). For that, the therapy starting day described in [105] was maintained for proper comparison, assuming that tumour volume would be similar enough in both cases since we use the same preclinical model. No significant difference in therapy efficacy was found between both groups (cured rate: 66.6% in E3D vs 60% in IMS), indicating that at least for this preclinical model, the same therapeutic effect would be obtained with less frequent administration. The mechanisms underlying here should be related to those previously described in section 4.1.4.1, the whole immune cycle usually takes about six days in the mice brain [39], thus the administration of anti-PD-1 therapy in consonance with this cycle would be more fruitful, while an application out of this window would not lead to increased efficacy, although no negative effect would be expected either. In other words, together with the strong dependence of immunotherapy on the host immune system, adequate synchrony with the host innate immune cycle may be a good strategy to maximize anti-PD-1 treatment effects. Moreover, while providing an equivalent anti-tumour efficacy, anti-PD-1 monotherapy applied with an IMS protocol allows us to reduce the cumulative amount of administered anti-PD-1, reducing the risk of development of dose-dependent autoimmune response [190]. Besides, mice survival rates (66.6% and 60%) we got from the high dosage (500/250 µg) anti-PD-1 treatment from day 6 p.i. were slightly better than Reardon et al [105] (50% long-term survival), and also better than another study, with anti-PD-1 given every 7 days [142](10% long-term survival).

4.1.4.3 IMS-TMZ, IMS-anti-PD-1/TMZ and anti-PD-1 monotherapy established varying degrees of long-term specific anti-tumour immunity.

In the present clinical landscape, patients with GB always relapse even after the best accepted therapeutic protocols are applied, including surgical resection. Accordingly, both response improvement and generation of tumour specific immunological memory would be crucial to improve prognosis. Thus, we tested how the different treatment modalities had an impact on

tumour recurrence after curing mice. A strong immune-memory effect (ca. 100% tumour rejection rate) is observed after GL261 tumour ablation with IMS-TMZ treatment or anti-PD-1 monotherapy, whereas a weaker anti-tumour immune memory capability (57% tumour rejection rate) was found in mice cured by anti-PD-1/TMZ combined therapy.

Alkylating agents such as CPA and TMZ have been described to induce immunogenic cell damage of tumour cells, further activating the immune system through the exposure and emission of damage-associated molecular patterns (DAMPs) [191][40][192][193]. However, as relevant as eliciting the immune system is avoiding impairing its amplification, and here the IMS gains importance. Alkylating agents, including TMZ, are known to induce side effects related to the immune system such as leukopenia and neutropenia, when administered daily [194]. If TMZ is administered in a continuous schedule, the anti-tumour immune cycle may be hampered due to the inhibition of the proliferation of immune cells, such as primed CD8+ T lymphocytes in proximal ganglia. On the other hand, in an every 6d metronomic administration schedule, TMZ would not interfere with the proliferation of immune cells, since each TMZ dose is administered after completion of the amplification step fostered by the previous therapeutic agent administration. In each time point of therapy administration, tumour cells are damaged, antigens presented to immune system cells and specific clones of lymphocytes arrive to the tumour milieu (figure 4.17). The sustained response could generate specific long-term anti-tumour immunity. Whereas all control, vehicle-treated mice developed rapidly growing GL261 tumours, 7/8 IMS-TMZ-cured mice resisted secondary re-challenge tumour development. Our preliminary findings in this indicate that anti-tumour immunological memory is established by the host immune system of IMS-TMZ cured mice. Previous unpublished work from our group showed that TMZ effect on GL261 tumour cells in vitro produces immunogenic cell damage [188] and this may be also taking place in vivo. Still in this respect, we cannot ignore that GL261 is a moderately immunogenic cell line [132]. Thus, a basal part of its response to therapies may be helped by this basal immunogenicity. Nonetheless, it seems clear that this basal immunogenicity alone is not able to make C57BL/6 mice resistant to GL261 GB growth, in the absence of therapy (Figure 4.5 control group). IMS-TMZ promotes very good overall response, with long-term therapeutic effects through generation of immunological memory with concomitant prevention of tumour relapse in 88% of the mice analysed in this thesis reaching 100% with only one additional therapy those upon

relapse. Wu and Waxman [38] found an increased number of CD8+ T cells and decreased number of circulating macrophages and MDSCs populations in cured mice treated with "metronomic" IMS-like CPA treatment, which rejected the GL261 tumour on re-challenge. In this sense, further work will be needed to explore the actual mechanism of anti-tumour immune memory in our system; thus, assessment of different immune populations could be performed in mice that rejected the re-implanted GL261 tumours compared to control tumours. It would be also of great interest to know which of the tumour antigens are responsible for the generation of the adaptive immune response, which could be helpful in case a future vaccination studied was planned.

One exciting feature of immunotherapy is its ability to conduct a dual-phase therapeutic benefit, which initially involves effective treatment of existing tumours, followed by a successful activation of tumour-specific immune response to fight a possible tumour recurrence. In a clinical study, Ribas and colleagues [195] analysed 102 tumour biopsies obtained from 53 patients treated with an PD-1 antibody (pembrolizumab) by multicolour flow cytometry. They found that PD-1 blockade therapy enhances the proliferation of T cells, B cells, and myeloid-derived suppressive cells (MDSCs) in the tumour site, being CD8+ memory T cells the main T-cell phenotype in patients with therapy response. In this sense, anti-PD-1 monotherapy in our study, which probably helped to generate a potent memory CD8+ T cell thus effectively (88-100% tumour rejection rate) would probably protect cured mice from tumour re-challenge. Moreover, some preclinical studies also reported that anti-PD-1 monotherapy could induce anti-tumour immunological memory in C57BL/6 immunocompetent mice bearing the GL261 tumour [105], [141].

Interestingly, weaker anti-tumour immune memory capability (i.e. 57-88% tumour rejection rate) was found in mice cured by anti-PD-1/TMZ combined therapy. Three of 7 re-implanted tumours in these cured mice grew after 6 days, although two of them disappeared immediately after repeated IMS-type therapy application. The kinetics of tumour growth after the re-challenge experiment was slower in these tumour-recurrence mice compared to control mice (mice whose GB tumour grew after re-challenge were shown to be easier to be cured after treatment re-instated), suggesting that combination therapy had been able to generate at least partial immune memory. Combination therapies are reported in literature with different outcomes. Authors in [141] reported that favourable immunological effects of

anti-PD-1 therapy were abrogated when TMZ was administered 5 days in a row before anti-PD-1 therapy administration. In their studies, the anti-tumour immunological memory was only observed with mice treated with anti-PD-1 monotherapy, which agrees with results described in this thesis. However, in our work even the combination therapy was able to mount some immune memory although at a lower rate (50%). These results support the concept of IMS-TMZ as an immune respectful administration protocol: in our case, TMZ did not abrogate the immunological memory provided by anti-PD-1. Furthermore, in another study [111], authors found that the anti-tumour immunity caused by anti-PD-1 therapy was abrogated by chemotherapy when the latter was administered in a systemic way (intraperitoneal injection in their case), with decreased immune memory in long-term survivors. However, when chemotherapy was administered locally (intra-tumoural), it allowed for persistent immunologic memory generated by anti-PD-1 therapy. This provides us new enlightenment for the combination therapy that is worth considering. In future research, we should not only focus on the therapy administration schedule but also consider different ways of chemotherapy delivery. We should expect that the right therapy combination and the preservation of host immune system functions, will result in improvement of GB outcome, probably even curing some cases, provided they are diagnosed at a relatively early stage, or, perhaps, therapy is given in a neoadjuvant fashion, prior to surgery [196]. The generation of immunity against same or similar clones of tumour would be an added and desirable result which may surely improve quality of life and progression free survival in GB patients.

4.1.5 Conclusions

- IMS-TMZ significantly improved survival in GL261 GB bearing mice in comparison with standard TMZ treatment, confirming and surpassing results previously reported by our group, even curing 61.5 % of the treated mice (average survival 298 ± 285 days). The "Enriched Environment (EE)"-like caging before tumour generation may be one of the reasons explaining the outstanding results and should be maintained in further studies.
- As expected, the combination of TMZ with anti-PD-1 immunotherapy even using low doses (100 μg/day), both in IMS administration, showed a great beneficial effect (100% cure), with much better therapeutic effect than monotherapies administration (0%-

75% cure) and may be considered for both preclinical and clinical translational studies. However, low doses of anti-PD-1 alone did not produce the previous described effect, and survival was not better than isotype-administered mice.

- Anti-PD-1 monotherapy was effective when applied at higher doses (500/250 µg) with protocols described in the literature for the same preclinical model. However, a word of caution may be raised regarding tumour volume at therapy starting point: smaller tumour volumes (2.1 ± 1.1 mm^3) will have much better response than larger ones (9.6 ±2.2 mm^3). In this sense, accurate measurement of tumour volume at immunotherapy starting day will be extremely important for efficacy evaluation in comparative work.
- No difference in survival was found while applying the anti-PD-1 (500/250 µg) every 3 days or every 6 days (66.6% vs 60%). This would be probably linked to immune system cycle length (ca. 6 days) and that most of the beneficial effects would be seen at this time frame, with no or few added benefits from an additional administration in the middle at 3 days. IMS protocols in this case will consume less therapeutic agent and reduce animal stress, with similar outcomes.
- The IMS treatment was able to raise strong immune memory effects in cured GL261 GB-bearing mice either with IMS-TMZ treatment or anti-PD-1 monotherapy (both 100% final rejection rate). The combination of anti-PD-1/TMZ, although was able to cure 100% of the studied mice, seemed to induce a weaker immune memory response (57% rejection rate), although 2 tumours disappeared after 1 additional cycle of therapy 88% final rejection rate). Further work will be needed to assess the different immune populations in cured mice after GL261 tumour cell re-challenge and to study the detailed mechanisms behind the generation of immune memory.

4.2 MRSI-BASED NOSOLOGICAL IMAGES IN GLIOBLASTOMA THERAPY MONITORING: AN OSILLATORY PATTERN COULD ACT AS IMMUNE SYSTEM EFFICACY BIOMARKER

4.2.1 Context and specific objectives

Magnetic resonance imaging (MRI) plays a crucial role in GB detection, treatment planning, and therapy response assessment, detecting tumour presence, size and characteristics in a non-invasive way [197]. MRI provides anatomical information and information about contrast enhancement or biophysical characteristics such as perfusion. On the other hand, magnetic resonance spectroscopy, or its multivolume variation, spectroscopic imaging (MRSI) provides additional information about millimolar concentrations of low molecular weight metabolites in studied tissue [198][199], which can inform about its biochemical/molecular environment. Previous studies from our group suggest that proper analysis of such metabolomic information could give hints about tumour response before changes observed in tumour size [151][158].

In previous studies from our group, the pattern recognition analysis of multi-slice MRSI technique, has allowed us to observe ca. 6 days period TRI (Tumour Responding Index, see definition and details in section 3.4.2) oscillations in GL261-tumour bearing mice treated with standard “three cycles” TMZ treatment [158]. In other words, the metabolomic pattern of the tumour showed a trend of oscillatory changes between response/non-response patterns while no significant changes were seen in tumour size measured by MRI. Our hypothesis was that local tissue effects triggered by the immune system could cause these changes in the metabolomics pattern. Some literature evidences support this hypothesis. It has been described that treatment with alkylating agents (e.g., TMZ) trigger the host immune system recruitment, eventually leading to tumour cell damage/death [191]. The whole immune cycle in mice brain usually requires around six days as already reported by others [39], which would be in agreement with the oscillation period found in our previous studies [158]. In the previous chapter, we have described the application of an “Immune-Enhancing Metronomic Schedule” (IMS) in therapeutic protocols [169], based in previous work from others [38] in which chemotherapy with consecutive cycles every 6 days in preclinical models triggered immune system activation. We have demonstrated that when TMZ and anti-PD-1 are administered in IMS alone or in combination, the survival rate of GL261 GB afflicted mice was significantly improved, and a certain degree of tumour-specific immune memory was

observed in all groups. These results suggest with the proposal that the host immune system is involved in tumour response processes. Since our previous MRSI studies suggested that the metabolomic pattern changes could be linked to local immune system effects, acting as a surrogate biomarker of therapy response through attack by the host immune system, we wondered whether the application of this non-invasive MRSI approach in our IMS therapeutic strategies would be indicative of these effects. Until now, the MRSI-based surrogate biomarker and the calculation of the TRI was only carried out with chemotherapeutic approaches. Studying the presence and behaviour of the surrogate biomarker in absence of chemotherapy, i.e. using chemo-immunotherapy combination or only immunotherapy, would be a consistent indicative that the metabolomic pattern changes are indeed linked to changes in immune system presence/action within the tumour, independently of the triggering agent used.

Consequently, our goals in this section were:

- To confirm the presence of 6-day frequency oscillations in the tumour responding index during IMS-TMZ treatment of GL261 GB mice in a large cohort of animals, and compare it with previous results from our group with the standard TMZ administration protocol.
- To explore whether such oscillatory pattern of therapy response is maintained, changed or abolished in GL261 GB treated with IMS-anti-PD-1/TMZ combination therapy and IMS-anti-PD-1 monotherapy.

The TMZ-related part of this work was recently published in NMR in Biomedicine [169].

4.2.2 Specific materials and methods

Mice mentioned in this section are part of the mice already described in section 4.1, which means they were not only followed-up by MRI for tumour volume detection, but also analysed by MRSI during their longitudinal survival experiment. Namely, n=10 mice from the IMS-TMZ group (C1263, C1276, C1264, C1281, C1270, C1285, C1380, C1286, C1383 and C1382), n=6 mice from the IMS-vehicle group (C1258, C1260, C1261, C1359 and C1360), n=1 mouse from the IMS-anti-PD-1/TMZ combination group (C1446) and n=3 mice from the IMS-anti-PD-1 monotherapy group (C1479, C1480 and C1484).

In this section, when tumour volumes of mice were not large enough to confidently perform MRSI segmentation, we defined it entering, or being in, the "below threshold detection period" (BTDP).

4.2.2.1 Multi-slice MRSI-based analysis of GL261 tumour treated with IMS-TMZ therapy

As mentioned before, the usual $1X10^5$ GL261 cells were stereotactically implanted intracranially in C57BL/6 mice. Mice were weighted twice a week and tumour volumes were followed using T2-weighted MRI acquisition after implantation; tumour volumes on day 11 p.i. were calculated. Mice with most homogeneous weights and tumour sizes were chosen to compose the experimental group, and therapy was launched. IMS-TMZ (60 mg/kg) was administered to n = 10 tumour-bearing mice using an oral gavage, every 6 days, from day 11 post inoculation (p.i.), while control mice (n = 6) received 10% DMSO vehicle. MRI studies were performed at least twice a week to monitor tumour volume evolution. Meanwhile, 3D MRSI acquisitions were performed every two days. The start of MRSI explorations was conditioned by the measured tumour volume. Technical details of MRSI acquisitions can be found in section 3.4.2. According to our experience and data described by our group [159], tumour volumes below 20 mm^3 are not properly segmented by MRSI, and this was the cut-off point to start MRSI acquisitions. Mice distribution is shown in Table 4.5, while the therapeutic and MRSI acquisition scheme is detailed in Figure 4.18.

Treatment	***IMS-TMZ***		***IMS-Vehicle***
Mice code	C1263	C1276#	C1258
	C1264	C1281#	C1260
	C1270	C1285#	C1261
	C1380	C1286#	C1359
	C1383	C1382#	C1360
Number of animals	10		6
MR data	MRSI/MRI		

Table 4.5 Table illustrating mice distribution in IMS-TMZ and IMS-vehicle group. # means cured cases.

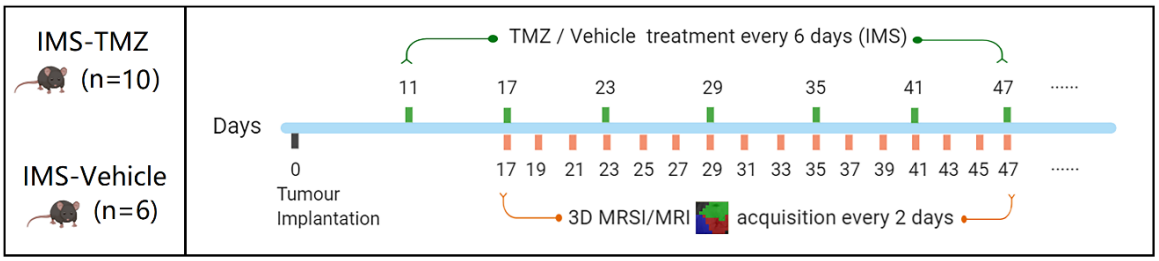

Figure 4.18 Therapeutic schedule and MRI/MRSI acquisition scheme used in this study.

All mice were allowed to endure 3 weeks of guarantee housing in "enriched environment"-like caging before tumour generation and were maintained there along the whole study. During the therapeutic period, mice were followed according to the supervision parameters for animal health status and weighted. Animals meeting endpoint criteria were euthanized by cervical dislocation according to the animal welfare protocol, the brain was removed, and tumour resected.

4.2.2.2 Multi-slice MRSI-based analysis of GL261 GB treated with IMS-anti-PD-1/TMZ combination therapy and IMS-anti-PD-1 monotherapy.

Assessing the presence of TRI oscillations in presence of immunotherapy (combined or alone) was envisioned to check whether the metabolomic pattern changes were maintained, changed or abolished. On the other hand, confirming its presence would reinforce the potential of our biomarker and its oscillatory behaviour to be used as a surrogate of immune system activity against tumours.

Thus, we performed a preliminary assessment with IMS-anti-PD-1/TMZ and IMS-anti-PD-1 monotherapy treated mice. Mice distribution is shown in Table 4.6

The usual $1X10^5$ GL261 cells were stereotactically implanted in C57BL/6 mice. Mice were weighted twice a week and tumour volumes were followed using T2-weighted MRI acquisition at day 6 and day 11 after implantation, then tumour volumes were calculated.

Treatment	***IMS-anti-PD-1/TMZ***	***IMS-anti-PD-1***
Mice code	C1446[#]	C1479 C1480[#] C1484
Number of animals	1	3

MR data	MRSI/MRI

Table 4.6 Table illustrating mice distribution in IMS-anti-PD-1/TMZ and IMS-anti-PD-1 group. # means cured cases.

In IMS-anti-PD-1/TMZ combination therapy group, mouse C1446 bearing the most suitable tumour size (6.35 mm^3 on day 11 p.i.) for MRSI segmentation was chosen to perform this study, and therapy was launched.

Therapeutic and MRSI acquisition scheme is shown in Figure 4.19. C1446 was given TMZ (60 mg/kg) by intragastric administration in the morning and anti-PD1 (100 µg /day) via intra-peritoneal injection in the late afternoon. Both were administered in IMS (every 6 days) from day 11 p.i. until tumour shrinkage to a stable scar or escape from therapy.

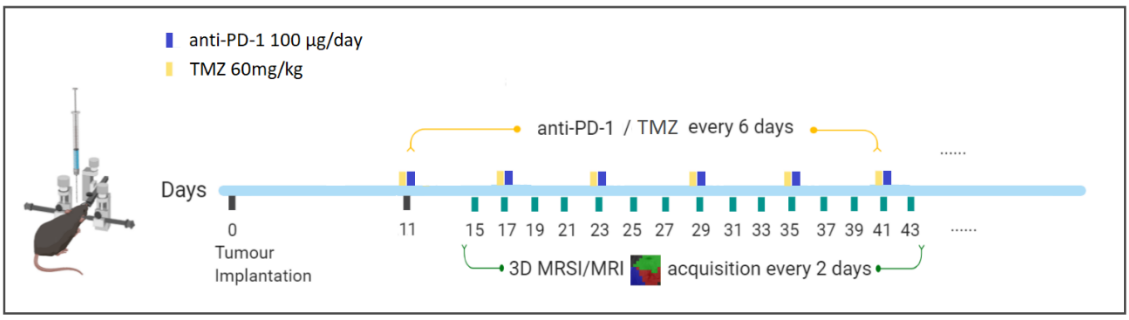

Figure 4.19 Therapeutic schedule and MRSI acquisition scheme used in this study.

Meanwhile, 3D MRSI acquisitions were performed every two days, starting at day 15 post-implantation. MRSI data was post-processed, then the obtained nosologic image was superimposed to the corresponding T2w image to calculate the Tumour Responding Index (TRI). Note that MRSI acquisitions were forced to be stopped from day 25 p.i. since C1446 tumour had shrunk down to a 2.73 mm^3 scar, entering the "below threshold detection period" (BTDP), i.e. not enough tumour volume to perform MRSI segmentation.

In the IMS-anti-PD-1 monotherapy group, mice with most homogeneous weights and tumour sizes (volume at day 6 p.i. ca. 0.4 mm^3) were chosen to compose the experimental group, and therapy was launched. Therapeutic and MRSI acquisition scheme is shown in Figure 4.20. PD-1 antibody was administered via intra-peritoneal injection beginning on day 6 p.i. (500 µg/dose) repeating injections every 6 days (250 µg/dose) until tumour escape from therapy or tumour disappearance.

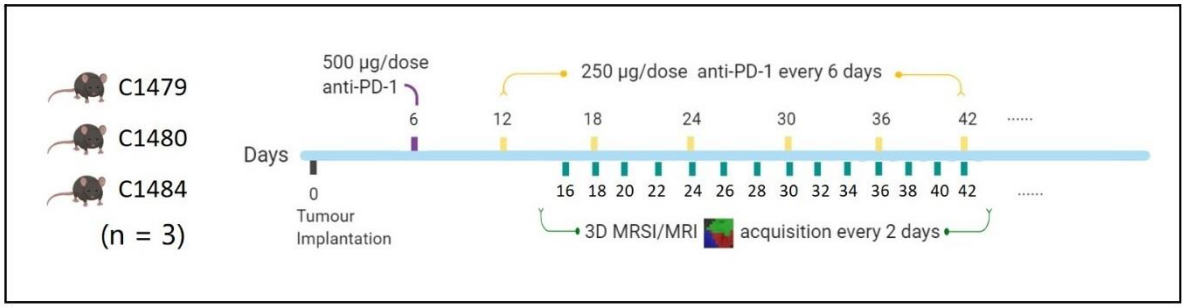

Figure 4.20 Therapeutic schedule and MRSI acquisition scheme used in this study.

MRI studies were performed at least twice a week to monitor tumour volume evolution. Meanwhile, 3D MRSI acquisitions were performed in 3 cases (C1479, C1480 and C1484) every two days, starting at day 16 post-implantation. During the therapeutic period, mice were followed according to the supervision parameters for animal health status and weighted. All mice were allowed to endure 3 weeks of guarantee housing in "enriched environment"-like caging before tumour generation, and were maintained there from beginning to end.

4.2.3 Results

4.2.3.1 Multi-slice MRSI-based volumetric analysis of therapy response assessment under IMS-TMZ treatment

A longitudinal study was performed with ten IMS-TMZ-treated GL261 tumour-bearing mice and six vehicle treated mice (see Table 4.5 for individual mice codes). Mice were studied every two days until endpoint, and the start of MRSI explorations was conditioned by the measured tumour volume. Results are summarized below.

IMS-TMZ-treated mice

The relationship between TRI and tumour volume evolution, as well as the corresponding nosological images of five most representative cases of TMZ treated mice are shown in Figure 4.21.

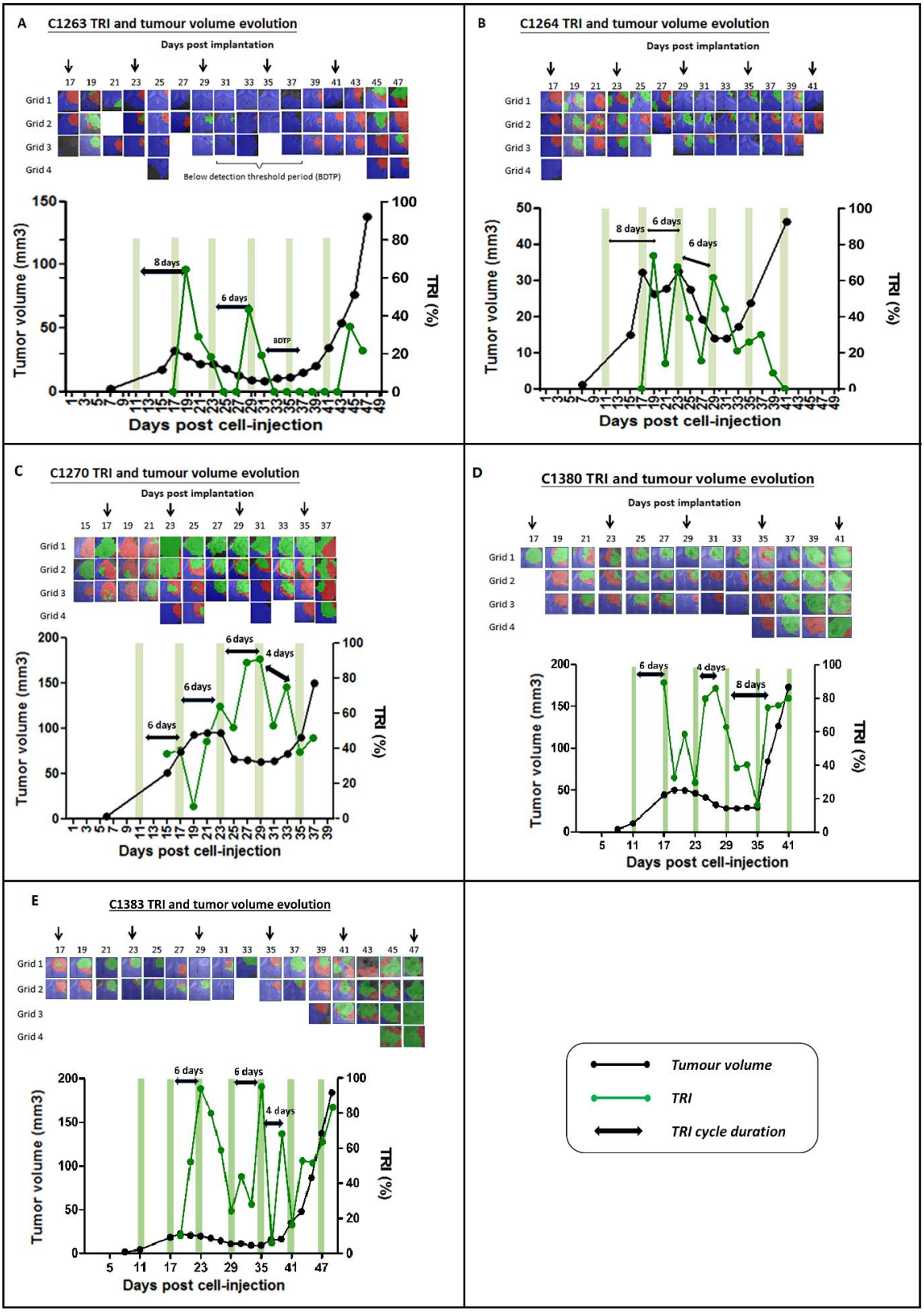

Figure 4.21 Nosological images and graphical representation of the tumour volume evolution for the tumour region in the cases (A) C1263, (B) C1264, (C) 1270, (D) C1380 and (E) C1383. *Tumour volume in mm^3 (black line, left axis) and the percentage of green, responding pixels (TRI)*

obtained taking into account total tumour pixels counting (green line, right axis). In the upper part of every image, chosen time points show the evolution of the nosological images in four rows of colour-coded grids superimposed to the T2w-MRI for each slice. Vertical arrows indicate days of therapy administration. In the bottom graphs, green shaded columns indicate TMZ administration days. TRI cycle duration (therapy administration to next peak maxima) is highlighted in every image. In (A), from days 31 to 37 it was not possible to evaluate TRI evolution because tumour volume was below the detection threshold period (BTDP). TRI peaks appear after TMZ administration time points with a frequency of 6.0 ± 1.3 days (n =5 mice with n = 15 total cycles counted).

In these five cases (C1263, C1264, C1270, C1380 and C1383), TRI peaks appear after TMZ administration time points with a frequency of 6.0 ± 1.3 days (n =5 mice with n = 15 total cycles counted), in agreement with values (6.3 ± 1.3 days) reported in [158]. Eventually, tumours escaped from therapy and met animal endpoint criteria, leading to the euthanasia of the mice. During this relapse, which started between days 35-41, either TRI cycles were not found anymore, or this value was no longer reliable. When the slope of the tumour growth increased dramatically or tumour relapsed beyond volumes of ca. 50 mm^3, TRI do not seem to suggest response, even if oscillating features are seen. Moreover, the combination of high tumour volume (>70mm^3) and relatively low TRI (e.g. C1270, TRI < 40%) resulted in bad survival outcome in comparison with other cases, and tumour grew uncontrolled until the second TRI oscillation appearance.

Additional cases from IMS-TMZ-cured mice

For mice with full MRI/MRSI follow-up, five of the TMZ treated mice analysed (C1276, C1281, C1285, C1286 and C1382) had tumours which disappeared after IMS-TMZ treatment, which obviously prevented the generation of nosological images. Still, tumour volume and TRI evolution of these mice are shown below (Figure 4.22).

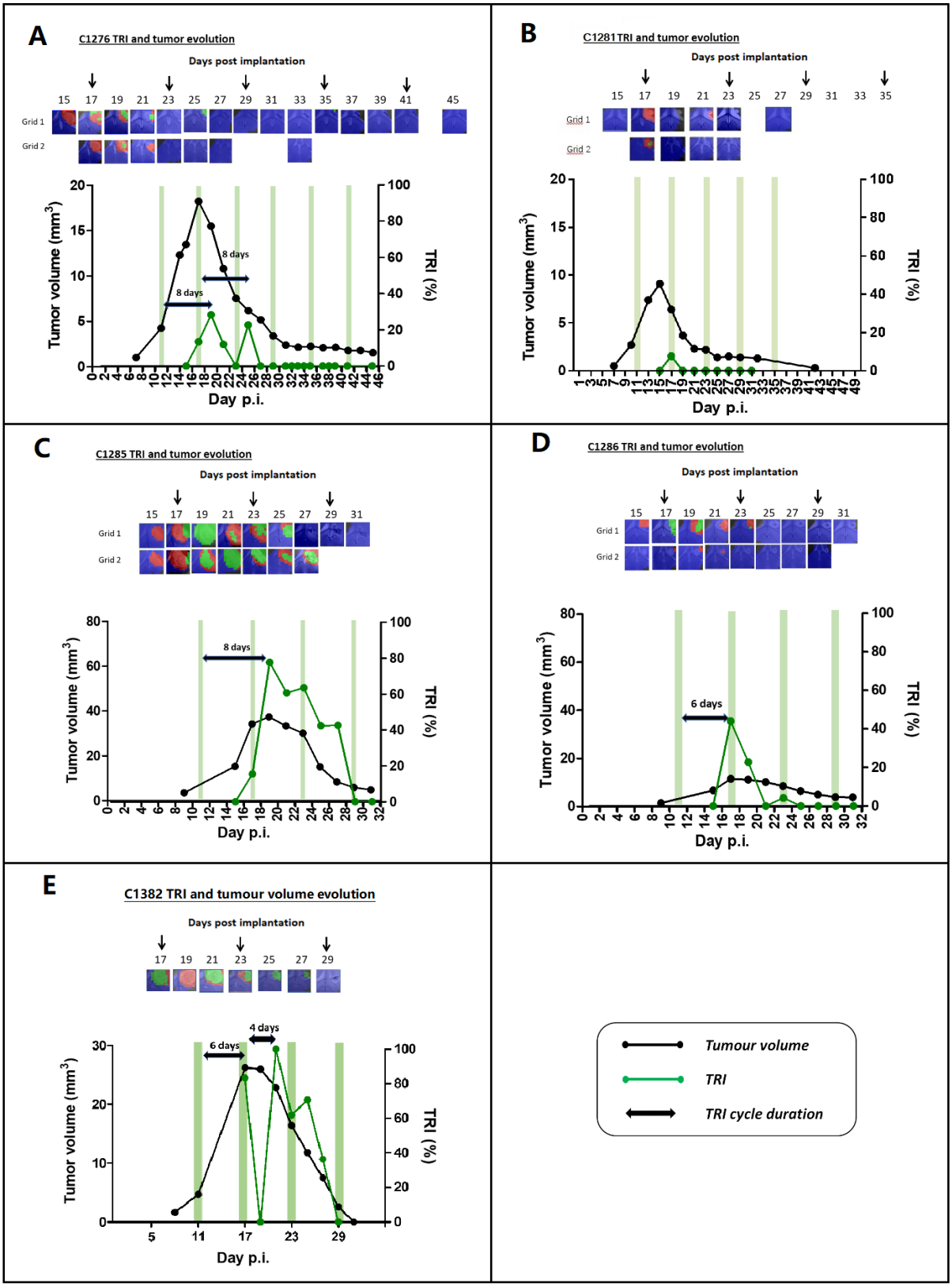

Figure 4.22 Nosological images and graphical representation of the tumour volume evolution for the tumour region in cases (A) C1276, (B) C1281, (C) C1285 (D) C1286 and (E) C1382 of "cured" animals. *Tumour volume in mm³ (black line, left axis) and the percentage of green, responding pixels (TRI)*

obtained taking into account total pixels counting (green line, right axis). In the upper part of every image chosen time points show the evolution of the nosological images in two rows of color-coded grids superimposed to the T2w-MRI for each slice. In bottom graphs, green shaded columns indicate TMZ administration days.

As in other TMZ-treated mice, TRI oscillations or punctual increases could be found for most cases. For example, in the first days of MRSI monitoring, TRI cycles were found in four out of five cases. After that time, the relationship between tumour volume evolution and TRI changes was different in every case.

The maximum volume achieved in this group was 37.4 mm^3, and tumour volume decrease was observed around the second TMZ therapy dose, lasting until ca. day 30 p.i. For cases with enough volume for nosological imaging segmentation, oscillations were seen during active response. For example, case C1276 (Figure 4.22 A) showed TRI oscillations from days 17 till 27 p.i., when the tumour was classified either as SDi or PRe. Case C1285 presented TRI oscillations at days 17 and 21 p.i., followed by a gradual decrease which concurred with tumour disappearance.

Regarding all IMS-TMS treated cases with complete follow-up, a total of 53 doses of TMZ were given, resulting in 26 TRI oscillation peaks, 21 of them corresponding with tumour growth arrest or volume decrease, whereas 5 TRI peaks were no longer able to coincide with controlled tumour growth (almost exclusively at relapsing time points). In addition, 8 TMZ doses corresponded to periods in which tumour volume were below the minimum volume for nosological imaging segmentation while 2 TMZ doses corresponded to endpoint with no further explorations made.

It is worth mentioning that TRI peaks appear ca. 6-8 days after the first therapy administration period. The only case which delayed this appearance – 12 days, but only 6 days after the second therapy dose, C1383– could be attributed to segmentation problems due to borderline tumour volume between therapy cycles one and two. For all followed tumours, the first TRI peak agreed with a certain decrease in the tumour growth slope.

IMS-Vehicle-treated mice

Six IMS-vehicle-treated mice were analysed for comparison purposes (Figure 4.23).

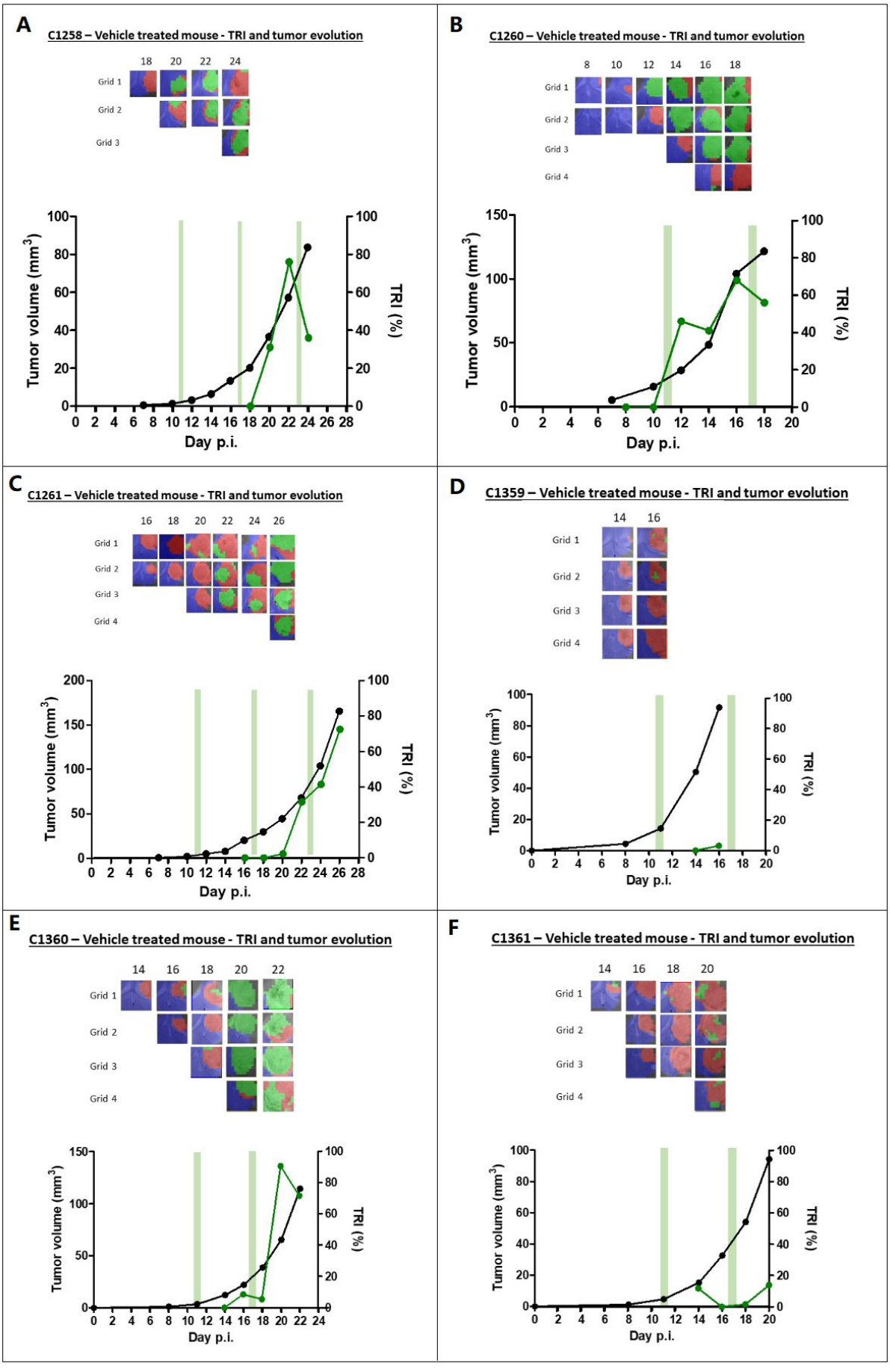
A
C1258 – Vehicle treated mouse - TRI and tumor evolution
18 20 22 24
Grid 1
Grid 2
Grid 3
Tumor volume (mm3)
TRI (%)
Day p.i.
B
C1260 – Vehicle treated mouse - TRI and tumor evolution
8 10 12 14 16 18
Grid 1
Grid 2
Grid 3
Grid 4
Tumor volume (mm3)
TRI (%)
Day p.i.
C
C1261 – Vehicle treated mouse - TRI and tumor evolution
16 18 20 22 24 26
Grid 1
Grid 2
Grid 3
Grid 4
Tumor volume (mm3)
TRI (%)
Day p.i.
D
C1359 – Vehicle treated mouse - TRI and tumor evolution
14 16
Grid 1
Grid 2
Grid 3
Grid 4
Tumor volume (mm3)
TRI (%)
Day p.i.
E
C1360 – Vehicle treated mouse - TRI and tumor evolution
14 16 18 20 22
Grid 1
Grid 2
Grid 3
Grid 4
Tumor volume (mm3)
TRI (%)
Day p.i.
F
C1361 – Vehicle treated mouse - TRI and tumor evolution
14 16 18 20
Grid 1
Grid 2
Grid 3
Grid 4
Tumor volume (mm3)
TRI (%)
Day p.i.

Figure 4.23 Nosological images and graphical representation of the tumour volume evolution for the tumour region in the vehicle treated cases (A) C1258, (B) C1260, (C) C1261, (D) C1359, (E) C1360 and (F) C1361. *Tumour volume in mm^3 (black line, left axis) and the percentage of green, responding pixels (TRI) obtained taking into account total pixels counting (green line, right axis). In the upper part of every image chosen time points show the evolution of the nosological images in two rows of color-coded grids superimposed to the T2w-MRI for each slice. In bottom graphs, green shaded columns indicate TMZ administration days.*

The TRI oscillatory pattern is not observed in any of the cases, except in the C1258, where a possible TRI cycle is observed, although tumour growth slope did not show any decrease. In the remaining 5 cases, no TRI cycles were observed, suggesting that clear TRI oscillations are only observed when tumour-bearing mice respond to IMS-TMZ treatment.

TRI oscillations were generally coincident with response

Several TRI oscillations were observed in the TMZ-treated mice and these were generally coincident with SDi and PRe tumour stages (Table 4.7), according to the adapted RECIST criteria (described in section 3.4.2). Oscillations were observed between days 17 and 39 p.i. depending on the case observed. It is worth mentioning that in the first MRSI time points (days 15-19 depending on the case), where the evolution tumour would be also classified as PD, TRI oscillations can already be seen. On the other hand, at last stages of the disease (PD, tumour escaping from therapy), the oscillations are no longer detected.

Case	Day p.i.	TRI behaviour	Classification of according to RECIST criteria
C1263	17-19	TRI cycles	Stable disease
	21-31		Partial Response
	33-47	BTDP and no cycles	Progressive disease
C1264	17	TRI cycles	Progressive disease
	19-31		Stable disease
	33-35		Progressive disease
	37	No cycles	Stable disease
	39-41		Progressive disease
C1270	15-19	TRI cycles	Progressive disease
	21-23		Stable disease
	25-31		Partial Response
	33		Stable disease

	35-37	No cycles	Progressive disease
C1276	15-17	TRI cycles	Progressive disease
	19		Stable disease
	21-27		Partial Response
C1281	15-17	No cycles	Stable disease
	19-27		Partial Response
C1285	15-17	TRI cycles	Progressive disease
	19-23	Unclear	Stable disease
	25-31	No cycles	Partial Response
C1286	15-17	TRI cycles	Progressive disease
	19-21		Stable disease
	23-31	No cycles	Partial Response
C1380	11-17	TRI cycles	Progressive disease
	19-25		Stable disease
	27-35		Partial Response
	37-41	No cycles	Progressive disease
C1382	17	TRI cycles	Progressive disease
	19-21		Stable disease
	23-29	No cycles	Partial Response
C1383	17	TRI cycles	Progressive disease
	19-25		Stable disease
	27-35		Partial Response
	37-49	TRI cycles / unclear	Progressive disease

Table 4.7 Evolution of the TMZ treated GL261 cases considering TRI and tumour volume changes over time. *Classification of adapted RECIST criteria were applied as described in section 3.4.2.*

The tumour evolution in control (vehicle treated) group was classified as PD throughout the period of MRSI analysis (Table 4.8), as expected. Among 6 mice, only one possible TRI behaver was observed.

Case	Day p.i.	TRI behaviour	Classification of RECIST criteria
C1258	18-24	One TRI cycle	Progressive disease
C1260	8-18	No cycles	Progressive disease

C1261	16-26	No cycles	Progressive disease
C1359	14-16	No cycles	Progressive disease
C1360	14-22	No cycles	Progressive disease
C1361	14-20	No cycles	Progressive disease

Table 4.8 Evolution of the vehicle-treated cases considering TRI and tumour volume changes over time. *Classification of adapted RECIST criteria were applied as described in section 3.4.2.*

The gathered data confirmed the oscillatory frequency of TRI (i.e. changes in the percentage of tumour area showing mostly metabolomics MRSI spectral pattern indicative of response), initially observed with the standard 5-*2-2* TMZ administration protocol [158]. The periodicity of oscillations was 4-8 **days (6.2 ± 1.4 days) which agrees** with the oscillations (6.3 ± 2.0 days and 6.3 ± 1.3 days) in previous work [151], [158] and is mostly related with periods in which tumour volume was stable or decreasing. These spectral pattern changes reflect local changes that are not being spotted by the MRI information, which is essentially stable during SDi periods, or showing a decreasing trend during PRe. Such information can be of great interest for tumour monitoring and early information about response. The next step would be to investigate whether this TRI behaviour was maintained while adding anti-PD-1 immunotherapy to TMZ or, more interestingly, while using only immunotherapy. Since no differences were seen where anti-PD-1 immunotherapy was administered every 3 or every 6 days (IMS), the IMS protocol was chosen for the MRSI analysis.

4.2.3.2 Multi-slice MRSI-based volumetric analysis of therapy response assessment under IMS-anti-PD-1/TMZ combined treatment or IMS-anti-PD1 monotherapy

A longitudinal study was performed with n=4 mice: one IMS-anti-PD-1/TMZ treated GL261 tumour-bearing mouse and three IMS-anti-PD-1 treated mice (see Table 4.6 for individual codes). Mice were studied every two days until endpoint, and the start of MRSI explorations was conditioned by the measured tumour volume. Results are summarized below.

IMS-anti-PD-1/TMZ treated mouse

As a representative case from IMS-anti-PD-1/TMZ combination therapy group, C1446 was analysed by MRI and multi-slice 3D MRSI from day 15 until day 23 post-implantation. Therapy

was administered at days 11, 17 and 23 p.i. right after MRSI analysis, and continued to be given in IMS until the animal was considered cured (day 41 p.i.). The relationship between TRI and tumour volume, as well as the corresponding nosological images, are shown in Figure 4.24.

In case C1446, TRI increased from 0% at day 15 p.i. to 74.2 % at day 19 p.i. and at day 23 TRI decayed to 0 % again. After this period, the tumour entered a BTDP period, then only one TRI peak could be observed. It is noteworthy that the tumour volume of C1446 reached the maximum size on day 17 p.i., when responding tumour pixels started to be observed. Along with the presence of TRI peak, the tumour volume dropped 78.9 % of its maximum between day 17 p.i. and day 23 p.i., probably due to the combined action of TMZ and immune system attack onto tumour during this shrinkage. The outstanding effectiveness of the treatment prevented us to observe further TRI cycles, but the appearance of a TRI maximum at day 8 is within the range of values observed for IMS-TMZ oscillation periods.

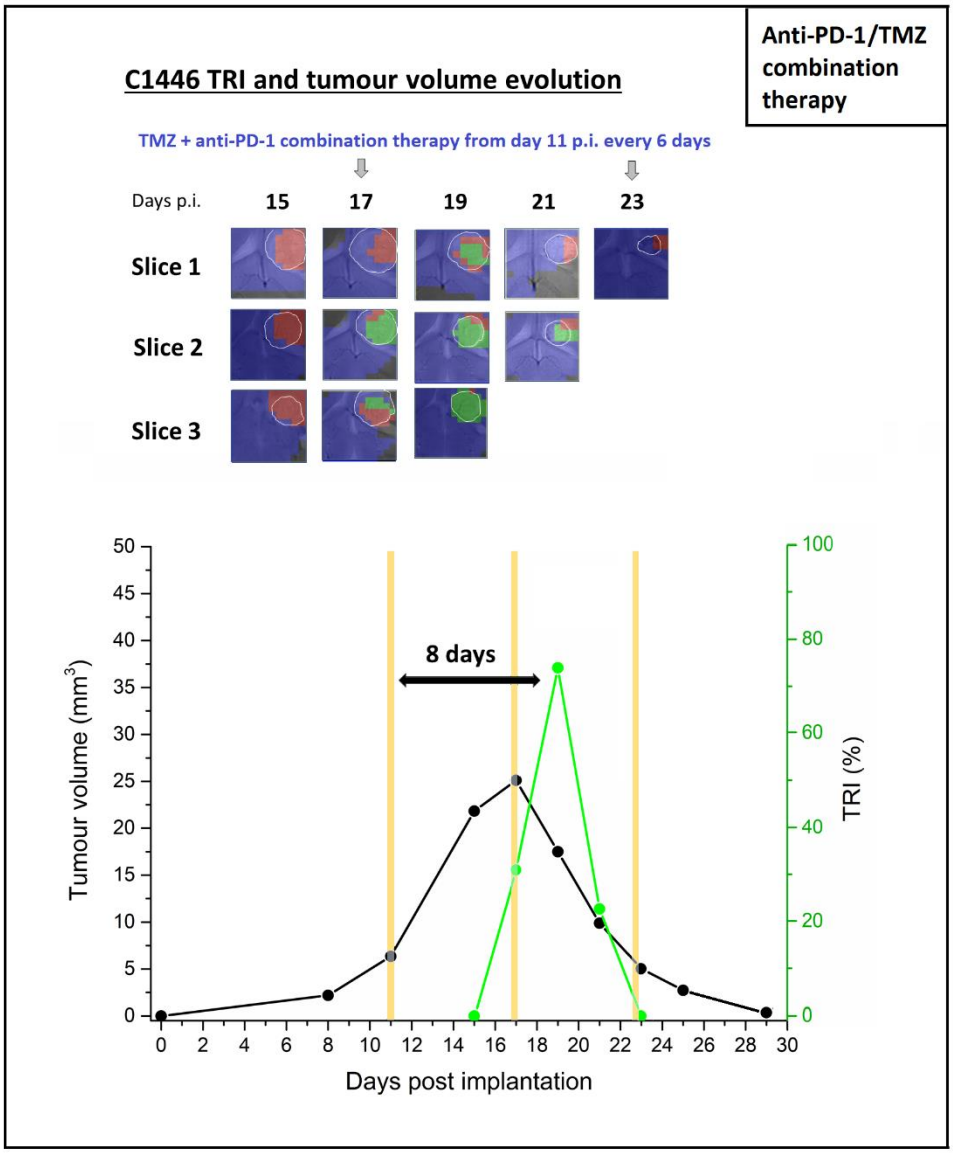

Figure 4.24 Nosological images and graphical representation of the tumour volume evolution for the tumour region in the case C1446. *Tumour volume in mm³ (black line, left axis) and the percentage of green, responding pixels (TRI) obtained taking into account total pixels counting (green line, right axis). In the upper part of every image, chosen time points show the evolution of the nosological images in three rows of colour-coded grids superimposed to the T2w-MRI for each slice. Vertical arrows indicate days of therapy administration. In the bottom graph, yellow columns indicate* anti-*PD-1/TMZ combination therapy administration days. TRI cycle duration (therapy administration to next peak maxima) are highlighted in the image. TRI peak appears 8 days after the first round of TMZ administration.*

IMS-anti-PD-1 monotherapy treated mice

The results of the multi-slice MRSI-based volumetric analysis of GL261 GB treated with anti-PD-1 monotherapy (C1479, C1480 and C1484, n = 3) are summarized below.

➢ *C1479 anti-PD-1 monotherapy*

Case C1479 was analysed by MRI and multi-slice 3D MRSI from day 16 until day 26 p.i. when it was euthanized for humanitarian reasons since tumour volume reached 163.4 mm^3. Therapy was administered at days 6, 12, 18 and 24, right after MRSI analysis. The relationship between tumour volume and TRI evolution accompanied by the corresponding nosological images are shown in Figure 4.25.

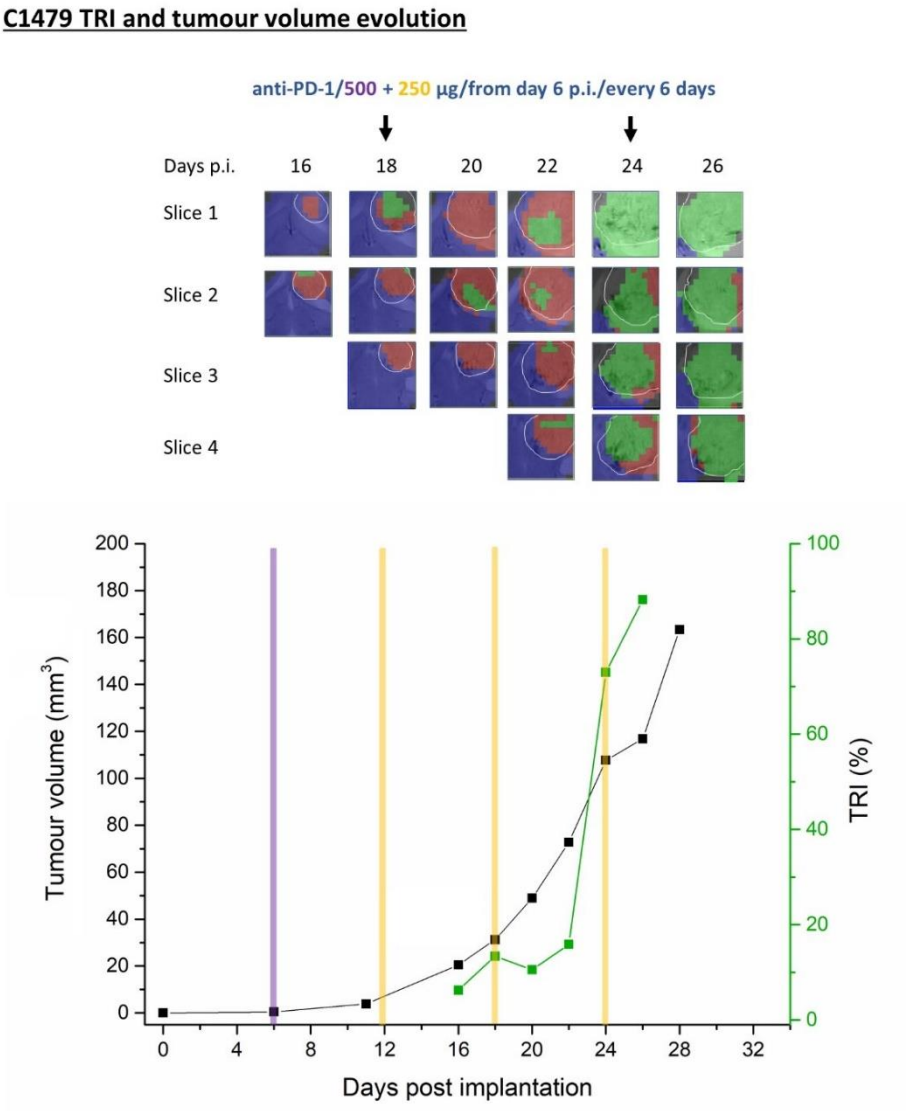

Figure 4.25 Nosological images and graphical representation of the tumour volume evolution for the tumour region in the case C1479. *Tumour volume in mm^3 (black line, left axis) and the percentage of green, responding pixels (TRI) obtained taking into account total pixels counting (green line, right axis). In the upper part of every image, chosen time points show the evolution of the nosological images in two-four rows of colour-coded grids superimposed to the T2w-MRI for*

each slice. Vertical arrows indicate days of therapy administration. In the bottom graph, the purple and yellow column (500 µg/dose and 250 µg/dose separately) indicate anti-PD-1 administration days. No TRI cycle was observed in this case.

The tumour evolution in this case was classified as PD throughout the period of MRSI analysis, except for a brief interval between days 24-26 p.i., being the overall trend similar to an untreated tumour with only slightly larger survival. The TRI oscillatory pattern is not observed in this case. The small variation observed at day 18 p.i. could be attributed to experimental variation, since a TRI cycle was defined provided a change between maximum and minimum TRI values was above 10%, and in this case variation was only 2.9%.

- *C1480 anti-PD-1 monotherapy*

Case C1480 was analysed by MRI and multi-slice 3D MRSI from day 16 until day 26 p.i. MRSI acquisitions were forced to be stopped from day 26 p.i. since C1480 tumour has shrunk down to a 4.12 mm^3 scar, entering the "below threshold detection period" (BTDP). Therapy was administered at days 6, 12, 18, 24, 30 and 36 p.i., and was maintained in IMS until the animal was considered cured. The relationship between tumour volume and TRI evolution accompanied by the corresponding nosological images are shown in Figure 4.26.

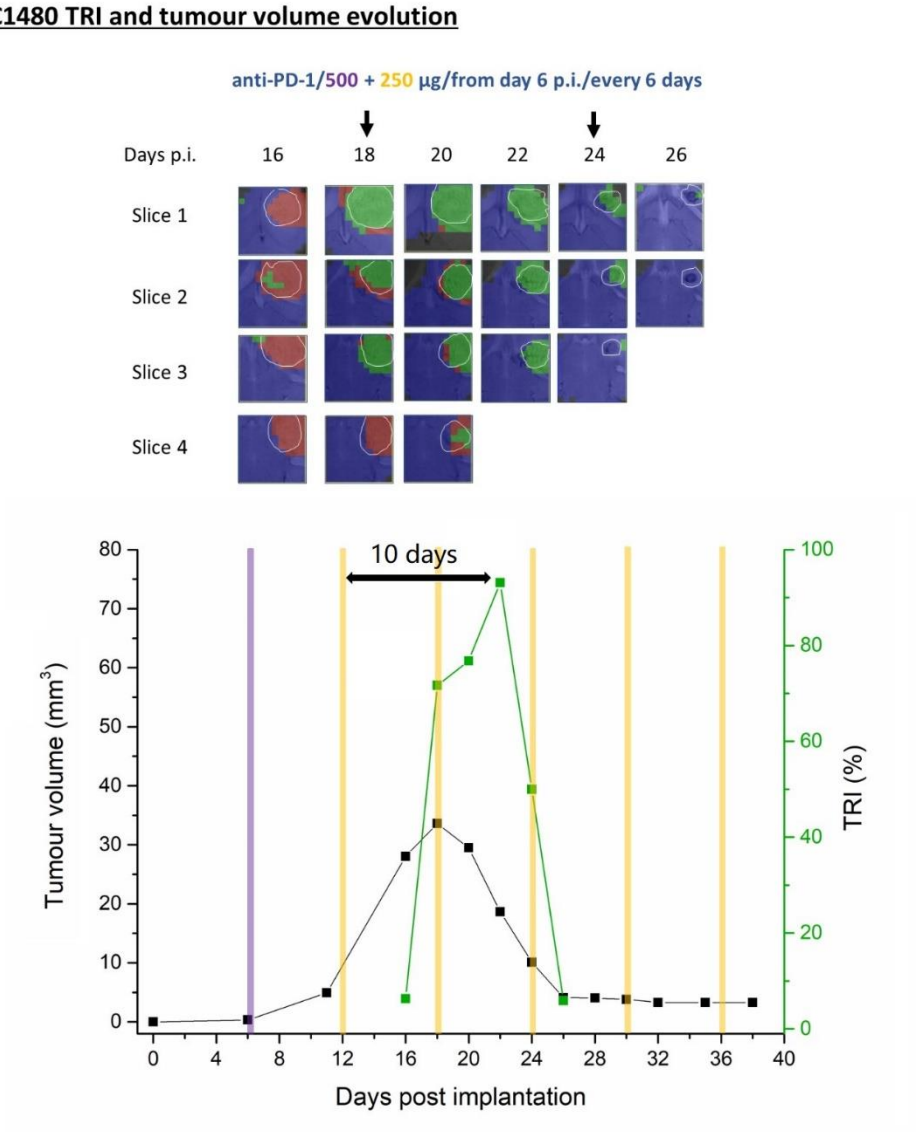

Figure 4.26 Nosological images and graphical representation of the tumour volume evolution for the tumour region in the case C1480. *Tumour volume in mm^3 (black line, left axis) and the percentage of green, responding pixels (TRI) obtained taking into account total pixels counting (green line, right axis). In the upper part of every image, chosen time points show the evolution of the nosological images in two-four rows of colour-coded grids superimposed to the T2w-MRI for each slice. Vertical arrows indicate days of therapy administration. In the bottom graph, the purple and yellow column (500 µg/dose and 250 µg/dose separately) indicate anti-PD-1 administration days. TRI cycle duration (therapy administration to next peak maxima) is highlighted in the image.*

In this case, TRI increased from 6.3 % at day 16 p.i. to 71.7 % at day 18 p.i. and a further increase to 93.1 % was measured at day 22 p.i. After this period, the tumour came to BTDP period so only one clear TRI peak was observed. It is noteworthy that it is unclear whether

the inflection point seen at day 20 p.i. has some biological meaning (i.e. a 'pseudo' cycle), which would place the maximum TRI at 6 days from the administration point. However, the criteria set to decide whether a TRI change was a cycle or not does not agree with this behaviour and the maximum TRI was considered to be reached at day 22 p.i., 10 days after the second anti-PD-1 round.

The tumour volume of mouse C1480 growth until day 18 p.i., when abundant responding tumour pixels started to be observed. Then, along with the presence of TRI peak, the tumour volume dropped 87.5 % between day 18 p.i. and day 26 p.i., probably due to immune system sustained attack onto tumour leading to shrinkage. One clear TRI cycle was observed in this case of 10 days length, which seemed slightly longer than the average observed with other therapy response TRI cycles. We cannot discard that a slower immune system build-up effect takes place from the effect of day 11 p.i. therapy administration.

- *C1484 anti-PD-1 monotherapy*

C1484 was analysed by MRI and multi-slice 3D MRSI from day 16 until day 28 p.i., when MRSI acquisitions were forced to be stopped from day 28 p.i. due to technical issues related to MR coil availability in this time period. Therapy was administered at days 6, 12, 18, 24, 30 and 36 p.i., continued been given in IMS until the animal escaped from therapy. Relationship between TRI and tumour volume as well as the corresponding nosological images are shown in Figure 4.27.

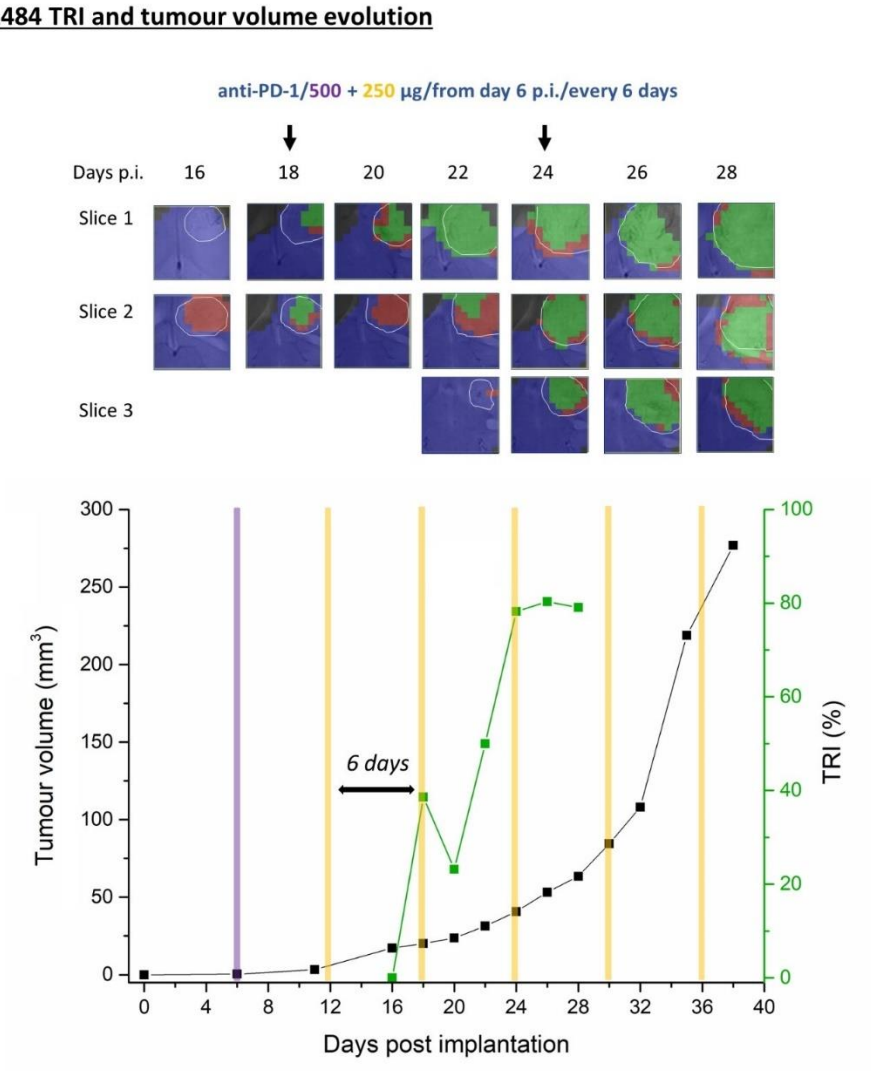

Figure 4.27 Nosological images and graphical representation of the tumour volume evolution for the tumour region in the case C1484. *Tumour volume in mm^3 (black line, left axis) and the percentage of green, responding pixels (TRI) obtained taking into account total pixels counting (green line, right axis). In the upper part of every image, chosen time points show the evolution of the nosological images in two-three rows of colour-coded grids superimposed to the T2w-MRI for each slice. Vertical arrows indicate days of therapy administration. In the bottom graph, the purple and yellow column (500 µg/dose and 250 µg/dose separately) indicate anti-PD-1 administration days. TRI cycle duration (therapy administration to next peak maxima) are highlighted in the image.*

In this case, there was no significant shrinkage during tumour evolution, however, according to the adapted RECIST criteria, two SDi stages of tumour growth were observed during the MRSI analysis period (16 - 20 days p.i.) along the TRI peaks. Moreover, the significantly longer survival time of C1484 also distinguished it from non-responding cases.

One clear TRI oscillation was observed between days 16 and 20 p.i.; such TRI peak appeared on day 18 p.i., 6 days after the second therapy administration. The lack of MRSI information from day 26 p.i. on due to the aforementioned technical issues which prevented us to check whether the second TRI rise would be followed by a minimum (second peak). However, the uncontrolled tumour volume increase does not seem to point towards this direction.

TRI oscillations were also present in monotherapy, but seem to appear later

Although the cohort studied was much smaller than the IMS-TMZ cohort and some technical issues prevented us to gather the whole set of information, it seems clear that some TRI oscillations can be spotted either during tumour shrinkage or transient response (stable disease). The first TRI maximum appeared in average 8 days after the second anti-PD-1 administration round. This is a relevant difference, since when TMZ was used either alone or in combination with anti-PD-1, the first TRI maximum appeared 6-8 days after the first administration round. The evident effect of anti-PD-1 therapy is relatively slow, authors reported the immune reinvigoration in the tumour would be detectable at 1-3 weeks after a single dose of anti-PD-1[200]. These results suggest that the build-up and action of immune system related to anti-PD-1 therapy alone may be slightly slower than the elicitation related to TMZ administration, although a higher number of mice would be needed to corroborate this observation. Another possible explanation is that the local effects triggered by the immune system enhanced after the first administration round was not enough to produce detectable changes in the metabolomic spectral pattern 6 days later and a new administration round was needed in order to raise enough immune system activity reflected in the metabolomics pattern. Probably the cell damage produced after the first anti-PD-1 round, relying only into local immune system cells favoured by immunotherapy, was not enough to elicit a relevant wave of new, primed cells to fight against the tumour, needing a new administration time point to be detectable with our approach.

TRI oscillations were generally coincident with response

Three TRI oscillations were observed in the IMS-anti-PD-1/TMZ and IMS-anti-PD-1 treated mice and these were generally coincident with SDi and PRe tumour stages (Table 4.9), according to the adapted RECIST criteria (described in section 3.4.2). Notably, similar to IMS-TMZ treated cases, in a first MRSI time point (case 1484 day 18 p.i.), where the tumour

evolution would be still classified as PD, TRI oscillation can already be seen, which confirms the idea that the information provided by MRSI appears in an early fashion compared with response evaluated by possible MRI sampled tumour volume changes.

Group	Case	Day p.i.	TRI behaviour	Classification of RECIST criteria
IMS-anti-PD-1/TMZ	**C1446**	15-17	TRI cycles	Stable disease
		17-23		Partial Response
		23-29	BTDP	Stable disease
IMS-anti-PD-1	**C1479**	16-26	No cycles	Progressive disease
	C1480	16-20	TRI cycles	Stable disease
		20-26		Partial Response
		26-34	BTDP	Stable disease
	C1484	16-20	TRI cycles	Stable disease
		20-28	No cycles	Progressive disease

Table 4.9 Evolution of the IMS-anti-PD-1/TMZ and IMS-anti-PD-1 treated GL261 cases considering TRI and tumour volume changes over time. Classification of adapted RECIST criteria were applied as described in section 3.4.2 .

4.2.3.3 Spectral quality

Spectra acquired were of overall good quality and examples of chosen MRSI spectra for cases C1270 (IMS-TMZ treated), C1480 (IMS-anti-PD-1 treated) and C1446 (IMS-anti-PD-1/TMZ treated) are shown in Figure 4.28. Major metabolites are identified in spectra classified as normal brain parenchyma, actively proliferating tumour or responding tumour. The good spectral quality, which was checked consistently to discard the presence of artifacts, ensure that differences detected with pattern recognition methods are not random or attributed to data lack of quality.

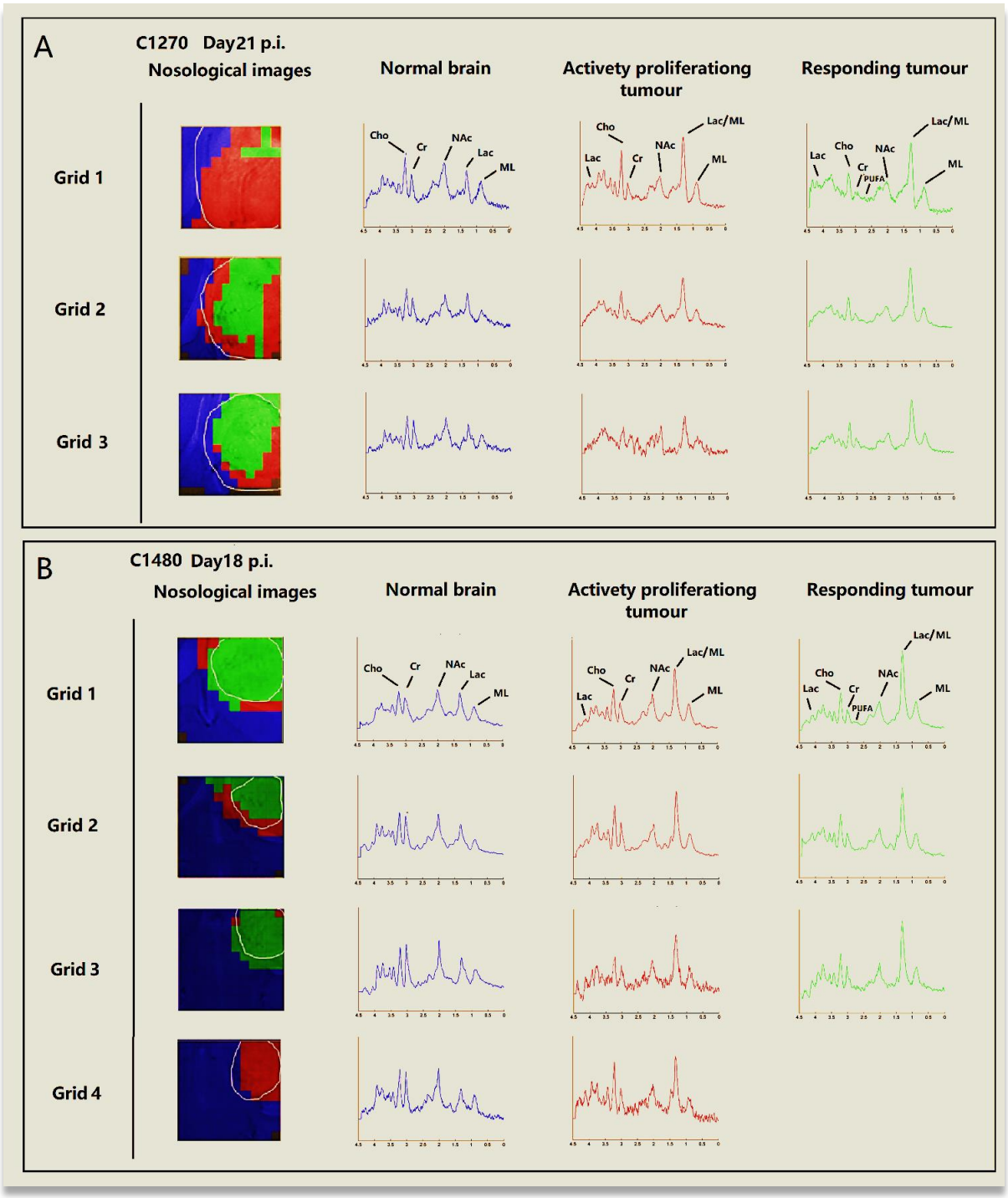
A
C1270 Day21 p.i.
Nosological images
Normal brain
Activety proliferationg tumour
Responding tumour
Grid 1
Grid 2
Grid 3
Cho
Cr
NAc
Lac
ML
Lac/ML
PUFA
B
C1480 Day18 p.i.
Nosological images
Normal brain
Activety proliferationg tumour
Responding tumour
Grid 1
Grid 2
Grid 3
Grid 4

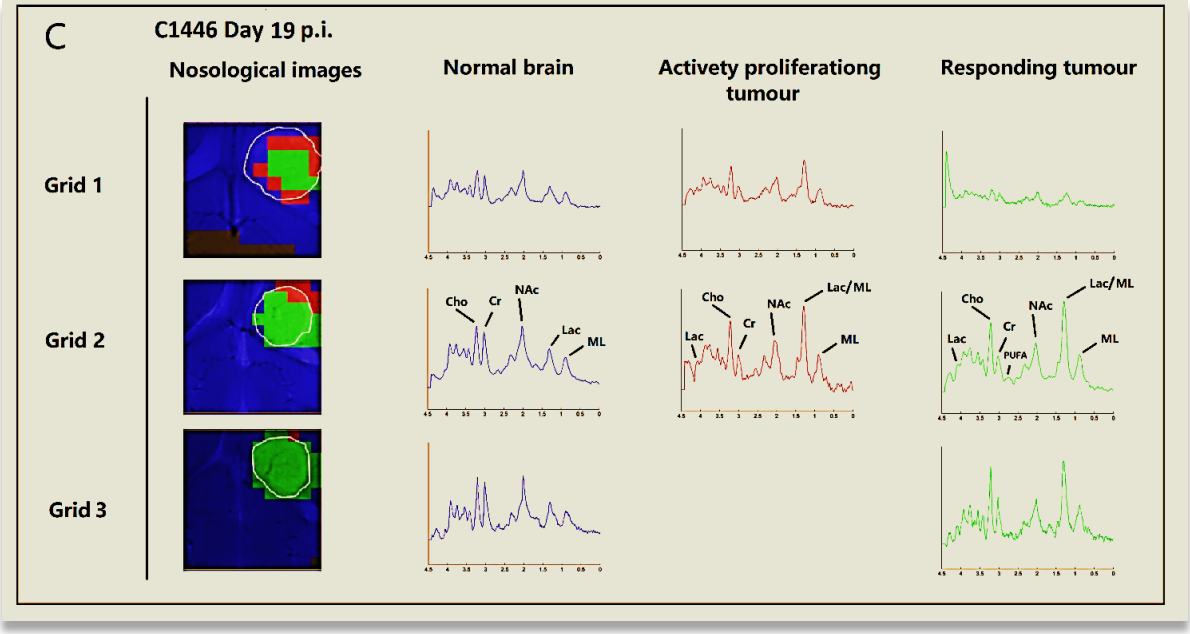

Figure 4.28 Examples of mean spectra calculated from chosen zones of nosological images classified as normal brain parenchyma, actively proliferating tumour and responding tumour. *(A) IMS-TMZ treated case C1270: Normal brain is shown in blue (n=164 pixels), actively proliferating tumour in red (n=81) and responding tumour in green (n=71). (B) IMS-anti-PD-1 treated case C1480: Normal brain is shown in blue (n=331 pixels), actively proliferating tumour in red (n=49) and responding tumour in green (n=108). (C) IMS-anti-PD-1/TMZ case C1446: Normal brain is shown in blue (n=298 pixels), actively proliferating tumour in red (n=18) and responding tumour in green (n=46). Cho= choline, Cr= creatine, NAc= N-acetyl containing compounds, Lac= lactate, ML= mobile lipids. As expected, tumour zones present higher Cho/Cr and Cho/NAc ratio in comparison with normal brain parenchyma and higher Lac/ML signals. Still, responding zones present more noticeable 2.8 ppm signal, compatible with Polyunsaturated fatty acids (PUFA) chemical shift, although differences are distributed all along the spectral pattern (compare with figure 1.14 for paradigmatic tissue sources).*

4.2.4 Discussion

4.2.4.1 Oscillatory TRI behaviour is confirmed in a large cohort of GL261 GB IMS-TMZ treated mice

Ten IMS-TMZ-treated and six vehicle treated GL261 GB-bearing mice were analysed by MRSI-based nosological images in longitudinal experiments. Results confirmed the oscillatory response level (i.e. % TRI values) produced by the IMS administration protocol, as expected. This was already shown in a previous study with the standard “three cycles” TMZ administration protocol in a smaller cohort of animals [158] but its reproducibility with the IMS-TMZ protocol had not yet been tested. Multi-slice MRSI acquisitions allowed us not only

to monitor TRI oscillations along the period of transient response to therapy, but also to sample intratumour heterogeneity. Our hypothesis to explain these oscillations is that TMZ administration would be responsible of "setting" cycles, since the period between therapy administration and appearance of a TRI peak is consistent along different cases, usually ranging between 4-8 days during regular transient response periods. Also, it has been shown that, prior or during tumour relapse, these oscillations disappeared, with a different TRI behaviour: it either assumed an increasing, non-oscillating trend or only showed small, incipient increases. This confirms that consistent TRI oscillations are related to metabolomic changes due to tumour response, but mostly absent during tumour relapse. The average value for time lapse recorded between TMZ administration and TRI peak appearance (being TRI peak average 66.8 ± 22.3 % in all studied cases, n = 10) was 6.2 ± 1.4 days.

In control cases (Figures 4.23), no TRI oscillations were observed, with the possible exception of case C1258, although no coherent tumour decrease was seen at the possible TRI peak in C1258. This suggests that the lack of response to therapy leads to absence of clear TRI oscillations. In such cases, an increase in TRI could suggest local metabolomics changes resembling the ones observed during therapy (e.g. spontaneous host immune response), although these are clearly not enough to arrest tumour growth.

Results from TMZ-treated mice suggest that TMZ administration "resets" the immune system cycle clock, since TRI maximum peaks appear in average 6.2 ± 1.4 days (n = 10) after therapy administration. This value is in agreement with work previously published by us with a non-metronomic TMZ administration schedule (distance between TRI maxima, 6.3 ± 1.3 days, n = 4, [158]) and also with calculations approached in single-slice acquired cases (distance between TRI maxima, 6.2 ± 2.0 days, calculated for n=3 cases from [151]). This value is also in line with the length of immune cycle in mice brain, described to be of ca. 6 days [39]. Moreover, taking into account that TMZ has already been described to behave as an immunogenic drug, which triggers the exposure and release of immunogenic signals [40][201], we hypothesize that each TMZ cycle is triggering a new 'turn' of the immune cycle leading to an arrival of new sub-clones of immune system cells within tumours ca. 6 days later. This would contribute to metabolomic pattern changes in the tumour microenvironment sampled by MRSI acquisitions, leading to changes in nosological images (see figure 4.29 for a schematic explanation). This explanation is supported by histopathological findings (related work from

our group), studied in samples reported in [158]: TMZ-treated samples presented a higher number of lymphocyte-like cells in comparison with untreated samples. This was further confirmed with immunostaining for CD3+ (T lymphocytes marker) and Iba-1 (microglia/macrophages marker), values for CD3+ were 4.8 ± 2.9 and 3.3 ± 2.5 CD3+ positive cells in responsive and unresponsive zones, respectively (n=53 and n=94 fields). For Iba-1, the percentage of positive immunostained area was 21.9 ± 11.4% for responsive and 16.8 ± 9.7% for unresponsive zones (n=53 and n=95 fields). Individual fields from responsive zones could achieve values up to 42% of area occupancy by Iba-1 positive cells while unresponsive zones could reach values as low as 1.4%. Values were significantly higher in tumour zones classified as "responding", in comparison with control cases or "unresponsive" areas. Moreover, the TRI imaging biomarker was proven to be correlated with the proliferation index Ki67 [158][151], also reflecting that metabolomics changes could be related to the proliferation status of tumour cells. Unpublished data from work in progress in our group showed glioma-associated microglia/macrophages (GAMs) population was larger and M1/M2 ratio was higher in responding tumours compared to control tumours. Since GAMs can represent up to 30% of the cells in the tumour tissue [202], and M1 and M2 macrophages have different metabolic profiles [203], this difference could be one of the key factors contributing to spectral pattern changes, acting MRSI response pattern as an immune system status biomarker.

It is important to remark that the 5-2-2 standard TMZ therapy does not follow an IMS schedule, although it also shows a close to 6-day oscillation of TRI. However, being true that the 5-2-2 protocol does not follow an IMS scheme, data gathered in [160] showed that a single cycle of TMZ during five days did not produce any improvement in animal survival (20.6 ± 6.8 days for 1 TMZ cycle vs. 20.5 ± 4.1 days for control animals). It was only when the two additional cycles were introduced with a three-day interleave between them that the survival rate increased significantly to 33.8 ± 8.7 days. A possible explanation is that in the 5-2-2 protocol the middle of the first 5 consecutive days is 2.5 days, which was about 5.5 days before the two additional cycles of TMZ administration, this duration maybe able to allow for some immune elicitation, by partially preserving lymphocyte proliferation at the proximal lymph node.

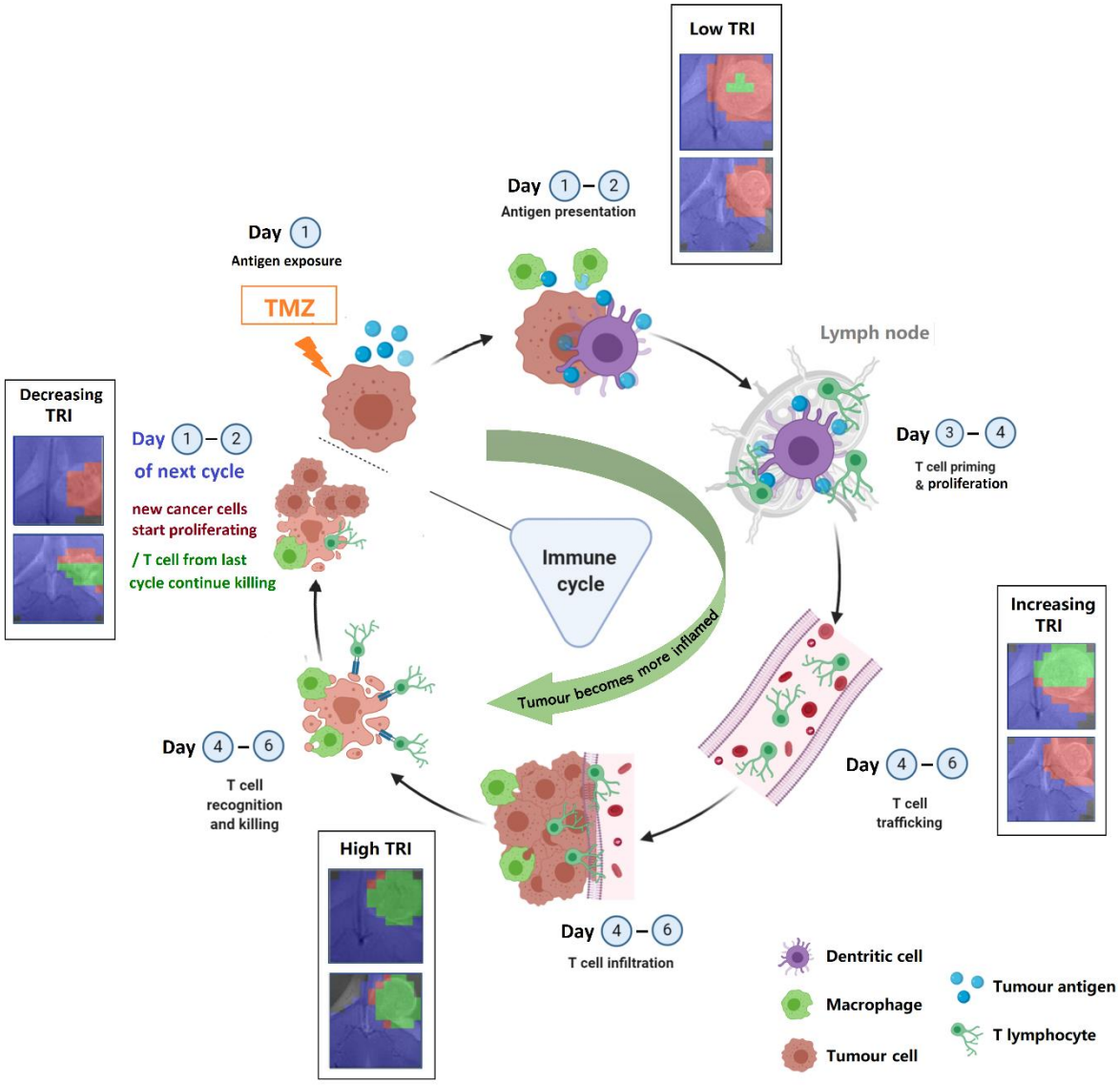

Figure 4.29 Hypothetic schema of the cycle for immune response against a preclinical GB tumour after two therapy cycles and resulting nosological images, using as example images from case C1383. *The cancer-immunity cycle is thought to last around 6 days in mouse brain: When treated with TMZ at day 1, tumour cells release and expose immunogenic signals which attract dendritic cells (DCs) and macrophages to the tumour site. Initially (day 2-3), the immune system is not especially active against those particular tumour cell clones and the nosological images correspond mostly to actively proliferating tumour, thus TRI is low. At days 3-4, DCs having migrated to the lymph nodes, prime naïve CD8+ effector T cells, which start to proliferate. TRI may start increasing between day 3-4 (allowing for inter-subject variability) partially due to innate immune system action against tumour. At days 4-6 of the cycle, a new wave of effector T cells arrive at the tumour site and jointly with macrophages efficiently attack the tumour. In this period, we may observe a TRI peak*

maximum and, in some instances, even reduction in tumour volume. During days 1-2 of next cycle, T cell from last cycle perhaps continue killing, while, simultaneously, new cancer cells start proliferating again, either because new subclones, resistant to lymphocytes appear or because present lymphocytes become anergic, in this period we may observe a decreasing TRI.

The monitoring of TRI evolution could enable the design of personalized therapeutic schemes, adapting the TMZ therapy schedule in order to obtain an optimal anti-tumour effect. Once fully validated that the 'green pattern', combined with a further consistent response of tumour growth arrest or shrinkage, is associated with a productive action of the host immune system against the tumour, its presence would indicate that no further TMZ doses are needed until TRI starts decreasing, meaning that a new, resistant clone of tumour cells is replacing cells killed by immune system action. An additional TMZ administration should trigger a new turn in the immune system cycle, with priming and amplification of lymphocytes enabling them to kill this new tumour cells sub-clone.

It is worth noting that the green "responding" pattern itself seems to be mostly a reflection of local events taking place in a given tissue, which are characteristic of therapy response, but not exclusive. Namely, relapsing tumours and even some controls can also present a "green pattern", but relapsing tumours, at a difference from controls will present TRI oscillations, which seem to be in our hands the main characteristic related to effective immune system local action against GL261 GB.

4.2.4.2 The oscillatory TRI behaviour is also confirmed in GL261 GB treated with immunotherapy

The classifier allowing recognition of the oscillatory TRI behaviour as a potentially useful biomarker for therapy response was developed with TMZ-treated cases [151], and one of the fundamental questions raised was whether it would be useful/applicable to assess the efficiency of other therapeutic agents, which would enhance its translational potential. In fact, it has also been shown to be robust to detect tumour response in cyclophosphamide (CPA) treated mice [159], indicating that the changes observed are not specific to TMZ, but rather linked to local tumour tissue changes during transiently successful treatment. However, CPA is an alkylating agent, similar to TMZ, and the robustness of the source-based classifier to follow up the behaviour of TRI have not been checked using therapeutic agents different from chemotherapeutic. This was assessed for the first time in this thesis. If our hypothesis was

correct, i.e. that TRI oscillations would be a reflection of local immune system action, it should be also observed with anti-PD-1 monotherapy or in combination treatments. Having this in mind, apart from IMS-TMZ treatment, one IMS-anti-PD-1/TMZ treated and three IMS-anti-PD-1 monotherapy treated tumour-bearing mice have been analysed up to now by MRSI-based nosological images. Results confirmed the presence of TRI oscillations in GL261 tumours treated with combination therapy and immunotherapy alone, although the smaller cohort and the variability of the mice population prevent us to generalize yet.

TRI oscillation (8 ± 2 days, n = 3) was observed in both groups, except by mouse C1479 which did not present any oscillation and did not respond to therapy. After therapy administration, TRI increased from near-zero to high values (68.6 ± 27.7 %, n=3) and decayed two days after the TRI peak. In this respect, it should be noticed that TRI peak maxima is also followed by a reduction in tumour volume in two out of three cases (C1446 and C1480), an effect which has been also observed in IMS-TMZ treated cases (see Figure 4.21). This reproducible behaviour may underlie that a rise in TRI combined with further tumour volume decrease is indicating an active anti-tumour response mediated by the host immune system. Unfortunately, in some cases such tumour volume decrease prevented assessment of further TRI cycles due to resolution limitations with MRSI approaches.

Indeed, one of the handicaps of the MRSI-based nosological image calculation technique is that small sized tumours do not produce confident segmentation (e.g. case C1446 after day23 p.i. and C1480 after day 26 p.i.). We named this period “below threshold detection period” (BTDP) since the semi-supervised source analysis software was not able to properly segment the tumour. However, since small tumours have a trend to better survival or either cure, the metabolomics signature would not be as relevant as in tumours with larger volumes, in which this information is relevant to assess the efficacy of a therapeutic strategy.

Results from previous work suggest that this oscillatory TRI behaviour could serve as a potential immune system efficiency biomarker during therapy response of GB. Our studies with immunotherapy have highlighted the importance of this biomarker, since the therapeutic effects of anti-PD-1 have been reported to be associated with changes in immune infiltration [185]. It has been seen in case C1479 that non-oscillating trend or only small, incipient increases in TRI are correlated with worst outcomes. Besides, preliminary TRI oscillation frequency (8 ± 2 days) seen in anti-PD-1 combination or monotherapy seems

slightly longer than in TMZ-treated cases (6.2 ± 1.4 days), but the difference does not reach significance.

It is worth mentioning that in final stages of tumour evolution in PD cases, high TRI values can be also seen, although without an oscillatory pattern (e.g. case C1479). This behaviour is similar to some cases studied in the IMS-TMZ treated section (see Figure 4.21 and 4.24), regardless these mice were from treated or control groups. The single fact that TRI value increases in these cases may indicate that the 'responding source' is not only related to a pattern of therapy response but also to local changes due to a rapid tumour expansion. For example, the presence of necrotic, non or low oxygenated areas that may cause cell death or the activation of the mouse immune system [204][205]. Still, the "responding" is the most similar source according to the classifier but we cannot discard that it belongs to a fourth, different source until a new mathematical study is eventually performed.

Last but not least, with anti-PD-1 monotherapy, the observed pattern changes should be essentially due to the action of the host immune system alone, without the confounding effect of chemotherapy. The oscillatory mode detected reinforces the translational potential of the MRSI-based biomarker for patient-tailored GB therapy, including immunotherapy.

4.2.4.3 The metabolite pattern detected in MRSI spectra of IMS-TMZ, IMS-anti-PD-1 and IMS-anti-PD-1/TMZ combination treated mice is similar

The reference sources used in the semi-supervised methodology were the same ones used in previous studies of our group [158]. Those sources have been robust enough to differentiate responding from non-responding tumours under different therapies (TMZ, anti-PD-1 and combination therapy), which suggests that metabolic changes contributing to those response patterns are reproducible and, possibly, similar among TMZ, anti-PD-1 and combination therapy (Figure 4.30), being both recognized by the previously extracted source. These metabolic changes such as PUFAs, Lactate etc sampled by the response source could be explained due to the mobilization of the immune system to fight against the tumour producing similar metabolomic pattern due to immune system-caused tumour cell death. It also confirmed that the pattern changes are not related to a chemotherapeutic agent but connected with the action of the immune system in tumour site.

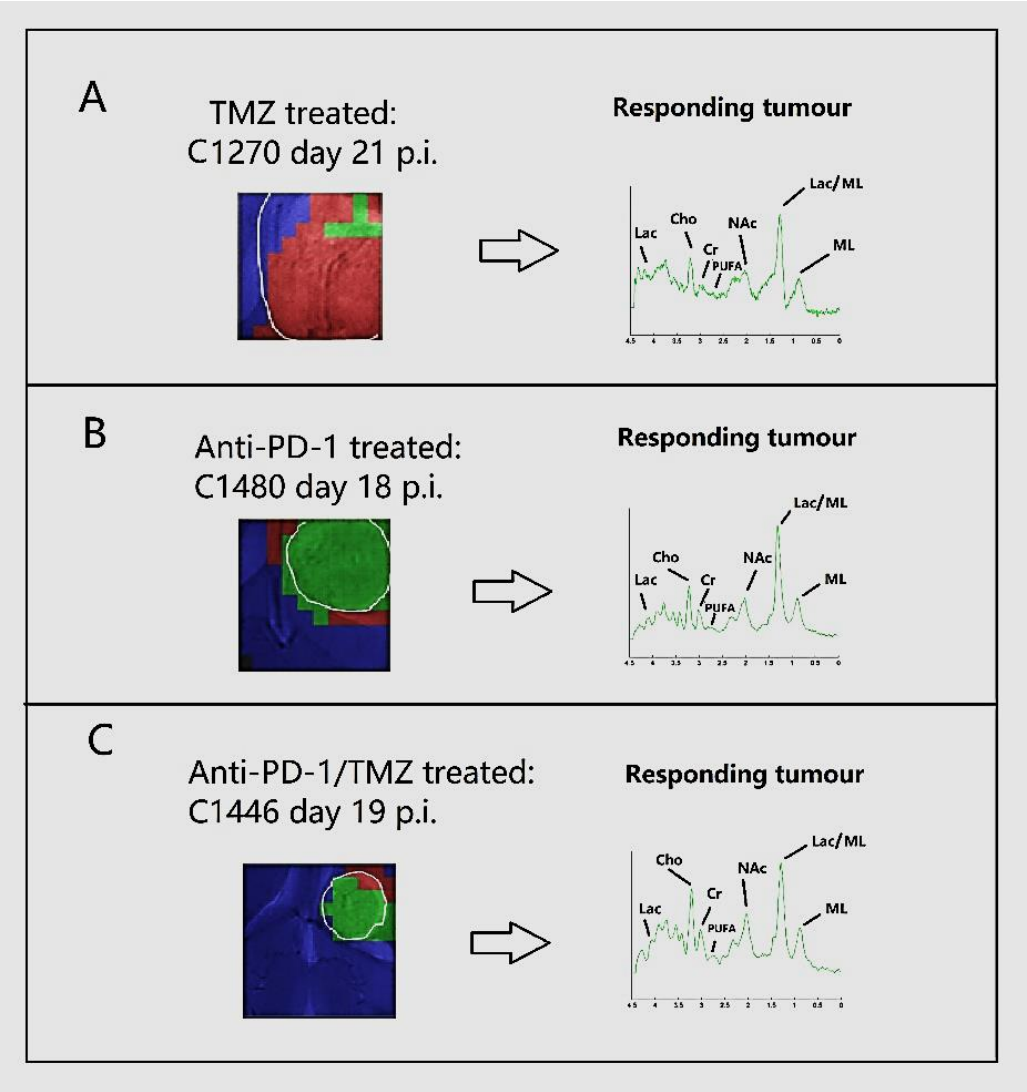

Figure 4.30 Responding pattern average spectra after semi-supervised source analysis. *(A) TMZ treated mouse (C1270 at day 21 p.i.), tumour responsive tissue (average of 6 green pixels), (B) Anti-PD-1 treated mouse (C1480 day 18 p.i.), tumour responsive tissue (average of 41 green pixels), (C) Anti-PD-1/TMZ treated mouse (C1446 day 19 p.i.), tumour responsive tissue (average of 22 green pixels).*

4.2.5 Conclusion

- Results confirmed that the IMS-TMZ protocol produced the expected oscillatory changes in the metabolomic pattern sampled by MRSI-based nosological images, with no significant differences from the standard 5-2-2 three cycles (6.2 ± 1.4 days vs 6.3 ± 1.3 days).
- This oscillatory behaviour of MRSI-based metabolomics pattern was also confirmed in mice treated with immunotherapy both in combination with TMZ and as monotherapy,

reinforcing preliminary results obtained in the group by histopathology or RT-PCR, hinting that responding tumours have a different immune system population that can be behind the observed metabolomic pattern changes.

- The range of the appearance of the first TRI maxima is slightly (not significantly) different between IMS-TMZ and IMS-anti-PD-1 therapy (4-8 days vs 6-10 days). Further studies with larger mice cohorts will be needed in order to clarify these differences and to elucidate the immune system populations in each case.
- TRI oscillations associated with corresponding tumour volume growth arrest or shrinkage seem to be related with host immune system attraction for tumour control. This indicates clear potential for therapy monitoring, further improving the scheduling of therapy and allowing its personalization. For that, studies with other GB preclinical lines are needed (e.g. CT-2A, spontaneous models) and in vitro validation will be needed.
- In order to propose a future clinical translational protocol, we are aware that it will be not feasible to propose an every 2 day longitudinal MRSI assessment of patients during treatment, due to both medical and resources constraints. In this sense, the combined use of MRSI and MRI information may be of help, and preliminary unpublished work from our group point that this would be feasible and if proven correct, fully applicable to clinical GB patients. In this sense, preclinical studies such as the one described in this thesis are of great relevance in the future improvement of clinical protocols and guidelines.

4.3 RESISTANCE TO TMZ THERAPY IN GL261 TUMOURS: POSSIBLE PATHWAYS

4.3.1 Context and Specific objectives

TMZ resistance in gliomas is one of the main reasons for the failure of chemotherapy in the adjuvant treatment of GB. The increased content of MGMT protein in tumour cells has been thought to be critical for resistance to TMZ therapy (See section 1.2.2.4). MGMT is consumed when counteracting TMZ-induced DNA damage, and it has been proposed that the intracellular level of MGMT should correlate with chemoresistance [206]. However, there is little literature data regarding MGMT expression in preclinical GL261 glioblastoma tumours, either control or under treatment, and its possible relevance in response.

Nevertheless, there may be other reasons for treatment failure in GB. Beyond the increased DNA repairing protein expressed by the tumour itself, the tumour immune microenvironment (TIM) also plays a role in tumour progression. PD-1 and its ligand PD-L1 play a key role in tumour immune escape and the modulation of tumour microenvironment, closely related with tumour evolution [207]. Chemotherapy can modify such tumour microenvironment. Increased PD-L1 expression was found after (radio) chemotherapy in thymic epithelial tumours [208] and rectal adenocarcinoma and breast cancer [209], [210], revealing a potential link between chemotherapy and tumour immune resistance. However, there is still controversial information about PD-L1 changes in GL261 GB after TMZ chemotherapy, some authors report that the expression of PD-L1 decreased in TMZ treated GL261 tumour[170], but others [211] described that after TMZ treatment, GL261 cells displayed a high level PD-L1 surface expression when compared to control.

Accordingly, our goal in this section was:

- To investigate the relevance of MGMT and PD-L1 content in chemoresistance by western blot (WB) analysis with special focus on tumours escaping therapy after transient response.
- To investigate basal differences in MGMT and PD-L1 expression in unresponsive tumours, control tumours and tumours transiently responding to therapy

4.3.2 Specific materials and methods

4.3.2.1 Protein extraction and WB analysis

Protein extraction

Cell extracts: GL261 cells were cultured in 75 cm^2 flasks and after the chosen time of treatment, cells were washed twice with 10 ml of PBS and collected. Next, for each 5,000,000 cells, 1 ml of cold lysis buffer was added and put on ice for 10 minutes (cell lysis buffer: 50 mM Tris-HCl pH 7.4, 150 mM NaCl, 1 % triton-X-100, 1 mM Dithiothreitol (DTT), 1 mM phenylmethylsulfonylfluoride (PMSF), 1mM Ethylenediaminetetraacetic acid (EDTA), 25 mM NaF, 0.2 mM Na_2VO_3, 2 mM PPi, 1 µg/mL protease inhibitors (leupeptin, benzamidine, aprotinin, pepstatin)). Then, samples were centrifuged at 13,000 × g for 15 min in cold-room (4 °C). After centrifugation, the supernatant was collected and stored at -20 °C.

Tumour tissue extracts: frozen GL261 tumour samples were weighed and 200 µl of cold lysis buffer for each 50 mg of tissue was added (tissue lysis buffer: 50 mM Tris-HCl pH 7.7, 150 mM NaCl, 15 mM $MgCl_2$, 0.4 mM EDTA, 0.5 mM DTT, 2 mM PMSF and 100 µg/mL of leupeptin, aprotinin and benzamidine). Then, tissue samples were homogenized with a 20 G needle 10 times and with a 26 G needle 10 more times. Sonication was performed 5 times for 5-second intervals at 30% amplification, and 0.5 % of Triton-X-100 was added. After that, samples remained on ice for 30 min. Then, the lysate was centrifuged at 13,000 × g for 20 min in cold-room (4 °C). After centrifugation, the supernatant was collected and stored at -20 °C.

WB analysis

The protein content of cells or tissue samples was quantified with Bradford assay (Bio-Rad) [212]. Equal amounts of protein (80 µg) were loaded on 12% Sodium Dodecyl Sulphate Polyacrylamide Gel Electrophoresis (SDS-PAGE) for separating purposes, then transferred from gel to polyvinylidene fluoride (PVDF) Immobilon-P membranes (Millipore, Darmstadt, Germany) by electroblotting. The membrane was incubated for 1 hour in 5% milk powder in Tris Buffered Saline (TBS) buffer (50 mM Tris-HCl, 150 mM NaCl, pH 7.4). After this blocking step, the membrane was washed with TTBS (TBS buffer containing 0.1% Tween-20) three times, 5 min each time. Membranes were incubated with antibodies against MGMT or PD-L1, and β-tubulin was used as a loading control (check details for each antibody in Table 4.10). After overnight incubation with the primary antibody in a cold-room (4 °C), membranes were washed three times with TTBS and incubated with the secondary antibodies (Immunoglobulin (Ig)G Goat Anti-Rabbit/Mouse IgG (h+L)- Horseradish Peroxidase conjugate, Bio-Rad) diluted in 5% milk – TTBS buffer for 1 h. After that, membranes were washed three times again with TTBS, and immunodetected using a chemiluminescent detection method (ClarityTM Western

ECL Blotting Substrates, Bio-Rad, California, U.S.A.). Chemiluminescent signal was obtained with Chemidoc MP Image System and quantified with the ImageJ software.

Target	Molecular Weight (kDa)	Trading house/origin	Reference number	Dilution	Origin
MGMT	21	Boster	PA1408	1: 1000	Mouse
PD-L1	33	Abcam	ab233482	1: 400	Rabbit
β-Tubulin	50	Cell signalling	2146	1: 1000	Rabbit

Table 4.10 List of primary antibodies used for WB analysis.

4.3.2.2 Investigate whether GL261 cells tend to express MGMT and PD-L1, in comparison with the expression of MGMT and PD-L1 in the LN18 cell line.

To evaluate whether our GL261 cells express MGMT and PD-L1, GL261 cells in exponential phase (the same growth phase we use in tumour implantation) were harvested and collected. Total protein of GL261 cells was extracted as described in 4.3.2.1, then WB analysis of MGMT and PD-L1 expression was carried out. To compare the expression of MGMT and PD-L1 in different cell lines and to estimate whether our GL261 cells will range in low or high expression level ones, LN18 cells (human glioblastoma, provided by Victor Yuste's group) were lysed for comparison. Tubulin was used as a loading control and comparable amounts of protein were loaded.

4.3.2.3 TMZ treatment of GL261 cells and tumours for MGMT expression analysis

To assess whether *in vitro* treatment of GL261 cells with TMZ would change their MGMT expression level, cells were treated during 72 h with TMZ at 2 mM, 0.748 mM and 0.298 mM (see concentration rationale in section 4.3.3.1) and cell viability was assessed with trypan blue. This step was designed to check if remaining TMZ-resistant cells were enough to detect MGMT through WB. Then, MGMT expression level was analysed by WB in either untreated or TMZ-treated GL261 cells after total protein extraction and values were normalized to tubulin content.

To assess the relevance of MGMT content in GL261 GB chemoresistance, the content of MGMT in n=3 control tumours were compared with n=3 tumour samples escaping from metronomic TMZ therapy (eight doses of TMZ 60 mg/Kg every 6 days, cumulative dose = 480

mg/Kg). Tissue homogenization, protein extraction and WB analysis were carried out as described in 4.3.2.1. Therapy was administered as described in section 4.1.2.1 and mice were followed-up with T2-weighted MRI at 7T as described in section 3.4.1.

4.3.2.4 IMS-TMZ treatment in GL261 GB for PD-L1 content analysis

To check whether PD-L1 may play a role in tumour TMZ-resistance, PD-L1 content was analysed by WB in 12 frozen dissected GL261 tumour samples from mice treated with IMS-TMZ. Tumour-bearing mice were screened with T2-weighted MRI at 7T for tumour follow-up as described in section 3.4.1. Fast-growing tumours escaping TMZ therapy from the start were categorized as “non-responding” (n=3), while cases showing growth arrest/shrinkage but eventually re-growing were defined as “relapsing” (n=6). Control cases received 10% DMSO vehicle (n=3). Animals were euthanized and samples extracted for WB analysis.

4.3.3 Results

4.3.3.1 Evaluation of GL261 cells content of MGMT and PD-L1, and comparison with the expression in the LN18 cell line.

Figure 4.31 A illustrates the WB results obtained according to the procedure described in section 4.3.2.2. The expression of MGMT and PD-L1 were detected in GL261 cells, clear MGMT and PD-L1 bands were revealed at the predicted molecular weight (21 and 33 kDa) and their expression level increased with the increased amount of total protein (80, 160, 320 and 640 µg) loaded from cell extracts. This suggests that our GL261 cells do express MGMT and PD-L1 protein, which provides the basis for later research.

Regarding the comparation with LN18 cell line, results of WB and its quantification are shown in Figure 4.31 B and C, indicating that the PD-L1 expression level of our GL261 cells is clearly higher than that of LN18 cells (n=3, 3.48-fold, both normalized to Tubulin). Furthermore, in the picture we can observe that MGMT protein is much overexpressed in the LN18 cell line as described in the literature [213], showing such intense band that in comparison for figure 4.31B would suggest it that GL261 had no MGMT expression at all.

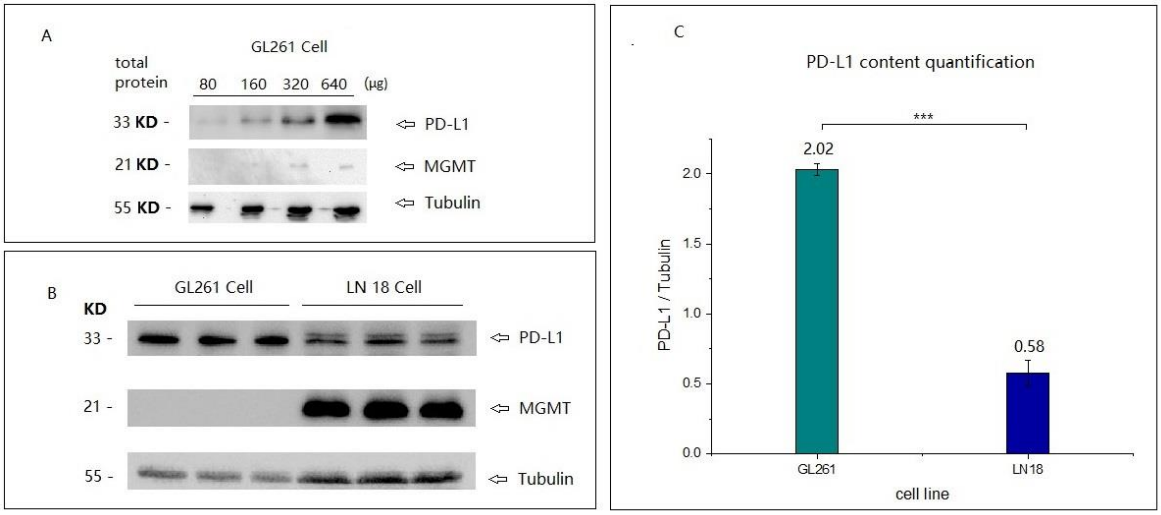

Figure 4.31 Result of Western Blotting analysis. *(A) different amounts (80, 160, 320 and 640 µg) of total protein were separated by 12% SDS-PAGE, after electro blotting, and the membrane was incubated with antibody against MGMT and PD-L1 (21 and 33 kDa). (B) Detection with both anti-PD-1 antibody and anti-MGMT antibody (total protein 640 µg). PD-L1 is highly expressed in the GL261 cell line, higher than in LN18, whereas much higher MGMT protein expression level is found in the LN18 cell line compared to GL261. (C) Quantification of WB result, experiments were performed with n=3, and mean +/- SD values are shown. ***p<0.001 for Student's t test for the comparison between GL261 and LN18 cells.*

4.3.3.2 Viability of TMZ-treated GL261 cells evaluated by trypan blue assay.

GL261 viability after 72h of TMZ treatment at 2 mM, 0.748 mM and 0.298 mM was assessed by trypan blue assay. The concentration of 2 mM has proven to decrease viability to 68.8 % in our group [188], whereas the 0.748 mM concentration (EC_{50} described by Ferrer-Font L et al [168]) proved to decrease viability to ca. 80%, with 100% cell viability assigned to control cells treated with 0.8% DMSO (v/v). Finally, 0.298mM is the actual drug concentration that was described to reach the tumour tissue in mice after equivalent oral administration to the one used in our system, described by Hao-Li Liu et al [214]. Results obtained suggested that TMZ treatment alone can only slightly compromise the viability of GL261 cells in vitro even at high concentrations, which would not be achieved in an *in vivo* treatment (Figure 4.32).

Figure 4.32 GL261 cell viability after 72h of TMZ treatment. *TMZ concentrations were 2 mM, 0.748 mM and 0.298 mM. Control cells were treated with 0.8% DMSO (v/v). Experiments were performed with n=3, and mean ± SD values are shown. *p<0.05, **p<0.01, ***p<0.001 for Student's t test for the comparison between control and treated cells.*

4.3.3.3 MGMT expression analysis of TMZ-treated GL261 cells in vitro.

To assess whether in vitro treatment of GL261 cells with TMZ would induce chemotherapy resistance, MGMT expression levels were assessed in the remaining TMZ treated cells at different concentrations after 72 hours, mimicking tumoral cells that would survive TMZ treatment in vivo. Parallel groups (n=3) were performed for each concentration. Tubulin expression were also analysed. Western-blot results suggest that TMZ treatment does not alter significantly the MGMT content in GL261 cultured cells after continuous treatment during 72 h with any of the studied concentrations (n=3 for each group, non-significant, p>0.05, Fig 4.33).

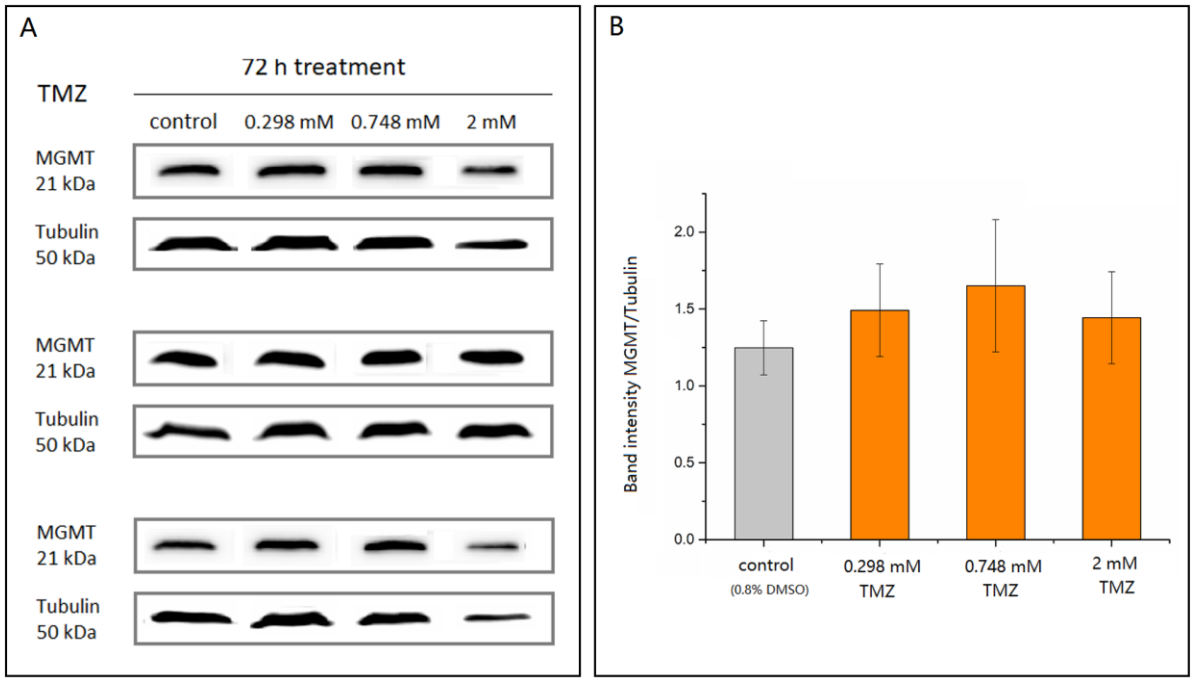

Figure 4.33 MGMT expression level in GL261 cultured cells. *(A) WB result of GL261 GB cells treated with different concentrations of TMZ for 72 hours, n=3 in each group. MGMT and Tubulin proteins were analysed. (B) Quantification of WB result, MGMT band intensity (after normalization to Tubulin) are 1.25 ± 0.18 in the control group, 1.49 ± 0.3 in 0.298 mM TMZ group, 1.65 ± 0.43 in 0.748 mM TMZ group and 1.44 ± 0.3 in 2 mM TMZ group. (n=3 in each group, non-significant p>0.05).*

4.3.3.4 MGMT expression analysis of TMZ-treated GL261 GB in vivo.

Results showed that MGMT expression level was about 1.16-fold higher in control tumour than in tumour escaping from TMZ therapy, although no significant changes were detected between the two groups (n=6 in each group, non-significant, p>0.05, Figure 4.34).

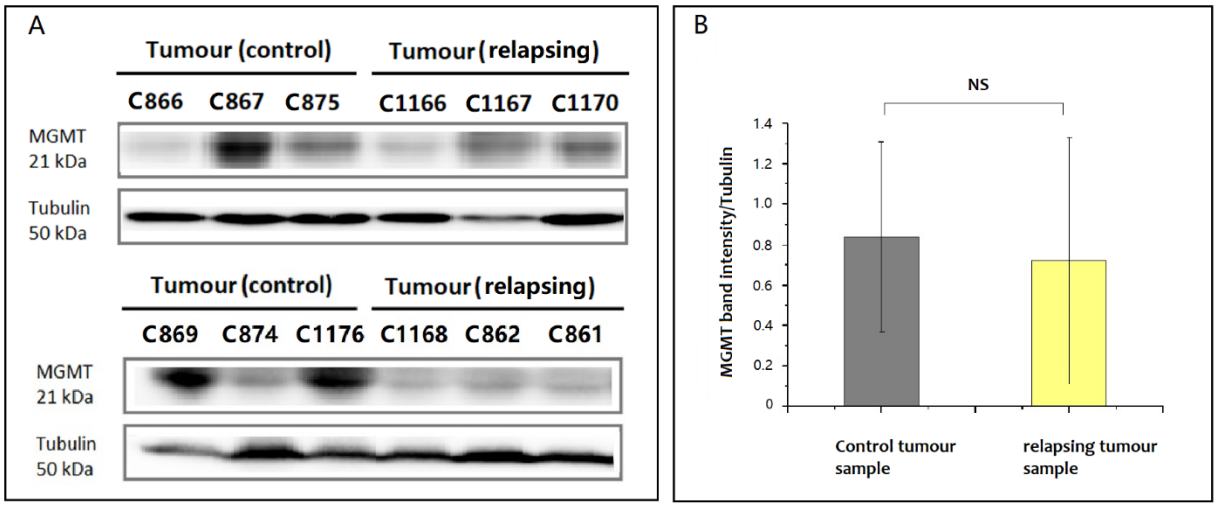

Figure 4.34 MGMT expression level in GL261 GB tumour samples. *(A) WB for tumour total protein homogenate (80 µg) from relapsing tumours treated with IMS-TMZ and control tumours treated with vehicle, n=3 in each group. MGMT and Tubulin proteins were analysed. (B) Quantification of WB result of relapsing and control tumour samples, MGMT band intensity (after normalization to Tubulin) are 0.85 ± 0.47 in the control group and 0.73 ± 0.61 in the relapsing group. (n=6 in each group, non-significant p>0.05). NS, non-significant.*

MGMT expression in control in comparison with TMZ-treated cells was sligthly different in vitro and in vivo, although non-significantly. Namely, in vitro treatment seemed to slightly increase MGMT expression (19%) while in vivo treatment showed a slight decrease in such expression (11%), although these non-significant differences could be also due to the interanimal variability, especially in case of in vivo tumour samples.

4.3.3.5 PD-L1 expression analysis of TMZ-treated GL261 GB in vivo.

PD-L1 content was analysed in 12 frozen dissected GL261 tumours: 9 from IMS-TMZ treated mice (n=3 non-responding and n=6 relapsing tumours), and 3 from control tumours. Western-blot results and quantification, as well as tumour growth curves are shown in Figure 4.35. After normalization to Tubulin, PD-L1 band intensity was 0.23 ± 0.04 in the GL261 control group whereas it was 0.64 ± 0.14 in the relapsing GL261 group and 0.19 ± 0.02 in non-responding group. The PD-L1 content was found significantly higher ($p<0.001$) in the relapsing group when comparing with control group (2.8-fold) and non-responding group (3.4-fold), whereas no differences were found for PD-L1 content between non-responding and control tumours.

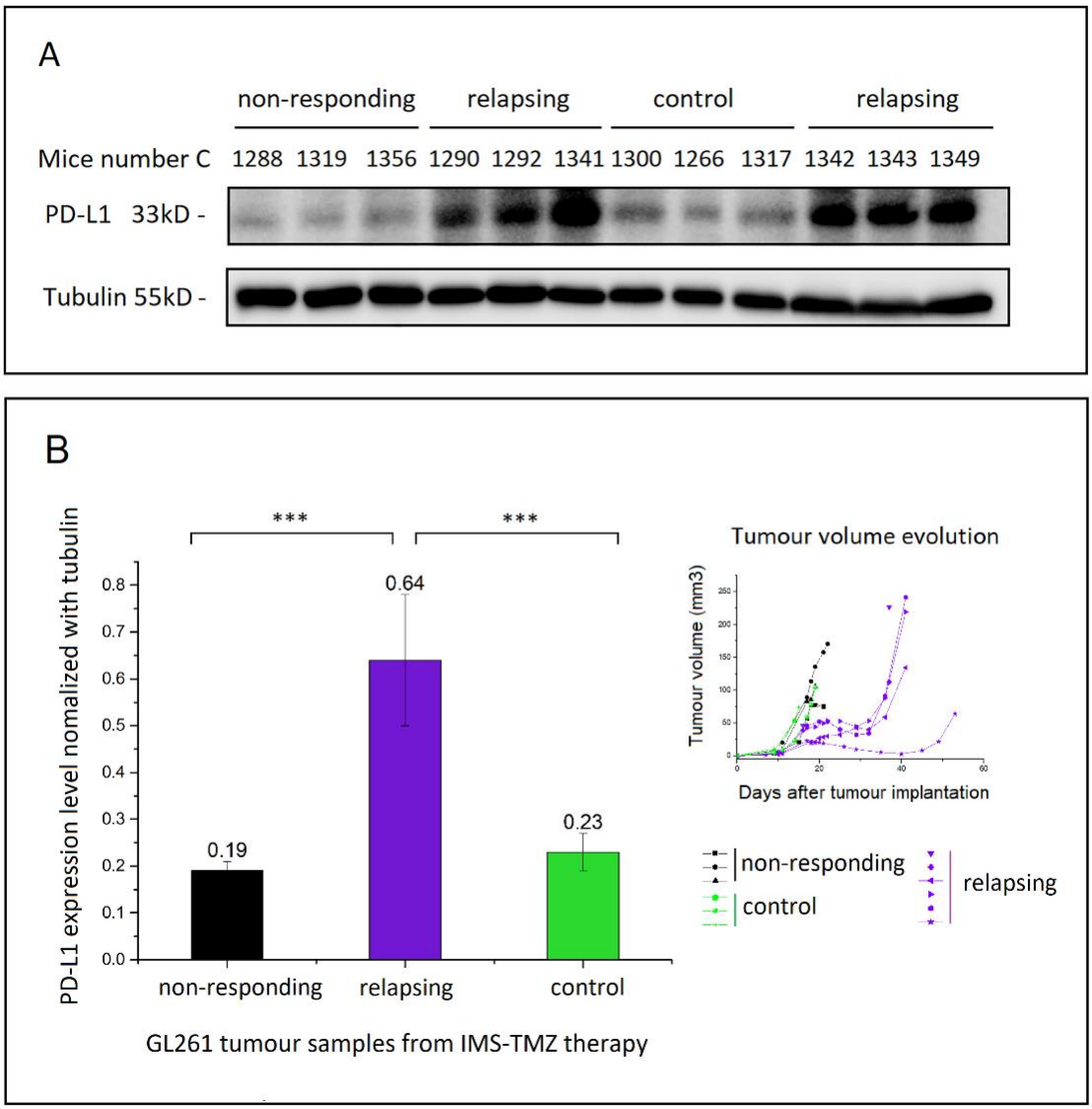

Figure 4.35 PD-L1 analysis in frozen dissected GL261 GB from IMS-TMZ treated mice. *(A) WB for tumour total protein homogenate (80 µg) from different mice treated with IMS-TMZ (n=3 non-responding and n=6 relapsing tumours), compared with vehicle treated mice, n=3. PD-L1 and Tubulin proteins were analysed. (B) Quantification of WB result including the non-responding, relapsing and control tumour samples, PD-L1 band intensity (after normalization to Tubulin) are 0.19 ± 0.02 in the non-responding group, 0.64 ± 0.14 in the relapsing group and 0.23 ± 0.04 in the control group. ***=p <0.001 for Student's t-test for the comparison among non-responding, relapsing and control group.*

4.3.4 Discussion

The DNA repair enzyme MGMT is of major clinical interest, since it is proposed that increases in MGMT content causes appearance of chemoresistance in human GB [215]. On the other hand, it was early described that patients with lower MGMT expression in their GB tumours

seem to benefit more from the alkylating agent TMZ [30], after treatment with temozolomide and radiotherapy, their median survival was 21.7 months as compared with 15.3 months among those who were assigned to only radiotherapy (P=0.007 by the log-rank test). In patients with higher MGMT expression, there was a small and statistically non-significant difference in survival between the treatment groups.

In our preclinical study, no significant increases in MGMT expression were observed, neither in late relapsing tumours escaping IMS-TMZ-treatment, neither in surviving cells after 72h of TMZ treatment, even using high TMZ concentrations. Such experimental results do not seem to indicate a relevant role for MGMT content changes in GL261 tumour chemoresistance after IMS-TMZ treatment. Still, there are reports of TMZ resistance that have been linked to increased levels of MGMT in LN229 preclinical GB tumour[216], T98 and TR-U373 cells [217].

The GL261 cell line is not in the range of high MGMT expression, besides, TMZ has only moderate effect in cultured cells in vitro at the dose reaching preclinical tumours in vivo. In vivo TMZ administration to GL261 bearing mice produces transient response when a three-cycle 5-2-2 administration protocol is used, while significantly better results are achieved with IMS protocols. Even in the IMS-TMZ case, there is a fraction of animals that escape treatment. Since MGMT does not seem to be involved in this therapy escape, there may be other reasons explaining these escape results.

The other possible pathway involved in TMZ therapy resistance studied in this thesis is related with the PD1-PDL1 axis. Our results show escaping tumours having 3-fold higher PD-L1 expression in comparison with control tumours, suggesting that overexpression of PD-L1 in the escaping tumour mass could be one possible explanation for resistance to TMZ in GL261 GB in these experimental conditions. Notably, the tumour mass is composed not only of tumour cells but also of immune cells, such as microglial and macrophage cells, which can contribute up to 30% of a brain tumour mass [218], and PD-L1 can also be expressed on their cell surface [219][220].

Immune evasion is one of the features of cancer [221], and the overexpression of PD-L1 on the surface of the cancer cells is one way of escaping the immune system attack [64] (see section 1.1.4.2 for a summary of the mechanism involved). Several studies reveal that up-regulated expression of PD-L1 on tumour cells could be a potential link between

chemotherapy and tumour immune resistance [208]–[210]. By far the best-known regulator of PD-L1 expression is IFN-γ, and it has been shown that both the JAK/STAT and MAP kinase signalling pathways are involved in IFN-γ-induced PD-L1 expression [67]. In 38.5% of the mice studied in this thesis with IMS-TMZ, we observed a transient therapy response followed by fast tumour regrowth. WB results with a selected group of those relapsing tumours showed that PD-L1 content was significantly increased in late relapsing tumours when comparing to vehicle-treated tumours, which could provide a possible explanation for relapse in these mice, although we cannot discard multiple pathways being involved in this resistance, not inspected during this PhD thesis.

In this respect, other authors have already described that treatment with alkylating agents (e.g., TMZ) trigger host immune system recruitment by elevated calreticulin, adenosine triphosphate (ATP) release, and nuclear protein high-mobility group box-1 (HMGB1) secretion. [191]. Our working hypothesis is that one of the reasons contributing to GL261 tumour regrowth during IMS-TMZ would be the appearance of tumour cell sub-clones which up-regulate PD-L1. These PD-L1 overexpressing tumour cells would be protected from productive T-lymphocyte attack and, consequently, would finally replace the tumour cell population not overexpressing PD-L1. This new, resistant cell population would finally lead to tumour escape due to the immunosuppressive effect of increased PD-L1 content. With respect to control tumours, they should barely trigger the production of immunogenic signals due to the lack of damage caused by TMZ, thus resulting in less T cell infiltration into tumour tissue. Accordingly, no pression for selection of tumour cells with increased PD-L1 expression for clonal expansion would happen.

In the case of “non-responding” GL261 tumours, results showed that the expression level of PD-L1 was equivalent to vehicle-treated tumours, and 3.4-fold lower than in late relapsing ones. Our hypothesis to explain this difference is that “non-responding” tumours would escape therapy by a different mechanism, not yet clarified, as opposed to “late relapsing” tumours, which could use high PD-L1 content for this. Initial tumour mass duplication times (“non-responding” 1.7 ± 0.6 days vs “late relapsing” 2.2 ± 0.4 days) and, eventually, overall tumour mass could probably hamper on its own immune system capability of the host [189], then, no positive selection for PD-L1 high expression clones would be required in this instance for tumours to grow unencumbered. This result brings us significant insight for future

research in preclinical GL261 GB, indicating that anti- PD-1 immunotherapy should be more effective as second line treatment in late relapsing GL261 tumours, while combined TMZ and kinase inhibitors such as CX-4945 may be best for fast growth, “non-responding” GL261 tumours [168]. In addition, CK2 kinase inhibitors could contribute an added value through another pathway, impairing hypoxia-inducible factor (HIF) stabilization which in turn could lead to decrease of PD-L1 content [222]. These hypotheses are amenable to test in future work and can lead to further improvement of the outcome of tumour-bearing mice.

4.3.5 Conclusions

- MGMT and PD-L1 were measured in vitro in the GL261 cell line with suitable results comparable to literature.
- MGMT does not seem to play a role in tumour escape in GL261 GB under TMZ therapy. No significant changes were observed in MGMT expression either in vitro (different TMZ concentrations) or in vivo (IMS-TMZ protocol).
- Regarding PD-L1 expression levels, a 3-fold increase was observed in IMS-TMZ relapsing tumours in comparison with control tumours. This result indicates that PD-L1 can be one of the pathways involved in TMZ resistance for GL261 GB in vivo, although we cannot discard that part of the measured PD-L1 expression would be present in macrophages within the tumour tissue
- “Non-responding” GL261 tumours, which escaped treatment from the beginning, did not show the same trend, presenting a PD-L1 expression similar to control tumours. In this type of tumours, the underlying resistance mechanism is still unclear and requires further exploration.
- These results indicate that anti-PD1 therapy may have a great potential, either in combination/monotherapy or as a second line to ‘rescue’ tumours escaping from TMZ therapy, at least in our experimental setting. Additional work with other GB preclinical models may help to evaluate the translational potential of this therapeutic strategy.

5 GENERAL DISCUSSION

5.1 The involvement of the immune system in preclinical GB treatment: challenges and opportunities

Although significant progress has been made in basic glioma research in recent years, the clinical outcome and prognosis is still poor in the clinical practice. GB patients treated with the current standard treatment, including maximum safe surgical resection, chemo-radiotherapy and adjuvant TMZ chemotherapy, only have a median survival time of 15-18 months. The standard first line protocols in clinics are still based in the Stupp and col studies [223][21]. Alternative approaches such as addition of tumour treating fields ([224], clinical trial NCT00916409), angiogenic agents [225], targeted therapies ([226], clinical trial NCT01582269) or immunotherapy [106], [107] did not produce relevant outstanding advances in GB outcome. This is probably a sum of different factors, including limitations in the current follow-up protocols which underline the urgent need of improving patient follow-up for early detection of relapse/resistance. Moreover, some therapeutic approaches being tested do not take into account (or not enough) the need to spare and/or enhance host immune system to fight tumours.

The last decades changed our understanding of brain and glioma microenvironment, including immune environment. In the traditional view, brain has been conceived as an immune-privileged organ due to lack of lymphatic drainage. The blood-brain barrier (BBB) was considered to limit entrance of pathogens and peripheral immune cells into the brain parenchyma. However, a study [227] published in 2015, reported that CNS can interact with the peripheral immune system through functional meningeal lymphatic vessels, which provides a basis for the immune system acting as a key player in cancer progression, also in brain [228]. In addition, the bioactive substances secreted by the tumour could change the tumour microenvironment Thus, vascular endothelial growth factor (VEGF) secreted by tumour cells can effectively disrupt tight junctions and vascular endothelial barrier integrity resulting in a severe compromise of the BBB [229]. In a sense, BBB disruption increases cerebrovascular permeability, allowing/enhancing the entrance of drugs and immune elements into the brain tumour site. Ultimately, if properly activated, these immune elements have a leading role in brain tumour fighting and this has been widely supported by several authors in literature [230][173].

As shown in Figure 5.1 (also Figure 4.17), the cancer-immune cycle is roughly divided into 6 steps : (1) tumour cell damage with release of DAMPs and cancer antigens, (2) cancer antigen presentation, (3) T cells priming and activation, (4) T cells trafficking to tumour, (5) infiltration of T cells into tumour, and (6) T cell recognition and killing tumour, probably with the help of tumour infiltrating macrophages with suitable phenotypes.

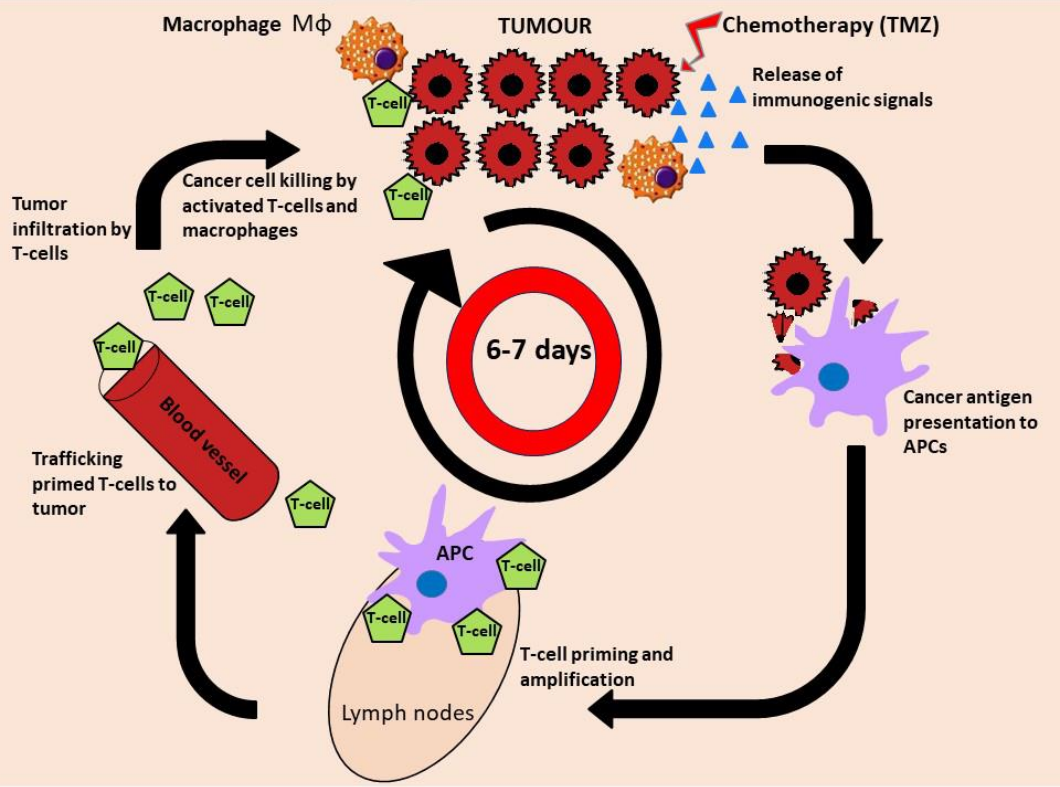

Figure 5.1 Cancer–immunity cycle. *Tumour antigens released from tumour cells are recognized by antigen-presenting cells (APCs). Matured APCs migrate to the lymph nodes, leading to priming and proliferation of T cells. T cells activated by APCs are transferred to tumour tissues, where they kill tumour cells with the help of tumour infiltrating macrophages. Finally, tumour antigens from killed cancer cells induce another round of the immune response, leading to a cancer–immunity cycle. Figure adapted from* [158].

It is worth noting that GBs are heterogeneous environments where neoplastic and non-neoplastic cell types interact, influencing their growth, progression and response to therapy. The tumour microenvironment (TME), i.e. non-neoplastic cells within tumour milieu, may help supporting tumour growth [231]. In addition, the epigenetic flexibility of GB cells may lead to a pluripotent environment that can adapt to changes and select resistant clones that can regrow after transient response to a given therapy [232]. Moreover, GB can create an immunosuppressive environment either through Tregs or generation of myeloid derived

suppressor cells (MDSC) through Il-10 and arginase production [233]. This immunosuppressive environment is one of the main challenges in GB treatment.

Accordingly, and having in mind the scheme depicted in figure 5.1, different items may be taken into account during therapy, namely: production of suitable immunogenic cell damage with release of DAMPs and antigen presentation; avoiding to apply unspecific antiproliferative strategies during the time of T-cell amplification; skipping or counteracting possible immunosuppressive strategies engaged by GB or other cells from the tumour microenvironment.

5.1.1 Different therapeutic strategies can enhance or spare host immune system

Historically, chemotherapy has been applied at maximum tolerated doses alternated with considerable rest periods in between, which usually involves tumour regrowth and selection of resistant clones [234]. However, this type of administration protocol is clearly neglecting the relevance of immune system participation in response to therapy. "Metronomic chemotherapy" refers to regular (equally spaced) administration of traditional chemotherapeutic agents at very low doses and was initially thought to act mainly against endothelial cells supporting the tumour vasculature; however, other mechanisms have been also observed, including activation of anti-tumour immunity [235].

In preclinical models of GB, regularly spaced (every 6-7 days) ‘metronomic’ administration of chemotherapy produced optimal results, inducing immunological memory and cure for some animals [38], [159], [192]. This is in agreement with the ca. 7-day period for brain T-cell lymphocytes peak increase after an antigen activation episode [39] and it is also in agreement with results described in this thesis and recently published [169]. We coined the expression Immune-Enhanced Metronomic Schedule (IMS) to make apparent the need for the every 6 days chemotherapeutic administration frequency.

TMZ has been described to be able to produce immunogenic cell damage with release of CRT [40] which is in agreement with in vitro results with GL261 cells [188]. In the same line, in a clinical study, authors reported that TMZ treatment leads to recruitment of the hosts' immune system, which ultimately leads to death of tumour cells [191]. Combining the ability to produce enough immunogenic cell damage and administration in an immune respectful protocol, avoiding affecting the T-cell amplification periods, gave TMZ treatment a much

more powerful perspective, since it is not a matter that TMZ must kill all tumour cells, but a) should damage enough cells to release DAMPs and cell antigens, and b) administration must be halted in the period of T-cell amplification to avoid its impairment. In this thesis we have gone one step further to facilitate reproducibility of results and implemented the enriched environment (EE) housing which was described to improve NK cell infiltration and anti-tumour activity in mice, increasing the survival time of mice harbouring GB [166]. Historical and present group results reflect a clear improvement of the survival of treated mice, allowing access to exploration time long enough for evaluation of response biomarkers. In previous studies of our group, TMZ (60 mg/kg) administered in IMS had been shown to produce an improved survival rate (38.7 ± 2.7 days) [168] in comparison to the standard "three cycles" schedule (33.8 ± 8.7 days) [160], which was better but still having much room for improvement to produce a good model for response biomarker development. In this thesis, the IMS-TMZ (60 mg/kg) administration protocol achieved a much better survival rate (135.8 ± 78.2 days) than the previous work [168]. We postulate that a possible reason for this high improvement may be attributed to the enhancement of mice living environment in combination with immune respectful administration protocols. In summary, we may have clear immune effects even without the use of a 'direct immunotherapeutic agent'. However, despite IMS-TMZ and EE inducing improved survival rates of GL261 tumour-bearing mice, 38.5% of tumours in our longitudinal studies eventually relapsed after transient tumour volume shrinkage, introducing variability into the cohort for potential biomarker performance evaluation and, as a consequence forcing extended follow-up studies (up to 2 year follow-up has been performed in this PhD) to potentially evaluate whether a certain biomarker profile would anticipate cure or relapse. Two of the described factors related to TMZ resistance in relation to GL261 relapse (MGMT and PD-L1 expression) were assessed in relapsed samples and only PD-L1 was found relevant in this context, which provided an additional rationale to study anti-PD-1 immunotherapy in this preclinical model, either as monotherapy or in combination with TMZ.

5.1.2 Lessons learned from TMZ/anti-PD-1 combination therapy studies

An important tumour survival strategy is immune escape. There are several tumour-immune escape mechanisms, including immunosuppression, which has become a research hotspot in recent years. The PD-L1 / PD-1 signalling pathway is an essential component of tumour immunosuppression, which can inhibit T lymphocyte activation and enhance tumour cell

immune tolerance, resulting in tumour immune escape. Thus, targeting the PD-L1 / PD-1 pathway will be an effective strategy for cancer treatment.

Indeed, results described in section 4.3 suggest that PD-L1 overexpression in relapsing GL261 GB tumours could be related to TMZ resistance, stressing again the relevance of the immune system cells in this process. In a variety of cancer types, the immune-suppressive function of the PD-1 / PD-L1 immune checkpoint pathway emerges as a promising oncological target and several preclinical and clinical studies are ongoing, including GB. Having the result regarding relapsing tumours in mind, we hypothesized that the combination of IMS-TMZ chemotherapy with anti-PD-1 immunotherapy would be a good strategy to improve the efficacy of GB treatment.

Our results, although based in a restricted cohort of mice yet, confirm this hypothesis. Namely, 100% of the mice treated with TMZ+anti-PD-1 combination were cured, an outstanding result that was not achieved before with similar strategies in the standard GL261 model (IMS-TMZ monotherapy cure rate was 61.5%). This is in line with work from other authors [141] which obtained 100% of cured mice with combination therapy, although with a different protocol of administration and using GL261-luc cells, which express luciferase, a potentially immunogenic product. Our hypothesis is that under the strategy of combination therapy, the use of anti-PD-1 counteracts the early appearance of overexpressing PD-L1 tumour cell subclones/phenotypes that could lead to escape from TMZ monotherapy without the adjuvant anti-PD-1 help. Therefore, these high PD-L1 cells may be also eliminated by activated effector T cells. In another similar study [170], mice received anti-PD-1/TMZ combination therapy from a very early stage (at day 2 p.i.). However, while their treated tumours were smaller than ours, the reported mice survival rate was much lower than in this PhD (long-term survival: 40%, their work, vs 100%, this work). This might reconciled with our data because they used different dose and therapy administration protocol: their mice received anti-PD-1 200 µg / times and three times in total, besides their TMZ was given at a slightly lower dose (50 µg/kg) and in during 5 consecutive days, which is not an immune respectful administration protocol.

Besides, considering the steps of the cancer-immunity cycle in anti-tumour therapy (figure 5.1), the combination of IMS-TMZ and anti-PD-1 therapy may contribute to different points. These two therapeutic agents may exert complementary anti-tumour effects through

different mechanisms. TMZ acting on step (1) lasting hours, and which releases antigens from the killed/damaged tumour cells and the anti-PD-1 therapy mostly acting on the final step (6), lasting days, but picking at day 6 of the cycle, enhancing T-cell-mediated cell killing, and the concomitant release of additional, potentially new, tumour-associated antigens from damaged tumour cells, to increase the breadth and depth of response in the subsequent cancer-immunity cycle.

Nonetheless, the experimental steps performed in this thesis have opened up additional questions to consider: first, even that combination therapy resulted successful, especially with initial small tumour volumes, anti-PD-1 alone at 100 μg in monotherapy did not produce the expected results from literature, showing no significant survival benefit when compared to the control group. Secondly, the tumour volume at therapy starting time proved to be closely related with outcome in combination therapy, with smaller tumours (5.4 ± 1.8 mm^3, average of volumes used in previous group studies) being more easily controlled than larger ones (10.8 ± 0.7 mm^3). This type of difference was already considered in literature from a generic perspective [189], and it is probably related to a balance (or lack of) between the pressure of actively proliferating cells and that of immune system cells in charge of abnormal cell killing. In addition, larger tumours can be more heterogeneous, having more hypoxic zones which could enhance PD-L1 expression [236] although more detailed studies will be needed to support this hypothesis. In our experimental conditions, the dose of 100 μg/day of anti-PD-1 used in combination therapy may have been too low to provide enough T-cell rescue, eventually leading to tumour recurrences when larger initial tumour volumes were encountered. The information about tumour volume at therapy starting point is usually missing or not detailed in many preclinical studies, thus direct comparisons with our results are not straightforward. For small tumour volumes, the combination therapy produced an excellent outcome and further work may be still performed in order to check whether it would be possible to decrease TMZ dose in combination schemes, which would have a clear interest in a translational landscape.

Our take-home messages from this section were that we would need to investigate a) the effect of anti-PD-1 monotherapy at higher doses, based in literature doses and protocol published in this regard, and also used in IMS protocols, and b) whether the tumour volume at therapy starting time would be also determinant in monotherapy protocols.

5.1.3 Anti-PD-1 monotherapy: facts about dose schedule and therapy starting volume

Finding an optimal combination of tumour starting volume and dosage was one of our main goals to proceed with further studies investigating non-invasive MR-based biomarkers of therapy response to evaluate whether we could also spot response by imaging, while including immunotherapy in therapy protocols, as already observed using TMZ monotherapy [151], [158].

5.1.3.1 Tumour volume at therapy start time

Since the 100 µg/day monotherapy did not produce the expected results from published literature (increasing median survival to 37 days, allowing 10% long term survivors [142]) we wondered whether a different dose had to be considered. Reardon et al [105] described in 2016 that anti-PD-1 monotherapy in a protocol with 500 µg initial dose followed by 250 µg/day every 3 days (see figure 4.3 B "E3D" for a schema) in a similar GL261 preclinical model would produce 50% long-term survival rate and induce 100% immune memory in cured mice. Preclinical doses described in literature are quite different from human dosage described in clinical trials. Doses described in murine glioma models ranged from 5-25mg/kg each application (doses transformed for comparison with human clinical trials), with application intervals ranging from every 2 to every 7 days, within a restricted time frame. Human patients received much lower doses ranging 2.6-3.2 mg/Kg, every 2 or 3 weeks depending on the study, probably due to the panoply of immune-related side effects described in patients receiving these therapeutic agents [237] which is either absent or not evident in mice. Some studies even proposed to administer anti-PD-1 agents prior to surgery [196], which was not attempted in this thesis because no surgery was performed in mice.

Since it was not feasible to investigate/reproduce all protocols described in literature, we chose to test Reardon and col anti-PD-1 protocol (500/250 µg /day) investigating the impact of tumour volume at therapy starting time, maintaining all timing and dose as described by authors, i.e. treatment started 6 days post implantation. The effectiveness of anti-PD-1 monotherapy might depend on the proliferation rate and initial tumour size. Thus, our treatment results demonstrate mice bearing small initial tumours (2.2 ± 1.1 mm^3) achieved significantly better survival rate than the relatively large initial tumour (9.6 ± 2.2 mm^3) group (75 % vs 0 %), which is still better than the results reported by Reardon et al [105] (75% vs

50%). Still, the same way we can have a large dispersion (1.1–11.8 mm^3 range) in tumour volumes at day 6, the same could occur in the Reardon et al study [105], thus we cannot really be sure which of our evaluated mice groups would be most comparable with their results. Research by others has suggested that the total tumour mass could potentially compromise the host's own immune system capability [189], therefore, estimation of the initial tumour volume at the therapy starting day may be needed for comparing immunotherapy efficacy among different studies. Our overall conclusion here is that tumours with a large volume at therapy starting time may not benefit as much as small tumours from immunotherapy, at the same dose. In these tumours, which, incidentally, show a shorter duplication time in our GL261 model (See Figure 5.2 "large initial tumour group") could benefit from other therapeutic strategies/combination (see for example good results obtained for TMZ/CK2 inhibitor combination)[168].

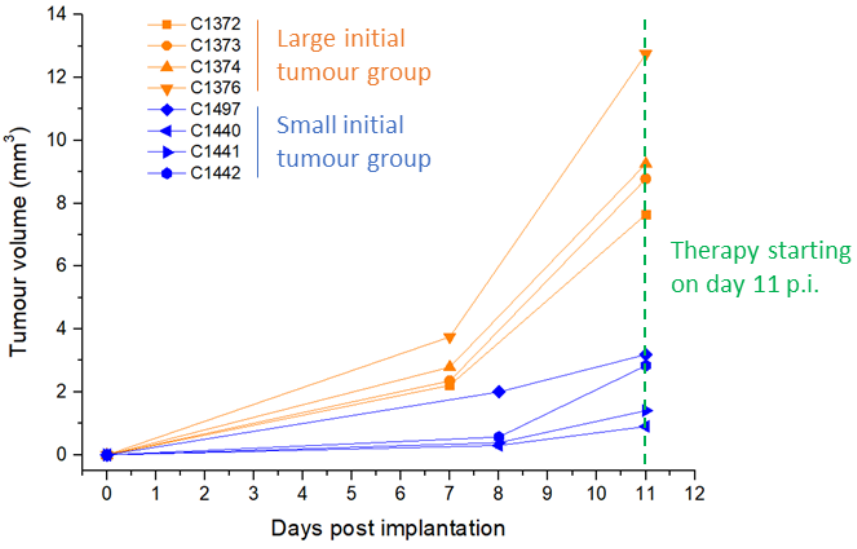

Figure 5.2 Example of tumour growth curve. GL261 *tumours in the "large initial tumour group" show a shorter duplication time, on the contrary, tumours in the "small initial tumour group" show a clearly slower duplication.*

Protein kinase CK2 has been described as linked to cell growth and proliferation [238][239] and GL261 tumours have been described to contain higher levels of it [240], being also sensitive to CK2 inhibitors in vitro [168]. One interesting item to be further investigated in "fast growing tumour" cases is whether CK2 inhibition can enhance glioma cells sensitivity to TMZ through CK2-STAT3-MGMT signaling [241].

5.1.3.2 Administration schedule

Once it was clear which tumour starting volumes should clearly benefit from anti-PD-1 immunotherapy, we wondered whether the anti-PD-1 dosage could be administered also in an IMS protocol. This would allow reduction of the overall dose received by mice and synchronization with TMZ administrations. For that, we compared anti-PD-1 administration "every 3 days (E3D)" protocol as described in [105] with our IMS protocol (i.e. every 6 days). The rates of cured mice were nearly identical in both groups (66.6% vs 60%), and this was better than Reardon et al [105] (50% long-term survival), also better than another study with applied anti-PD-1 every 7 days [142] (10% long-term survival). Furthermore, the overall dosage was almost halved. Immunotherapy (anti-PD-1) administered in every 6 days cycle could comply with the cancer-immunity cycle being administered in the time point that it would be more beneficial, i.e. when a new wave of immune system cells arriving to the tumour site is peaking. Additional doses, although did not exert a negative effect, did not seem to result in an added survival benefit. Moreover, reducing the cumulative amount of anti-PD-1 administered is relevant to decrease the risk of developing dose-dependent autoimmune response [190], although future complementary studies may be needed to investigate which protocol may be feasible in human patients.

It is worth noting that GL261 tumour escaping from anti-PD-1 monotherapy showed a different tumour growth behaviour in comparison with transiently responding? TMZ treated tumours. Different from showing an obvious transient tumour volume shrinkage, the escaping tumour treated with anti-PD-1 would only slow down the growth rate, but no reduction of tumour mass was observed during the entire period of investigation (Figure 4.14 and Figure 4.15), similarly to some TMZ treated tumours not responding at the start point. This suggests that these tumours were only slowed down in their growth by immunotherapy, but no partial response was detected according to adapted RECIST criteria. Although the exact mechanism for tumour escape is unclear in this case, it is worth mentioning that resistance to immunotherapy has been described to be either primary resistance (a cancer does not respond to an immunotherapy strategy), adaptive immune resistance (cancer is recognized by the immune system but it protects itself by adapting to the immune attack) or acquired resistance (cancer initially responded to immunotherapy but after a period of time it relapsed)

(see [242] for a comprehensive review). The main reason behind PD-1 blockade treatment failing, however, seems to be lack of proper immune cell infiltration at tumour site, which could be mediated by several mechanisms such as lack of antigenic mutations, disruption of the interferon (IFN) signaling pathway, among others. Recent literature reported that P21-activated kinase 4 (PAK4) is enriched in tumour biopsies with low-T-cell and dendritic cell infiltration [243]. This opens the door for future work by combining of anti-PD-1 with PAK4 inhibitors (e.g. KPT-9274) in case of initially unresponsive/escaping tumours.

5.1.4 Immune memory

Our previous results, in addition to unpublished results from still ongoing work, suggest that the host immune system is having a key role in both IMS chemotherapy and immunotherapy in our preclinical model. Some authors [38] have previously described that every 6 day CPA-based chemotherapy produced cure in 64.2% of mice with a subcutaneous GL261 model, also with immune memory in 66.7% of the cured cohort, rejecting tumour reimplantation. They examined levels of immune cells in mice that rejected GL261 re-implanted tumours and compared it to mice with growing GL261 tumours. Using FACS they found an increased number of CD8+ T cells and a decreased number of circulating macrophages and myeloid-derived suppressive cells (MDSCs) populations in cured mice treated with “metronomic” IMS-like CPA treatment, which rejected the GL261 tumour on re-challenge. Additionally, other authors [105] demonstrated that anti-PD-1 monotherapy was effective against intracranial preclinical glioblastoma tumours (50% long-term survival), and with immune memory in 100 % of anti-PD-1 monotherapy cured mice. Similarly, they found local infiltration of effector CD8+ cells and increased content of activated NK cells in the draining cervical lymph nodes of treated tumours. Likewise, the proportion of immunosuppressive lymphocytes, including Tregs, PD-1+ lymphocytes, PD-1+/TIM-3+ exhausted T cells and MDSCs, simultaneously decreased.

We wanted to investigate whether immune memory would also take place in our mice cohorts and performed tumour re-challenge experiments with all cured mice. Animals bearing GL261 tumour ablated with IMS-TMZ or anti-PD-1 monotherapy displayed a strong immune-memory effect (i.e. 88% tumour rejection rate), whereas a weaker anti-tumour immune memory (57% tumour rejection rate) was observed in mice cured with anti-PD-1 / TMZ combination therapy. In case of IMS-TMZ, sequential administration of TMZ produces cell

damage and antigen presentation to immune system cells, while halting administration during 5 days enable lymphocyte proliferation after LN priming. This may probably allow host familiarization with major tumour antigens to unleash a strong immune response whenever a tumour re-challenge is attempted. Regarding the high tumour rejection rate in anti-PD-1 monotherapy cured mice, this type of tumour-specific immune response to a possible tumour re-challenge is one of features of immunotherapy as described by different authors [105], [141], [195]. Surprisingly, with the anti-PD-1/ TMZ combination therapy, poorer anti-tumour immune memory capacity (57% tumour rejection rate) was observed in the studied cohort. It is not fully clear why the combination therapy is not as effective as monotherapy regarding immune memory and further studies with different cell populations such as CD8+ T cells, circulating macrophages and MDSCs (the same described by Wu & Waxman [38]) would be helpful to elucidate the ongoing mechanisms. Park et al [141] treated GL261 GB bearing mice with anti-PD-1/TMZ combination therapy and were not able to generate immune memory in their cohort, as opposed to the result obtained in our case with anti-PD-1 monotherapy. However, this result may be explained by differences in the protocols of administration, especially of TMZ, which was administered 5 days in a row which should mostly abolish immune memory generation by inhibiting adequate T-lymphocyte amplification at the proximal ganglia. In this respect, the immune memory establishment rate (50%) with our combination therapy group reinforced the concept of IMS-TMZ as an immune-respectful administration protocol with potential to be further improved and applied in clinical trials, if properly administered. In addition, another research team, found that the anti-tumour immunity bolstered by anti-PD-1 therapy is abrogated by chemotherapy when chemotherapy is administered in a systemic manner (e.g. oral administration) compared to local administration, with reduced immune memory in long-term survivors [111]. However, it allowed persistent immunological memory generated by anti-PD-1 therapy when chemotherapy was administered in a local modality (intratumour), i.e. avoiding the harmful effects in lymph nodes which would impair T-cell amplification. This gives us new insight into combination therapy, and in future research we should not only focus on the schedule of treatment administration, but also consider different modes of chemotherapy delivery.

It is worth mentioning that our main goals in this PhD thesis went beyond finding an optimal therapy recipe for GL261 cure or to extensively study all types of cells involved in the immune

memory, although this was an interesting outcome of the work done and may have translational interest for future collaboration. Thus, one of the major focus of our research group is the investigation of early, robust, non-invasive therapy response biomarkers for GB, using MR-based approaches. If proven consistent, those imaging biomarkers could be translated to clinics in future work, and benefit GB-afflicted patients while saving resources to the public health system through discontinuation of unsuccessful therapies or early switching to second-line therapeutic protocols. However, in order to be translated, these approaches should be extensively tested and molecularly validated in preclinical models, such in our case the GL261 GB immunocompetent model. For that, we needed therapeutic approaches that produced transient responses in such preclinical GB models. We already described in the GABRMN group that the MRSI-based metabolomics pattern, when properly analysed with advanced pattern recognition methods, could act as a surrogate biomarker of therapy response when a standard three cycles 5-2-2 TMZ protocol was administered to GL261 GB bearing C57BL/6 mice, and histopathological/molecular data suggested that this surrogate biomarker and its oscillatory behaviour was at least partially explained by changes in cellular populations of host immune system. We wondered whether the inclusion of immunotherapy in the GL261 GB treatment, either as monotherapy or in combination therapy would still produce similar metabolomic changes and response could then be detected using the same MRSI-based biomarker.

5.2 Immune system participation in therapy response sampled by MRSI-based nosological imaging

Monitoring of therapy response in GB is generally carried out through non-invasive techniques, especially magnetic resonance, since repeated biopsy is not feasible or advisable in these cases. Clinical guidelines are mostly based in MRI regarding tumour volume/contrast enhancement, while MRS (spectroscopic information) is not fully integrated in clinical pipeline due to complex processing and not straightforward interpretation by radiologists. In addition, since MRI information can be misinterpreted due to phenomena such as pseudoresponse or pseudoprogression, the information about therapy efficiency is delayed. Moreover, therapies that do not properly trigger/stimulate the host immune system will fail, and having this information as early as possible would help clinicians in patient management: ineffective

therapies could be halted and patients switched to possible second line or combinations, while effective therapies should be maintained even if changes in contrast enhancement/tumour volume are not informative enough. Our MRSI-based surrogate biomarker can provide this type of information and the suitable postprocessing and analysis of MRSI data allow its transformation into an image-like output which can be easily interpreted by radiologists. Exhaustive longitudinal studies are needed in order to characterize such biomarkers and preclinical GL261 GB models were used in this thesis to conduct systematic studies of the monitoring of response to therapy.

As expected, an oscillatory behaviour of the MRSI-based surrogate biomarker was also observed with the IMS-TMZ treatment in GL261 GB tumour-bearing mice. The period between treatment administration and the appearance of the first TRI peak is consistent across different cases, ranging from 4-8 days during regular transient response periods. The average time period value recorded between TMZ administrations and TRI peak appearance was 6.2 ± 1.4 days, in agreement with previous data from our group with the standard three-cycle TMZ administration protocol (distance between TRI maxima, 6.3 ± 1.3 days, n = 4) [158]. It has also been shown that, before or during the relapse of the tumour, these oscillations disappeared or we encountered a different TRI behaviour: either TRI assumed an increasing, non-oscillating trend, or only showed small, incipient increases. This confirms that consistent TRI oscillations are related to metabolic changes due to tumour response to therapy, but are mostly absent during relapse of the tumour.

TMZ is nowadays accepted as a drug that causes release of immunogenic signals by target cells [40][201]. Our hypothesis for these TRI maximum peaks is that each turn of TMZ administration triggers a new 'turn' in the immune cycle, and the arrival of a new immune system T-cell subclones to the tumour site displays local effects over tumour cells and the tumour microenvironment, ultimately leading to changes in the spectral pattern, sampled by MRSI acquisitions. Previous work from our group with standard TMZ treatment (samples from [158] and unpublished work) showed several histological/molecular differences between tissues recognized as “responding” or “unresponsive/control” by the MRSI-based surrogate biomarker, which could explain such changes. Regions identified as “responding” were analysed by immunohistochemistry and showed higher CD3 + (marker of lymphocytes) and Iba-1+ (microglia / macrophages marker) immunostaining in contrast with control cases or

"unresponsive" regions. In addition, the imaging biomarker was demonstrated to be associated with the Ki67 proliferation index [158][151], higher in unresponsive/control zones, as expected. Still, treated samples showed presence of giant multinucleated cells and higher percentage of acellular spaces which could have been contributed by extracellular matrix. Moreover, unpublished data from work in progress shows that the population of glioma-associated microglia / macrophages (GAMs) was larger and the ratio of M1 / M2 macrophage phenotype was higher in responding tumours. Since the overall changes in the MRSI-based biomarker are probably a sum of several factors, we may not forget that in order to be spotted by MRSI, changes should represent enough volume inside the sampled region. This means that low percentage cellular populations (e.g. lymphocytes which account for ca. 1% of tumour volume in evaluated GL261 tumours) will not produce direct noticeable changes in the MRSI pattern. On the other hand, GAMs can account for up to 30% of the cells in the tumour tissue [202] and M1 and M2 macrophages have various metabolic profiles [203], and most probably would be one of the key variations contributing to spectral patterns changes in responding tumours. In summary, all these related factors listed above could make the MRSI response pattern an immune system efficiency biomarker.

All those changes in the spectral pattern which are reflected in changes in the nosological images with the observation of TRI maximum peaks, which appear in average 6.2 ± 1.4 days (n = 10) after TMZ therapy administration, which is in line with the length of immune cycle in mice brain, described to be of ca. 6 days [39]. Available data strongly suggest that these changing metabolic patterns are related to immune system action within the tumour tissue, but there were no studies without chemotherapy (TMZ, CPA) and one of the reasonable doubts arising was whether this biomarker were induced by the chemotherapeutic drug specific local action, or whether this would be also observed with using direct immunotherapy therapeutic agents.

In this sense, longitudinal studies with nosological images based on MRSI were performed with GL261 GB bearing mice under IMS-anti-PD-1/TMZ or IMS-anti-PD-1 monotherapy treatment. For the first time, appearance of TRI maxima (8 ± 2 days, n = 3) followed by decrease was observed both in the combination therapy group and the immunotherapy alone group. The TRI oscillation frequency of these series seems slightly longer than in TMZ-treated cases (6.2 ± 1.4 days, n = 21), but non-significantly. Since two of the evaluated cases got cured,

this prevented us to check whether subsequent TRI cycles would be observed. However, in the small cohort of mice evaluated for this purpose, the TRI oscillation seems to appear while tumour is either transiently responding to therapy or getting cured, as with the TMZ therapy. In addition, especially with anti-PD-1 monotherapy, the spectral pattern changes detected and used by the source-based classifier to colour code the nosological images, should be due to the action of host immune system alone, without any confusing effects due to chemotherapy.

Visual inspection of the spectral pattern of immunotherapy-treated cases showed that the spectral quality is good and the metabolomic profiles are the expected according to previous work, with contribution of metabolites such as lactate, mobile lipids, PUFAs, choline, creatine, alanine, glutamate/glutamine, with no unexpected major contributions. The semi-supervised pattern recognition approach promptly recognized local tissue changes in the same way that was described for TMZ- or CPA-treated cases.

Data obtained supports that the responding ("green") MRSI-based spectral pattern appearing in form of maximum/minimum during tumour response can be correlated with the effective action of the host immune system against the tumour. This would enable the application of such biomarker development concept for monitoring the evolution of GB patients assessing TRI variations and could make it possible to design personalized therapeutic schemes for GB patients. Low TRI values or lack of oscillation would be considered a negative signal pointing to weak local immune action and treatment regimen switch would have to be considered as early as possible.

However, this will require extensive validation of the local changes taking place in responding zones, currently in progress in our group in PhD theses still ongoing. Further confirmation of such changes in immunotherapy treated mice may be also considered in a future work. Finally, we are aware that a translational proposal of our biomarker including repeated MRSI exploration in patients would not be easy/feasible. In this sense, the collaboration with the bioinformatics branch of the group is starting to combine MRSI and advanced MRI data analysis, which may help to improve the future translational potential and application of this knowledge in clinics.

6 GENERAL CONCLUSIONS

Suitable combination of oncology and immunology knowledge will pave the way for future GB treatment and improve patient outcome. We have explored in an immunocompetent, aggressive GB preclinical model how using immune respectful administration protocols can strongly stimulate anti-tumour immune responses, even leading to cure and immune memory again new tumour re-challenges. Furthermore, we have explored GB treatment with direct mitigation of the tumour-based immune suppression microenvironment (PD-1 / PD-L1 pathway blockade) either as monotherapy or in combination with TMZ, with outstanding results not achieved before with comparable treatments in the GL261 GB model. We have also proved, for the first time, that the metabolomic spectral patterns spotted by our MRSI-based surrogate biomarker of therapy response are also observed using anti-PD-1 monotherapy, in agreement with these changes being, at least partially, contributed by the local immune system action against tumour cells. This finding confirms that the MRSI-derived biomarker is not linked to a given therapeutic agent or protocol and should be investigated in any therapeutic approach for GB involving host immune system activation. Possible translation of these protocols would allow to assess, in an early and confident way, therapy efficacy and help in patient management. Further studies may be needed in order to fully characterize the molecular/cellular changes related to the spectral pattern changes detected. Last, but not least, such imaging biomarker could be useful in the follow-up of other brain pathologies in which the immune system can play a role such as stroke or neurodegenerative diseases.

7 REFERENCES

[1] Q. T. Ostrom, G. Cioffi, H. Gittleman, N. Patil, K. Waite, C. Kruchko, and J. S. Barnholtz-Sloan, “CBTRUS Statistical Report: Primary Brain and Other Central Nervous System Tumors Diagnosed in the United States in 2012–2016,” *Neuro. Oncol.*, vol. 21, no. Supplement_5, pp. v1–v100, 2019, doi: 10.1093/neuonc/noz150.

[2] A. Omuro and L. M. DeAngelis, “Glioblastoma and other malignant gliomas: A clinical review,” *JAMA - J. Am. Med. Assoc.*, vol. 310, no. 17. pp. 1842–1850, 2013, doi: 10.1001/jama.2013.280319.

[3] M. Weller, W. Wick, K. Aldape, M. Brada, M. Berger, S. M. Pfister, R. Nishikawa, M. Rosenthal, P. Y. Wen, R. Stupp, and G. Reifenberger, “Glioma,” *Nat. Rev. Dis. Prim.*, vol. 1, no. 1, p. 15017, 2015, doi: 10.1038/nrdp.2015.17.

[4] K. Kwan, J. R. Schneider, N. V. Patel, and J. A. Boockvar, “Tracing the Origin of Glioblastoma: Subventricular Zone Neural Stem Cells,” *Neurosurgery*, vol. 84, no. 1, pp. E15–E16, 2019, doi: 10.1093/neuros/nyy512.

[5] J. H. Lee, J. E. Lee, J. Y. Kahng, S. H. Kim, J. S. Park, S. J. Yoon, J.-Y. Um, W. K. Kim, J.-K. Lee, J. Park, E. H. Kim, J.-H. Lee, J.-H. Lee, W.-S. Chung, Y. S. Ju, S.-H. Park, J. H. Chang, S.-G. Kang, and J. H. Lee, “Human glioblastoma arises from subventricular zone cells with low-level driver mutations,” *Nature*, vol. 560, no. 7717, pp. 243–247, 2018, doi: 10.1038/s41586-018-0389-3.

[6] G. S. Stoyanov, D. Dzhenkov, P. Ghenev, B. Iliev, Y. Enchev, and A. B. Tonchev, “Cell biology of glioblastoma multiforme: from basic science to diagnosis and treatment,” *Med. Oncol.*, vol. 35, no. 3, p. 27, 2018, doi: 10.1007/s12032-018-1083-x.

[7] S. Yadavalli, V. M. Yenugonda, and S. Kesari, “Repurposed Drugs in Treating Glioblastoma Multiforme: Clinical Trials Update,” *Cancer J.*, vol. 25, no. 2, pp. 139–146, 2019, doi: 10.1097/PPO.0000000000000365.

[8] T. J. Brown, M. C. Brennan, M. Li, E. W. Church, N. J. Brandmeir, K. L. Rakszawski, A. S. Patel, E. B. Rizk, D. Suki, R. Sawaya, and M. Glantz, “Association of the extent of resection with survival in glioblastoma a systematic review and meta-Analysis,” *JAMA Oncol.*, vol. 2, no. 11, pp. 1460–1469, 2016, doi: 10.1001/jamaoncol.2016.1373.

[9] S. A. Toms, W.-C. Lin, R. J. Weil, M. D. Johnson, E. D. Jansen, and A. Mahadevan-Jansen, “Intraoperative Optical Spectroscopy Identifies Infiltrating Glioma Margins with High Sensitivity,” *Oper. Neurosurg.*, vol. 57, no. 4 SUPPL., pp. 382–391, 2005, doi: 10.1227/01.NEU.000176855.39826.2D.

[10] B. van der Sanden, F. Appaix, F. Berger, L. Selek, J.-P. Issartel, and D. Wion, “Translation of the ecological trap concept to glioma therapy: the cancer cell trap concept,” *Futur. Oncol.*, vol. 9, no. 6, pp. 817–824, 2013, doi: 10.2217/fon.13.30.

[11] J. Mann, R. Ramakrishna, R. Magge, and A. G. Wernicke, “Advances in radiotherapy for glioblastoma,” *Front. Neurol.*, vol. 8, no. JAN. Frontiers Media S.A., p. 748, 2018, doi: 10.3389/fneur.2017.00748.

[12] E. J. Hall and A. J. Giaccia, *“Radiobiology for the radiologist: Seventh edition,” Lippincott Williams & Wilkins*. 2012.

[13] J. J. Grau and E. Verger, “Radiotherapy of the brain in elderly patients - Pro:,” *Eur. J. Cancer*, vol. 36, no. 4, pp. 443–447, 2000, doi: 10.1016/S0959-8049(99)00321-4.

[14] T. Bhattacharyya, K. Purushothaman, S. S. Vadakke Puthiyottil, A. Bhattacharjee, and G. Muttah, “Immunological interactions in radiotherapy-opening a new window of opportunity,” *Ann. Transl. Med.*, vol. 4, no. 3, p. 51, 2016, doi: 10.3978/j.issn.2305-5839.2015.10.44.

[15] I. J. Barani and D. A. Larson, “Radiation therapy of glioblastoma,” *Cancer Treat. Res.*, vol. 163, pp. 49–73, 2015, doi: 10.1007/978-3-319-12048-5_4.

[16] M. S. Ricci, “Chemotherapeutic Approaches for Targeting Cell Death Pathways,” *Oncologist*, vol. 11, no. 4, pp. 342–357, 2006, doi: 10.1634/theoncologist.11-4-342.

[17] R. Stupp, M. Brada, M. J. van den Bent, J. C. Tonn, and G. Pentheroudakis, “High-grade glioma: ESMO clinical practice guidelines for diagnosis, treatment and follow-up,” *Ann. Oncol.*, vol. 25, pp. 93–101, 2014, doi: 10.1093/annonc/mdu050.

[18] M. F. G. Stevens, J. A. Hickman, S. P. Langdon, D. Chubb, L. Vickers, R. Stone, G. Baig, C. Goddard, N. W. Gibson, J. A. Slack, C. Newton, E. Lunt, C. Fizames, and F. Lavelle, “Antitumor Activity and Pharmacokinetics in Mice of 8-Carbamoyl-3-methyl-imidazo[5, 1-d], 2, 3, 5-tetrazin-4(3/f)-one (CCRG 81045; M & B 39831), a Novel Drug with Potential as an Alternative to Dacarbazine,” *Cancer Res.*, vol. 47, no. 22, pp. 5846–5852, 1987.

[19] E. S. Newlands, M. F. G. Stevens, S. R. Wedge, R. T. Wheelhouse, and C. Brock, “Temozolomide: A review of its discovery, chemical properties, pre-clinical development and clinical trials,” *Cancer Treat. Rev.*, vol. 23, no. 1, pp. 35–61, 1997, doi: 10.1016/S0305-7372(97)90019-0.

[20] R. Rai, M. Banerjee, D. H. Wong, E. McCullagh, A. Gupta, S. Tripathi, E. Riquelme, R. Jangir, S. Yadav, M. Raja, P. Melkani, V. Dixit, U. Patil, R. Shrivastava, S. Middya, F. Olivares, J. Guerrero, A. Surya, S. M. Pham, *et al.*, “Temozolomide analogs with improved brain/plasma ratios – Exploring the possibility of enhancing the therapeutic index of temozolomide,” *Bioorg. Med. Chem. Lett.*, vol. 26, no. 20, pp. 5103–5109, 2016, doi: 10.1016/j.bmcl.2016.08.064.

[21] R. Stupp, M. E. Hegi, W. P. Mason, M. J. van den Bent, M. J. Taphoorn, R. C. Janzer, S. K. Ludwin, A. Allgeier, B. Fisher, K. Belanger, P. Hau, A. A. Brandes, J. Gijtenbeek, C. Marosi, C. J. Vecht, K. Mokhtari, P. Wesseling, S. Villa, E. Eisenhauer, *et al.*, “Effects of radiotherapy with concomitant and adjuvant temozolomide versus radiotherapy alone on survival in glioblastoma in a randomised phase III study: 5-year analysis of the EORTC-NCIC trial,” *Lancet Oncol.*, vol. 10, no. 5, pp. 459–466, 2009, doi: 10.1016/S1470-2045(09)70025-7.

[22] F. Nassiri, K. Aldape, and G. Zadeh, “The multiforme of glioblastoma,” *Neuro-Oncology*, vol. 20, no. 4, pp. 437–438, 2018, doi: 10.1093/neuonc/noy025.

[23] H. S. Friedman, T. Kerby, and H. Calvert, “Temozolomide and treatment of malignant glioma,” *Clin Cancer Res*, vol. 6, no. 7. pp. 2585–2597, 2000.

[24] M. Esteller, J. Garcia-Foncillas, E. Andion, S. N. Goodman, O. F. Hidalgo, V.

Vanaclocha, S. B. Baylin, and J. G. Herman, “Inactivation of the DNA-Repair Gene *MGMT* and the Clinical Response of Gliomas to Alkylating Agents,” *N. Engl. J. Med.*, vol. 343, no. 19, pp. 1350–1354, 2000, doi: 10.1056/NEJM200011093431901.

[25] S. G. Younis, R. A. E. G. Khedr, and S. H. El-Shorbagy, “Immunohistochemical analysis of O6-methylguanine-DNA methyltransferase (MGMT) protein expression as prognostic marker in glioblastoma patients treated with radiation therapy with concomitant and adjuvant Temozolomide,” *J. Egypt. Natl. Canc. Inst.*, vol. 28, no. 1, pp. 23–30, 2016, doi: 10.1016/j.jnci.2015.11.003.

[26] L. Cen, B. L. Carlson, J. L. Pokorny, A. C. Mladek, P. T. Grogan, M. A. Schroeder, P. A. Decker, S. K. Anderson, C. Giannini, W. Wu, K. V. Ballman, G. J. Kitange, and J. N. Sarkaria, “Efficacy of protracted temozolomide dosing is limited in MGMT unmethylated GBM xenograft models,” *Neuro. Oncol.*, vol. 15, no. 6, pp. 735–746, 2013, doi: 10.1093/neuonc/not010.

[27] C. Melguizo, J. Prados, B. González, R. Ortiz, A. Concha, P. Alvarez, R. Madeddu, G. Perazzoli, J. Oliver, R. López, F. Rodríguez-Serrano, and A. Aránega, “MGMT promoter methylation status and MGMT and CD133 immunohistochemical expression as prognostic markers in glioblastoma patients treated with temozolomide plus radiotherapy,” *J. Transl. Med.*, vol. 10, no. 1, p. 250, 2012, doi: 10.1186/1479-5876-10-250.

[28] R. P. Thomas, L. Recht, and S. Nagpal, “Advances in the management of glioblastoma: The role of temozolomide and MGMT testing,” *Clin Pharmacol.*, vol. 5, no. 1, pp. 1–9, 2012, doi: 10.2147/CPAA.S26586.

[29] J. Felsberg, N. Thon, S. Eigenbrod, B. Hentschel, M. C. Sabel, M. Westphal, G. Schackert, F. W. Kreth, T. Pietsch, M. Löffler, M. Weller, G. Reifenberger, and J. C. Tonn, “Promoter methylation and expression of MGMT and the DNA mismatch repair genes MLH1, MSH2, MSH6 and PMS2 in paired primary and recurrent glioblastomas,” *Int. J. Cancer*, vol. 129, no. 3, pp. 659–670, 2011, doi: 10.1002/ijc.26083.

[30] M. E. Hegi, A. C. Diserens, T. Gorlia, M. F. Hamou, N. De Tribolet, M. Weller, J. M. Kros, J. A. Hainfellner, W. Mason, L. Mariani, J. E. C. Bromberg, P. Hau, R. O. Mirimanoff, J. G. Cairncross, R. C. Janzer, and R. Stupp, “MGMT gene silencing and benefit from temozolomide in glioblastoma,” *N. Engl. J. Med.*, vol. 352, no. 10, pp. 997–1003, 2005, doi: 10.1056/NEJMoa043331.

[31] C. Happold and M. Weller, “New insights into acquired temozolomide resistance in glioblastoma?,” *Brain*, vol. 138, no. 12, pp. 3468–3470, 2015, doi: 10.1093/brain/awv301.

[32] M. Hermisson, A. Klumpp, W. Wick, J. Wischhusen, G. Nagel, W. Roos, B. Kaina, and M. Weller, “O6-methylguanine DNA methyltransferase and p53 status predict temozolomide sensitivity in human malignant glioma cells,” *J. Neurochem.*, vol. 96, no. 3, pp. 766–776, 2006, doi: 10.1111/j.1471-4159.2005.03583.x.

[33] J. Stritzelberger, L. Distel, R. Buslei, R. Fietkau, and F. Putz, “Acquired temozolomide resistance in human glioblastoma cell line U251 is caused by mismatch repair deficiency and can be overcome by lomustine,” *Clin. Transl. Oncol.*, vol. 20, no. 4, pp.

508–516, 2018, doi: 10.1007/s12094-017-1743-x.

[34] G. Perazzoli, J. Prados, R. Ortiz, O. Caba, L. Cabeza, M. Berdasco, B. Gónzalez, and C. Melguizo, “Temozolomide resistance in glioblastoma cell lines: Implication of MGMT, MMR, P-glycoprotein and CD133 expression,” *PLoS One*, vol. 10, no. 10, p. e0140131, 2015, doi: 10.1371/journal.pone.0140131.

[35] D. Zhu, M. Tu, B. Zeng, L. Cai, W. Zheng, Z. Su, and Z. Yu, “Up-regulation of miR-497 confers resistance to temozolomide in human glioma cells by targeting mTOR/Bcl-2,” *Cancer Med.*, vol. 6, no. 2, pp. 452–462, 2017, doi: 10.1002/cam4.987.

[36] E. Vacchelli, F. Aranda, A. Eggermont, C. Sautès-Fridman, E. Tartour, E. P. Kennedy, M. Platten, L. Zitvogel, G. Kroemer, and L. Galluzzi, “Trial watch: IDO inhibitors in cancer therapy,” *Oncoimmunology*, vol. 3, no. 10, pp. e957994-1-e957994-10, 2014, doi: 10.4161/21624011.2014.957994.

[37] L. Zitvogel, L. Apetoh, F. Ghiringhelli, and G. Kroemer, “Immunological aspects of cancer chemotherapy,” *Nat. Rev. Immunol.*, vol. 8, no. 1, pp. 59–73, 2008, doi: 10.1038/nri2216.

[38] J. Wu and D. J. Waxman, “Metronomic cyclophosphamide eradicates large implanted GL261 gliomas by activating antitumor Cd8+ T-cell responses and immune memory,” *Oncoimmunology*, vol. 4, no. 4, p. e1005521, 2015, doi: 10.1080/2162402X.2015.1005521.

[39] J. Karman, C. Ling, M. Sandor, and Z. Fabry, “Initiation of Immune Responses in Brain Is Promoted by Local Dendritic Cells,” *J. Immunol.*, vol. 173, no. 4, pp. 2353–2361, 2004, doi: 10.4049/jimmunol.173.4.2353.

[40] T. G. Kim, C. H. Kim, J. S. Park, S. D. Park, C. K. Kim, D. S. Chung, and Y. K. Hong, “Immunological factors relating to the antitumor effect of temozolomide chemoimmunotherapy in a murine glioma model,” *Clin. Vaccine Immunol.*, vol. 17, no. 1, pp. 143–153, 2010, doi: 10.1128/CVI.00292-09.

[41] M. Tabbekh, M. Mokrani-Hammani, G. Bismuth, and F. Mami-Chouaib, “T-cell modulatory properties of CD5 and its role in antitumor immune responses,” *Oncoimmunology*, vol. 2, no. 1, p. e22841, 2013, doi: 10.4161/onci.22841.

[42] C. Laplagne, M. Domagala, A. Le Naour, C. Quemerais, D. Hamel, J.-J. Fournié, B. Couderc, C. Bousquet, A. Ferrand, and M. Poupot, “Latest Advances in Targeting the Tumor Microenvironment for Tumor Suppression,” *Int. J. Mol. Sci.*, vol. 20, no. 19, p. 4719, 2019, doi: 10.3390/ijms20194719.

[43] I. Mellman, G. Coukos, and G. Dranoff, “Cancer immunotherapy comes of age,” *Nature*, vol. 480, no. 7378, pp. 480–489, 22, 2011, doi: 10.1038/nature10673.

[44] C. Voena and R. Chiarle, “Advances in cancer immunology and cancer immunotherapy,” *Discov. Med.*, vol. 21, no. 114, pp. 125–133, 2016.

[45] M. A. Postow, M. K. Callahan, and J. D. Wolchok, “Immune Checkpoint Blockade in Cancer Therapy,” *J. Clin. Oncol.*, vol. 33, no. 17, pp. 1974–1982, 2015, doi: 10.1200/JCO.2014.59.4358.

[46] W. J. Lesterhuis, J. B. A. G. Haanen, and C. J. A. Punt, “Cancer immunotherapy-revisited,” *Nat. Rev. Drug Discov.*, vol. 10, no. 8, pp. 591–600, 2011, doi: 10.1038/nrd3500.

[47] A. Ribas and J. D. Wolchok, “Cancer immunotherapy using checkpoint blockade,” *Science*, vol. 359, no. 6382, pp. 1350–1355, 2018, doi: 10.1126/science.aar4060.

[48] T. M. Johanns and G. P. Dunn, “The Immune Response to Glioblastoma: Overview and Focus on Checkpoint Blockade,” in *Handbook of Brain Tumor Chemotherapy, Molecular Therapeutics, and Immunotherapy: Second Edition*, Elsevier Inc., 2018, pp. 653–668.

[49] S.-M. Razavi, K. E. Lee, B. E. Jin, P. S. Aujla, S. Gholamin, and G. Li, “Immune Evasion Strategies of Glioblastoma,” *Front. Surg.*, vol. 3, no. 11, 2016, doi: 10.3389/fsurg.2016.00011.

[50] D. M. Pardoll, “The blockade of immune checkpoints in cancer immunotherapy,” *Nat. Rev. Cancer*, vol. 12, no. 4., pp. 252–264, 2012, doi: 10.1038/nrc3239.

[51] K. N. Berger and J. J. Pu, “PD-1 pathway and its clinical application: A 20 year journey after discovery of the complete human PD-1 gene,” *Gene*, vol. 638, pp. 20–25, 2018, doi: 10.1016/j.gene.2017.09.050.

[52] M. E. Keir, M. J. Butte, G. J. Freeman, and A. H. Sharpe, “PD-1 and Its Ligands in Tolerance and Immunity,” *Annu. Rev. Immunol.*, vol. 26, no. 1, pp. 677–704, 2008, doi: 10.1146/annurev.immunol.26.021607.090331.

[53] L. V. Riella, A. M. Paterson, A. H. Sharpe, and A. Chandraker, “Role of the PD-1 Pathway in the Immune Response,” *Am. J. Transplant.*, vol. 12, no. 10, pp. 2575–2587, 2012, doi: 10.1111/j.1600-6143.2012.04224.x.

[54] E. J. Wherry, “T cell exhaustion,” *Nat. Immunol.*, vol. 12, no. 6, pp. 492–499, 2011, doi: 10.1038/ni.2035.

[55] A. Liston and D. H. D. Gray, “Homeostatic control of regulatory T cell diversity,” *Nat. Rev. Immunol.*, vol. 14, no. 3, pp. 154–165, 2014, doi: 10.1038/nri3605.

[56] S. Sakaguchi, M. Miyara, C. M. Costantino, and D. A. Hafler, “FOXP3 + regulatory T cells in the human immune system,” *Nat. Rev. Immunol.*, vol. 10, no. 7, pp. 490–500, 2010, doi: 10.1038/nri2785.

[57] C. Sun, R. Mezzadra, and T. N. Schumacher, “Regulation and Function of the PD-L1 Checkpoint,” *Immunity*, vol. 48, no. 3, pp. 434–452, 2018, doi: 10.1016/j.immuni.2018.03.014.

[58] J. Wang, L. Cheng, Z. Wondimu, M. Swain, P. Santamaria, and Y. Yang, “Cutting Edge: CD28 Engagement Releases Antigen-Activated Invariant NKT Cells from the Inhibitory Effects of PD-1,” *J. Immunol.*, vol. 182, no. 11, pp. 6644–6647, 2009, doi: 10.4049/jimmunol.0804050.

[59] T. Okazaki, A. Maeda, H. Nishimura, T. Kurosaki, and T. Honjo, “PD-1 immunoreceptor inhibits B cell receptor-mediated signaling by recruiting src homology 2-domain-containing tyrosine phosphatase 2 to phosphotyrosine,” *Proc. Natl. Acad. Sci. U. S. A.*,

vol. 98, no. 24, pp. 13866–13871, 2001, doi: 10.1073/pnas.231486598.

[60] J. Gong, A. Chehrazi-Raffle, S. Reddi, and R. Salgia, “Development of PD-1 and PD-L1 inhibitors as a form of cancer immunotherapy: A comprehensive review of registration trials and future considerations,” *J. ImmunoTher. Cancer.*, vol. 6, no. 1, p. 8, 2018, doi: 10.1186/s40425-018-0316-z.

[61] S. Yao, S. Wang, Y. Zhu, L. Luo, G. Zhu, S. Flies, H. Xu, W. Ruff, M. Broadwater, I. H. Choi, K. Tamada, and L. Chen, “PD-1 on dendritic cells impedes innate immunity against bacterial infection,” *Blood*, vol. 113, no. 23, pp. 5811–5818, 2009, doi: 10.1182/blood-2009-02-203141.

[62] S. Ostrand-Rosenberg, L. A. Horn, and S. T. Haile, “The Programmed Death-1 Immune-Suppressive Pathway: Barrier to Antitumor Immunity,” *J. Immunol.*, vol. 193, no. 8, pp. 3835–3841, 2014, doi: 10.4049/jimmunol.1401572.

[63] T. Yamazaki, H. Akiba, H. Iwai, H. Matsuda, M. Aoki, Y. Tanno, T. Shin, H. Tsuchiya, D. M. Pardoll, K. Okumura, M. Azuma, and H. Yagita, “Expression of Programmed Death 1 Ligands by Murine T Cells and APC,” *J. Immunol.*, vol. 169, no. 10, pp. 5538–5545, 2002, doi: 10.4049/jimmunol.169.10.5538.

[64] H. Dong, S. E. Strome, D. R. Salomao, H. Tamura, F. Hirano, D. B. Flies, P. C. Roche, J. Lu, G. Zhu, K. Tamada, V. A. Lennon, E. Cells, and L. Chen, “Tumor-associated B7-H1 promotes T-cell apoptosis: A potential mechanism of immune evasion,” *Nat. Med.*, vol. 8, no. 8, pp. 793–800, 2002, doi: 10.1038/nm730.

[65] V. A. Boussiotis, “Molecular and Biochemical Aspects of the PD-1 Checkpoint Pathway,” *N. Engl. J. Med.*, vol. 375, no. 18, pp. 1767–1778, 2016, doi: 10.1056/NEJMra1514296.

[66] P. Ritprajak and M. Azuma, “Intrinsic and extrinsic control of expression of the immunoregulatory molecule PD-L1 in epithelial cells and squamous cell carcinoma,” *Oral Oncol.*, vol. 51, no. 3, pp. 221–228, 2015, doi: 10.1016/j.oraloncology.2014.11.014.

[67] J. Liu, A. Hamrouni, D. Wolowiec, V. Coiteux, K. Kuliczkowski, D. Hetuin, A. Saudemont, and B. Quesnel, “Plasma cells from multiple myeloma patients express B7-H1 (PD-L1) and increase expression after stimulation with IFN-γ and TLR ligands via a MyD88-, TRAF6-, and MEK-dependent pathway,” *Blood*, vol. 110, no. 1, pp. 296–304, 2007, doi: 10.1182/blood-2006-10-051482.

[68] J. Chen, Y. Feng, L. Lu, H. Wang, L. Dai, Y. Li, and P. Zhang, “Interferon-γ-induced PD-L1 surface expression on human oral squamous carcinoma via PKD2 signal pathway,” *Immunobiology*, vol. 217, no. 4, pp. 385–393, 2012, doi: 10.1016/j.imbio.2011.10.016.

[69] M. Marzec, Q. Zhang, A. Goradia, P. N. Raghunath, X. Liu, M. Paessler, Y. W. Hong, M. Wysocka, M. Cheng, B. A. Ruggeri, and M. A. Wasik, “Oncogenic kinase NPM/ALK induces through STAT3 expression of immunosuppressive protein CD274 (PD-L1, B7-H1),” *Proc. Natl. Acad. Sci. U. S. A.*, vol. 105, no. 52, pp. 20852–20857, 2008, doi: 10.1073/pnas.0810958105.

[70] O. Bloch, C. A. Crane, R. Kaur, M. Safaee, M. J. Rutkowski, and A. T. Parsa, “Gliomas

Promote Immunosuppression through Induction of B7-H1 Expression in Tumor-Associated Macrophages," *Clin. Cancer Res.*, vol. 19, no. 12, pp. 3165–3175, 2013, doi: 10.1158/1078-0432.CCR-12-3314.

[71] M. Ahmadzadeh, L. A. Johnson, B. Heemskerk, J. R. Wunderlich, M. E. Dudley, D. E. White, and S. A. Rosenberg, "Tumor antigen-specific CD8 T cells infiltrating the tumor express high levels of PD-1 and are functionally impaired," *Blood*, vol. 114, no. 8, pp. 1537–1544, 2009, doi: 10.1182/blood-2008-12-195792.

[72] D. Q. Zeng, Y. F. Yu, Q. Y. Ou, X. Y. Li, R. Z. Zhong, C. M. Xie, and Q. G. Hu, "Prognostic and predictive value of tumor-infiltrating lymphocytes for clinical therapeutic research in patients with non-small cell lung cancer," *Oncotarget*, vol. 7, no. 12, pp. 13765–13781, 2016, doi: 10.18632/oncotarget.7282.

[73] L. Carbognin, S. Pilotto, R. Nortilli, M. Brunelli, A. Nottegar, I. Sperduti, D. Giannarelli, E. Bria, and G. Tortora, "Predictive and Prognostic Role of Tumor-Infiltrating Lymphocytes for Early Breast Cancer According to Disease Subtypes: Sensitivity Analysis of Randomized Trials in Adjuvant and Neoadjuvant Setting," *Oncologist*, vol. 21, no. 3, pp. 283–291, 2016, doi: 10.1634/theoncologist.2015-0307.

[74] A. W. Turksma, V. M. H. Coupé, M. C. Shamier, K. L. H. Lam, V. A. De Weger, J. A. M. Belien, A. J. Van Den Eertwegh, G. A. Meijer, C. J. L. M. Meijer, and E. Hooijberg, "Extent and location of tumor-infiltrating lymphocytes in microsatellite-stable colon cancer predict outcome to adjuvant active specific immunotherapy," *Clin. Cancer Res.*, vol. 22, no. 2, pp. 346–356, 2016, doi: 10.1158/1078-0432.CCR-13-2462.

[75] B. Wei, L. Wang, X. Zhao, C. Du, Y. Guo, and Z. Sun, "The upregulation of programmed death 1 on peripheral blood T cells of glioma is correlated with disease progression," *Tumor Biol.*, vol. 35, no. 4, pp. 2923–2929, 2014, doi: 10.1007/s13277-013-1376-9.

[76] T. B. Davidson, A. Lee, M. Hsu, S. Sedighim, J. Orpilla, J. Treger, M. Mastall, S. Roesch, C. Rapp, M. Galvez, A. Mochizuki, J. Antonios, A. Garcia, N. Kotecha, N. Bayless, D. Nathanson, A. Wang, R. Everson, W. H. Yong, *et al.*, "Expression of PD-1 by T cells in malignant glioma patients reflects exhaustion and activation," *Clin. Cancer Res.*, vol. 25, no. 6, pp. 1913–1922, 2019, doi: 10.1158/1078-0432.CCR-18-1176.

[77] X. Gu, X. S. Gao, W. Xiong, W. Guo, L. Han, Y. Bai, C. Peng, M. Cui, and M. Xie, "Increased programmed death ligand-1 expression predicts poor prognosis in hepatocellular carcinoma patients," *Onco. Targets. Ther.*, vol. 9, pp. 4805–4813, 2016, doi: 10.2147/OTT.S110713.

[78] K. Inamura, Y. Yokouchi, R. Sakakibara, M. Kobayashi, S. Subat, H. Ninomiya, H. Nagano, K. Nomura, S. Okumura, and Y. Ishikawa, "Relationship of tumor PD-L1 expression with *EGFR* wild-type status and poor prognosis in lung adenocarcinoma," *Jpn. J. Clin. Oncol.*, vol. 46, no. 10, pp. 935–941, 2016, doi: 10.1093/jjco/hyw087.

[79] U. Joneja, S. Vranic, J. Swensen, R. Feldman, W. Chen, J. Kimbrough, N. Xiao, S. Reddy, J. Palazzo, and Z. Gatalica, "Comprehensive profiling of metaplastic breast carcinomas reveals frequent overexpression of programmed death-ligand 1," *J. Clin. Pathol.*, vol. 70, no. 3, pp. 255–259, 2017, doi: 10.1136/jclinpath-2016-203874.

[80] M. X. Zou, A. B. Peng, G. H. Lv, X. Bin Wang, J. Li, X. L. She, and Y. Jiang, "Expression of

programmed death-1 ligand (PD-L1) in tumor-infiltrating lymphocytes is associated with favorable spinal chordoma prognosis," *Am. J. Transl. Res.*, vol. 8, no. 7, pp. 3274–3287, 2016, doi: 10.13140/RG.2.1.1007.0649

[81] P. Aguiar, G. Lopes, I. Santoro, H. Tadokoro, C. Barreto, and R. De Mello, "The Role of PD-L1 Expression as a Predictive Biomarker in Advanced NSCLC: An Update of a Network Meta-Analysis," *J. Thorac. Oncol.*, vol. 11, no. 10, pp. S247–S248, 2016, doi: 10.1016/j.jtho.2016.08.118.

[82] C.-L. Chen, Q.-Z. Pan, J.-J. Zhao, Y. Wang, Y.-Q. Li, Q.-J. Wang, K. Pan, D.-S. Weng, S.-S. Jiang, Y. Tang, X.-F. Zhang, H.-X. Zhang, Z.-Q. Zhou, Y.-X. Zeng, and J.-C. Xia, "PD-L1 expression as a predictive biomarker for cytokine-induced killer cell immunotherapy in patients with hepatocellular carcinoma," *Oncoimmunology*, vol. 5, no. 7, p. e1176653, 2016, doi: 10.1080/2162402X.2016.1176653.

[83] Z. Wang, C. Zhang, X. Liu, Z. Wang, L. Sun, G. Li, J. Liang, H. Hu, Y. Liu, W. Zhang, and T. Jiang, "Molecular and clinical characterization of PD-L1 expression at transcriptional level via 976 samples of brain glioma," *Oncoimmunology*, vol. 5, no. 11, p. e1196310, 2016, doi: 10.1080/2162402X.2016.1196310.

[84] S. Xue, G. Song, and J. Yu, "The prognostic significance of PD-L1 expression in patients with glioma: A meta-analysis," *Sci. Rep.*, vol. 7, no. 1, p. 4231, 2017, doi: 10.1038/s41598-017-04023-x.

[85] E. K. Nduom, J. Wei, N. K. Yaghi, N. Huang, L.-Y. Kong, K. Gabrusiewicz, X. Ling, S. Zhou, C. Ivan, J. Q. Chen, J. K. Burks, G. N. Fuller, G. A. Calin, C. A. Conrad, C. Creasy, K. Ritthipichai, L. Radvanyi, and A. B. Heimberger, "PD-L1 expression and prognostic impact in glioblastoma," *Neuro. Oncol.*, vol. 18, no. 2, pp. 195–205, 2016, doi: 10.1093/neuonc/nov172.

[86] Y. Liu, R. Carlsson, M. Ambjørn, M. Hasan, W. Badn, A. Darabi, P. Siesjö, and S. Issazadeh-Navikas, "PD-L1 expression by neurons nearby tumors indicates better prognosis in glioblastoma patients," *J. Neurosci.*, vol. 33, no. 35, pp. 14231–14245, 2013, doi: 10.1523/JNEUROSCI.5812-12.2013.

[87] K. S. Lee, K. Lee, S. Yun, S. Moon, Y. Park, J. H. Han, C.-Y. Kim, H. S. Lee, and G. Choe, "The prognostic significance of PD-L1 expression in patients with glioma: A meta-analysis," *J. Neurooncol.*, vol. 136, no. 3, pp. 453–461, 2018, doi: 10.1007/s11060-017-2675-6.

[88] D. Pratt, G. Dominah, G. Lobel, A. Obungu, J. Lynes, V. Sanchez, N. Adamstein, X. Wang, N. A. Edwards, T. Wu, D. Maric, A. J. Giles, M. R. Gilbert, M. Quezado, and E. K. Nduom, "Programmed Death Ligand 1 Is a Negative Prognostic Marker in Recurrent Isocitrate Dehydrogenase-Wildtype Glioblastoma," *Neurosurgery*, vol. 85, no. 2, pp. 280–289, 2019, doi: 10.1093/neuros/nyy268.

[89] A. S. Berghoff, B. Kiesel, G. Widhalm, O. Rajky, G. Ricken, A. Wohrer, K. Dieckmann, M. Filipits, A. Brandstetter, M. Weller, S. Kurscheid, M. E. Hegi, C. C. Zielinski, C. Marosi, J. A. Hainfellner, M. Preusser, and W. Wick, "Programmed death ligand 1 expression and tumor-infiltrating lymphocytes in glioblastoma," *Neuro. Oncol.*, vol. 17, no. 8, pp. 1064–1075, 2015, doi: 10.1093/neuonc/nou307.

[90] J. Zeng, X. K. Zhang, H. D. Chen, Z. H. Zhong, Q. L. Wu, and S. X. Lin, “Expression of programmed cell death-ligand 1 and its correlation with clinical outcomes in gliomas,” *Oncotarget*, vol. 7, no. 8, pp. 8944–8955, 2016, doi: 10.18632/oncotarget.6884.

[91] T. Miyazaki, E. Ishikawa, M. Matsuda, H. Akutsu, S. Osuka, N. Sakamoto, S. Takano, T. Yamamoto, K. Tsuboi, and A. Matsumura, “Assessment of PD-1 positive cells on initial and secondary resected tumor specimens of newly diagnosed glioblastoma and its implications on patient outcome,” *J. Neurooncol.*, vol. 133, no. 2, pp. 277–285, 2017, doi: 10.1007/s11060-017-2451-7.

[92] M. Mirghorbani, S. Van Gool, and N. Rezaei, “Myeloid-derived suppressor cells in glioma,” *Expert Rev. Neurother.*, vol. 13, no. 12. Expert Rev Neurother, pp. 1395–1406, 2013, doi: 10.1586/14737175.2013.857603.

[93] J. P. Antonios, H. Soto, R. G. Everson, D. Moughon, J. R. Orpilla, N. P. Shin, S. Sedighim, J. Treger, S. Odesa, A. Tucker, W. H. Yong, G. Li, T. F. Cloughesy, L. M. Liau, and R. M. Prins, “Immunosuppressive tumor-infiltrating myeloid cells mediate adaptive immune resistance via a PD-1/PD-L1 mechanism in glioblastoma,” *Neuro. Oncol.*, vol. 19, no. 6, pp. 796–807, 2017, doi: 10.1093/neuonc/now287.

[94] C. I. Jan, W. C. Tsai, H. J. Harn, W. C. Shyu, M. C. Liu, H. M. Lu, S. C. Chiu, and D. Y. Cho, “Predictors of response to autologous dendritic cell therapy in Glioblastoma multiforme,” *Front. Immunol.*, vol. 9, no. MAY, p. 727, 2018, doi: 10.3389/fimmu.2018.00727.

[95] K. M. Zak, R. Kitel, S. Przetocka, P. Golik, K. Guzik, B. Musielak, A. Dömling, G. Dubin, and T. A. Holak, “Structure of the Complex of Human Programmed Death 1, PD-1, and Its Ligand PD-L1,” *Structure*, vol. 23, no. 12, pp. 2341–2348, 2015, doi: 10.1016/j.str.2015.09.010.

[96] K. A. Hofmeyer, H. Jeon, and X. Zang, “The PD-1/PD-L1 (B7-H1) Pathway in Chronic Infection-Induced Cytotoxic T Lymphocyte Exhaustion,” *J. Biomed. Biotechnol.*, vol. 2011, p. 451694, 2011, doi: 10.1155/2011/451694.

[97] R. V. Parry, J. M. Chemnitz, K. A. Frauwirth, A. R. Lanfranco, I. Braunstein, S. V. Kobayashi, P. S. Linsley, C. B. Thompson, and J. L. Riley, “CTLA-4 and PD-1 Receptors Inhibit T-Cell Activation by Distinct Mechanisms,” *Mol. Cell. Biol.*, vol. 25, no. 21, pp. 9543–9553, 2005, doi: 10.1128/mcb.25.21.9543-9553.2005.

[98] J. Long, J. Lin, A. Wang, L. Wu, Y. Zheng, X. Yang, X. Wan, H. Xu, S. Chen, and H. Zhao, “PD-1/PD-L blockade in gastrointestinal cancers: Lessons learned and the road toward precision immunotherapy,” *J. Hematol. Oncol.*, vol. 10, no. 1, p. 146, 2017, doi: 10.1186/s13045-017-0511-2.

[99] X. Zang and J. P. Allison, “The B7 Family and Cancer Therapy: Costimulation and Coinhibition,” *Clin. Cancer Res.*, vol. 13, no. 18, pp. 5271–5279, 2007, doi: 10.1158/1078-0432.CCR-07-1030.

[100] L. B. John, C. Devaud, C. P. M. Duong, C. S. Yong, P. A. Beavis, N. M. Haynes, M. T. Chow, M. J. Smyth, M. H. Kershaw, and P. K. Darcy, “Anti-PD-1 antibody therapy potently enhances the eradication of established tumors by gene-modified T cells,” *Clin. Cancer Res.*, vol. 19, no. 20, pp. 5636–5646, 2013, doi: 10.1158/1078-0432.CCR-

13-0458.

[101] K. C. Ohaegbulam, A. Assal, E. Lazar-Molnar, Y. Yao, and X. Zang, “Human cancer immunotherapy with antibodies to the PD-1 and PD-L1 pathway,” *Trends Mol. Med.*, vol. 21, no. 1, pp. 24–33, 2015, doi: 10.1016/j.molmed.2014.10.009.

[102] N. A. Rizvi, J. Mazières, D. Planchard, T. E. Stinchcombe, G. K. Dy, S. J. Antonia, L. Horn, H. Lena, E. Minenza, B. Mennecier, G. A. Otterson, L. T. Campos, D. R. Gandara, B. P. Levy, S. G. Nair, G. Zalcman, J. Wolf, P. J. Souquet, E. Baldini, *et al.*, “Activity and safety of nivolumab, an anti-PD-1 immune checkpoint inhibitor, for patients with advanced, refractory squamous non-small-cell lung cancer (CheckMate 063): A phase 2, single-arm trial,” *Lancet Oncol.*, vol. 16, no. 3, pp. 257–265, 2015, doi: 10.1016/S1470-2045(15)70054-9.

[103] D. Cella, V. Grünwald, P. Nathan, J. Doan, H. Dastani, F. Taylor, B. Bennett, M. DeRosa, S. Berry, K. Broglio, E. Berghorn, and R. J. Motzer, “Quality of life in patients with advanced renal cell carcinoma given nivolumab versus everolimus in CheckMate 025: a randomised, open-label, phase 3 trial,” *Lancet Oncol.*, vol. 17, no. 7, pp. 994–1003, 2016, doi: 10.1016/S1470-2045(16)30125-5.

[104] S. M. Ansell, A. M. Lesokhin, I. Borrello, A. Halwani, E. C. Scott, M. Gutierrez, S. J. Schuster, M. M. Millenson, D. Cattry, G. J. Freeman, S. J. Rodig, B. Chapuy, A. H. Ligon, L. Zhu, J. F. Grosso, S. Y. Kim, J. M. Timmerman, M. A. Shipp, and P. Armand, “PD-1 Blockade with Nivolumab in Relapsed or Refractory Hodgkin’s Lymphoma,” *N. Engl. J. Med.*, vol. 372, no. 4, pp. 311–319, 2015, doi: 10.1056/NEJMoa1411087.

[105] D. A. Reardon, P. C. Gokhale, S. R. Klein, K. L. Ligon, S. J. Rodig, S. H. Ramkissoon, K. L. Jones, A. S. Conway, X. Liao, J. Zhou, P. Y. Wen, A. D. Van Den Abbeele, F. S. Hodi, L. Qin, N. E. Kohl, A. H. Sharpe, G. Dranoff, and G. J. Freeman, “Glioblastoma Eradication Following Immune Checkpoint Blockade in an Orthotopic, Immunocompetent Model,” *Cancer Immunol. Res.*, vol. 4, no. 2, pp. 124–135, 2016, doi: 10.1158/2326-6066.CIR-15-0151.

[106] S. N. Reiss, P. Yerram, L. Modelevsky, and C. Grommes, “Retrospective review of safety and efficacy of programmed cell death-1 inhibitors in refractory high grade gliomas,” *J. Immunother. Cancer*, vol. 5, no. 1, p. 99, 2017, doi: 10.1186/s40425-017-0302-x.

[107] I. Fried, A. Lossos, T. Ben Ami, R. Dvir, H. Toledano, M. W. Ben Arush, S. Postovski, A. Abu Kuidar, M. Yalon, M. Weintraub, and M. Benifla, “Preliminary results of immune modulating antibody MDV9300 (pidilizumab) treatment in children with diffuse intrinsic pontine glioma,” *J. Neurooncol.*, vol. 136, no. 1, pp. 189–195, 2018, doi: 10.1007/s11060-017-2643-1.

[108] J. R. Brahmer, S. S. Tykodi, L. Q. M. Chow, W.-J. Hwu, S. L. Topalian, P. Hwu, C. G. Drake, L. H. Camacho, J. Kauh, K. Odunsi, H. C. Pitot, O. Hamid, S. Bhatia, R. Martins, K. Eaton, S. Chen, T. M. Salay, S. Alaparthy, J. F. Grosso, *et al.*, “Safety and Activity of Anti–PD-L1 Antibody in Patients with Advanced Cancer,” *N. Engl. J. Med.*, vol. 366, no. 26, pp. 2455–2465, 2012, doi: 10.1056/NEJMoa1200694.

[109] S. S. Chang, “Re: MPDL3280A (Anti-PD-L1) Treatment Leads to Clinical Activity in

Metastatic Bladder Cancer," *J. Urol.*, vol. 194, no. 4, pp. 956–956, 2015, doi: 10.1016/j.juro.2015.07.017.

[110] J. Zeng, A. P. See, J. Phallen, C. M. Jackson, Z. Belcaid, J. Ruzevick, N. Durham, C. Meyer, T. J. Harris, E. Albesiano, G. Pradilla, E. Ford, J. Wong, H. J. Hammers, D. Mathios, B. Tyler, H. Brem, P. T. Tran, D. Pardoll, *et al.*, "Anti-PD-1 blockade and stereotactic radiation produce long-term survival in mice with intracranial gliomas," *Int. J. Radiat. Oncol. Biol. Phys.*, vol. 86, no. 2, pp. 343–349, 2013, doi: 10.1016/j.ijrobp.2012.12.025.

[111] D. Mathios, J. E. Kim, A. Mangraviti, J. Phallen, C. K. Park, C. M. Jackson, T. Garzon-Muvdi, E. Kim, D. Theodros, M. Polanczyk, A. M. Martin, I. Suk, X. Ye, B. Tyler, C. Bettegowda, H. Brem, D. M. Pardoll, and M. Lim, "Anti-PD-1 antitumor immunity is enhanced by local and abrogated by systemic chemotherapy in GBM," *Sci. Transl. Med.*, vol. 8, no. 370, p. 370ra180, 2016, doi: 10.1126/scitranslmed.aag2942.

[112] P. C. Huszthy, I. Daphu, S. P. Niclou, D. Stieber, J. M. Nigro, P. O. Sakariassen, H. Miletic, F. Thorsen, and R. Bjerkvig, "In vivo models of primary brain tumors: pitfalls and perspectives," *Neuro. Oncol.*, vol. 14, no. 8, pp. 979–993, 2012, doi: 10.1093/neuonc/nos135.

[113] M. Acosta González, "Mejora de los modelos preclínicos de tumores cerebrales. Aplicación a la caracterización ex vivo e in vivo de agentes de contraste nanoparticulados para imagen de resonancia magnetica." PhD Thesis, Universitat Autònoma de Barcelona, 2013. https://tdx.cat/handle/10803/128995

[114] L. Ferrer Font, "Tuning response to therapy in preclinical GL261 glioblastoma through CK2 targeting and temozolomide metronomic approaches: non-invasive assessment with MRI and MRSI-based molecular imaging strategies," PhD Thesis, Universitat Autònoma de Barcelona, 2017. https://tdx.cat/handle/10803/402400

[115] D. P. Houchens, A. A. Ovejera, S. M. Riblet, and D. E. Slagel, "Human brain tumor xenografts in nude mice as a chemotherapy model," *Eur. J. Cancer Clin. Oncol.*, vol. 19, no. 6, pp. 799–805, 1983, doi: 10.1016/0277-5379(83)90012-3.

[116] M. Candolfi, J. F. Curtin, W. S. Nichols, A. K. M. G. Muhammad, G. D. King, G. E. Pluhar, E. A. McNiel, J. R. Ohlfest, A. B. Freese, P. F. Moore, J. Lerner, P. R. Lowenstein, and M. G. Castro, "Intracranial glioblastoma models in preclinical neuro-oncology: Neuropathological characterization and tumor progression," *J. Neurooncol.*, vol. 85, no. 2, pp. 133–148, 2007, doi: 10.1007/s11060-007-9400-9.

[117] R. P. Deshpande and P. P. Babu, "Animal Model for Glioma : A Brief Overview," *Arch. Med. Biotechnol.*, vol. 1, no. 1, pp. 1–4, 2018.

[118] J. Pontén, "Neoplastic Human Glia Cells in Culture," in *Human Tumor Cells in Vitro*, Springer US, pp. 175–206, 1975, doi: 10.1007/978-1-4757-1647-4_7

[119] M. Kirsch, J. Strasser, R. Allende, L. Bello, J. Zhang, and P. M. Black, "Angiostatin suppresses malignant glioma growth in vivo.," *Cancer Res.*, vol. 58, no. 20, pp. 4654–9, 1998.

[120] J. A. Ecsedy, K. A. Holthaus, H. C. Yohe, and T. N. Seyfried, "Expression of mouse sialic

acid on gangliosides of a human glioma grown as a xenograft in SCID mice," *J. Neurochem.*, vol. 73, no. 1, pp. 254–259, 1999, doi: 10.1046/j.1471-4159.1999.0730254.x.

[121] M. Allen, M. Bjerke, H. Edlund, S. Nelander, and B. Westermark, "Origin of the U87MG glioma cell line : Good news and bad news," *Sci. Transl. Med*., vol. 8, no. 354, p. 354re3, 2016. doi: 10.1126/scitranslmed.aaf6853

[122] D. L. Peterson, P. J. Sheridan, and W. E. Brown, "Animal models for brain tumors: historical perspectives and future directions," *J. Neurosurg.*, vol. 80, no. 5, pp. 865–876, 1994, doi: 10.3171/jns.1994.80.5.0865.

[123] N. Nagano, H. Sasaki, M. Aoyagi, and K. Hirakawa, "Invasion of experimental rat brain tumor: early morphological changes following microinjection of C6 glioma cells," *Acta Neuropathol.*, vol. 86, no. 2, pp. 117–125, 1993, doi: 10.1007/BF00334878.

[124] I. R. Whittle, D. C. Macarthur, G. P. Malcolm, M. Li, K. Washington, and J. W. Ironside, "Can experimental models of rodent implantation glioma be improved? A study of pure and mixed glioma cell line tumours," *J. Neurooncol.*, vol. 36, no. 3, pp. 231–242, 1998, doi: 10.1023/A:1005831111337.

[125] D. Giakoumettis, A. Kritis, and N. Foroglou, "C6 cell line: the gold standard in glioma research," *Hippokratia*, vol. 22, no. 3, pp. 105–112, 2018.

[126] F. San-Galli, P. Vrignaud, J. Robert, J. M. Coindre, and F. Cohadon, "Assessment of the experimental model of transplanted C6 glioblastoma in wistar rats," *J. Neurooncol.*, vol. 7, no. 3, pp. 299–304, 1989, doi: 10.1007/BF00172924.

[127] A. T. Parsa, I. Chakrabarti, P. T. Hurley, J. H. Chi, J. S. Hall, M. G. Kaiser, and J. N. Bruce, "Limitations of the C6/Wistar rat intracerebral glioma model: Implications for evaluating immunotherapy," *Neurosurgery*, vol. 47, no. 4, pp. 993–1000, 2000, doi: 10.1097/00006123-200010000-00050.

[128] H. M. Zimmerman and H. Arnold, "Experimental Brain Tumors I . Tumors Produced with Methylcholanthrene," *Cancer Res.*, vol. 1, no. 12, pp. 919–938, 1941.

[129] O. C. A. Scott, "Tumor Transplantation and Tumor Immunity : A Personal View," *Cancer Res.*, vol. 51, no. 2, pp. 757–763, 1991.

[130] G. H. Vince, M. Bendszus, T. Schweitzer, R. H. Goldbrunner, S. Hildebrandt, J. Tilgner, R. Klein, L. Solymosi, J. C. Tonn, and K. Roosen, "Spontaneous regression of experimental gliomas - An immunohistochemical and MRI study of the C6 glioma spheroid implantation model," *Exp. Neurol.*, vol. 190, no. 2, pp. 478–485, 2004, doi: 10.1016/j.expneurol.2004.08.015.

[131] N. Ishii, M. Tada, M. F. Hamou, R. C. Janzer, K. Meagher-Villemure, O. D. Wiestler, N. De Tribolet, and E. G. Van Meir, "Cells with TP53 mutations in low grade astrocytic tumors evolve clonally to malignancy and are an unfavorable prognostic factor," *Oncogene*, vol. 18, no. 43, pp. 5870–5878, 1999, doi: 10.1038/sj.onc.1203241.

[132] T. Szatmári, K. Lumniczky, S. Désaknai, S. Trajcevski, E. J. Hídvégi, H. Hamada, and G. Sáfrány, "Detailed characterization of the mouse glioma 261 tumor model for experimental glioblastoma therapy," *Cancer Sci.*, vol. 97, no. 6, pp. 546–553, 2006,

doi: 10.1111/j.1349-7006.2006.00208.x.

[133] J. I. Ausman, W. R. Shapiro, and D. P. Rall, “Studies on the chemotherapy of experimental brain tumors: development of an experimental model.,” *Cancer Res.*, vol. 30, no. 9, pp. 2394–400, 1970.

[134] T. N. Seyfried, M. El-Abbadi, and M. L. Roy, “Ganglioside distribution in murine neural tumors,” *Mol. Chem. Neuropathol.*, vol. 17, no. 2, pp. 147–167, 1992, doi: 10.1007/BF03159989.

[135] R. Martínez-Murillo and A. Martínez, “Standardization of an orthotopic mouse brain tumor model following transplantation of CT-2A astrocytoma cells,” *Histol. Histopathol.*, vol. 22, no. 10–12, pp. 1309–1326, 2007, doi: 10.14670/HH-22.1309.

[136] P. Mukherjee, L. E. Abate, and T. N. Seyfried, “Antiangiogenic and proapoptotic effects of dietary restriction on experimental mouse and human brain tumors,” *Clin. Cancer Res.*, vol. 10, no. 16, pp. 5622–5629, 2004, doi: 10.1158/1078-0432.CCR-04-0308.

[137] E. Binello, Z. A. Qadeer, H. P. Kothari, L. Emdad, and I. M. Germano, “Stemness of the CT-2A immunocompetent mouse brain tumor model: Characterization in vitro,” *J. Cancer*, vol. 3, no. 1, pp. 166–174, 2012, doi: 10.7150/jca.4149.

[138] L. M. Shelton, P. Mukherjee, L. C. Huysentruyt, I. Urits, J. A. Rosenberg, and T. N. Seyfried, “A novel pre-clinical in vivo mouse model for malignant brain tumor growth and invasion,” *J. Neurooncol.*, vol. 99, no. 2, pp. 165–176, 2010, doi: 10.1007/s11060-010-0115-y.

[139] S. Semenkow, S. Li, U. D. Kahlert, E. H. Raabe, J. Xu, A. Arnold, M. Janowski, B. C. Oh, G. Brandacher, J. W. M. Bulte, C. G. Eberhart, and P. Walczak, “An immunocompetent mouse model of human glioblastoma,” *Oncotarget*, vol. 8, no. 37, pp. 61072–61082, 2017, doi: 10.18632/oncotarget.17851.

[140] W. Maes and S. W. Van Gool, “Experimental immunotherapy for malignant glioma: lessons from two decades of research in the GL261 model,” *Cancer Immunol. Immunother.*, vol. 60, no. 2, pp. 153–160, 2011, doi: 10.1007/s00262-010-0946-6.

[141] J. Park, C. G. Kim, J.-K. Shim, J. H. Kim, H. Lee, J. E. Lee, M. H. Kim, K. Haam, I. Jung, S.-H. Park, J. H. Chang, E.-C. Shin, and S.-G. Kang, “Effect of combined anti-PD-1 and temozolomide therapy in glioblastoma,” *Oncoimmunology*, vol. 8, no. 1, p. e1525243, 2019, doi: 10.1080/2162402X.2018.1525243.

[142] A. D. Garg, L. Vandenberk, M. Van Woensel, J. Belmans, M. Schaaf, L. Boon, S. De Vleeschouwer, and P. Agostinis, “Preclinical efficacy of immune-checkpoint monotherapy does not recapitulate corresponding biomarkers-based clinical predictions in glioblastoma,” *Oncoimmunology*, vol. 6, no. 4, p. e1295903, 2017, doi: 10.1080/2162402X.2017.1295903.

[143] L. C. Hygino Da Cruz, I. Rodriguez, R. C. Domingues, E. L. Gasparetto, and A. G. Sorensen, “Pseudoprogression and pseudoresponse: Imaging challenges in the assessment of posttreatment glioma,” *Am. J. Neuroradiol.*, vol. 32, no. 11. American Journal of Neuroradiology, pp. 1978–1985, 01, 2011, doi: 10.3174/ajnr.A2397.

[144] M. B. Weishaupt D, Köchli V D, “How Does MRI Work? An Introduction to the Physics and Function of Magnetic Resonance Imaging, 2nd ed,” *Springer Sci. Bus. Media*, 2006. https://www.springer.com/gp/book/9783540300670

[145] F. Kiessling, B. Morgenstern, and C. Zhang, “Contrast Agents and Applications to Assess Tumor Angiogenesis In Vivo by Magnetic Resonance Imaging,” *Curr. Med. Chem.*, vol. 14, no. 1, pp. 77–91, 2006, doi: 10.2174/092986707779313516.

[146] P. Weybright, P. Maly, D. Gomez-Hassan, C. Blaesing, and P. C. Sundgren, “MR spectroscopy in the evaluation of recurrent contrast-enhancing lesions in the posterior fossa after tumor treatment,” *Neuroradiology*, vol. 46, no. 7, pp. 541–549, 2004, doi: 10.1007/s00234-004-1195-1.

[147] D. P. Soares and M. Law, “Magnetic resonance spectroscopy of the brain : review of metabolites and clinical applications,” *Clin. Radiol.*, vol. 64, no. 1, pp. 12–21, 2009, doi: 10.1016/j.crad.2008.07.002.

[148] S. Kalra, “Magnetic Resonance Spectroscopy in ALS,” *Front. Neurol.*, vol. 10, no. MAY, p. 482, 2019, doi: 10.3389/fneur.2019.00482.

[149] V. Govindaraju, K. Young, and A. A. Maudsley, “Proton NMR chemical shifts and coupling constants for brain metabolites,” *NMR Biomed.*, vol. 13, no. 3, pp. 129–153, 2000, doi: 10.1002/1099-1492(200005)13:3<129::AID-NBM619>3.0.CO;2-V.

[150] E. Kousi, I. Tsougos, and K. Eftychi, “Proton Magnetic Resonance Spectroscopy of the Central Nervous System,” in *Novel Frontiers of Advanced Neuroimaging*, InTech, 2013, doi: 10.5772/53892

[151] T. Delgado-Goñi, S. Ortega-Martorell, M. Ciezka, I. Olier, A. P. Candiota, M. Julià-Sapé, F. Fernández, M. Pumarola, P. J. Lisboa, and C. Arús, “MRSI-based molecular imaging of therapy response to temozolomide in preclinical glioblastoma using source analysis,” *NMR Biomed.*, vol. 29, no. 6, pp. 732–743, 2016, doi: 10.1002/nbm.3521.

[152] J. M. Hakumäki, H. Poptani, A.-M. Sandmair, S. Ylä-Herttuala, and R. A. Kauppinen, “1H MRS detects polyunsaturated fatty acid accumulation during gene therapy of glioma: Implications for the in vivo detection of apoptosis,” *Nat. Med.*, vol. 5, no. 11, pp. 1323–1327, Nov. 1999, doi: 10.1038/15279.

[153] E. R. Danielsen and B. Ross, *Magnetic Resonance Spectroscopy Diagnosis of Neurological Diseases*. CRC Press, 1999.

[154] S. J. Nelson, A. K. Kadambi, I. Park, Y. Li, J. Crane, M. Olson, A. Molinaro, R. Roy, N. Butowski, S. Cha, and S. Chang, “Association of early changes in 1H MRSI parameters with survival for patients with newly diagnosed glioblastoma receiving a multimodality treatment regimen,” *Neuro. Oncol.*, vol. 19, no. 3, pp. 430–439, 2017, doi: 10.1093/neuonc/now159.

[155] F. S. De Edelenyi, C. Rubin, F. Estève, S. Grand, M. Décorps, V. Lefournier, J. F. Le Bas, and C. Rémy, “A new approach for analyzing proton magnetic resonance spectroscopic images of brain tumors: Nosologic images,” *Nat. Med.*, vol. 6, no. 11, pp. 1287–1289, 2000, doi: 10.1038/81401.

[156] S. Ortega-Martorell, P. J. G. Lisboa, A. Vellido, R. V. Simões, M. Pumarola, M. Julià-

Sapé, and C. Arús, “Convex Non-Negative Matrix Factorization for Brain Tumor Delimitation from MRSI Data,” *PLoS One*, vol. 7, no. 10, p. e47824, 2012, doi: 10.1371/journal.pone.0047824.

[157] N. Zarinabad, L. J. Abernethy, S. Avula, N. P. Davies, D. Rodriguez Gutierrez, T. Jaspan, L. MacPherson, D. Mitra, H. E. L. Rose, M. Wilson, P. S. Morgan, S. Bailey, B. Pizer, T. N. Arvanitis, R. G. Grundy, D. P. Auer, and A. Peet, “Application of pattern recognition techniques for classification of pediatric brain tumors by in vivo 3T 1H-MR spectroscopy—A multi-center study,” *Magn. Reson. Med.*, vol. 79, no. 4, pp. 2359–2366, 2018, doi: 10.1002/mrm.26837.

[158] N. Arias-Ramos, L. Ferrer-Font, S. Lope-Piedrafita, V. Mocioiu, M. Julià-Sapé, M. Pumarola, C. Arús, and A. Candiota, “Metabolomics of Therapy Response in Preclinical Glioblastoma: A Multi-Slice MRSI-Based Volumetric Analysis for Noninvasive Assessment of Temozolomide Treatment,” *Metabolites*, vol. 7, no. 2, p. 20, 2017, doi: 10.3390/metabo7020020.

[159] L. Ferrer-Font, N. Arias-Ramos, S. Lope-Piedrafita, M. Julià-Sapé, M. Pumarola, C. Arús, and A. P. Candiota, “Metronomic treatment in immunocompetent preclinical GL261 glioblastoma: effects of cyclophosphamide and temozolomide,” *NMR Biomed.*, vol. 30, no. 9, p. e3748, 2017, doi: 10.1002/nbm.3748.

[160] T. Delgado-Goñi, M. Julià-Sapé, A. P. Candiota, M. Pumarola, and C. Arús, “Molecular imaging coupled to pattern recognition distinguishes response to temozolomide in preclinical glioblastoma,” *NMR Biomed.*, vol. 27, no. 11, pp. 1333–1345, 2014, doi: 10.1002/nbm.3194.

[161] R. V. Simões, M. L. García-Martín, S. Cerdán, and C. Arús, “Perturbation of mouse glioma MRS pattern by induced acute hyperglycemia,” *NMR Biomed.*, vol. 21, no. 3, pp. 251–264, 2008, doi: 10.1002/nbm.1188.

[162] R. V. Simões, T. Delgado-Goñi, S. Lope-Piedrafita, and C. Arús, “1H-MRSI pattern perturbation in a mouse glioma: The effects of acute hyperglycemia and moderate hypothermia,” *NMR Biomed.*, vol. 23, no. 1, pp. 23–33, 2010, doi: 10.1002/nbm.1421.

[163] T. Delgado-Goñi, J. Martín-Sitjar, R. V. Simões, M. Acosta, S. Lope-Piedrafita, and C. Arús, “Dimethyl sulfoxide (DMSO) as a potential contrast agent for brain tumors,” *NMR Biomed.*, vol. 26, no. 2, pp. 173–184, 2013, doi: 10.1002/nbm.2832.

[164] A. P. Candiota, M. Acosta, R. V. Simões, T. Delgado-Goñi, S. Lope-Piedrafita, A. Irure, M. Marradi, O. Bomati-Miguel, N. Miguel-Sancho, I. Abasolo, S. Schwartz, J. Santamaria, S. Penadés, and C. Arús, “A new ex vivo method to evaluate the performance of candidate MRI contrast agents: A proof-of-concept study,” *J. Nanobiotechnology*, vol. 12, no. 12, 2014, doi: 10.1186/1477-3155-12-12.

[165] M. Sánchez-Osuna, M. Garcia-Belinchón, V. Iglesias-Guimarais, E. Gil-Guiñón, E. Casanelles, and V. J. Yuste, “Caspase-activated DNase Is Necessary and Sufficient for Oligonucleosomal DNA Breakdown, but Not for Chromatin Disassembly during Caspase-dependent Apoptosis of LN-18 Glioblastoma Cells,” *J. Biol. Chem.*, vol. 289, no. 27, pp. 18752–18769, 2014, doi: 10.1074/jbc.M114.550020.

[166] S. Garofalo, G. D’Alessandro, G. Chece, F. Brau, L. Maggi, A. Rosa, A. Porzia, F.

Mainiero, V. Esposito, C. Lauro, G. Benigni, G. Bernardini, A. Santoni, and C. Limatola, “Enriched environment reduces glioma growth through immune and non-immune mechanisms in mice,” *Nat. Commun.*, vol. 6, no. 1, p. 6623, 2015, doi: 10.1038/ncomms7623.

[167] E. A. Eisenhauer, P. Therasse, J. Bogaerts, L. H. Schwartz, D. Sargent, R. Ford, J. Dancey, S. Arbuck, S. Gwyther, M. Mooney, L. Rubinstein, L. Shankar, L. Dodd, R. Kaplan, D. Lacombe, and J. Verweij, “New response evaluation criteria in solid tumours: Revised RECIST guideline (version 1.1),” *Eur. J. Cancer*, vol. 45, no. 2, pp. 228–247, 2009, doi: 10.1016/j.ejca.2008.10.026.

[168] L. Ferrer-Font, L. Villamañan, N. Arias-Ramos, J. Vilardell, M. Plana, M. Ruzzene, L. Pinna, E. Itarte, C. Arús, and A. Candiota, “Targeting Protein Kinase CK2: Evaluating CX-4945 Potential for GL261 Glioblastoma Therapy in Immunocompetent Mice,” *Pharmaceuticals*, vol. 10, no. 4, p. 24, 2017, doi: 10.3390/ph10010024.

[169] S. Wu, P. Calero-Pérez, L. Villamañan, N. Arias-Ramos, M. Pumarola, S. Ortega-Martorell, M. Julià-Sapé, C. Arús, and A. P. Candiota, “Anti-tumour immune response in GL261 glioblastoma generated by Temozolomide Immune-Enhancing Metronomic Schedule monitored with MRSI-based nosological images,” *NMR Biomed.*, vol. 33, no. 4, p. e4229, 2020, doi: 10.1002/nbm.4229.

[170] B. Dai, N. Qi, J. Li, and G. Zhang, “Temozolomide combined with PD-1 Antibody therapy for mouse orthotopic glioma model,” *Biochem. Biophys. Res. Commun.*, vol. 501, no. 4, pp. 871–876, 2018, doi: 10.1016/j.bbrc.2018.05.064.

[171] A. Karachi, C. Yang, F. Dastmalchi, E. J. Sayour, J. Huang, H. Azari, Y. Long, C. Flores, D. A. Mitchell, and M. Rahman, “Modulation of temozolomide dose differentially affects T-cell response to immune checkpoint inhibition,” *Neuro. Oncol.*, vol. 21, no. 6, pp. 730–741, 2019, doi: 10.1093/neuonc/noz015.

[172] M. Ciezka, M. Acosta, C. Herranz, J. M. Canals, M. Pumarola, A. P. Candiota, and C. Arús, “Development of a transplantable glioma tumour model from genetically engineered mice: MRI/MRS/MRSI characterisation,” *J. Neurooncol.*, vol. 129, no. 1, pp. 67–76, 2016, doi: 10.1007/s11060-016-2164-3.

[173] A. M. Dunn-Pirio and G. Vlahovic, “Immunotherapy approaches in the treatment of malignant brain tumors,” *Cancer*, vol. 123, no. 5, pp. 734–750, 2017, doi: 10.1002/cncr.30371.

[174] P. Balermpas, Y. Michel, J. Wagenblast, O. Seitz, C. Weiss, F. Rödel, C. Rödel, and E. Fokas, “Tumour-infiltrating lymphocytes predict response to definitive chemoradiotherapy in head and neck cancer,” *Br. J. Cancer*, vol. 110, no. 2, pp. 501–509, 2014, doi: 10.1038/bjc.2013.640.

[175] G. Kroemer, L. Galluzzi, O. Kepp, and L. Zitvogel, “Immunogenic Cell Death in Cancer Therapy,” *Annu. Rev. Immunol.*, vol. 31, no. 1, pp. 51–72, 2013, doi: 10.1146/annurev-immunol-032712-100008.

[176] N. Casares, M. O. Pequignot, A. Tesniere, F. Ghiringhelli, S. Roux, N. Chaput, E. Schmitt, A. Hamai, S. Hervas-Stubbs, M. Obeid, F. Coutant, D. Métivier, E. Pichard, P. Aucouturier, G. Pierron, C. Garrido, L. Zitvogel, and G. Kroemer, “Caspase-dependent

immunogenicity of doxorubicin-induced tumor cell death," *J. Exp. Med.*, vol. 202, no. 12, pp. 1691–1701, 2005, doi: 10.1084/jem.20050915.

[177] R. Samaritani, G. Corrado, E. Vizza, and C. Sbiroli, "Cyclophosphamide 'metronomic' chemotherapy for palliative treatment of a young patient with advanced epithelial ovarian cancer," *BMC Cancer*, vol. 7, p. 65, 2007, doi: 10.1186/1471-2407-7-65.

[178] P. Fedele, A. Marino, L. Orlando, P. Schiavone, A. Nacci, F. Sponziello, P. Rizzo, N. Calvani, E. Mazzoni, M. Cinefra, and S. Cinieri, "Efficacy and safety of low-dose metronomic chemotherapy with capecitabine in heavily pretreated patients with metastatic breast cancer," *Eur. J. Cancer*, vol. 48, no. 1, pp. 24–29, 2012, doi: 10.1016/j.ejca.2011.06.040.

[179] R. S. Kerbel and B. A. Kamen, "The anti-angiogenic basis of metronomic chemotherapy," *Nat. Rev. Cancer*, vol. 4, no. 6, pp. 423–436, 2004, doi: 10.1038/nrc1369.

[180] M. Colleoni, L. Orlando, G. Sanna, A. Rocca, P. Maisonneuve, G. Peruzzotti, R. Ghisini, M. T. Sandri, L. Zorzino, F. Nolè, G. Viale, and A. Goldhirsch, "Metronomic low-dose oral cyclophosphamide and methotrexate plus or minus thalidomide in metastatic breast cancer: Antitumor activity and biological effects," *Ann. Oncol.*, vol. 17, no. 2, pp. 232–238, 2006, doi: 10.1093/annonc/mdj066.

[181] J. Wu and D. J. Waxman, "Metronomic cyclophosphamide schedule-dependence of innate immune cell recruitment and tumor regression in an implanted glioma model," *Cancer Lett.*, vol. 353, no. 2, pp. 272–280, 2014, doi: 10.1016/j.canlet.2014.07.033.

[182] J. Wu and D. J. Waxman, "Immunogenic chemotherapy: Dose and schedule dependence and combination with immunotherapy," *Cancer Lett.*, vol. 419, pp. 210–221, 2018, doi: 10.1016/j.canlet.2018.01.050.

[183] C. S. Chen, J. C. Doloff, and D. J. Waxman, "Intermittent metronomic drug schedule is essential for activating antitumor innate immunity and tumor xenograft regression," *Neoplasia*, vol. 16, no. 1, pp. 84–96, 2014, doi: 10.1593/neo.131910.

[184] A. A. Brandes, A. Tosoni, E. Franceschi, V. Blatt, A. Santoro, M. Faedi, P. Amistà, M. Gardiman, R. Labianca, C. Bianchini, M. Ermani, and M. Reni, "Fotemustine as second-line treatment for recurrent or progressive glioblastoma after concomitant and/or adjuvant temozolomide: A phase II trial of Gruppo Italiano Cooperativo di Neuro-Oncologia (GICNO)," *Cancer Chemother. Pharmacol.*, vol. 64, no. 4, pp. 769–775, 2009, doi: 10.1007/s00280-009-0926-8.

[185] J. Zhao, A. X. Chen, R. D. Gartrell, A. M. Silverman, L. Aparicio, T. Chu, D. Bordbar, D. Shan, J. Samanamud, A. Mahajan, I. Filip, R. Orenbuch, M. Goetz, J. T. Yamaguchi, M. Cloney, C. Horbinski, R. V. Lukas, J. Raizer, A. I. Rae, *et al.*, "Immune and genomic correlates of response to anti-PD-1 immunotherapy in glioblastoma," *Nat. Med.*, vol. 25, no. 3, pp. 462–469, 2019, doi: 10.1038/s41591-019-0349-y.

[186] D. S. Chen and I. Mellman, "Elements of cancer immunity and the cancer–immune set point," *Nature*, vol. 541, no. 7637, pp. 321–330, 2017, doi: 10.1038/nature21349.

[187] P. S. Hegde, V. Karanikas, and S. Evers, "The where, the when, and the how of

immune monitoring for cancer immunotherapies in the era of checkpoint inhibition," *Clin. Cancer Res.*, vol. 22, no. 8, pp. 1865–1874, 2016, doi: 10.1158/1078-0432.CCR-15-1507.

[188] L. Villamañán, "Unraveling CK2 inhibition and temozolomide contribution to therapy response in preclinical GL261 glioblastoma: immune system implications and magnetic resonance based nosological imaging," PhD Thesis, Universitat Autònoma de Barcelona, 2019. https://tdx.cat/handle/10803/666881

[189] H. L. Hanson, D. L. Donermeyer, H. Ikeda, J. M. White, V. Shankaran, L. J. Old, H. Shiku, R. D. Schreiber, and P. M. Allen, "Eradication of established tumors by CD8+ T cell adoptive immunotherapy," *Immunity*, vol. 13, no. 2, pp. 265–276, 2000, doi: 10.1016/S1074-7613(00)00026-1.

[190] C. H. June, J. T. Warshauer, and J. A. Bluestone, "Is autoimmunity the Achilles' heel of cancer immunotherapy?," *Nat. Med.*, vol. 23, no. 5, pp. 540–547, 2017, doi: 10.1038/nm.4321.

[191] I. Liikanen, L. Ahtiainen, M. L. Hirvinen, S. Bramante, V. Cerullo, P. Nokisalmi, O. Hemminki, I. Diaconu, S. Pesonen, A. Koski, L. Kangasniemi, S. K. Pesonen, M. Oksanen, L. Laasonen, K. Partanen, T. Joensuu, F. Zhao, A. Kanerva, and A. Hemminki, "Oncolytic adenovirus with temozolomide induces autophagy and antitumor immune responses in cancer patients," *Mol. Ther.*, vol. 21, no. 6, pp. 1212–1223, 2013, doi: 10.1038/mt.2013.51.

[192] J. Wu, M. Jordan, and D. J. Waxman, "Metronomic cyclophosphamide activation of anti-tumor immunity: tumor model, mouse host, and drug schedule dependence of gene responses and their upstream regulators," *BMC Cancer*, vol. 16, no. 1, p. 623, 2016, doi: 10.1186/s12885-016-2597-2.

[193] G. Schiavoni, A. Sistigu, M. Valentini, F. Mattei, P. Sestili, F. Spadaro, M. Sanchez, S. Lorenzi, M. T. D'Urso, F. Belardelli, L. Gabriele, E. Proietti, and L. Bracci, "Cyclophosphamide synergizes with type I interferons through systemic dendritic cell reactivation and induction of immunogenic tumor apoptosis," *Cancer Res.*, vol. 71, no. 3, pp. 768–778, 2011, doi: 10.1158/0008-5472.CAN-10-2788.

[194] M. R. Gilbert, M. Wang, K. D. Aldape, R. Stupp, M. E. Hegi, K. A. Jaeckle, T. S. Armstrong, J. S. Wefel, M. Won, D. T. Blumenthal, A. Mahajan, C. J. Schultz, S. Erridge, B. Baumert, K. I. Hopkins, T. Tzuk-Shina, P. D. Brown, A. Chakravarti, W. J. Curran, *et al.*, "Dose-dense temozolomide for newly diagnosed glioblastoma: A randomized phase III clinical trial," *J. Clin. Oncol.*, vol. 31, no. 32, pp. 4085–4091, 2013, doi: 10.1200/JCO.2013.49.6968.

[195] A. Ribas, D. S. Shin, J. Zaretsky, J. Frederiksen, A. Cornish, E. Avramis, E. Seja, C. Kivork, J. Siebert, P. Kaplan-Lefko, X. Wang, B. Chmielowski, J. A. Glaspy, P. C. Tumeh, T. Chodon, D. Pe'er, and B. Comin-Anduix, "PD-1 blockade expands intratumoral memory T cells," *Cancer Immunol. Res.*, vol. 4, no. 3, pp. 194–203, 2016, doi: 10.1158/2326-6066.CIR-15-0210.

[196] K. A. Schalper, M. E. Rodriguez-Ruiz, R. Diez-Valle, A. López-Janeiro, A. Porciuncula, M. A. Idoate, S. Inogés, C. de Andrea, A. López-Diaz de Cerio, S. Tejada, P. Berraondo, F.

Villarroel-Espindola, J. Choi, A. Gúrpide, M. Giraldez, I. Goicoechea, J. Gallego Perez-Larraya, M. F. Sanmamed, J. L. Perez-Gracia, *et al.*, “Neoadjuvant nivolumab modifies the tumor immune microenvironment in resectable glioblastoma,” *Nat. Med.*, vol. 25, no. 3, pp. 470–476, 2019, doi: 10.1038/s41591-018-0339-5.

[197] F. G. Dhermain, P. Hau, H. Lanfermann, A. H. Jacobs, and M. J. van den Bent, “Advanced MRI and PET imaging for assessment of treatment response in patients with gliomas,” *Lancet Neurol.*, vol. 9, no. 9. Lancet Neurol, pp. 906–920, 2010, doi: 10.1016/S1474-4422(10)70181-2.

[198] E. Hattingen, A. Jurcoane, O. Bähr, J. Rieger, J. Magerkurth, S. Anti, J. P. Steinbach, and U. Pilatus, “Bevacizumab impairs oxidative energy metabolism and shows antitumoral effects in recurrent glioblastomas: A 31P/ 1H MRSI and quantitative magnetic resonance imaging study,” *Neuro. Oncol.*, vol. 13, no. 12, pp. 1349–1363, 2011, doi: 10.1093/neuonc/nor132.

[199] S. J. Nelson, “Assessment of therapeutic response and treatment planning for brain tumors using metabolic and physiological MRI,” *NMR Biomed*, vol. 24, no. 6. NMR Biomed, pp. 734–749, 2011, doi: 10.1002/nbm.1669.

[200] A. C. Huang, R. J. Orlowski, X. Xu, R. Mick, S. M. George, P. K. Yan, S. Manne, A. A. Kraya, B. Wubbenhorst, L. Dorfman, K. D’Andrea, B. M. Wenz, S. Liu, L. Chilukuri, A. Kozlov, M. Carberry, L. Giles, M. W. Kier, F. Quagliarello, *et al.*, “A single dose of neoadjuvant PD-1 blockade predicts clinical outcomes in resectable melanoma,” *Nat. Med.*, vol. 25, no. 3, pp. 454–461, 2019, doi: 10.1038/s41591-019-0357-y.

[201] J. F. Curtin, M. R. Edwards, K. S. Michelsen, K. M. Kroeger, M. Candolfi, C. Liu, M. C. Clark, M. Arditi, B. Comin-Andiux, A. Ribas, P. R. Lowenstein, and M. G. Castro, “HMGB1 Mediates Endogenous TLR2 Activation And Brain Tumor Regression.,” *FASEB J.*, vol. 22, no. S2, pp. 515–515, 2008, doi: 10.1096/fasebj.22.2_supplement.515.

[202] R. Glass and M. Synowitz, “CNS macrophages and peripheral myeloid cells in brain tumours,” *Acta Neuropathol.*, vol. 128, no. 3, pp. 347–362, 2014, doi: 10.1007/s00401-014-1274-2.

[203] J. Van den Bossche, L. A. O’Neill, and D. Menon, “Macrophage Immunometabolism: Where Are We (Going)?,” *Trends Immunol.*, vol. 38, no. 6, pp. 395–406, 2017, doi: 10.1016/j.it.2017.03.001.

[204] I. Montalbán del Barrio, C. Penski, L. Schlahsa, R. G. Stein, J. Diessner, A. Wöckel, J. Dietl, M. B. Lutz, M. Mittelbronn, J. Wischhusen, and S. F. M. Häusler, “Adenosine-generating ovarian cancer cells attract myeloid cells which differentiate into adenosine-generating tumor associated macrophages - a self-amplifying, CD39- and CD73-dependent mechanism for tumor immune escape,” *J. Immunother. Cancer*, vol. 4, p. 49, 2016, doi: 10.1186/s40425-016-0154-9.

[205] C. Lewis and C. Murdoch, “Macrophage responses to hypoxia: Implications for tumor progression and anti-cancer therapies,” *Am. J. Clin. Pathol.*, vol. 167, no. 3. American Society for Investigative Pathology Inc., pp. 627–635, 2005, doi: 10.1016/S0002-9440(10)62038-X.

[206] C. Happold, P. Roth, W. Wick, N. Schmidt, A.-M. Florea, M. Silginer, G. Reifenberger,

and M. Weller, “Distinct molecular mechanisms of acquired resistance to temozolomide in glioblastoma cells,” *J. Neurochem.*, vol. 122, no. 2, pp. 444–455, 2012, doi: 10.1111/j.1471-4159.2012.07781.x.

[207] J. He, Y. Hu, M. Hu, and B. Li, “Development of PD-1/PD-L1 Pathway in Tumor Immune Microenvironment and Treatment for Non-Small Cell Lung Cancer,” *Sci. Rep.*, vol. 5, no. 1, p. 13110, 2015, doi: 10.1038/srep13110.

[208] Y. Katsuya, H. Horinouchi, T. Asao, S. Kitahara, Y. Goto, S. Kanda, Y. Fujiwara, H. Nokihara, N. Yamamoto, S. ichi Watanabe, K. Tsuta, and Y. Ohe, “Expression of programmed death 1 (PD-1) and its ligand (PD-L1) in thymic epithelial tumors: Impact on treatment efficacy and alteration in expression after chemotherapy,” *Lung Cancer*, vol. 99, pp. 4–10, 2016, doi: 10.1016/j.lungcan.2016.05.007.

[209] M. Hecht, M. Büttner-Herold, K. Erlenbach-Wünsch, M. Haderlein, R. Croner, R. Grützmann, A. Hartmann, R. Fietkau, and L. V. Distel, “PD-L1 is upregulated by radiochemotherapy in rectal adenocarcinoma patients and associated with a favourable prognosis,” *Eur. J. Cancer*, vol. 65, pp. 52–60, 2016, doi: 10.1016/j.ejca.2016.06.015.

[210] P. Zhang, D. M. Su, M. Liang, and J. Fu, “Chemopreventive agents induce programmed death-1-ligand 1 (PD-L1) surface expression in breast cancer cells and promote PD-L1-mediated T cell apoptosis,” *Mol. Immunol.*, vol. 45, no. 5, pp. 1470–1476, 2008, doi: 10.1016/j.molimm.2007.08.013.

[211] A. Derer, M. Spiljar, M. Bäumler, M. Hecht, R. Fietkau, B. Frey, and U. S. Gaipl, “Chemoradiation Increases PD-L1 Expression in Certain Melanoma and Glioblastoma Cells,” *Front. Immunol.*, vol. 7, no. DEC, p. 610, 2016, doi: 10.3389/fimmu.2016.00610.

[212] M. M. Bradford, “A rapid and sensitive method for the quantitation of microgram quantities of protein utilizing the principle of protein-dye binding,” *Anal. Biochem.*, vol. 72, no. 1–2, pp. 248–254, 1976, doi: 10.1016/0003-2697(76)90527-3.

[213] Z. Yu, Y. Chen, S. Wang, P. Li, G. Zhou, and Y. Yuan, “Inhibition of NF-κB results in anti-glioma activity and reduces temozolomide-induced chemoresistance by down-regulating MGMT gene expression,” *Cancer Lett.*, vol. 428, pp. 77–89, 2018, doi: 10.1016/j.canlet.2018.04.033.

[214] H.-L. Liu, C.-Y. Huang, J.-Y. Chen, H.-Y. J. Wang, P.-Y. Chen, and K.-C. Wei, “Pharmacodynamic and Therapeutic Investigation of Focused Ultrasound-Induced Blood-Brain Barrier Opening for Enhanced Temozolomide Delivery in Glioma Treatment,” *PLoS One*, vol. 9, no. 12, p. e114311, 2014, doi: 10.1371/journal.pone.0114311.

[215] T. Nakagawa, K. Ido, T. Sakuma, H. Takeuchi, K. Sato, and T. Kubota, “Prognostic significance of the immunohistochemical expression of O^6-methylguanine-DNA methyltransferase, P-glycoprotein, and multidrug resistance protein-1 in glioblastomas,” *Neuropathology*, vol. 29, no. 4, pp. 379–388, 2009, doi: 10.1111/j.1440-1789.2008.00983.x.

[216] P. Wu, J. Cai, Q. Chen, B. Han, X. Meng, Y. Li, Z. Li, R. Wang, L. Lin, C. Duan, C. Kang,

and C. Jiang, “Lnc-TALC promotes O6-methylguanine-DNA methyltransferase expression via regulating the c-Met pathway by competitively binding with miR-20b-3p,” *Nat. Commun.*, vol. 10, no. 1, p. 2045, 2019, doi: 10.1038/s41467-019-10025-2.

[217] H. H. Wang, T. Y. Chang, W. C. Lin, K. C. Wei, and J. W. Shin, “GADD45A plays a protective role against temozolomide treatment in glioblastoma cells,” *Sci. Rep.*, vol. 7, p. 8814, 2017, doi: 10.1038/s41598-017-06851-3.

[218] M. Lorger, “Tumor Microenvironment in the Brain,” *Cancers*, vol. 4, no. 1, pp. 218–243, 2012, doi: 10.3390/cancers4010218.

[219] Y. De Vlaeminck, A. González-Rascón, C. Goyvaerts, and K. Breckpot, “Cancer-associated myeloid regulatory cells,” *Front. Immunol.*, vol. 7, no. MAR, p. 113, 2016, doi: 10.3389/fimmu.2016.00113.

[220] C. D. Carey, D. Gusenleitner, M. Lipschitz, M. G. M. Roemer, E. C. Stack, E. Gjini, X. Hu, R. Redd, G. J. Freeman, D. Neuberg, F. S. Hodi, X. S. Liu, M. A. Shipp, and S. J. Rodig, “Topological analysis reveals a PD-L1-associated microenvironmental niche for Reed-Sternberg cells in Hodgkin lymphoma,” *Blood*, vol. 130, no. 22, pp. 2420–2430, 2017, doi: 10.1182/blood-2017-03-770719.

[221] D. Hanahan and R. A. Weinberg, “Hallmarks of cancer: The next generation,” *Cell*, vol. 144, no. 5, pp. 646–674, 2011, doi: 10.1016/j.cell.2011.02.013.

[222] D. Samanta, Y. Park, X. Ni, H. Li, C. A. Zahnow, E. Gabrielson, F. Pan, and G. L. Semenza, “Chemotherapy induces enrichment of CD47+/CD73+/PDL1+ immune evasive triple-negative breast cancer cells,” *Proc. Natl. Acad. Sci. U. S. A.*, vol. 115, no. 6, pp. E1239–E1248, 2018, doi: 10.1073/pnas.1718197115.

[223] R. Stupp, W. P. Mason, M. J. van den Bent, M. Weller, B. Fisher, M. J. B. Taphoorn, K. Belanger, A. A. Brandes, C. Marosi, U. Bogdahn, J. Curschmann, R. C. Janzer, S. K. Ludwin, T. Gorlia, A. Allgeier, D. Lacombe, J. G. Cairncross, E. Eisenhauer, and R. O. Mirimanoff, “Radiotherapy plus Concomitant and Adjuvant Temozolomide for Glioblastoma,” *N. Engl. J. Med.*, vol. 352, no. 10, pp. 987–996, 2005, doi: 10.1056/NEJMoa043330.

[224] R. Stupp, S. Taillibert, A. Kanner, W. Read, D. M. Steinberg, B. Lhermitte, S. Toms, A. Idbaih, M. S. Ahluwalia, K. Fink, F. Di Meco, F. Lieberman, J. J. Zhu, G. Stragliotto, D. D. Tran, S. Brem, A. F. Hottinger, E. D. Kirson, G. Lavy-Shahaf, *et al.*, “Effect of tumor-treating fields plus maintenance temozolomide vs maintenance temozolomide alone on survival in patients with glioblastoma a randomized clinical trial,” *JAMA - J. Am. Med. Assoc.*, vol. 318, no. 23, pp. 2306–2316, 2017, doi: 10.1001/jama.2017.18718.

[225] W. Taal, H. M. Oosterkamp, A. M. E. Walenkamp, H. J. Dubbink, L. V. Beerepoot, M. C. J. Hanse, J. Buter, A. H. Honkoop, D. Boerman, F. Y. F. de Vos, W. N. M. Dinjens, R. H. Enting, M. J. B. Taphoorn, F. W. P. J. van den Berkmortel, R. L. H. Jansen, D. Brandsma, J. E. C. Bromberg, I. van Heuvel, R. M. Vernhout, *et al.*, “Single-agent bevacizumab or lomustine versus a combination of bevacizumab plus lomustine in patients with recurrent glioblastoma (BELOB trial): A randomised controlled phase 2 trial,” *Lancet Oncol.*, vol. 15, no. 9, pp. 943–953, 2014, doi: 10.1016/S1470-2045(14)70314-6.

[226] J. Rodon, M. A. Carducci, J. M. Sepulveda-Sánchez, A. Azaro, E. Calvo, J. Seoane, I.

Braña, E. Sicart, I. Gueorguieva, A. L. Cleverly, N. S. Pillay, D. Desaiah, S. T. Estrem, L. Paz-Ares, M. Holdhoff, J. Blakeley, M. M. Lahn, and J. Baselga, “First-in-human dose study of the novel transforming growth factor-β receptor I kinase inhibitor LY2157299 monohydrate in patients with advanced cancer and glioma,” *Clin. Cancer Res.*, vol. 21, no. 3, pp. 553–560, 2015, doi: 10.1158/1078-0432.CCR-14-1380.

[227] A. Louveau, I. Smirnov, T. J. Keyes, J. D. Eccles, S. J. Rouhani, J. D. Peske, N. C. Derecki, D. Castle, J. W. Mandell, K. S. Lee, T. H. Harris, and J. Kipnis, “Structural and functional features of central nervous system lymphatic vessels,” *Nature*, vol. 523, no. 7560, pp. 337–341, 2015, doi: 10.1038/nature14432.

[228] R. D. Schreiber, L. J. Old, and M. J. Smyth, “Cancer Immunoediting: Integrating Immunity’s Roles in Cancer Suppression and Promotion,” *Science.*, vol. 331, no. 6024, pp. 1565–1570, 2011, doi: 10.1126/science.1203486.

[229] E. Iwado, T. Ichikawa, H. Kosaka, S. Otsuka, H. Kambara, T. Tamiya, S. Kondo, and I. Date, “Role of VEGF and matrix metalloproteinase-9 in peritumoral brain edema associated with supratentorial benign meningiomas,” *Neuropathology*, vol. 32, no. 6, pp. 638–646, 2012, doi: 10.1111/j.1440-1789.2012.01312.x.

[230] I. Golán, L. Rodríguez de la Fuente, and J. Costoya, “NK Cell-Based Glioblastoma Immunotherapy,” *Cancers*, vol. 10, no. 12, p. 522, 2018, doi: 10.3390/cancers10120522.

[231] M. L. Broekman, S. L. N. Maas, E. R. Abels, T. R. Mempel, A. M. Krichevsky, and X. O. Breakefield, “Multidimensional communication in the microenvirons of glioblastoma,” *Nat. Rev. Neurol.*, vol. 14, no. 8, pp. 482-495, 2018, doi: 10.1038/s41582-018-0025-8.

[232] P. M. Woo, Y. Li, A. Y. Chan, S. P. Ng, H. F. Loong, D. M. Chan, G. C. Wong, and W.-S. Poon, “A multifaceted review of temozolomide resistance mechanisms in glioblastoma beyond O-6-methylguanine-DNA methyltransferase,” *Glioma*, vol. 2, no. 2, p. 68, 2019, doi: 10.4103/glioma.glioma_3_19.

[233] R. Domenis, D. Cesselli, B. Toffoletto, E. Bourkoula, F. Caponnetto, I. Manini, A. P. Beltrami, T. Ius, M. Skrap, C. Di Loreto, and G. Gri, “Systemic T cells immunosuppression of glioma stem cell-derived exosomes is mediated by monocytic myeloid-derived suppressor cells,” *PLoS One*, vol. 12, no. 1, p. e0169932, 2017, doi: 10.1371/journal.pone.0169932.

[234] M. W. Schmitt, L. A. Loeb, and J. J. Salk, “The influence of subclonal resistance mutations on targeted cancer therapy,” *Nat. Rev. Clin. Oncol.*, vol. 13, no. 6, pp. 335–347, 2016, doi: 10.1038/nrclinonc.2015.175.

[235] R. Maiti, “Metronomic chemotherapy,” *J. Pharmacol. Pharmacother.*, vol. 5, no. 3, p. 186, 2014, doi: 10.4103/0976-500X.136098.

[236] S. Xue, M. Hu, V. Iyer, and J. Yu, “Blocking the PD-1/PD-L1 pathway in glioma: A potential new treatment strategy,” *J. Hematol. Oncol.*, vol. 10, no. 1, p. 81, Apr. 07, 2017, doi: 10.1186/s13045-017-0455-6.

[237] L. Spiers, N. Coupe, and M. Payne, “Toxicities associated with checkpoint inhibitors-

An overview," *Rheumatol*, vol. 58, pp. vii7–vii16, 2019, doi: 10.1093/rheumatology/kez418.

[238] D. W. Litchfield, "Protein kinase CK2: Structure, regulation and role in cellular decisions of life and death," *Biochem. J.*, vol. 369, no. 1. Portland Press, pp. 1–15, Jan. 01, 2003, doi: 10.1042/BJ20021469.

[239] L. A. Pinna and F. Meggio, "Protein kinase CK2 ('casein kinase-2') and its implication in cell division and proliferation.," *Prog. Cell. Cycle. Res.*, vol. 3, pp. 77–97, 1997, doi: 10.1007/978-1-4615-5371-7_7.

[240] L. Ferrer-Font, E. Alcaraz, M. Plana, A. P. Candiota, E. Itarte, and C. Arús, "Protein Kinase CK2 Content in GL261 Mouse Glioblastoma," *Pathol. Oncol. Res.*, vol. 22, no. 3, pp. 633–637, 2016, doi: 10.1007/s12253-015-9987-7.

[241] X. Liu, J. Chen, W. Li, C. Hang, and Y. Dai, "Inhibition of Casein Kinase II by CX-4945, But Not Yes-associated protein (YAP) by Verteporfin, Enhances the Antitumor Efficacy of Temozolomide in Glioblastoma," *Transl. Oncol.*, vol. 13, no. 1, pp. 70–78, 2020, doi: 10.1016/j.tranon.2019.09.006.

[242] P. Sharma, S. Hu-Lieskovan, J. A. Wargo, and A. Ribas, "Primary, Adaptive, and Acquired Resistance to Cancer Immunotherapy," *Cell*, vol. 168, no. 4, pp. 707–723, 2017, doi: 10.1016/j.cell.2017.01.017.

[243] G. Abril-Rodriguez, D. Y. Torrejon, W. Liu, J. M. Zaretsky, T. S. Nowicki, J. Tsoi, C. Puig-Saus, I. Baselga-Carretero, E. Medina, M. J. Quist, A. J. Garcia, W. Senapedis, E. Baloglu, A. Kalbasi, G. Cheung-Lau, B. Berent-Maoz, B. Comin-Anduix, S. Hu-Lieskovan, C. Wang, *et al.*, "PAK4 inhibition improves PD-1 blockade immunotherapy," *Nat. Cancer*, vol. 1, no. 1, pp. 46–58, 2020, doi: 10.1038/s43018-019-0003-0.

[244] D. A. Reardon, P. C. Gokhale, S. R. Klein, K. L. Jones, P. T. Kirschmeier, M. Speranza, H. Koblish, P. Scherle, L. Leopold, R. Newton, and G. J. Freeman, "Abstract 572: Inhibition of IDO1 with epacadostat enhances anti-tumor efficacy of PD-1 blockade in a syngeneic glioblastoma (GBM) model," *Cancer Res.*, vol. 77, no. 13 Supplement, pp. 572–572, 2017, doi: 10.1158/1538-7445.am2017-572.

[245] J. E. Kim, M. A. Patel, A. Mangraviti, E. S. Kim, D. Theodros, E. Velarde, A. Liu, E. W. Sankey, A. Tam, H. Xu, D. Mathios, C. M. Jackson, S. Harris-Bookman, T. Garzon-Muvdi, M. Sheu, A. M. Martin, B. M. Tyler, P. T. Tran, X. Ye, *et al.*, "Combination therapy with anti-PD-1, anti-TIM-3, and focal radiation results in regression of murine gliomas," *Clin. Cancer Res.*, vol. 23, no. 1, pp. 124–136, 2017, doi: 10.1158/1078-0432.CCR-15-1535.

Annex I

SUPERVISION OF LABORATORY ANIMALS

Procedure CEEAH-3665

MONITORING PARAMETERS (scale: 0-3 points):

Weight Loss

0) Normal Weight

1) Less than 10% loss

2) Between 10 and 15% loss

3) Consistent or rapid, exceeding 20% loss maintained for 72h

Physical appearance

0) Normal

1) More than 10% dehydration, skin tenting

2) Erected hair. Cyanosis

3) Hunched back. Loss of muscle mass

Clinical signs

0) None

1) Circular motion of the animal

2) Mucous secretions and/or bleeding from any orifice. Detectable hypertrophy of organs (lymph nodes, spleen, liver).

3) Shortness of breath (particularly if accompanied by nasal discharge and / or cyanosis). Cachexia.

Changes in behaviour

0) No

1) Inability to move normally

2) Inability to get to the food / drink. Isolation from the rest of the animals in the cage

3) Unconsciousness or comatose. Lack of response (Dying)

Wounds

0) No

1) Scratches

2) Nonhealing wounds. Infection at the surgical site

3) Ulcerating, festering wounds. Ulcerating or necrotic tumours

The animal condition according to the parameters and overall score:

a) 0 points: Healthy animal

b) 1-2 points: Minor signs, follow established protocol

c) 3-11 points: Daily supervision of the animal. Analgesics* or sacrifice of the animal **

d) 12-30 points: sacrifice **

* Analgesic: Meloxicam (subcutaneously: 1 mg /kg)

** The *Servei d'Estabulari* veterinary staff informs a group member as soon as possible to consider halting of the protocol / experiment.

NOTE: As the tumour grows, it affects the motor function of the brain. Animals may suffer from: paresis, decreased strength, paralysis. In these cases, food and water (i.e. hydrogel or water-soaked food) should be placed inside the cage to facilitate access by the animal.

Annex II

In order to develop a more effective treatment strategy for GL261 GB mice, some related literature was read and analysed. Table A lists the information about PD-1 antibody as a monotherapy for GL261 tumour in different studies, including anti-PD-1 dosing frequency, cumulative dose and corresponding therapeutic effect.

Among these strategies, the last one [142] should have been the optimal choice: in this study the least amount of anti-PD-1 was used (100 μg per day, every 7 days, with a total amount of 300 μg). In our hands, this protocol lead to a satisfactory yet not curative therapeutic effect, it prolonged the median survival to 37 days (vs 26 days in control mice) and allowing 10% mice with long-term survival (≧ 100 days). Therefore, we could be more confident to get better therapeutic effects when combined it with metronomic TMZ therapy and using less total anti-PD-1.

Literature name and year	Cell line and Mice model	Anti-PD-1 Dosing frequency	Cumulative dose	Therapeutic effect
Inhibition of IDO1 with epacadostat enhances anti-tumour efficacy of PD-1 blockade in a syngeneic glioblastoma (GBM) model (2017) [244]	100,000 luciferized GL261 cells, C57BL/6 mice	500 μg (IP) on day 6, 250 μg every 3 days with 7 repeat injections	2,250 μg	4 of 8 mice (50%) treated with anti-PD-1 were long-term survivors (≥ 100 days). (median survival was not mentioned)
Glioblastoma Eradication Following Immune Checkpoint Blockade in an Orthotopic, Immunocompetent Model （2015）[105]	100,000 luciferized GL261 cells, C57BL/6 mice	500 μg (IP) on day 6, 250 μg every 3 days with 7 repeat injections	2,250 μg	12 of 24 mice (50%) treated with anti-PD-1 were long-term survivors (≥ 100 days). (median survival was not mentioned)
Anti-PD-1 Blockade and Stereotactic Radiation Produce Long-Term Survival in Mice with Intracranial Gliomas (2012)[110]	130,000 GL261-Luc cells, C57BL/6J mice	Anti-PD-1 antibody 200 μg (IP) per animal, administered on days 10, 12, and 14.	600 μg	Anti-PD-1 monotherapy prolonged median survival to 30 days, compared with control (26 days). No long-term survival
Combination Therapy with Anti-PD-1, Anti-TIM-3, and Focal Radiation Results in Regression of Murine Gliomas (2016)[245]	130,000 GL261-Luc cells, C57BL/6J mice	Anti-PD-1 antibody 200 μg (IP) per animal, administered on days 10, 12, and 14.	600 μg	Anti-PD-1 improved median survival (33 days) compared with control (22 days). 27.8% long-term survival (≥ 100 days)

Temozolomide combined with PD-1 Antibody therapy for mouse orthotopic glioma model (2018)[170]	50,000 GL261 glioma cells, C57BL/6 mice	200 μg /day (ip), Administration at day1, day3 and day5 (alternate dose) post implantation	600 μg	Anti-PD-1 monotherapy prolonged median survival to 28 days, compared with control (25 days). No long-term survival
Preclinical efficacy of immune-checkpoint monotherapy does not recapitulate corresponding biomarkers-based clinical predictions in glioblastoma (2017)[142]	500,000 GL261 glioma cells, C57BL/6 mice	100 μg /day(ip), Administration at day7, day14, day21 (every 7 days) post implantation	300 μg	Anti-PD1 therapy prolonged the median survival (37 days), compared with control (26 days), allowing 10% long-term survival ($\geqslant$ 100 days).

Table A, information about PD-1 antibody as a monotherapy for GL261 tumour in different studies.